A MULTISCALE MODEL FOR COUPLED HEAT CONDUCTION AND DEFORMATIONS OF VISCOELASTIC COMPOSITES

A Dissertation

by

KAMRAN AHMED KHAN

Submitted to the Office of Graduate Studies of
Texas A&M University
in partial fulfillment of the requirements for the degree of

DOCTOR OF PHILOSOPHY

May 2011

Major Subject: Mechanical Engineering

A Multiscale Model for Coupled Heat Conduction and Deformations of Viscoelastic Composites

A MULTISCALE MODEL FOR COUPLED HEAT CONDUCTION AND DEFORMATIONS OF VISCOELASTIC COMPOSITES

A Dissertation

by

KAMRAN AHMED KHAN

Submitted to the Office of Graduate Studies of
Texas A&M University
in partial fulfillment of the requirements for the degree of

DOCTOR OF PHILOSOPHY

Approved by:

Chair of Committee,	Anastasia H. Muliana
Committee Members,	J.N. Reddy
	Arun R. Srinivasa
	Rashid K. Abu Al Rub
Head of Department,	Dennis O'Neal

May 2011

Major Subject: Mechanical Engineering

ABSTRACT

A Multiscale Model for Coupled Heat Conduction and Deformations of Viscoelastic Composites. (May 2011)

Kamran Ahmed Khan, B.E., NED University of Engineering and Technology, Karachi, Pakistan; M.S., Texas A&M University

Chair of Advisory Committee: Dr. Anastasia Muliana

This study introduces a multiscale model for analyzing nonlinear thermo-viscoelastic responses of particulate composites. A simplified micromechanical model consisting of four sub-cells, i.e., one particle and three matrix sub-cells is formulated to obtain the effective thermal and mechanical properties and time-dependent response of the composites. The particle and matrix constituents are made of isotropic homogeneous viscoelastic bodies undergoing small deformation gradients. Perfect bonds are assumed along the sub-cell's interfaces. The coupling between the thermal and mechanical response is attributed to the dissipation of energy due to the viscoelastic deformation and temperature dependent material parameters in the viscoelastic constitutive model. The micromechanical relations are formulated in terms of incremental average field quantities, i.e., stress, strain, heat flux and temperature gradient, in the sub-cells. The effective mechanical properties and coefficient of thermal expansion are derived by satisfying displacement- and traction continuities at the interfaces during the thermo-viscoelastic deformations. The effective thermal conductivity is formulated by imposing heat flux- and temperature continuities at the subcells' interfaces. A time integration

algorithm for simultaneously solving the equations that govern heat conduction and thermoviscoelastic deformations of isotropic materials is developed. The algorithm is then incorporated within each sub-cell of the micromechanical model together with the macroscopic energy equation to determine the effective coupled thermoviscoelastic response of the particulate composite. The numerical formulation is implemented within the ABAQUS, general purpose displacement based FE software, allowing for analyzing coupled heat conduction and deformations of composite structures. Experimental data on the effective thermal properties and time-dependent responses of particulate composites available in the literature are used to verify the micromechanical model formulation. The multiscale model capability is also examined by comparing the field variables, i.e., temperature, displacement, stresses and strains, obtained from heterogeneous and homogeneous composite structures, during the transient heat conduction and deformations. It is found that the multiscale framework can predicts the microscopic temperature and displacements fields with a reasonable accuracy. However, it is conclude that the multiscale framework is not suitable to represent accurately the discontinuities at the interfaces within the composite. Examples of coupled thermoviscoelastic analyses of particulate composites and functionally graded structures are also presented. The present micromechanical modeling approach is found to be computationally efficient and shows good agreement with experiments in predicting the effective thermo-mechanical response of particulate composites and functionally graded materials. Our analyses forecast a better design for creep resistant and less dissipative structures using particulate composites and functionally graded materials.

DEDICATION

To my parents

ACKNOWLEDGEMENTS

Above all, I am very thankful to almighty Allah who gave me courage and strength to obtain my Ph.D. degree.

I am grateful to my advisor and committee chair, Dr. Anastasia Muliana, for her continuous guidance and encouragement throughout my doctoral program and my stay at Texas A&M. Her support at every stage of this project was really valuable for me. I would like to extend my gratitude to Dr. J. N. Reddy, Dr. Arun R. Srinivasa and Dr. Rashid for their invaluable and constructive comments on my dissertation.

There is something very special about my dissertation committee. All members, including the chair of my committee, are the teachers who introduced me to their respective courses for the first time ever in my life. Dr. Srinivasa was my first teacher of elasticity and plasticity with whom I have learned fundamental mechanics in-depth. His valuable comments always served as a guideline for me to complete my dissertation. Dr. Reddy was my first teacher of linear and nonlinear finite element methods. He has always been an inspiration to me. In addition to finite elements, I have learned some of the very basic concepts in the field of solids, as well as fluid mechanics from him. Dr. Rashid was my first teacher of damage mechanics who gave me the basic understanding of fracture and damage mechanics and provided me the motivation to further explore this area.

I would like to express my sincere gratitude to my advisor, Dr. Muliana who has been very supportive in all aspects of my studies. She introduced me to the field of viscoelasticity. I have learned various analytical, numerical and experimental techniques from her. She provided invaluable guidance and constant supervision during my doctoral studies. I would like to thank her from the bottom of my heart for providing financial support during the entire duration of my doctoral studies. I would also like to thank her, for her financial support and continuous encouragement for me to attend various conferences and disseminate my research work. She is a great advisor and mentor to work with.

I would like to extend my gratitude to Dr. Harry Hilton for sharing his knowledge on mechanics of materials in general, and with whom I co-authored a journal paper on functionally graded materials. He is a nice person to work with. I would like to thank Dr. Martin Levesque for providing the FE mesh of the heterogeneous composites. His valuable comments on the micromechanics of composites are very much appreciated.

I am very thankful to all my friends who guided and supported me throughout my doctoral program. I am thankful to Pradeep, Kim, Abid, Ammar, Sohaib, Tariq, Ali, Salman and all others who supported and provided me constant motivation during my studies. I am also thankful to my roommates who provided constant support during my doctoral studies. I would like to thank Shahbaz Bhai from the bottom of my heart for his continuous support and encouragement during my stay at Texas A&M. In the end, I am very thankful to my beloved mother, father, grandmother, brother and sisters for their support.

NOMENCLATURE

AEH	Asymptotic Expansion Homogenization
BVP	Boundary Value Problem
CTE	Coefficient of Linear Thermal Expansion
ETC	Effective Thermal Conductivity
FC	Field Coupling
FE	Finite Element
FGM	Functionally Graded Materials
FRP	Fiber Reinforced Composites
HDPE	High Density Polyethylene
ISV	Internal State Variable
MOC	Method of Cells
MT	Mori-Tanaka
NR	Newton Raphson
RVE	Representative Volume Element
SCM	Self Consistent Method
TBC	Thermal Barrier Coatings
TSM	Thermo-rheologically Simple Material
UEXPAN	User Subroutine to Define Incremental Thermal Strains
UMAT	User Subroutine to Define a Material's Mechanical Behavior
UMATH	User Subroutine to Define a Material's Thermal Behavior

VCFEM	Voronoi Cell FE Method
VF	Volume Fraction

TABLE OF CONTENTS

CHAPTER Page

LIST OF FIGURES

Page

Page

Page

Page

Page

Page

Page

Page

Page

Page

Page

LIST OF TABLES

Page

CHAPTER I

INTRODUCTION

Composite materials have been utilized in various engineering applications that involves temperature changes ranging from low to elevated temperatures such as thermal barrier coatings, turbine blades, etc. Different composite performances can be achieved by combining constituents with different thermal and mechanical properties. Metal, ceramic and polymer have been used for the matrix which is reinforced with various types of fiber and/or particles. Polymer matrix composites are used due to their light weight characteristics and low cost of manufacturing; however they exhibit significant time-dependent behaviors when subjected to elevated temperatures. For extremely high temperature applications like in gas turbines and diesel engines, metal and ceramic matrix composites are preferred as an alternate to polymeric composites. A resistance to high temperature and mechanical loadings is one of many attractive features of metal matrix composite. These composites also show creep behavior under extreme environmental conditions.

During their life time composites are often exposed to coupled mechanical and non-mechanical effects, such as diffusion of fluid, heat conduction, chemical reactions that affect the mechanical properties of the composites. To reduce complexity in

---

This dissertation follows the style of *Mechanics of Time-Dependent Materials*.

analyzing the response of materials and structures, the interactions of the field variables are often ignored and the governing equations of the different fields are solved independently. This approach can lead to sensible response predictions when the effect of field coupling on the overall performance of materials is insignificant. For example, viscoelastic materials are considered as dissipative materials and during the deformation significant heat could be generated affecting the temperature of the viscoelastic bodies. However, in extremely high temperature applications, the heat generation due to the dissipation effect of the viscoelastic bodies may be negligible compared to the ambient temperature of the bodies. In other applications, when an inertia effect is considerable, such as in dynamics and impact loadings, the thermo-mechanical coupling effects become significant. In addition to that when a quasi-static cyclic loading is applied to a viscoelastic body over a long period of time considerable amount of heat is generated; depending on the boundary conditions, the temperature increase in the body could be significant and could accelerate creep/relaxation in the body. To gain fundamental understanding on the effects of constituents' properties and microstructural geometries on the overall response of composites, various micromechanical models have been formulated. Limited studies have been performed to analyze the coupled thermo-viscoelastic responses of composites, mainly for fiber reinforced composite. In most of these studies, the temperature fields obtained from first solving the heat transfer equations are used to analyze the thermo-viscoelastic responses of composites. Micromechanical models capable of predicting the effective behavior of composite

subjected to concurrent mechanical and thermal stimuli and incorporating heat generation due to the dissipation effect are still lacking.

The primary objective of this study is to develop a multiscale framework for analyzing coupled heat conduction and thermoviscoelastic deformation of a particulate composite. A micro-macro approach is adopted to determine the homogenized thermo-viscoelastic response of composites and solve the equations that govern the heat conduction and deformation in the composite at multiple length scales. The effect of heat generation from the dissipation of energy during the viscoelastic deformation on the overall response of the composite is also considered. The framework is implemented in ABAQUS (FE code) to analyze the thermoviscoelastic behavior of composite structures and functionally graded materials (FGMs). The suitability to analyze FGMs using the proposed multi-scale computational framework will be assessed by comparing the results from the available experimental data or FE simulations. As a structural application, coupled heat conduction and viscoelastic deformation analyses of composite plates and beams are presented.

This chapter presents a literature review of analytical, experimental and numerical studies on the thermo-viscoelastic response of composites. Various micromechanical and multiscale modeling approaches to analyze coupled heat conduction and deformation of viscoelastic composites with an emphasis given to particulate composites are discussed. The objectives of the present study are also given.

1.1 LITERATURE REVIEW

Particulate composites have been extensively used in many high temperature applications. Experimental results show that the spatial distribution of the reinforced particles and composition of the constituents greatly influenced the mechanical behavior of the composites (Watt et. al., 1996 and Chawla et. al., 1998). Particulate composites having SiC particles and Aluminum alloy matrix show creep behavior at moderate temperatures, between 300-600 ˚C (Mishra and Pandey, 1990; Doncel and Sherby, 1993; Yong et.al., 1997) and at extremely high temperatures, above 1000 ˚C (Butt et al., 1996). Thermal barrier coatings (TBC) are used in many high temperature applications like diesel engine and turbine blades, to protect these components from high temperature gases and prevent corrosion and oxidation. A TBC system is composed of different layers. These layers can be made of functionally graded materials (FGMs) or composites with uniformly distributed particles. The TBC system shows creep at high temperatures, above 900 ˚C (Ali et. al., 2004, Oruganti and Ghosh, 2003) which can be detrimental to the performance of these coating systems and can cause failure of the structural components.

In designing composite structures, it is necessary to determine the macroscopic effective properties of the composite and understand responses of the constituents when the composite are subjected to various external stimuli. Conducting experiments to obtain the effective response of composites under various loading histories and at different compositions and properties of the constituents is often costly and time consuming. In some cases it is challenging or impractical to perform experiments on

determining coupled thermoviscoelastic behavior of composite structures. Modeling response of composites that include detailed microstructural characteristics allows obtaining macroscopic response of the structural components and detailed response of the constituents. However, it is impossible to incorporate detailed characteristics of the constituents and microstructural geometries in designing and analyzing response of the composite structures. Thus, several homogenization techniques with simplified microstructural morphologies have been developed to predict the effective response of composites and their microstructural behaviors.

1.1.1 MULTISCALE AND MICROMECHANICAL MODELS

The overall behavior of composites depends strongly on the shape, size, properties and spatial distribution of the microstructural constituents. Bridging the micro-macro or global-local responses has been done through the multi-scale and micromechanical models. Depending on the complexity of the responses and microstructural geometries, approximate solutions are often used within the multiscale and micromechanical models.

Within the framework of linearized elasticity, several analytical models have been proposed to predict the effective response of composites at the macroscopic level from the characteristics of microstructures. Based on the uniform strain and stress approximations, Voigt (1910) and Reuss (1929) introduced simple rule of mixtures to average elastic moduli of composites. This model gives a rough estimate of effective properties by considering only constituents properties and compositions. Hill (1952) has shown that the Voigt and Reuss models yield to upper and lower bounds, respectively. Tighter bounds are given by Walpole (1966) and Hashin and Shtrikman (1963). A

refined model is given by Eshelby (1957), which is the pioneer work in micromechanics of composites. According to this solution, the strain and stress fields in the ellipsoid inclusion subjected to a remotely applied uniform strain or stress are uniform. Further development in micromechanics is done by various authors, e.g., composite spheres model, Hashin (1962); self consistent approach, Budiansky (1965) and Hill (1965); generalized self consistent scheme, Christensen and Lo (1979,1986); effective field theory, Mori-Tanaka (1973); probabilistic approach, Chen and Acrivos, (1978); differential Method, McLaughlin, (1977), Norris, (1985). Detailed discussion of various micromechanical models and bounds on the effective mechanical properties can be found in Aboudi (1991), Mura (1987), Nemat-Nasser and Hori (1999).

The above analytical models are limited in predicting the effective properties of composites having simple microstructural geometries. The micromechanical models based on representative volume element (RVE) are widely used to predict the effective inelastic and nonlinear properties of composites having a complex geometry of microstructures. The RVE concept was originally introduced by Hill (1963). Two approaches have been considered in selecting RVEs. The first approach includes all possible microstructural characteristics (Zohdi and Wriggers 2001; Nogales and Bohm 2008, Segurado and Llorca 2002; Lévesque et al. 2004, 2008). The second approach determines the smallest size of the microstructure as an RVE that can give reasonably accurate effective response of the composite (Mori-Tanaka 1973; Aboudi 1991; Muliana et al. 2007, 2009). Once the RVE has been selected, macroscopic boundary conditions are imposed on the RVE. Most of these models assume local periodicity. The

homogenized material properties are obtained by incorporating the results of detailed micromechanical relations of the RVE (typically performed by the finite element method) with the macroscopic constitutive equations. Examples of such work can be found in Aboudi (1991), Haj-ali and Pecknold (1996), Christman et. al. (1989), Tvergaard (1990), Brockenbrough et. al. (1991), Nakamura and Suresh (1993), McHugh et. al. (1993) and Smit et. al. (1999), which formulate the macroscopic constitutive relations based on a single RVE subjected to loading history and periodic boundary conditions. These methods are suitable for small deformation problems as discussed by McHugh et. al. (1993). The main drawback of this approach is that it assumes the periodic spatial distribution of the microstructures but the actual composite materials have non-periodic microstructures. But, for elastic response of materials, Suquet (1987) found that the use of periodic boundary conditions with the homogenization formulation gave the closest agreement with the experimental results.

In the last few decades, there has been considerable advancement in the homogenization theory. A mathematical homogenization approach based on a two-scale asymptotic expansion of field variable (displacements, temperature, etc) was developed for composites with periodic or quasi periodic microstructures. Earlier work on this homogenization theory can be attributed to Babuska (1976), Keller (1977), Tartar (1990), Sanchez-Palencia (1974, 1980), Bensoussan et al. (1978), Lions (1978), Francfort and Suquet (1986), Bakhvalov and Panasenko (1989). The modeling by homogenization techniques is done by considering the RVE which represents the microstructure of the composite and solving the microscopic boundary value problem to

obtain the macroscopic constitutive properties. A microscale boundary value problem is formulated in a unit cell, which is defined within the basic period of the composite. A solution of the composites with periodic microstructures converges to the solution of the homogenized problem as the periodicity of the microstructure goes to zero. By considering higher order terms in expansion of field variables, the influence of microstructures on the macroscopic approximation, as well as both macroscopic constitutive equation and microscopic distribution of stress, strain in composites can be computed. The asymptotic expansion homogenization (AEH) method has been employed successfully to solve not only elastic but also elastoplastic problems. For example the method was applied to linear thermoelasticity (Ene, 1983; Francfort, 1983) and plasticity with internal variables (Suquet 1982, 1985, 1986, 1987).

The FE method has been used in conjunction with the homogenization theory for the analysis of linear elastic response of composites by Toledana and Murakami (1987), Devries et al. (1989), Guedes and Kikuchi (1991), Michel et. al., 1999, Allen, 2001 and Duvaut, 1976, Drugan and Willis, 1996, Auriault, 1991. Moreover, the method has been used for analyzing elastoplastic constitutive properties of composites (Jansson, 1992), Hollister and Kikuchi (1992), Terada and Kikuchi (1995), Ghosh et al. (1995, 1996) and Fish et. al. (1998, 1999), further improved by Smit et. al. (1998), Miehe et al., (2002), Michel et al. (1999), Terada and Kikuchi (2001), Kouznetsova et al. (2001).

Polymers which are often used as matrix in composites exhibit time-dependent responses in the form of creep and stress relaxation when subjected to a mechanical

loading. The time-dependent behaviors have also been observed in metal-matrix composites at high temperatures. The effective properties of composites exhibiting linear viscoelastic behavior can be solved using the correspondence principle*, e.g., Nguyen (1995). For problems involving complex geometries and boundary conditions, in addition to nonlinear responses, it is often impossible to obtain exact analytical solutions. It is due to this reason that approximate (numerical) solutions are sought.

Several studies have been done on formulating micromechanical models for predicting effective linear viscoelastic responses of composites, e.g. Christensen (1969), Brinson and co-authors (1991, 1998), Rougier et al. (1993) and Li and Weng (1997). Micromechanical models based on simplified microstructural geometries of composites for obtaining effective viscoelastic behaviors with stress/strain dependent constituents (nonlinear viscoelasticity) have been proposed, mainly for fiber reinforced plastic (FRP) composites, e.g., Aboudi (1990, 2005), Haj-Ali and Muliana (2003 and 2004), Muliana and Sawant (2008). The AEH has been employed to formulate the macroscopic constitutive equation in viscoelasticity (Sanchez-Palencia, 1980; Francfort and Suquet, 1986). Numerical procedures using a homogenization theory with a two-scale asymptotic expansion has been developed for linear viscoelasticity, e.g., Shibuya (1997); Yi et al. (1998); Noel and Suquet (2007), thermoviscoelasticity, e.g., Chung et. al. (2000) and Maghous and Creus (2003). Rigorous mathematical formulations (using

* The solutions to boundary value problems in linear viscoelastic bodies can be obtained from the corresponding solutions of linear elastic bodies through the use of Laplace transform.

Nguetseng's notion of two-scale convergence) are also developed for the homogenization of the nonlinear viscoelastic behavior of the composites with periodic microstructures by Augusto (2006 and 2008) and Wu and Ohno (1999), mostly for nonlinear Maxwell and Kelvin Voigt type models. Recently, Muliana and Kim (2007) formulated a micromechanical model for analyzing stress dependent viscoelastic response of solid spherical particle reinforced polymers. Their micromechanical formulation is suitable for small deformation gradient problems. The homogenization schemes are formulated in terms of average stress-strain relations of the particle and matrix constituents, which give approximated values of the effective properties.

Micromechanical models have also been formulated to obtain effective coefficient of thermal expansion (CTE) and effective thermal conductivity (ETC) of composite. For composite with arbitrary phase geometries and composites with spherical inclusions, Turner (1946), Kerner (1956), Levin (1967), Schapery (1968), Fahmi and Ragai (1970) and Rosen and Hashin (1970) have derived equations for the effective CTEs. The effective CTEs are functions of the CTE and linear elastic modulus of each constituent. Tseng (2004) introduced a statistical micromechanics model to determine an effective CTE of particle reinforced composites. Volume averaging scheme was used to determine the effective CTE. Stress and strain concentrations tensors were introduced to relate the local average fields to the global (effective) fields. The interaction effects among the particles were considered by introducing an interaction tensor. Closed form solutions of the effective elastic moduli and effective CTE was derived in terms of the constituent's properties and interaction tensor. Hsieh and Tuan (2006) proposed a modified unit cell

model composed of a continuous matrix phase and an elongated particle. Upper and lower bounds for the effective CTE have been obtained by solving boundary value problems of linear elastic composite bodies.

Referring to the above discussion, the effective CTE of composites depends on the mechanical properties and CTEs of the constituents in the composites. The mechanical and physical properties of materials change with field variables such as stress, deformation, and temperature, resulting in nonlinear response of materials. This has been experimentally reported in several literatures. Odegard and Kumosa (2000), Rupnowski et al. (2006), and Marias and Villoutreix (1998) have shown that the moduli of composites having polymer matrix and their constituents vary with temperatures. Cho et al. (2006) showed the stress-dependent elastic modulus of particle composites, while Lai and Bakker (1995, 1996) and Muliana et al. (2006) are among researchers who experimentally show the stress-dependent viscoelastic responses of polymers and composites. Available methods for predicting the effective CTE were formulated with constant constituent properties (independent of stress, strain, temperature etc.). Moreover, the effective CTE of composites having time-dependent constituent properties are not well understood. Although, it is possible to extend the available micromechanical models to incorporate non-constant (nonlinear) constituent properties and form a set of equations to determine the non-linear effective CTE, it is not always easy to obtain the closed form solutions. To the best knowledge of the author only Feltham and Martin (1982) have experimentally shown the variation of effective CTEs with temperature for a particle reinforced composite.

The averaging procedures developed for the effective linear elastic material constants have been modified to homogenize non-mechanical (thermal, electrical, magnetic) properties of composites. Many analytical and numerical models have been proposed to predict the effective thermal conductivity (ETC) of the composites. Maxwell (1954), Baschirow and Selenew (1976) and Verma (1991) derived ETC for two phase composites. The particles were randomly distributed in a homogeneous medium and there was no interaction among them which is suitable for predicting ETC of composites with relatively low particle contents. Benveniste (1987) formulated ETC for multiphase systems by determining the average flux in each constituent and the homogenization was then performed using the Mori Tanaka (1973) and generalized self consistent method. Several empirical studies have also been conducted to investigate the effect of shape and orientation of the dispersed particles on the overall ETC of the composites, e.g., Cheng and Vachon (1969) and Lewis and Nielsen (1970).

It has been experimentally shown by Agri and Uno (1985, 1986) and recently by Zhang et. al. (2005) that at higher particle volume fractions and high ratios of the particle's thermal conductivity to the one of the matrix, i.e., VF > 20% and K_p/K_m*>100, there exists particle interactions in the form of a conductive chain mechanism. This mechanism accelerates the heat conduction process, which was shown by an increase in the overall ETC. Khan and Muliana (2009) modified the previously developed micromechanical model of stress dependent viscoelastic responses of solid spherical

*K_p is the thermal conductivity of particle and K_m is the thermal conductivity of matrix, assuming isotropic constituents.

particle reinforced polymers (Muliana and Kim, 2007) to include the temperature-dependent material properties and to determine the effective CTE. Furthermore, a new micromechanical formulation is also presented for the effective thermal conductivity of particle-reinforced composites.

1.1.2 MULTISCALE ANALYSES OF COUPLED THERMO-MECHANICAL BEHAVIOR

In a multiscale analysis macro-scale material response is obtained by solving the boundary value problem (BVP) defined on a RVE that represents the microstructure of a composite. Limited studies on multi-scale modeling are available for analyzing the coupled mechanical and non-mechanical response of composite, mostly for thermoelastic (Feng and Cui, 2004 and Daneshjo and Ramezani, 2004) and thermo-mechanical with inelastic behavior by Williams and Aboudi, 1999 and Aboudi, 2008. Recently, Ozdemir (2008) employed a computational homogenization technique to analyze the thermo-mechanical elastic-plastic and damage behavior of heterogeneous solids. The interactions between the mechanical and thermal fields are incorporated through thermal stresses, temperature dependent material properties and influence of the geometrical changes on the thermal fields. However, the effects of energy dissipation from the mechanical work on the thermal field were not taken into account.

There are limited multi-scale studies on analyzing quasi-static coupled thermoviscoelastic behavior of the particulate composites. Yu and Fish (2002) employed an asymptotic homogenization method to develop a space-time homogenization procedure for a class of homogenized solids interacting at multiple

spatial and temporal scales during combined thermal and mechanical loadings. The homogenization framework was applied to analyze the coupled thermoviscoelastic response of fiber reinforced composites. The Kelvin-Voigt viscoelastic model was considered for each constituent. The coupling between the mechanical and thermal fields was taken into account through the dissipation of energy during the viscoelastic deformation of composite. Chung et al. (2000) used FE to analyze coupled thermoviscoelastic response of polymer matrix composite structures containing microscopic homogeneities. The homogenization of Kelvin-Voigt viscoelastic model was performed using the asymptotic homogenization scheme. At each time step, the heat generation due to dissipation of the mechanical work was calculated and supplied to the energy equation to perform heat transfer analysis. The temperature distribution obtained from the heat transfer analysis was then used as input into the equations that govern the thermoviscoelastic deformations.

1.2 MOTIVATION AND RESEARCH OBJECTIVES

Polymeric composite (reinforced with polymer, metal or ceramic particles) structural components such as plates, beam, rods, etc. when subjected to a cyclic deformation (or stress) for a longer period of time generate significant amount of heat due to the dissipation of the viscoelastic body. As a result the temperature of the body rises and the conduction cannot take place as fast as it requires to cool down the body due to a low thermal conductivity of polymers. Significant temperature changes can alter the mechanical and thermal properties of the composite structure. Available studies for analyzing the coupled thermoviscoelastic behaviors are mainly done for linear

viscoelastic solids, i.e., Kelvin-Voigt viscoelastic model and mainly for fiber reinforced composites. This study presents a simplified homogenization scheme to obtain the effective thermomechanical property and micro-macro field variables of coupled heat conduction and quasi-static thermoviscoelastic deformation of a particulate composite that takes into account the dissipation of energy from the viscoelastic constituents. The purpose is to use this micro-macro scale framework for analyzing response of viscoelastic composite structures subjected to a coupled mechanical and thermal effect and at the same time recognizing different nonlinear response of the constituents. This can lead to rigorous design of composite structures without the need of expensive computational costs. Schapery's nonlinear thermo-viscoelastic constitutive model with stress and temperature dependent material properties is used for each constituent. A micromechanical model for predicting the effective nonlinear thermal and mechanical properties of viscoelastic composites reinforced with solid spherical particles is developed. The previously developed micromechanical model of stress dependent viscoelastic responses of solid spherical particle reinforced polymers (Muliana and Kim, 2007) is modified to include the temperature-dependent material properties and to determine the effective thermal properties, i.e., CTE, ETC. A unit-cell model with four particle and polymer subcells is generated. Simplified micromechanical relations are formulated in terms of incremental average field quantities, i.e., stress, strain, heat flux and temperature gradient, in the subcells of the micromodels. Perfect bonds are assumed along the subcell's interfaces. Linearized prediction and iterative schemes are incorporated to solve the nonlinear constitutive equations at the composite and

constituents' levels in order to satisfy the micromechanical relations and the nonlinear constitutive equations. The effective thermo-mechanical response derived from the simplified micromechanical model is compatible with FE framework and used for structural analyses. Verifications of the proposed micromechanical model and comparisons with available analytical models, numerical solutions and experimental data are also shown.

This study consists of the following major tasks:

1. Formulate a time-integration algorithm to solve the governing equations of the thermoviscoelastic deformations and heat conduction for an isotropic material. Small deformation gradient problems are considered. The constitutive model for the viscoelastic material follows a single-integral function having stress and temperature dependent material parameters. The constitutive model for the heat flux follows the Fourier's law with a temperature dependent thermal conductivity. The thermomechanical coupling is due to the dissipation of the energy during the viscoelastic deformation and temperature dependent material properties in the viscoelastic constitutive model.
2. Develop a micromechanical model for predicting the effective thermal and mechanical responses of particulate composites. This task addresses the procedure to homogenize mechanical properties, coefficient of thermal expansion, thermal conductivity and specific heat, and formulate the macroscopic energy equation which involves the thermo-mechanical coupling effects.

3. Analyze the coupled thermo-elastic and thermo-viscoelastic behavior of particulate composites. Two models for particle reinforced composites that represent homogenized and heterogeneous composite media are generated using FE. The matrix region in the FE model of the heterogeneous composite medium incorporates the coupled thermoviscoelastic algorithm developed in task 1 while the particle follows the linear thermo-elastic response. The micromechanical model described in task 2 is used to determine the effective thermo-mechanical response of the homogenized composite medium. Both composite models are subjected to same boundary conditions. The effective responses and field variables determined using the two models are compared and discussed.
4. Use the integrated micromechanical and FE framework to analyze coupled heat conduction and deformations of viscoelastic composite structures such as a composite plate with a hole and a composite beam under cyclic loadings and beams made of functionally graded materials (FGMs).

CHAPTER II

A RECURSIVE-ITERATIVE ALGORITHM FOR COUPLED THERMO-VISCOELASTIC DEFORMATION

This chapter introduces a time integration algorithm for solving equations that govern heat conduction and thermoviscoelastic deformations in isotropic materials. This involves obtaining simultaneous solutions of time-dependent deformation and temperature fields. The constitutive model for the viscoelastic material, suitable for small deformation gradient problems, follows a single-integral function having temperature and stress dependent material parameters (nonlinear integrand). The constitutive model for the heat flux follows classical Fourier's law with a temperature dependent thermal conductivity. The coupling between the thermal and mechanical response is attributed to the dissipation of energy due to the viscoelastic deformation and stress-temperature dependent material parameters in the viscoelastic constitutive model. A recursive-iterative method is employed to integrate the time-dependent dissipation function in the energy equation and the nonlinear thermoviscoelastic integral model of Schapery. This approach is similar to the work of Haj-Ali and Muliana (2004) and Muliana and Khan (2008) for uncoupled thermo-viscoelastic problems. The numerical formulation is implemented within the ABAQUS, general purpose displacement based FE software.

Viscoelastic materials dissipate energy that is converted into heat; thus increasing the temperature of the materials. When a viscoelastic material undergoes a small deformation gradient with a relatively slow loading rate, which can be considered as a

quasi-static loading, and at a relatively short duration, the effect of temperature changes due to energy dissipation on the deformation of the material is usually negligible. Under high loading rates or cyclic loadings over a longer period of time, temperature increases can be significant even in small deformation gradient problems. Experimental evidences show that the thermomechanical dissipation can significantly increase the temperature of metals (Dillon, 1962, 1963) and polymers (Wolosewick and Gratch, 1965; Tauchert, 1967 (a, b, c), 1968; Schapery and Cantey, 1966a; Huang and Lee, 1967; Schapery, 1965, 1966b; and Cost, 1969b) during a cyclic loading under small strains and frequency ranges of 1-20 Hz. A temperature increase up to 80°F was observed after few hours of the cyclic loading.

Within the framework of thermodynamics and continuum mechanics, several theories were proposed to describe the dissipation of energy during viscoelastic deformations. There are three approaches based on which the thermomechanical constitutive equations for coupled thermoviscoelastic responses were derived. These are classified as follows: the phenomenological approach by Staverman and Schwarzl (1952), the theory of irreversible thermodynamics by Biot (1958) and the rational mechanics (functional thermodynamics) approach by Coleman (1964). Although these approaches are different in concept but the results obtained from these constitutive equations and dissipation functions are practically the same as discussed by Cost (1969a, b,c). Several dissipation functions for viscoelastic materials have been proposed. Schapery (1964), Christensen and Naghdi (1967), and Huang (1968) used Biot's approach and Cost (1969c) employed Coleman's (1964) approach to express the

dissipation function for non-isothermal viscoelastic solids. Hunter (1961) and Parkus (1966) described that once the dissipation function for a viscoelastic material is determined the energy equation for such material can be obtained by simply adding the dissipation function to the energy equation in the classical thermo-elastic materials.

Analytical solutions of the coupled viscoelastic deformations and dissipation of energy under a simple loading, like a uniaxial cyclic loading and torsional oscillations can be found in Schapery and Cantey (1966a) and Tauchert (1967a,b,c). Finite element (FE) has also been used for solving coupled thermoviscoelastic problems. Examples of using FE method to solve the problems of a quasi-static coupled thermoelasticity can be found in Kasti et al. (1991), Oden and Kauss (1968) and for a dynamic coupled thermoelasticity can be found in Oden (1969) and Oden and Poe (1970). Holzapfel and Reiter (1995) proposed a 2D FE formulation for linear viscoelastic solids including the thermomechanical coupling effects. A four parameter model, the so-called Burgers model is used to describe the constitutive behavior of a viscoelastic fluid. Cost (1969b) presented a 2D FE formulation of the thermorheologically simple materials (TSMs) including the thermo-mechanical coupling effects for linear viscoelastic materials. Oden and Armstrong (1971) developed 3D FE formulation for dynamic coupled linear thermoviscoelastic response for a class of TSMs. The constitutive equations and dissipation function proposed by Cost (1969c) were used. Several studies on the coupled viscoelastic deformations and dissipation of energy have been done for linear thermoviscoelastic materials and TSMs. Coupled thermoviscoelastic behaviors that include temperature and stress/strain dependent material properties (nonlinear responses)

are currently lacking. This chapter considers nonlinear coupled thermoviscoelastic behaviors for homogeneous isotropic materials undergoing small deformations. The nonlinear viscoelastic model proposed by Schapery (1969) is used and modified to incorporate the temperature dependent material properties. The nonlinear energy equation along with the dissipation function is also derived. It is also assumed that loadings are relatively slow such that the inertial effects on the deformation of a viscoelastic body can be ignored.

2.1 LOCAL GOVERNING EQUATIONS OF COUPLED THERMOVISCOELASTIC SOLIDS

For an isotropic homogeneous material, in the absences of body force, body couple and inertial effects, the conservation of mass and momenta lead to the following equations:

$$\dot{\rho} = 0 \tag{2.1}$$

$$\sigma_{ij,j} = 0 \tag{2.2}$$

$$\sigma_{ij} = \sigma_{ji} \tag{2.3}$$

where, ρ and σ_{ij} denote the mass density and the scalar components of the Cauchy stress tensor, respectively. Over dot denotes the derivative with respect to time. The infinitesimal symmetric Green strain tensor, ε_{ij}, is defined as:

$$\varepsilon_{ij} = \frac{1}{2}\left(u_{i,j} + u_{j,i}\right) \tag{2.4}$$

where $u_{i,j}$ is the displacement gradient.

The balance of energy states that the rate of change in the kinetic and internal energy of the portion of the body is a result of the rate at which the surface tractions and body forces do work on the portion of the body plus the rate at which the energy is transferred into it by heat conduction and internal heat generation. As a consequence of this postulate, the local form of the energy equation, in the absence of internal heat generation, can be written as;

$$\dot{\mathcal{E}} = \sigma_i \dot{\varepsilon}_i - q_{i,i} \tag{2.5}$$

where $\mathcal{E}$, $\sigma_i \dot{\varepsilon}_i$, and q_i denote the internal energy per unit volume, mechanical work rate, and the components of the heat flux, respectively.

The second law of thermodynamics, which was introduced by Clausius (1862) deals with an entropy production. Let η be the entropy per unit volume, the local form of the entropy equation, also called as Clausius-Duhem inequality, is:

$$\dot{\eta} + \frac{q_{i,i}}{T} - \frac{q_i T_{,i}}{T^2} \geq 0 \tag{2.6}$$

$$T\dot{\gamma} \equiv T\dot{\eta} + q_{i,i} - \frac{q_i T_{,i}}{T} \geq 0 \tag{2.7}$$

where $\dot{\gamma}$ is the entropy production rate per unit volume and T is the temperature. Truesdell and Noll (1965) split the entropy production into internal entropy production (γ_{int}) and entropy production by a conduction (γ_{cond}).

$$T\dot{\gamma} \equiv T\dot{\gamma}_{\text{int}} + T\dot{\gamma}_{cond} \tag{2.8}$$

$$T\dot{\gamma}_{\text{int}} \equiv T\dot{\eta} + q_{i,i} \geq 0 \tag{2.9}$$

$$T\dot{\gamma}_{cond} \equiv -\frac{q_i T_{,i}}{T} \geq 0 \tag{2.10}$$

As a consequence of irreversible thermodynamics, the entropy production by conduction, γ_{cond} at any material point is always positive. It is assumed that the constitutive equation for the heat flux can be defined by the classical Fourier's law:

$$q_i = -k_{ij} T_{,j} \tag{2.11}$$

where, k_{ij} denote the components of the thermal conductivity tensor. The thermal conductivity is temperature dependent. Substituting heat flux in Eq. (2.11) to the entropy production due to conduction in Eq. (2.10) yields,

$$k_{ij} T_{,i} T_{,j} \geq 0 \tag{2.12}$$

The thermal conductivity tensor k_{ij} must be symmetric to satisfy a positive definite quadratic form. The inequality given in Eq. (2.10) states that heat flows from the hotter part of the body to the colder part of the body. Thus, the inequality of entropy production become

$$T\dot{\gamma} \equiv T\dot{\eta} + q_{i,i} + \frac{k_{ij} T_{,i} T_{,j}}{T} \geq 0 \tag{2.13}$$

It is noted that the second law of thermodynamics imposed restriction on the constitutive models. During any deformation process, the thermoviscoelastic materials must satisfy the Clausius-Duhem inequality, i.e., Eq (2.6). The first law places no restriction on the constitutive models of thermoviscoelastic materials.

The framework for deriving constitutive models of materials can be established by choosing thermodynamics functions, such as the Helmholtz (1882) and Gibbs (1873)

free energy potentials. Using thermodynamics of irreversible processes, Schapery (1964) proposed a thermodynamic framework for deriving a general constitutive theory. These theories have been developed for the cases when strains and temperature are applied and the corresponding stresses are determined (Helmholtz free energy, Schapery 1966b) and when stresses and temperature are applied and the corresponding strains are obtained (Gibbs free energy, Schapery 1969). In this study we follow the Schapery (1997) Gibbs free energy in terms of stresses (σ_i), internal state variables (ISVs) ζ_m and temperature *T*. The ISVs has been introduced to account for the viscoelastic effects. The first law of thermodynamics in terms of the Gibbs free energy can be written as:

$$\dot{G} + \dot{T}\eta + T\dot{\eta} + \varepsilon_i \dot{\sigma}_i + q_{i,i} = 0 \tag{2.14}$$

and the second law becomes

$$T\dot{\gamma} \equiv -\dot{G} - \dot{T}\eta - \dot{\sigma}_i \varepsilon_i - \frac{q_i T_{,i}}{T} \geq 0 \tag{2.15}$$

The time derivative of the Gibbs free energy is

$$\frac{\partial G}{\partial t} = \frac{\partial G}{\partial \sigma_i}\dot{\sigma}_i + \frac{\partial G}{\partial T}\dot{T} + \frac{\partial G}{\partial \zeta_m}\dot{\zeta}_m \tag{2.16}$$

Substituting the above time derivative into the inequality in Eq. (2.15) and grouping terms to obtain

$$T\dot{\gamma} \equiv \left(-\varepsilon_i - \frac{\partial G}{\partial \sigma_i}\right)\dot{\sigma}_i + \left(-\eta - \frac{\partial G}{\partial T}\right)\dot{T} - \frac{\partial G}{\partial \zeta_m}\dot{\zeta}_m - \frac{q_i T_{,i}}{T} \geq 0 \tag{2.17}$$

The inequality must hold for arbitrary values of $\dot{\sigma}_i$ and $\dot{T}$. Accordingly, the constitutive equation for the strain is

$$\varepsilon_i = -\frac{\partial G}{\partial \sigma_i} \tag{2.18}$$

Similarly, the constitutive relation for the entropy is obtained as

$$\eta = -\frac{\partial G}{\partial T} \tag{2.19}$$

Furthermore, the inequality (2.17) with Eqs. (2.18) and (2.19) yield the condition

$$T\dot{\gamma} \equiv -\frac{\partial G}{\partial \zeta_m}\dot{\zeta}_m - \frac{q_i T_{,i}}{T} \geq 0 \tag{2.20}$$

Using Eqs. (2.8)- (2.10), we can write the volumetric heat generation rate $\dot{w}_{dis}^t$ as

$$\dot{w}_{dis}^t \equiv T\dot{\gamma}_{\text{int}} = f_m \dot{\zeta}_m \geq 0 \tag{2.21}$$

where $f_m = -\partial G/\partial \zeta_m$ is the thermodynamic force associated with each ISV. The first law of thermodynamics using Eq. (2.9) can be expressed as

$$T\dot{\eta} = -T\frac{\partial}{\partial t}\left\{\frac{\partial G}{\partial T}\right\} = -q_{i,i} + \dot{w}_{dis}^t \tag{2.22}$$

Schapery (1997) introduces the following form of the Gibbs free energy (G) in terms of the second order of ISVs ζ_m as

$$G = G_0 - A_m\zeta_m + \frac{1}{2}B_{mn}\zeta_m\zeta_n \tag{2.23}$$

where G_0, A_m and B_{mn} are the functions of σ_i and T. Under isothermal conditions, the constitutive equation for a uniaxial strain using Eq. (2.18) and Eq. (2.23) can be determined and expressed as (see Schapery 1969, 1997 or appendix A for detail)

$$\varepsilon^t \equiv \varepsilon(t) = g_0(\sigma^t)D_0\sigma^t + g_1(\sigma^t)\int_0^t dD\left(\psi^t - \psi^\tau\right)\frac{d\left[g_2(\sigma^\tau)\sigma^\tau\right]}{d\tau}d\tau \tag{2.24}$$

where D_0 and dD are the uniaxial instantaneous elastic and transient compliances, respectively, and g_o, g_1 and g_2 are the nonlinear parameters and defined as functions of the applied stress σ^t . The superscript 't' indicates a variable at time t. The parameter g_o is the nonlinear instantaneous elastic compliance and it measures the reduction or increase in the compliance as a function of stress and/or temperature. The transient creep parameter g_1 measures the nonlinearity effect in the transient compliance. The parameter g_2 accounts for the loading rate effect on the creep response. ψ^t is the reduced-time given by

$$\psi^t \equiv \psi(t) = \int_0^t \frac{d\xi}{a_\sigma^\xi} \quad , \quad \psi^\tau \equiv \psi(\tau) = \int_0^\tau \frac{d\xi}{a_\sigma^\xi} \tag{2.25}$$

The function a_σ is a stress-dependent that is used to define a time scale shift factor for stress dependent behaviors. The dissipation function $(T\dot{\gamma}_{\text{int}} = f_m \dot{\zeta}_m)$ for a uniaxial case, incorporating the stress and temperature dependent material parameters, can be found as (see appendix A for detail)

$$\dot{w}_{dis}^t = f_m \dot{\zeta}_m = g_1(\sigma^t, T^t)\sigma^{vis,t}\left(\frac{d}{dt}\int_0^t dD\left(\psi^t - \psi^\tau\right)\frac{d\left[g_2(\sigma^\tau, T^t)\sigma^\tau\right]}{d\tau}d\tau\right) \tag{2.26}$$

where $\sigma^{vis,t}$ is the viscous stress at time t and expressed as

$$\sigma^{vis,t} = g_2(\sigma^t, T^t)\sigma^t - \int_0^t \sum_{m=1}^{N}\left\{1 - \exp\left[-\lambda_m\left(\psi^t - \psi^\tau\right)\right]\right\}\frac{d\left[g_2(\sigma^\tau, T^t)\sigma^\tau\right]}{d\tau}d\tau \tag{2.27}$$

The energy equation using Eq. (2.22) and Eq. (2.26) and neglecting the dissipation due to the transient components of thermal expansion and specific heat becomes (see appendix A for detail)

$$\frac{\partial}{\partial t}\left(\frac{\partial C_{th}}{\partial T}\right)+T^t\alpha(T^t)\dot{\sigma}^t+T^t\frac{\partial\alpha(T^t)}{\partial T}\dot{T}\sigma^t+T^t\frac{\partial\alpha(T^t)}{\partial T}\theta^t\dot{\sigma}^t+T^t\frac{\partial g_0(\sigma^t,T^t)}{\partial T}D_0\sigma^t\dot{\sigma}^t$$
$$=-q^t+g_1(\sigma^t,T^t)\sigma^{vis,t}\left(\frac{d}{dt}\int_0^t dD\left(\psi^t-\psi^\tau\right)\frac{d\left[g_2(\sigma^\tau,T^t)\sigma^\tau\right]}{d\tau}d\tau\right) \tag{2.28}$$

where $\theta^t=T^t-T_0$, T_0 is the reference temperature. Where C_{th}, α, D_0, q^t, $d\alpha\left(\psi^t\right)$, $dC\left(\psi^t\right)$ and $dD\left(\psi^t\right)$ are the pure thermal part of the thermoelastic Gibbs free energy, coefficient of linear thermal expansion, instantaneous elastic compliance, heat flux, the transient components of the thermal expansion, specific heat and mechanical creep compliances, respectively.

In this study, the generalized three dimensional viscoelastic constitutive model of Schapery (1969) with stress and temperature dependent behavior for non-aging materials is formulated. For isotropic materials, the multiaxial (3D) constitutive relations can be separated into deviatoric and volumetric strain-stress relations and thermal strains as:

$$\varepsilon_{ij}^t=e_{ij}^t+\frac{1}{3}\varepsilon_{kk}^t\delta_{ij}+\alpha_{ij}^t\left(T^t-T_0\right) \tag{2.29}$$

$$\varepsilon_{ij}^{M,t}=e_{ij}^t+\frac{1}{3}\varepsilon_{kk}^t\delta_{ij} \tag{2.30}$$

$$\varepsilon_{ij}^{T,t}=\alpha_{ij}^t\left(T^t-T_0\right) \tag{2.31}$$

$$e_{ij}^t=\frac{1}{2}g_0(\bar{\sigma}^t,T^t)J_0S_{ij}^t+\frac{1}{2}g_1(\bar{\sigma}^t,T^t)\int_0^t dJ\left(\psi^t-\psi^\tau\right)\frac{d\left[g_2(\bar{\sigma}^\tau,T^\tau)S_{ij}^\tau\right]}{d\tau}d\tau \tag{2.32}$$

$$\varepsilon_{kk}^t=\frac{1}{3}g_0(\bar{\sigma}^t,T^t)B_0\sigma_{kk}^t+\frac{1}{3}g_1(\bar{\sigma}^t,T^t)\int_0^t dB\left(\psi^t-\psi^\tau\right)\frac{d\left[g_2(\bar{\sigma}^\tau,T^\tau)\sigma_{kk}^\tau\right]}{d\tau}d\tau \tag{2.33}$$

where $\varepsilon_{ij}^{M,t}$ and $\varepsilon_{ij}^{T,t}$ are the total mechanical and thermal strains, respectively. The parameters *Jo* and *Bo* are the instantaneous elastic shear and bulk compliances, respectively. The terms *dJ* and *dB* are the time-dependent shear and bulk compliances,

respectively. The corresponding linear elastic Poisson's ratio v is assumed to be time-independent, which allows expressing the shear and bulk compliances as:

$$\begin{aligned} J_0 &= 2(1+v)D_0 & B_0 &= 3(1-2v)D_0 \\ dJ^{\psi^t} &= 2(1+v)dD^{\psi^t} & dB^{\psi^t} &= 3(1-2v)dD^{\psi^t} \end{aligned} \tag{2.34}$$

Here D_0 and dD are the instantaneous elastic and transient compliances under a uniaxial (extensional) creep loading. The uniaxial transient compliance dD is expressed in terms of Prony series as:

$$dD^{\psi^t} = \sum_{n=1}^{N} D_n \left(1 - \exp[-\lambda_n \psi^t]\right) \tag{2.35}$$

Here $\alpha_{ij}^t \equiv \alpha_{ij}(T^t)$ are the components of coefficient of thermal expansion (CTE) tensor and can depend on temperatures. Knauss and Emri (1987) have suggested that the CTEs of polymers are also time-dependent. The parameter T^t is the current temperature. ψ^t is the reduced-time (effective time) given by:

$$\psi^t \equiv \psi(t) = \int_0^t \frac{d\xi}{a_T^\xi a_\sigma^\xi} \qquad \psi^\tau \equiv \psi(\tau) = \int_0^\tau \frac{d\xi}{a_T^\xi a_\sigma^\xi}, \tag{2.36}$$

where the function a_T is a temperature dependent that is used to define a time scale shift factor for TSMs. Where g_o, g_1, g_2 in Eq. (2.32) and a_σ in Eq. (2.36) are the nonlinear parameters and defined as functions of current temperature T^t and effective stress $\bar{\sigma}^t$. These non-linear material parameters or functions can be determined from a series of creep and recovery tests at different temperatures and stress levels.

For isotropic materials, neglecting the dissipation due to transient components of the thermal expansion and specific heat, the energy equation in Eq. (2.28) using the heat flux in Eq. (2.11) can be expressed as

$$\begin{aligned}&\rho c_\sigma(T^t)\dot{T}+T^t\frac{\partial\alpha(T^t)}{\partial T}\dot{T}\sigma_{kk}^t+T^t\frac{\partial\alpha(T^t)}{\partial T}\theta^t\dot{\sigma}_{kk}^t+T^t\frac{\partial g_0(\bar{\sigma},T^t)}{\partial T}D_{ijkl}^e\sigma_{kl}^t\dot{\sigma}_{ij}^t\\&+T^t\alpha(T^t)\dot{\sigma}_{kk}^t=k^tT_{,ii}^t+g_1(\bar{\sigma}^t,T^t)\sigma_{ij}^{vis,t}\left(\frac{d}{dt}\int_0^t dD_{ijkl}\left(\psi^t-\psi^\tau\right)\frac{d}{d\tau}\left(g_2(\bar{\sigma}^\tau,T^t)\sigma_{kl}^\tau\right)d\tau\right)\end{aligned}\tag{2.37}$$

where k^t is a thermal conductivity and C_{th} is assumed such that it accounts for the temperature dependent specific heat at a constant stress. Where $\sigma_{ij}^{vis,t}$ are the components of the viscous stress and can be expressed as

$$\sigma_{ij}^{vis,t}=g_2(\bar{\sigma}^t,T^t)\sigma_{ij}^t-\int_0^t\sum_{m=1}^N\left\{1-\exp\left[-\lambda_m\left(\psi^t-\psi^\tau\right)\right]\right\}\frac{d\left[g_2(\bar{\sigma}^\tau,T^t)\sigma_{ij}^\tau\right]}{d\tau}d\tau\tag{2.38}$$

For nonlinear viscoelastic solids, considering temperature independent material properties, the energy equation (Eq. 2.37) becomes

$$\begin{aligned}&\rho c_\sigma\dot{T}+T\alpha\dot{\sigma}_{kk}=k^tT_{,ii}^t\\&+g_1(\bar{\sigma}^t)\left\{g_2(\bar{\sigma}^t)\sigma_{ij}^t-\int_0^t\sum_{m=1}^N\left\{1-\exp\left[-\lambda_m\left(\psi^t-\psi^\tau\right)\right]\right\}\frac{d\left[g_2(\bar{\sigma}^\tau)\sigma_{ij}^\tau\right]}{d\tau}d\tau\right\}\\&\left\{\frac{d}{dt}\int_0^t dD_{ijkl}\left(\psi^t-\psi^\tau\right)\frac{d}{d\tau}\left(g_2(\bar{\sigma}^\tau)\sigma_{kl}^\tau\right)d\tau\right\}\end{aligned}\tag{2.39}$$

2.2 COUPLED THERMOMECHANICAL NUMERICAL INTEGRATION ALGORITHM

A recursive iterative method developed by Muliana and Khan (2008) is used to solve the deviatoric and volumetric components of the mechanical strains in Eq. (2.30). The

formulation is derived with a constant incremental strain rate during each time increment, which is compatible with displacement based FE analyses. The incremental form of the deviatoric and volumetric strains, indicated by prefix *d*, at a current time is expressed as:

$$\begin{aligned} de_{ij}^{t} &= e_{ij}^{t} - e_{ij}^{t-dt} \\ &= \overline{J}^{t} S_{ij}^{t} - \overline{J}^{t-dt} S_{ij}^{t-dt} - \frac{1}{2}\sum_{n=1}^{N} J_n (g_1^{t} \exp[-\lambda_n d\psi^{t}] - g_1^{t-dt}) q_{ij,n}^{t-dt} - \\ &\quad \frac{1}{2} g_2^{t-dt} \sum_{n=1}^{N} J_n \left[g_1^{t-dt} \left(\frac{1-\exp[-\lambda_n d\psi^{t-dt}]}{\lambda_n d\psi^{t-dt}} \right) - g_1^{t} \left(\frac{1-\exp[-\lambda_n d\psi^{t}]}{\lambda_n d\psi^{t}} \right) \right] S_{ij}^{t-dt} \end{aligned} \tag{2.40}$$

$$\begin{aligned} d\varepsilon_{kk}^{t} &= \varepsilon_{kk}^{t} - \varepsilon_{kk}^{t-dt} \\ &= \overline{B}^{t} \sigma_{kk}^{t} - \overline{B}^{t-dt} \sigma_{kk}^{t-dt} - \frac{1}{3}\sum_{n=1}^{N} B_n (g_1^{t} \exp[-\lambda_n d\psi^{t}] - g_1^{t-dt}) q_{kk,n}^{t-dt} - \\ &\quad \frac{1}{2} g_2^{t-dt} \sum_{n=1}^{N} B_n \left[g_1^{t-dt} \left(\frac{1-\exp[-\lambda_n d\psi^{t-dt}]}{\lambda_n d\psi^{t-dt}} \right) - g_1^{t} \left(\frac{1-\exp[-\lambda_n d\psi^{t}]}{\lambda_n d\psi^{t}} \right) \right] \sigma_{kk}^{t-dt} \end{aligned} \tag{2.41}$$

where the parameters $\overline{J}^{t}$ and $\overline{B}^{t}$ are the effective shear and bulk compliances at the current time, respectively. For simplicity, the notation $g_{\beta}^{t} (\beta = 0, 1, 2)$ is used to represent the stress and temperature dependent material parameters at current time *t*. The parameters $q_{ij,n}^{t}$ and $q_{kk,n}^{t}$, $n = 1 \ldots N$ are the hereditary integrals for every term in the Prony series in the form of deviatoric and volumetric strains, which are:

$$q_{ij,n}^{t} = \exp[-\lambda_n d\psi^{t}] q_{ij,n}^{t-dt} + \left(g_2^{t} S_{ij}^{t} - g_2^{t-dt} S_{ij}^{t-dt} \right) \frac{1-\exp[-\lambda_n d\psi^{t}]}{\lambda_n d\psi^{t}} \tag{2.42}$$

$$q_{kk,n}^{t} = \exp[-\lambda_n d\psi^{t}] q_{kk,n}^{t-dt} + \left(g_2^{t} \sigma_{kk}^{t} - g_2^{t-dt} \sigma_{kk}^{t-dt} \right) \frac{1-\exp[-\lambda_n d\psi^{t}]}{\lambda_n d\psi^{t}} \tag{2.43}$$

The parameters $q_{ij,n}^{t-dt}$ and $q_{kk,n}^{t-dt}$ are the hereditary integral (history state variables) stored from the last converged step at time $(t - dt)$. The incremental reduced time is

expressed as $d\psi^t \equiv \psi^t - \psi^{t-dt}$. Eqs. (2.40)- (2.41) define complete solutions for the current incremental strain tensor. The nonlinear parameters in Eqs. (2.40)- (2.41) are expressed as functions of current temperature T^t and effective stress $\bar{\sigma}^t$, which at the current time (t), are not known. Linearized trial stress tensors are used as starting points for solving the stress tensor using Eqs. (2.40)-(2.41). An iterative scheme is included in order to find the correct stress tensor for a given strain tensor and temperature. The current temperature is obtained from the solution of energy equation (2.37). The initial approximation (trial) stress tensor is determined using the following approximation of the nonlinear parameters:

$$\begin{aligned} g_\beta^{t,tr} &= g_\beta(\bar{\sigma}^{t\text{-}dt}, T^{t\text{-}dt}), \qquad \beta = 0,1,2 \\ a^{t,tr} &= a\ (\bar{\sigma}^{t\text{-}dt}, T^{t\text{-}dt}) \end{aligned} \tag{2.44}$$

The superscript '*tr*' means trial value of that variable. The g_β (β = 0, 1, 2) represent the nonlinear parameters g_o, g_1 and g_2, given in Eqs. (2.32)-(2.33). The trial current stress tensor is formed based on the given variables and history variables from the previous converged step:

$$\sigma_{ij}^{t,tr} = \sigma_{ij}^{t\text{-}dt} + d\sigma_{ij}^{t,tr} \tag{2.45}$$

$$d\sigma_{ij}^{t,tr} = dS_{ij}^{t,tr} + \frac{1}{3} d\sigma_{kk}^{t,tr}\delta_{ij} \tag{2.46}$$

where the trial incremental deviatoric and volumetric stresses are given by:

$$dS_{ij}^{t,tr} = \frac{1}{\bar{J}^{t,tr}}\left[de_{ij}^t + \frac{1}{2} g_1^{t,tr} \sum_{n=1}^{N} J_n (\exp[-\lambda_n d\psi^t] - 1) q_{ij,n}^{t\text{-}dt} \right] \tag{2.47}$$

$$d\sigma_{kk}^{t,tr} = \frac{1}{\bar{B}^{t,tr}}\left[d\varepsilon_{kk}^t + \frac{1}{3} g_1^{t,tr} \sum_{n=1}^{N} B_n (\exp[-\lambda_n d\psi^t] - 1) q_{kk,n}^{t\text{-}dt} \right] \tag{2.48}$$

The correct stress tensor at current time is solved by minimizing a residual vector, which is defined in terms of incremental strains and expressed by:

$$R_{ij}^{t} = de_{ij}^{t} + \frac{1}{3} d\varepsilon_{kk}^{t} \delta_{ij} - d\varepsilon_{ij}^{M,t} \tag{2.49}$$

where $d\varepsilon_{ij}^{M,t} = d\varepsilon_{ij}^{\mathrm{A},t} - d\varepsilon_{ij}^{\mathrm{T},t}$ with $d\varepsilon_{ij}^{\mathrm{A},t}$ is the total strain obtained from the displacement at a structural scale. Finally, the consistent tangent stiffness matrix is defined by taking the inverse of the partial derivative of the incremental strain with respect to the incremental stress at the end of the current time step. The consistent tangent stiffness, C_{ijkl}^{t}, at the converged state, are:

$$C_{ijkl}^{t} \equiv \frac{\partial d\sigma_{ij}^{t}}{\partial d\varepsilon_{kl}^{M,t}} = \left[\frac{\partial R_{ij}^{t}}{\partial d\sigma_{kl}^{t}} \right]^{-1} ; \quad \left\| R_{ij}^{t} \right\| \to 0 \tag{2.50}$$

Equation (2.50) defines material properties at current time t for each integration point in FE mesh. The components of the consistent tangent stiffness tensor vary with time, temperature, and stress. The total thermal strains at current time are expressed by:

$$\varepsilon_{ij}^{T,t} = \varepsilon_{ij}^{T,t\text{-}dt} + d\varepsilon_{ij}^{T,t} \tag{2.51}$$

where for an isotropic material, the incremental thermal strains are:

$$d\varepsilon_{ij}^{T,t} = \alpha(T^{t}) dT^{t} \delta_{ij} \tag{2.52}$$

where dT^{t} is the change in temperature at time *t*. The energy equation given in Eq. (2.37) is solved by integrating the dissipation function within the ABAQUS defined fully coupled thermomechanical analysis. For most coupled thermal-stress analyses, the unconditional stability of the backward difference operator (implicit method) is desirable, ABAQUS (2005). Therefore, at each incremental time-step, temperatures are

integrated using a backward-difference scheme, and the nonlinear coupled system is solved using Newton-Raphson method (Reddy, 2004). The first term in the left-hand side of the energy equation, Eq. (2.39), is approximated by:

$$\rho c_\sigma(T^t)\dot{T} \approx \frac{\rho c_\sigma(T^t)}{dt}\left(T^t - T^{t-dt}\right) = \frac{\rho\, c_\sigma(T^t)}{dt} dT^t \tag{2.53}$$

The temperature and temperature gradient (φ_i^t) at current time are expressed as:

$$T^t = T^{t\text{-}dt} + dT \tag{2.54}$$

$$\varphi_i^t = \varphi_i^{t\text{-}dt} + d\varphi_i^t \text{ , where } d\varphi_i^t = \partial dT/\partial x_i \tag{2.55}$$

The solution for the heat flux is done incrementally and the total heat flux at current time is defined as:

$$q_i^t = q_i^{t\text{-}dt} + dq_i^t \tag{2.56}$$

$$dq_i^t = \text{-}k_{ij}^t d\varphi_j^t \tag{2.57}$$

In this case, k_{ij}^t is the component of the consistent tangent thermal conductivity matrix, which varies with temperature at current time *t*. The constitutive equation is solved iteratively to obtain correct solutions of the thermal constitutive relation. The heat flux with respect to temperature at the end of increments is:

$$\frac{\partial dq_i^t}{\partial T^t} = \text{-}\frac{\partial k_{ij}^t}{\partial T^t} d\varphi_j^t \tag{2.58}$$

The recursive scheme is used to integrate Eq. (2.38) and the evolution of viscous stress can be written as:

$$\sigma_{ij}^{vis,t} = \sum_{m=1}^{N}\left\{\exp[\text{-}\lambda_m d\psi^t]P_{ij,m}^{t\text{-}dt} + \left(g_2^t\sigma_{ij}^t - g_2^{t\text{-}dt}\sigma_{ij}^{t\text{-}dt}\right)\frac{1\text{-}\exp[\text{-}\lambda_m d\psi^t]}{\lambda_m d\psi^t}\right\} \tag{2.59}$$

The parameters $P_{ij,m}^{t-dt}$ are history state variables stored from the last converged step at time ($t-dt$). The expression of history state variables at current time *t*, i.e., $P_{ij,m}^{t}$ is

$$P_{ij,m}^{t} = \exp[-\lambda_m d\psi^t]P_{ij,m}^{t-dt} + \left(g_2^t\sigma_{ij}^t - g_2^{t-dt}\sigma_{ij}^{t-dt}\right)\frac{1-\exp[-\lambda_m d\psi^t]}{\lambda_m d\psi^t} \tag{2.60}$$

At the end of time increment *dt* the incremental heat generation is written as:

$$\mathrm{d}w_{dis}^t = g_1^t\sigma_{ij}^{vis,t}\, d\varepsilon_{ij}^{vis,t} \tag{2.61}$$

It should be noted that the rate of heat generation per unit volume, i.e., $\dot{w}_{dis}^t = dw_{dis}^t/dt$, is required, which is added to the energy equation in Eq. (2.22).

The proposed numerical algorithm of the nonlinear coupled thermoviscoelastic constitutive model is implemented at each material point (Gaussian integration point) within the 3D continuum elements. The material subroutines (UMAT) and UMATH of the ABAQUS FE code are used. At each integration point, the input variables are the total strain (ε_{ij}^t), increment of the total strain ($d\varepsilon_{ij}^t$), previous converged stress (σ_{ij}^{t-dt}), temperature (T^{t-dt}), increment of the temperature (dT^t) and history variables. At the end of each increment, the output variables are the current stress components (σ_{ij}^t), temperature (T^t), volumetric heat generation rate ($\dot{w}_{dis}^t$), and updated history variables.

In a typical thermo-mechanical problem, the incremental stress is a function of strain and temperature, which are given by

$$d\sigma_{ij}^{t} = \frac{\partial \sigma_{ij}^{t}}{\partial \varepsilon_{kl}^{t}} d\varepsilon_{kl}^{t} + \frac{\partial \sigma_{ij}^{t}}{\partial T^{t}} dT^{t} \tag{2.62}$$

Similarly, the increment of the volumetric heat generation, which must be added into the thermal energy balance equation for a coupled thermo-mechanical problem, is

$$d\dot{w}_{dis}^{t} = \frac{\partial \dot{w}_{dis}^{t}}{\partial \varepsilon_{ij}^{t}} d\varepsilon_{ij}^{t} + \frac{\partial \dot{w}_{dis}^{t}}{\partial T^{t}} dT^{t} \tag{2.63}$$

In addition, it is necessary to define the Jacobians for mechanical load ($\partial \sigma_{ij}^{t} \big/ \partial \varepsilon_{kl}^{t}$) and temperature ($\partial \sigma_{ij}^{t} \big/ \partial T^{t}$), variations of the volumetric heat generation with respect to the strain ($\partial \dot{w}_{dis}^{t} \big/ \partial \varepsilon_{ij}^{t}$) and temperature ($\partial \dot{w}_{dis}^{t} \big/ \partial T^{t}$). From elasticity the stress increment can be written as (Lim and McDowell, 2002; Bassiouny and Maugin, 1988)

$$d\sigma_{ij}^{t} = C_{ijkl}^{el,t} d\varepsilon_{kl}^{el,t} = C_{ijkl}^{el,t} \left(d\varepsilon_{kl}^{t} - d\varepsilon_{kl}^{vis,t} - \frac{\partial \varepsilon_{kl}^{T,t}}{\partial T^{t}} dT^{t} \right) \tag{2.64}$$

where $C_{ijkl}^{el,t}$ is the elasticity stiffness tensor. For a thermo-viscoelastic problem,

$$\varepsilon_{ij}^{el,t} = \varepsilon_{ij}^{t} - \varepsilon_{ij}^{vis,t} - \varepsilon_{ij}^{T,t} \tag{2.65}$$

where ε_{ij}^{t}, $\varepsilon_{ij}^{el,t}$ $\varepsilon_{ij}^{vis,t}$ and $\varepsilon_{ij}^{T,t}$ are the total, elastic, viscous and thermal strain tensors, respectively. In this study, it is assumed that the thermal strains are the function of temperature, i.e.,

$$\varepsilon_{ij}^{T,t} \equiv \varepsilon_{ij}^{T,t} \left(T^{t} \right) \tag{2.66}$$

The incremental stress can now be written as follows

$$d\sigma_{ij}^{t} = C_{ijkl}^{el,t} d\varepsilon_{kl}^{t} - C_{ijkl}^{el,t} d\varepsilon_{kl}^{vis,t} - C_{ijkl}^{el,t} \frac{\partial \varepsilon_{kl}^{T,t}}{\partial T^{t}} dT^{t} \tag{2.67}$$

The variation in the viscoelastic strain can be written as:

$$d\varepsilon_{ij}^{vis,t} = \frac{\partial \varepsilon_{ij}^{vis,t}}{\partial \sigma_{kl}^{t}} d\sigma_{kl}^{t} + \frac{\partial \varepsilon_{ij}^{vis,t}}{\partial T^{t}} dT^{t} \tag{2.68}$$

Substituting $d\varepsilon_{ij}^{vis,t}$ into Eq. (2.67) yields

$$d\sigma_{ij}^{t} = C_{ijkl}^{el,t} d\varepsilon_{kl}^{t} - C_{ijkl}^{el,t} \left(\frac{\partial \varepsilon_{kl}^{vis,t}}{\partial \sigma_{mn}^{t}} d\sigma_{mn}^{t} + \frac{\partial \varepsilon_{kl}^{vis,t}}{\partial T^{t}} dT^{t} \right) - C_{ijkl}^{el,t} \frac{\partial \varepsilon_{kl}^{T,t}}{\partial T^{t}} dT^{t} \tag{2.69}$$

which can be further simplified as

$$d\sigma_{ij}^{t} = X_{ijmn}^{t} C_{mnkl}^{el,t} d\varepsilon_{kl}^{t} - X_{ijmn}^{t} \left\{ C_{mnkl}^{el,t} \left(\frac{\partial \varepsilon_{kl}^{vis,t}}{\partial T^{t}} + \frac{\partial \varepsilon_{kl}^{T,t}}{\partial T^{t}} \right) \right\} dT^{t} \tag{2.70}$$

$$\text{where } X_{ijmn}^{t} = \left(Y_{ijmn}^{t} \right)^{-1} \text{ and } Y_{ijmn}^{t} = \delta_{im}\delta_{jn} + C_{ijkl}^{el,t} \frac{\partial \varepsilon_{kl}^{vis,t}}{\partial \sigma_{mn}^{t}} \tag{2.71}$$

The incremental stress in Eq.(2.70) can be written as

$$d\sigma_{ij}^{t} = H_{ijkl}^{t} d\varepsilon_{kl}^{t} + h_{ij}^{t} dT^{t} \tag{2.72}$$

$$\text{where } H_{ijkl}^{t} = X_{ijmn}^{t} C_{mnkl}^{el,t} \text{ and} \tag{2.73}$$

$$h_{ij}^{t} = -X_{ijmn}^{t} C_{mnkl}^{el,t} \left(\frac{\partial \varepsilon_{kl}^{vis,t}}{\partial T^{t}} + \frac{\partial \varepsilon_{kl}^{T,t}}{\partial T^{t}} \right) \tag{2.74}$$

The rate of volumetric heat generation using Eq. (2.61) can be written as:

$$\dot{w}_{dis}^{t} = \frac{g_1^{t}}{dt} \sigma_{ij}^{vis,t} d\varepsilon_{ij}^{vis,t} \tag{2.75}$$

To obtain the variation of the volumetric heat generation per unit time with respect to strain and temperature, the variations of the quantities at current time in the $\dot{w}_{dis}^{t}$ expression are required. Using the product rule of differentiation Eq. (2.75) yields,

$$d\dot{w}_{dis}^{t} = \frac{1}{dt} dg_1^t d\varepsilon_{ij}^{vis,t} \sigma_{ij}^{vis,t} + \frac{1}{dt} g_1^t \partial d\varepsilon_{ij}^{vis,t} \sigma_{ij}^{vis,t} + \frac{1}{dt} g_1^t d\varepsilon_{ij}^{vis,t} d\sigma_{ij}^{vis,t} \tag{2.76}$$

Substituting $\partial d\varepsilon_{ij}^{vis,t}$ from Eq. (2.68) gives

$$\begin{aligned} d\dot{w}_{dis}^{t} =& \frac{1}{dt} dg_1^t \left(\frac{\partial \varepsilon_{ij}^{vis,t}}{\partial \sigma_{kl}} d\sigma_{kl} + \frac{\partial \varepsilon_{ij}^{vis,t}}{\partial T} dT \right) \sigma_{ij}^{vis,t} + \frac{1}{dt} g_1^t \frac{\partial d\varepsilon_{ij}^{vis,t}}{\partial \sigma_{kl}} d\sigma_{kl} \sigma_{ij}^{vis,t} \\ &+ \frac{1}{dt} g_1^t \left(\frac{\partial \varepsilon_{ij}^{vis,t}}{\partial \sigma_{kl}} d\sigma_{kl} + \frac{\partial \varepsilon_{ij}^{vis,t}}{\partial T} dT \right) d\sigma_{ij}^{vis,t} + \frac{1}{dt} g_1^t \frac{\partial d\varepsilon_{ij}^{vis,t}}{\partial T} \sigma_{ij}^{vis,t} dT \end{aligned} \tag{2.77}$$

$$\begin{aligned} d\dot{w}_{dis}^{t} =& \frac{1}{dt} dg_1^t \frac{\partial \varepsilon_{ij}^{vis,t}}{\partial \sigma_{kl}} d\sigma_{kl} \sigma_{ij}^{vis,t} + \frac{1}{dt} g_1^t \frac{\partial \varepsilon_{ij}^{vis,t}}{\partial \sigma_{kl}} d\sigma_{kl} d\sigma_{ij}^{vis,t} + \frac{1}{dt} g_1^t \frac{\partial d\varepsilon_{ij}^{vis,t}}{\partial \sigma_{kl}} d\sigma_{kl} \sigma_{ij}^{vis,t} \\ &+ \frac{1}{dt} dg_1^t \frac{\partial \varepsilon_{ij}^{vis,t}}{\partial T} \sigma_{ij}^{vis,t} dT + \frac{1}{dt} g_1^t \frac{\partial \varepsilon_{ij}^{vis,t}}{\partial T} d\sigma_{ij}^{vis,t} dT + \frac{1}{dt} g_1^t \frac{\partial d\varepsilon_{ij}^{vis,t}}{\partial T} \sigma_{ij}^{vis,t} dT \end{aligned} \tag{2.78}$$

Using, Eq. (2.72), we can write Eq. (2.78) as:

$$\begin{aligned} d\dot{w}_{dis}^{t} =& \frac{1}{dt} \left[dg_1^t \frac{\partial \varepsilon_{ij}^{vis,t}}{\partial \sigma_{kl}} H_{klmn} \sigma_{mn}^{vis,t} + g_1^t \frac{\partial \varepsilon_{ij}^{vis,t}}{\partial \sigma_{kl}} H_{klmn} d\sigma_{mn}^{vis,t} + g_1^t \frac{\partial d\varepsilon_{ij}^{vis,t}}{\partial \sigma_{kl}} H_{klmn} \sigma_{mn}^{vis,t} \right] d\varepsilon_{ij} \\ &+ \frac{1}{dt} \left[dg_1^t \frac{\partial \varepsilon_{ij}^{vis,t}}{\partial \sigma_{kl}} h_{kl} \sigma_{ij}^{vis,t} + g_1^t \frac{\partial \varepsilon_{ij}^{vis,t}}{\partial \sigma_{kl}} h_{kl} d\sigma_{ij}^{vis,t} + g_1^t \frac{\partial d\varepsilon_{ij}^{vis,t}}{\partial \sigma_{kl}} h_{kl} \sigma_{ij}^{vis,t} \right] dT \\ &+ \frac{1}{dt} \left[dg_1^t \frac{\partial \varepsilon_{ij}^{vis,t}}{\partial T} \sigma_{ij}^{vis,t} + g_1^t \frac{\partial \varepsilon_{ij}^{vis,t}}{\partial T} d\sigma_{ij}^{vis,t} + g_1^t \frac{\partial d\varepsilon_{ij}^{vis,t}}{\partial T} \sigma_{ij}^{vis,t} \right] dT \end{aligned} \tag{2.79}$$

Differentiating Eq. (2.79) with respect to the strain and temperature increments, respectively, gives

$$\frac{\partial d\dot{w}_{dis}^{t}}{\partial d\varepsilon_{ij}} = \frac{1}{dt} dg_1^t \frac{\partial \varepsilon_{ij}^{vis,t}}{\partial \sigma_{kl}} H_{klmn} \sigma_{mn}^{vis,t} + \frac{1}{dt} g_1^t \frac{\partial \varepsilon_{ij}^{vis,t}}{\partial \sigma_{kl}} H_{klmn} d\sigma_{mn}^{vis,t} + \frac{1}{dt} g_1^t \frac{\partial d\varepsilon_{ij}^{vis,t}}{\partial \sigma_{kl}} H_{klmn} \sigma_{mn}^{vis,t} \tag{2.80}$$

$$\frac{\partial d\dot{w}_{dis}^{t}}{\partial dT}=\left[\frac{1}{d\mathrm{t}}dg_1^t\frac{\partial\varepsilon_{ij}^{vis,t}}{\partial\sigma_{kl}}h_{kl}\sigma_{ij}^{vis,t}+\frac{1}{d\mathrm{t}}g_1^t\frac{\partial\varepsilon_{ij}^{vis,t}}{\partial\sigma_{kl}}h_{kl}d\sigma_{ij}^{vis,t}+\frac{1}{d\mathrm{t}}g_1^t\frac{\partial d\varepsilon_{ij}^{vis,t}}{\partial\sigma_{kl}}h_{kl}\sigma_{ij}^{vis,t}\right]$$
$$+\left[\frac{1}{d\mathrm{t}}dg_1^t\frac{\partial\varepsilon_{ij}^{vis,t}}{\partial T}\sigma_{ij}^{vis,t}+\frac{1}{d\mathrm{t}}g_1^t\frac{\partial\varepsilon_{ij}^{vis,t}}{\partial T}d\sigma_{ij}^{vis,t}+\frac{1}{d\mathrm{t}}g_1^t\frac{\partial d\varepsilon_{ij}^{vis,t}}{\partial T}\sigma_{ij}^{vis,t}\right] \tag{2.81}$$

Next, a numerical algorithm for the nonlinear coupled thermoviscoelastic behavior of isotropic homogeneous materials under general mechanical and temperature loading histories is presented. The viscoelastic constitutive model with stress and temperature dependent behavior for non-aging materials is considered (Eqs. 2.32-2.34). The algorithm is derived based on implicit stress integration solutions within general displacement based FE structural analyses for small deformations and coupled thermo-mechanical problems. Linearized solutions of the nonlinear constitutive equations and iterative schemes are performed at the structural (global) and material (local) levels. At the structural level, the iterative correction alone is not sufficient to minimize errors at the material level. For nonlinear viscoelastic materials, Haj-Ali and Muliana (2004) showed that the linearized stress-update at material level leads to large residual strain, even with a small time increment. Therefore, an iterative scheme is added at the material level in order to minimize errors arising from the linearization; otherwise very small time increments are required which is computationally expensive. Furthermore, consistent tangent matrices are developed to accelerate convergence and avoid divergence at both structural and material levels.

To simulate the coupled thermoviscoelastic response the numerical algorithm is integrated with ABAQUS/standard FE code. At each integration point in the FE mesh, the user subroutines UMATH and UMAT are called. Within UMAT, the numerical

algorithm for the nonlinear thermo-viscoelastic material model is defined, which is used to provide the total stresses, viscous stress, viscoelastic strain, consistent tangent stiffness matrix $C_{ijkl}^{t,(k)}$, stress variation with respect to strain ($\partial\sigma_{ij}^{t}/\partial T^{t}$), rate of heat generation ($\dot{w}_{dis}^{t}$), variation of heat generation with respect to strain ($\partial\dot{w}_{dis}^{t}/\partial\varepsilon_{ij}^{t}$) and temperature ($\partial\dot{w}_{dis}^{t}/\partial T^{t}$). The thermal constitutive behavior is defined within UMATH which is used to define and update internal energy $\mathcal{E}^{\mathrm{t,(k)}}$, variation of internal energy with respect to temperature $\left(\mathrm{d}\mathcal{E}/\mathrm{dT}\right)^{\mathrm{t,(k)}}$ and temperature gradient $\left(\mathrm{d}\mathcal{E}/\mathrm{dg}\right)^{\mathrm{t,(k)}}$, heat flux $q_i^{\mathrm{t,(k)}}$, heat flux variation with respect to temperature $\left(\mathrm{d}q_i/\mathrm{dT}\right)^{\mathrm{t,(k)}}$ and temperature gradient $\left(\mathrm{d}q_i/\mathrm{dg}\right)^{\mathrm{t,(k)}}$. Where g is the temperature gradient vector. The numerical algorithm for the fully coupled thermoviscoelastic analyses of isotropic solids is summarized in Figure 2.1.

Now, the numerical algorithm within the UMAT subroutine is described in detail. Let the superscript (*k*) denotes the global iteration counter within the current incremental time step. At each global iteration within the incremental time-step $dt^{(k)}$, trial incremental strain tensor $d\varepsilon_{ij}^{t,(k)}$ and temperature $dT^{t,(k)}$ are obtained, as illustrated in Figure 2.1. The goal is to calculate current total stresses σ_{ij}^{t}, C_{ijkl}^{t}, ($\partial\sigma_{ij}^{t}/\partial T^{t}$), ($\dot{w}_{dis}^{t}$), ($\partial\dot{w}_{dis}^{t}/\partial\varepsilon_{ij}^{t}$) and ($\partial\dot{w}_{dis}^{t}/\partial T^{t}$) from given current variables and history variables stored from the previous converged solution at time $(t-dt)$. The converged σ_{ij}^{t} and Jacobians (Eqs. 2.62-2.63) after *K* global iteration at the current time *t* will be used to provide

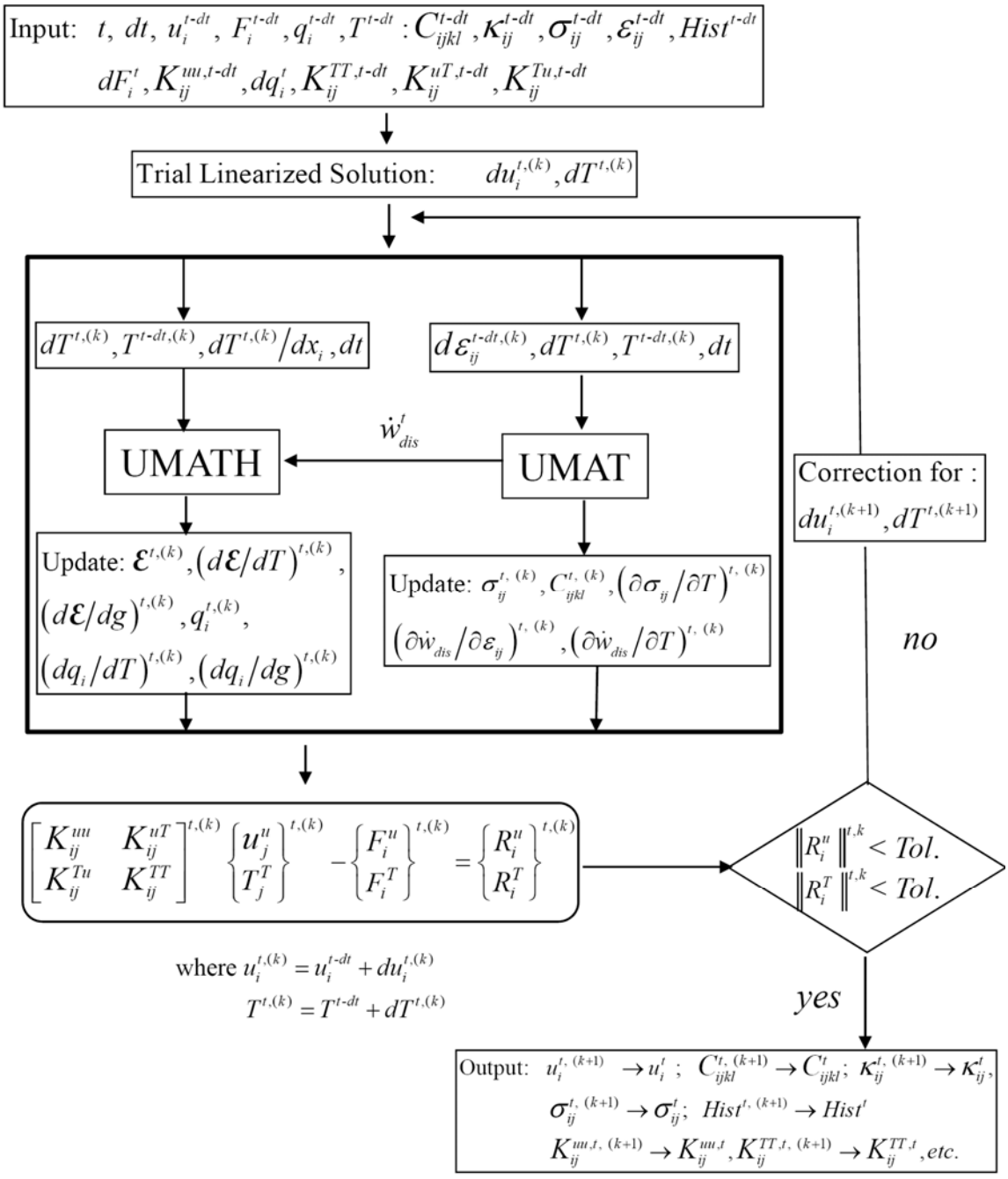

Figure 2.1 Numerical algorithm for the coupled thermo-viscoelastic behavior of isotropic homogeneous solids.

incremental trial strains for the next time step $(t+dt)$. Due to the coupled thermo-mechanical problems, the trial incremental temperature $dT^{t,(k)}$ is directly linked to the incremental time step. However, for each global iteration, the temperature is obtained from solving the energy equation (2.37). The procedure given below is performed at every material (Gaussian) integration point within elements at each structural iteration to achieve structural and material convergence simultaneously. Thus, an efficient and accurate numerical algorithm for solving the constitutive material model becomes necessary. For simplicity, the superscript (*k*) that indicates the global iteration counter will be ignored in the rest of this manuscript and the local iteration counter will be denoted by the superscript (*m*).

The complete recursive iterative algorithm (within UMAT subroutine) at the material level is summarized in the following steps:

1. Input variables: (At the k^{th} global iteration)
   $\varepsilon_{ij}^{t-\Delta t}, \quad d\varepsilon_{ij}^{t,(k)}, \quad dt^{(k)}, dT^{t,(k)}$
   History : $\sigma_{ij}^{t-dt}, T^{t-dt}, \sigma_{ij}^{vis,t-dt}, q_{ij,n}^{t-dt}, q_{kk,n}^{t-dt}$

2. Initial approximation variables:
   $g_{\beta}^{t,tr} = g_{\beta}(\bar{\sigma}^{t-dt}, T^{t-dt}); \beta = 0,1,2 \qquad a^{t,tr} = a\ (\bar{\sigma}^{t-dt}, T^{t-dt})$
   $d\sigma_{ij}^{t,tr} = d\sigma_{ij}^{t,tr}(dS_{ij}^{t,tr}, d\sigma_{kk}^{t,tr}) \qquad \sigma_{ij}^{t,(0)} = \sigma_{ij}^{t-dt} + d\sigma_{ij}^{t,tr}$

3. Iterate for *m*=0,1,2,3... (m=local iteration counter)
   3.1 Compute nonlinear parameters:
   $g_{\beta}^{t,(m)} = g_{\beta}(\bar{\sigma}^{t,(m)}, T^{t,(k)}); \ \beta = 0,1,2 \qquad a^{t,(m)} = a\ (\bar{\sigma}^{t,(m)}, T^{t,(k)})$
   where $T^{t,(k)} = T^{t-\Delta t} + dT^{t,(k)}$

3.2 Compute current stress:

$$d\sigma_{ij}^{t,(m+1)} = d\sigma_{ij}^{t,(m)} + \left[\frac{\partial R_{ij}^{t,(m)}}{\partial d\sigma_{kl}}\right]^{-1} R_{kl}^{t,(m)};\ \sigma_{ij}^{t,(m+1)} = \sigma_{ij}^{t-\Delta t} + d\sigma_{ij}^{t,(m+1)}$$

3.3 Evaluate residual tensor:

$$R_{ij}^{t,(m+1)} = de_{ij}^{t,(m+1)} + \frac{1}{3}\delta_{ij} d\varepsilon_{kk}^{t,(m+1)} - d\varepsilon_{ij}^{M,t,(k)}$$

IF $\| R_{ij}^{t,(m+1)} \| \leq$ Tol THEN GOTO 4 and EXIT

ENDIF GOTO 3

4. Update stress, consistent tangent stiffnesses, and history variables:

$$\sigma_{ij}^{t,(m+1)} \to \sigma_{ij}^{t},\ \sigma_{ij}^{vis,t,(m+1)} \to \sigma_{ij}^{vis,t},\ C_{ijkl}^{t},\quad q_{ij,n}^{t,(m+1)} \to q_{ij,n}^{t},\ q_{kk,n}^{t,(m+1)} \to q_{kk,n}^{t}$$

$$\dot{w}_{dis}^{t},\ \partial\sigma_{ij}^{t}/\partial T^{t},\ \partial\dot{w}_{dis}^{t}/\partial\varepsilon_{ij}^{t},\ \partial\dot{w}_{dis}^{t}/\partial T^{t}$$

2.3 NUMERICAL VERIFICATION AND IMPLEMENTATION

The proposed numerical algorithm can be used to simulate nonlinear coupled thermo-mechanical responses of viscoelastic bodies subjected to various loading histories. The numerical scheme is verified by comparing the results obtained from FE simulations to the ones obtained analytically. The responses are also compared to the analytical solution of Medri (1988) and Tauchert (1967c) and experimental data of Tauchert (1967a). The numerical algorithm is implemented at each integration point in the FE mesh. All FE simulations are performed using ABAQUS (2005). The efficiency and accuracy of the algorithm are also discussed.

First, the analytical solution for the creep response of a linear viscoelastic material subjected to a single step shear creep stress is used to verify the proposed numerical algorithm. The analytical solution for one-dimensional strain and temperature increase is

obtained analytically using linearized form of Eq. (2.24) and Eq. (2.37). The analytical solution can be found in appendix B. To describe the linear viscoelastic solid behavior the mechanical analog model also called the Zener solid model (three parameter solid model) is equivalent to a linearized form of Eq. (2.24). The proposed model is also validated with an analytical solution of temperature and strain obtained from Zener solid model obtained using the Laplace transform (appendix B). Under a simple shear loading, the Zener solid model yields the following governing differential equation (Flugge 1975, Wineman and Rajagopal 2001, Reddy 2008):

$$\sigma_{12} + p_1\dot{\sigma}_{12} = q_0\varepsilon_{12} + q_1\dot{\varepsilon}_{12} \tag{2.82}$$

where p_1, q_0, q_1 are the material constants and $\gamma_{12} = 2\varepsilon_{12}$. The energy equation, assuming an adiabatic process and no internal heating source, for an isotropic viscoelastic material can be expressed as:

$$\rho c_\sigma \dot{T} = \dot{w}^I_{dis} \tag{2.83}$$

The schematic of the Zener solid model and material constants for the above differential equation are shown in Figure 2.2(b). The shear creep compliance under a constant shear stress can be represented as:

$$J(t) = \frac{p_1}{q_1}\exp[-\frac{q_0}{q_1}t] + \frac{1}{q_0}\left(1 + \exp[-\frac{q_0}{q_1}t]\right) \tag{2.84}$$

For the above creep compliance function the equivalent Prony series coefficients are characterized using Eqs. (2.34)- (2.35). Table 2.1 shows the material constants, thermal properties (taken from Medri 1988) and Prony series coefficients, respectively that are used in the FE simulations. The constitutive model given in Eq. (2.82) was used to

obtain the analytical solution for a viscoelastic material subjected to a constant stress (see Appendix B).

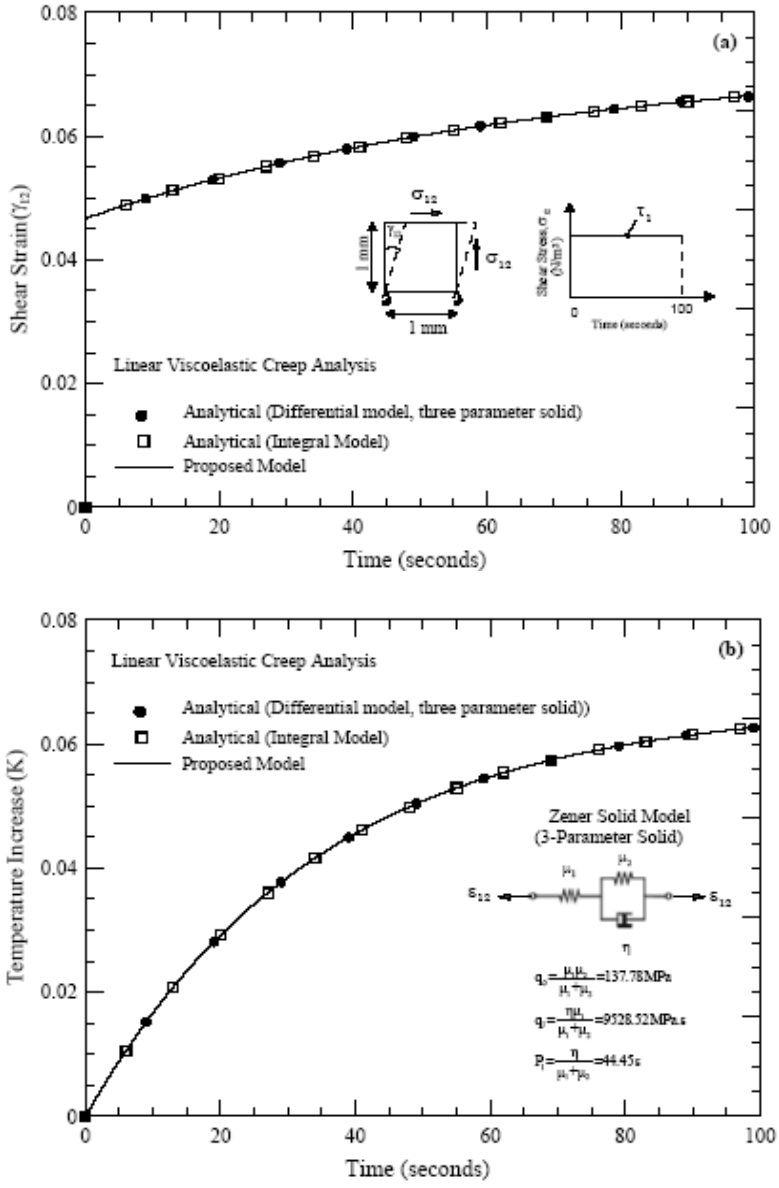

Figure 2.2 Dissipative heating under creep loading. (a) geometry, applied loading and shear strain, γ_{12}. (b) material parameter and increase of temperature, *T*.

Table 2.1 Prony series coefficients, mechanical and thermal properties for polymer.

n	$\lambda_n(\sec^{-1})$	$D_n \times 10^{-6}(\mathrm{MPa}^{-1})$
1	0.0145	0.00096
Young modulus, (E) (MPa)= 578.2 Poisson ratio, (v)=0.35 Coefficient of Thermal Expansion, (α) 10^{-6}, 1/°K =101.0 Thermal Conductivity, (k), W/m/°K = 1.0 Specific heat, (c), J/Kg. °K= 2180.0 Density, (ρ), Kg/m^3= 902.0		

The problem is discretized with one eight node linear brick element (ABAQUS generic name, C3D8T). The mechanical boundary conditions are shown in Figure 2.2(a) while for thermal boundary conditions all boundaries of the specimen are assumed to be insulated, i.e, no heat loss across the boundary.

Figures 2.2(a) and 2.2(b) show the comparison of shear strain and temperature rise, respectively, during the application of shear stress of magnitude $\tau_1 = 10\ MPa$. The results obtained from FE simulations (proposed model) are found in good agreement with both analytical solutions.

In the next example, the shear strain and temperature rise is obtained under a sinusoidal loading. The sinusoidal shear stress σ_{12}^t with $\omega = \pi/4$ and amplitude of 10MPa is applied, as shown in Figure 2.3. The same values of material constants and Prony series parameters that were used in previous problem are considered. The numerical simulation is performed using one eight node linear brick element, with

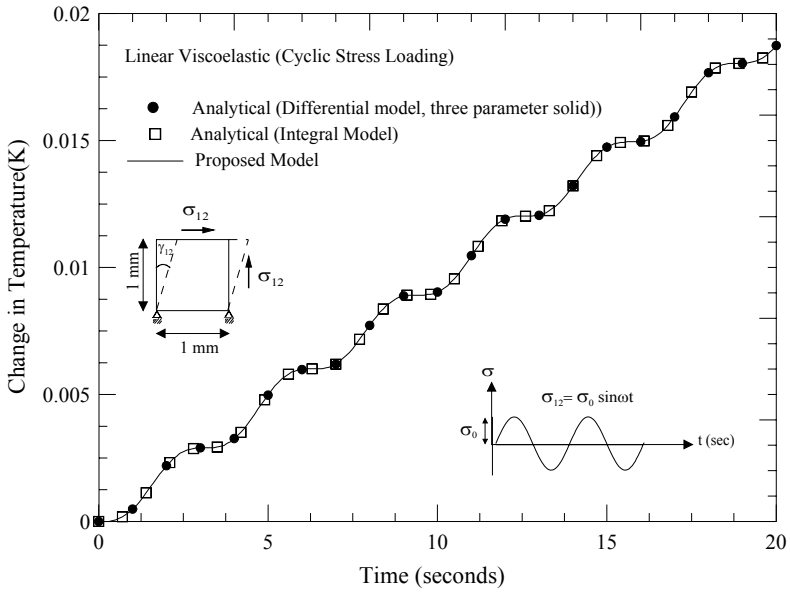

Figure 2.3 Dissipative heating under cyclic loading with geometry, applied sinusoidal loading and increase of temperature, *T*.

thermally insulated boundary conditions. The mechanical boundary conditions are shown in Figure 2.3. The solution for the temperature is in good agreement with both analytical solutions (see appendix B).

Tauchert (1967c) studied a cyclic torsional loading of a thin wall tube and used the Zener solid model to describe the viscoelastic behavior of the studied material. For a sinusoidal shear strain loading, Tauchert (1967c) obtained the analytical solution of stress and temperature increase using Fourier series expansion and Laplace transform methods. Under a pure torsional loading, the Zener solid model yields the following governing differential equation:

$$\sigma_{23} + p_1\dot{\sigma}_{23} = q_0\varepsilon_{23} + q_1\dot{\varepsilon}_{23} \tag{2.85}$$

where p_1, q_0, q_1 are the material constants. Table 2.2 shows the material constants, thermal properties (taken from Tauchert (1967c)) and Prony series coefficients,

respectively that are used in the FE simulations. Temperature history resulting from the cyclic strain amplitude of 0.35% and with frequency of 200 cps is shown in Figure 2.4. The time increment of 0.002 sec was used. It is found that the proposed model agrees with the analytical solution.

Table 2.2 Prony series coefficients, mechanical and thermal properties for pure aluminum at temperature 680˚F.

n	$\lambda_n(\sec^{-1})$	$D_n \times 10^{-6}(Psi^{-1})$
1	0.677	0.0318
Young modulus, (E) = 2.08x10^6 Psi Poisson ratio, (v) = 0.35 Thermal Conductivity, (k) = 0.002681 Btu/in.sec.˚F Specific heat, (c) = 205. Btu/lb.F Density, (ρ) = 1. lb/in^3		

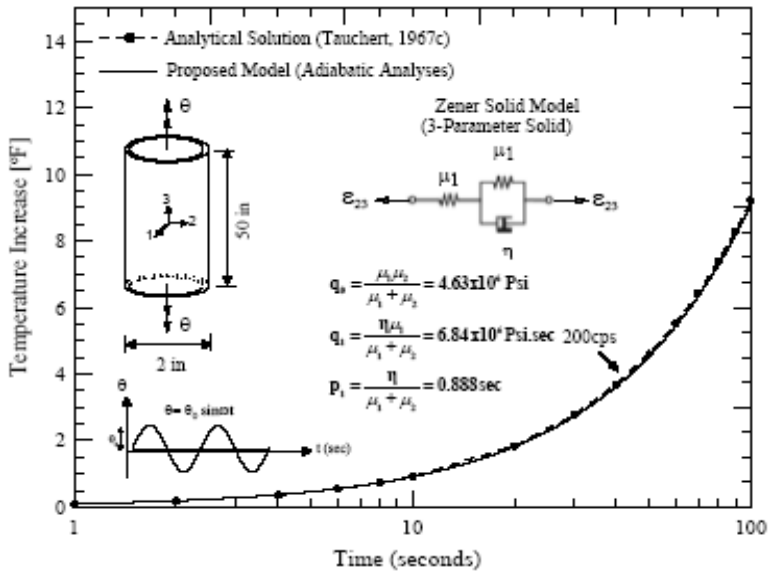

Figure 2.4 Comparison of analytical and FE results under torsional strain oscillations at constant frequency of 200 cps and angle of twist of θ_0=10˚. (Adiabatic solution)

Medri (1988) obtained an analytical solution for a viscoelastic solid under a simple tension at a constant stress rate of 2.246 MPa/sec. The Zener solid model (standard linear solid model) was used to describe the viscoelastic behavior of the solid. Under a uni-axial stress, the Zener solid model yields the following governing differential equation:

$$\sigma_{11} + p_1\dot{\sigma}_{11} = q_0\varepsilon_{11} + q_1\dot{\varepsilon}_{11} \tag{2.86}$$

where p_1, q_0, q_1 are the material constants. The material constants and Prony series coefficients, respectively that are used in the FE simulation are given in Table 2.1. For an isotropic thermo-viscoelastic material the energy equation, assuming an adiabatic process, no internal heating source, and considering temperature independent material properties, can be expressed as:

$$\left(\rho c_\varepsilon + 9KT_0\alpha^2\right)\dot{T} + \alpha T_0\dot{\sigma}_{kk} = \dot{w}^t_{dis} \tag{2.87}$$

where K is the elastic bulk modulus and c_ε is the specific heat at a constant strain. The uniaxial creep compliance $D(t)$ under a constant stress can be represented as:

$$D(t) = \frac{p_1}{q_1}\exp[-\frac{q_0}{q_1}t] + \frac{1}{q_0}\left(1 + \exp[-\frac{q_0}{q_1}t]\right) \tag{2.88}$$

The energy equation was derived for the Zener model and expression for the temperature change at a constant stress rate was then determined analytically. Figure 2.5 shows the comparison of the temperature change obtained analytically, numerically from the proposed model and analytical solution obtained by Medri (1988). Good agreements are observed.

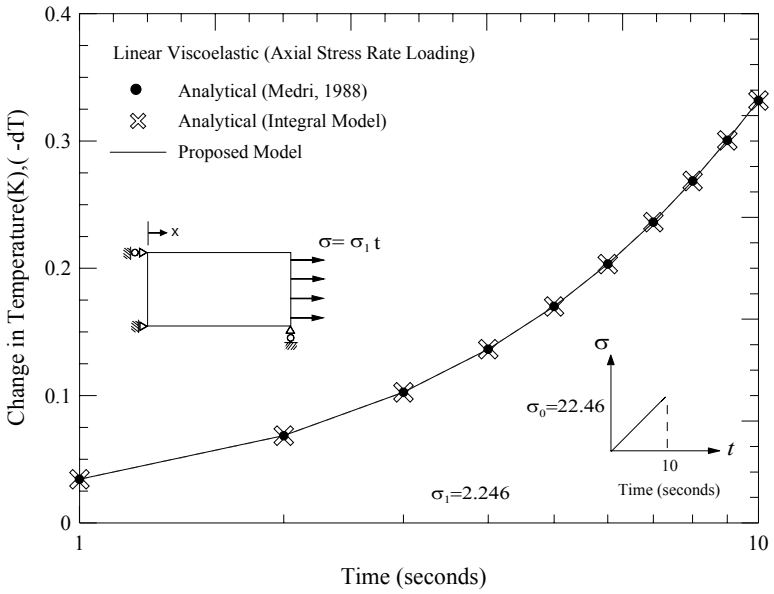

Figure 2.5 Temperature increase under tension at constant stress rate loading.

Tauchert (1967a) performed experiments to study the heat generation in polyethylene rods undergoing torsional oscillations. The twisting of each specimen was done at a constant frequency and at strain amplitude which were within the linear viscoelastic range. It was experimentally shown that the material behaved linearly up to 3.3% shear strain. The recorded temperature during the oscillation tests under various frequencies are predicted using the proposed numerical algorithm. Table 2.3 shows the Prony series parameters used in the simulation which are characterized using the experimental creep data of 60 seconds reported by Tauchert (1967a) under a fixed torsional load of 6 lb-in. By extending the experimental data of the creep curve on log-log scale the Prony series coefficients are characterized up to 3000 seconds.

Table 2.3 Prony series coefficients, mechanical and thermal properties for polyethylene.

n	$\lambda_n(\text{sec}^{-1})$	$D_n \times 10^{-6}(\text{Psi}^{-1})$
1	1.0	3.7
2	$1\text{x}10^{-1}$	3.7
3	$1\text{x}10^{-2}$	7.41
4	$1\text{x}10^{-3}$	6.85
5	$1\text{x}10^{-4}$	14.8
Young modulus, (E) = 58006.0 Psi Poisson ratio, (v) = 0.45 Thermal Conductivity, (k) = 0.0125 Btu/in.sec.˚F Specific heat, (c) = 180. Btu/lb.F Density, (ρ) = 1. lb/in^3		

Temperature histories obtained from the experiments and FE simulations corresponding to frequencies of 0.3833 and 1.33 cycles per second and shear strain amplitude of 3.3% are shown in Figure 2.6. Tauchert (1967a) explained that there is an interval of time in every experiment when the adiabatic condition exists. Heat loss to surroundings is prevented by the insulation and heat conduction is negligible due to a relatively low thermal conductivity of the polyethylene for certain time interval. The simulations performed in this study assumed adiabatic heating while during an experiment there exists a balance between the rate at which the heat is transferred by conduction out of an element and the rate at which heat is dissipated in the element that resulted in steady state temperature distribution ($\partial T/\partial t = 0$), as shown in Figure 2.6. The results obtained from FE simulations assuming adiabatic condition and temperature independent material properties over predict the experimental data. This deviation might be due to ignoring the effect of temperature dependence on the material properties. The

mechanical properties of polymers are very sensitive to temperature changes and with the increase of temperature the polymer relaxes faster and consequently results in reduction of heat generation rate. Therefore, the effect of temperature dependence on the material properties must be taken into account when there is a significant temperature change due to torsional oscillations. For a linear viscoelastic behavior, the effect of temperature on the relaxation behavior is carried through the shift factor (a_T). Such materials are called as thermorheologically simple materials (Schwarzl and Staverman, 1952). Since the properties of the polyethylene at different temperatures are not available in Tauchert (1967a), the following form of shift factor as function of the temperature is considered to simulate the effect of temperature dependent material properties on heat generation.

$$a^{T'} = \exp\left[-40\frac{T-T_0}{T_0}\right] \tag{2.89}$$

where T_0 is a reference temperature which is taken as 303˚K. Figure 2.6(b) shows that the temperature generation decreases when the above shift factor is considered, which implies that the polymer relaxes faster as temperature increases. Although the results are

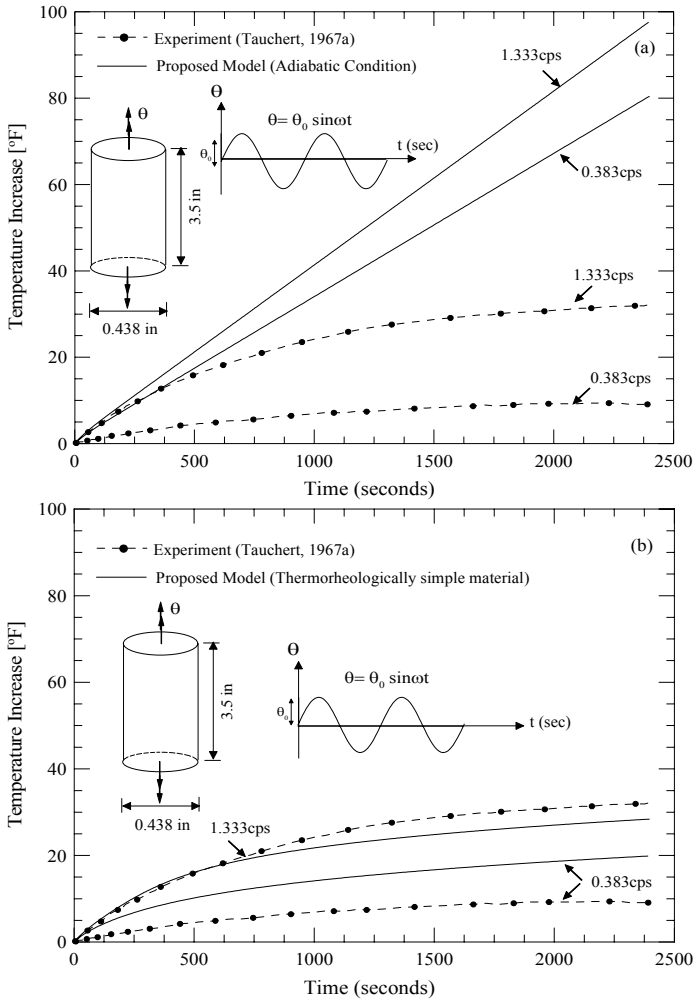

Figure 2.6 Comparison of experimental and finite element results under torsional oscillations at different constant frequencies and angle of twist of θ_0=30˚a) Adiabatic solution with temperature independent material properties, b) Adiabatic solution with an assumption of TSM behavior.

not in agreement with the experimental data but it shows that the steady state temperature distributions can be reached if the temperature dependent properties are considered. In addition to the shift factor there are some other parameters that can also affect the heat generation rate, such as heat transfer due to convection, stress and temperature dependent material properties. Later, the effect of temperature as well as

stress dependent parameters will be shown on the heat generation in the rod undergoing torsional oscillations.

Until now, the coupled behavior was studied for materials exhibiting linear viscoelastic behaviors. The numerical algorithm shows promising outcome under various types of loading conditions and agree to some extent with the available experimental data and analytical solution. Next, the simulation will be performed to study the effect of nonlinear stress and temperature dependent parameters on the temperature generation. The analyses are carried out for a short time period to demonstrate the need of performing the nonlinear analyses in predicting the long term coupled thermoviscoelastic responses of materials.

In this study a FM73 adhesive polymer is considered. FM73 adhesive is commonly used as adhesive to bond polymeric based composite and to strengthen the structure locally. The yield stress of FM73 under tension, compression and shear is 42MPa, 60MPa and 38MPa, respectively. The nonlinear stress and temperature dependent parameters for FM73 adhesive characterized by Peretz and Weitsman (1982, 1983) are used in this study to carry out simulations under various types of loadings. The Prony series coefficients, mechanical and thermal properties are given in Table 2.4. The nonlinear stress and temperature dependent parameters are shown in Figure 2.7(a)-(b).

In the first simulation, the temperature increase due to creep at different stress levels and stress relaxation due to an instantaneous applied strain is reported. Different magnitude of shear stresses ranging from 20-30MPa at isothermal temperature 303˚K are applied. The instantaneous strains obtained from these creep analyses are used as input for

Table 2.4 Prony series coefficients, mechanical and thermal properties for FM73 adhesive polymer.

n	$\lambda_n(\text{sec}^{-1})$	$D_n \times 10^{-6}(\text{MPa}^{-1})$
1	1.0	21.00
2	$1\text{x}10^{-1}$	21.60
3	$1\text{x}10^{-2}$	11.84
4	$1\text{x}10^{-3}$	15.88
5	$1\text{x}10^{-4}$	21.58
6	$1\text{x}10^{-5}$	20.05
Young modulus, (E)= 2710 MPa Poisson ratio, (v)=0.35 Thermal Conductivity, (k) = 0.2 W/m ˚K Specific heat, (c) =1300. J/kg ˚K Density, (ρ) = 980 Kg/m^3		

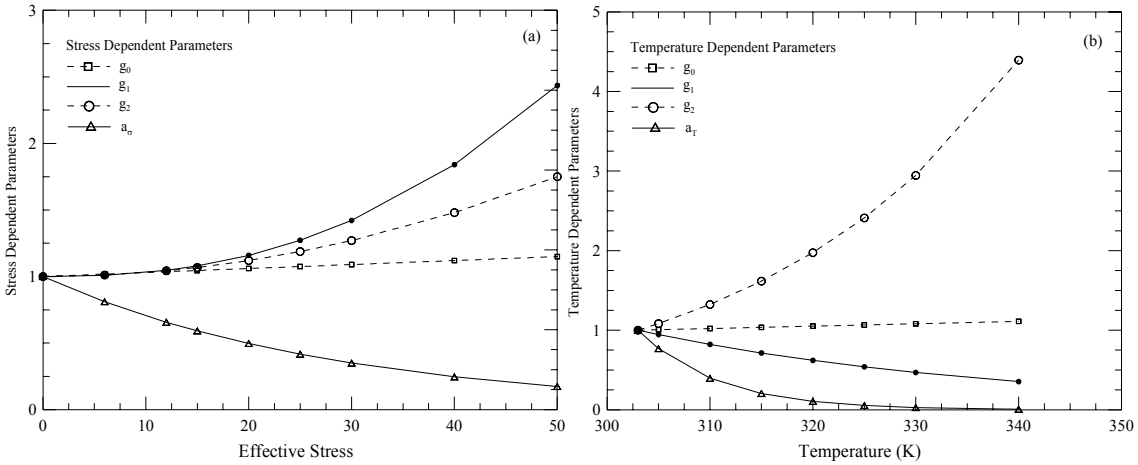

Figure 2.7 Nonlinear material parameters for FM73 adhesive a) stress dependent and b) temperature dependent. (Peretz and Weitsman, 1982, 1983)

the stress relaxation simulations. The simulations performed in this study assumed an adiabatic heating due to the viscoelastic deformation. Both linear and nonlinear viscoelastic behaviors of the material are considered. Figure 2.8 (a) shows temperature

changes during creep at various stress levels. The nonlinear parameters tend to increase the compliance or decrease the modulus more rapidly and causing high level of stresses as compares to the linear viscoelastic materials. This phenomenon is observed at all the stress levels studied and yield more temperature rise as compare to the linear case. Note that the temperature changes are very small and no temperature boundary conditions are applied, therefore, for a given loading history the contribution from temperature dependent material parameters in heat generation is negligible. Figure 2.8 (b) shows temperature changes during the relaxation at various strain levels. More temperature is

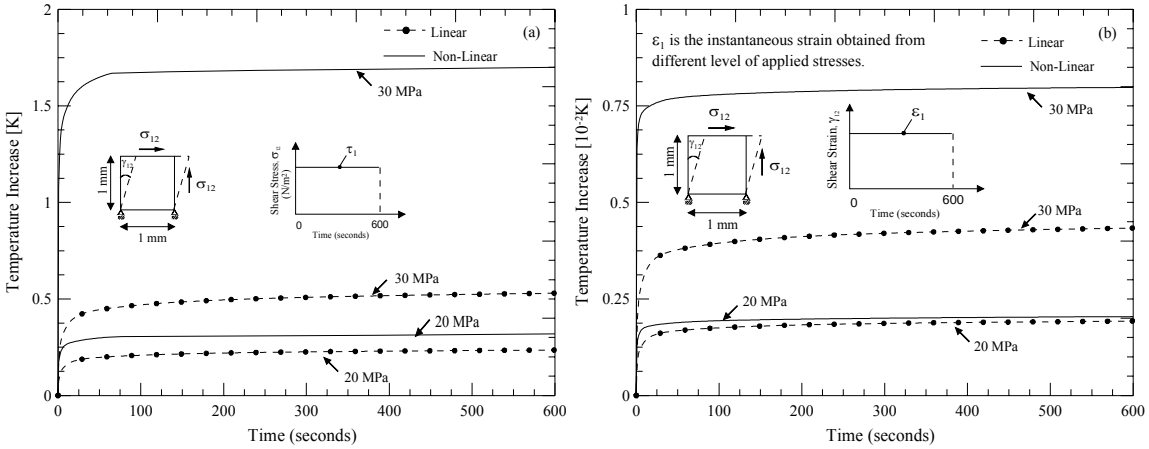

Figure 2.8 Comparison of linear and nonlinear viscoelastic material behaviors on heat generation subjected to a) creep at different stress and b) relaxation at different strain levels.

generated during relaxation of a nonlinear viscoelastic behavior than the linear ones. However, the temperature increases during the relaxation are less for both linear and nonlinear viscoelastic materials as compare to the ones that rises during the creep.

Next the effects of stress and temperature dependent parameters are determined on the viscoelastic material subjected to cyclic shear stress and strain loading. First, the cyclic stress with amplitude of 20MPa and $\omega = \pi/4$ is applied and the maximum strain

attained during the linear viscoelastic analysis is used as strain amplitude for the cyclic strain loading for both linear and nonlinear viscoelastic behaviors. For the cyclic stress loading, similar trends are observed as were noticed in the previous analyses and the temperature generation is higher with stress and temperature dependent parameters as shown in Figure 2.9 (b). However, for the cyclic strain loading, stress and temperature dependent parameters do not affect much on the temperature generation and less value of temperature increase was observed as compare to the linear behavior shown in Figure 2.9 (a). With temperature dependent material parameters, the temperature rise in both loading types is less than the ones obtained for linear viscoelastic responses. Polymer relaxes faster as temperature increases and therefore in the analyses with temperature dependent material parameters always less temperature change is obtained as compare to the analyses with stress dependent material parameters. Figure 2.9(c) shows the comparison of linear and nonlinear viscoelastic behaviors of materials subjected to sinusoidal stress and strain loadings. It is observed that for both linear and nonlinear viscoelastic cases the cyclic stress loading generates more heat as compare to the cyclic strain loading. Under cyclic stress, more heat is generated per cycle for non-linear viscoelastic behavior due to the presence of nonlinear parameters as compare to the linear viscoelastic case, as shown in Figure 2.9 (d).

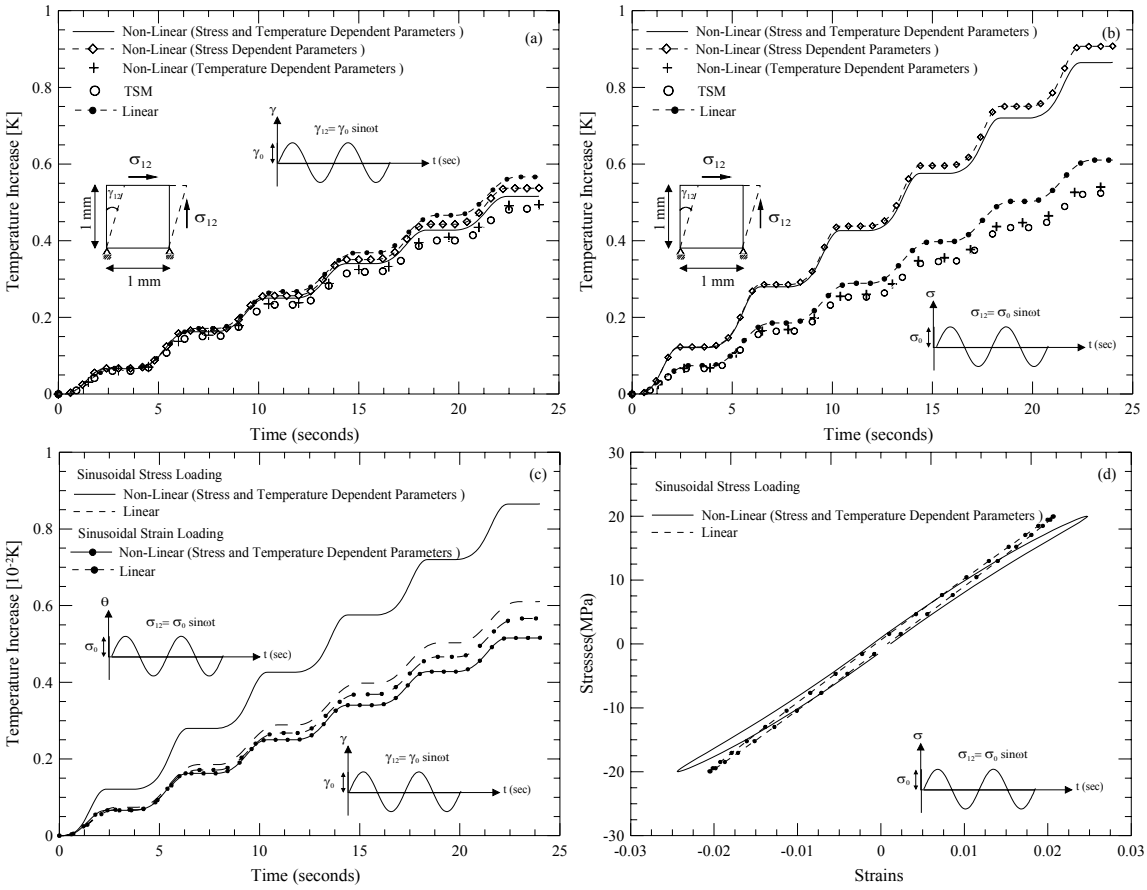

Figure 2.9 Comparison of linear and nonlinear viscoelastic material behaviors on heat generation subjected to cyclic a) strain and b) stress loading. c) comparison of heat generation in cyclic strain and stress loading d) comparison of stress-strain plot for cyclic stress and strain loading.

Tauchert (1967a) showed that enormous amount of heat generated when a polymer was subjected to torsional oscillations. Therefore, the effect of temperature dependent properties on the generation of temperature of a viscoelastic material can be analyzed using cyclic torsion analyses. The twisting of the specimen shown in Figure 2.10(a) is done at constant frequencies of 0.3833 and 1.33 cycles per second (cps) and shear strain amplitude of 1.0%. The simulations performed in this study assumed adiabatic heating due to viscoelastic deformation. Both Linear and non linear viscoelastic responses are

considered. The comparison of temperature histories obtained from FE simulations corresponding to frequencies of 0.3833 and 1.33 cycles per second are shown in Figure 2.10(a).

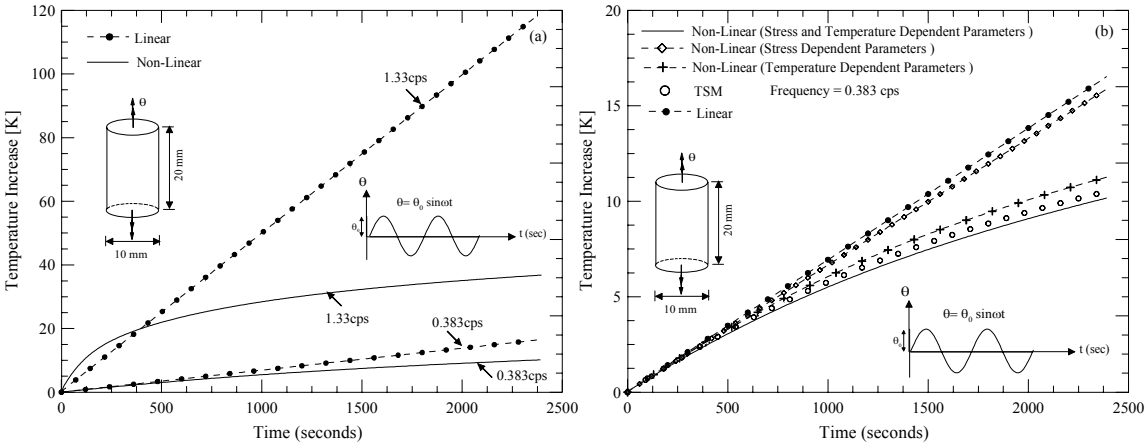

Figure 2.10 Comparison of heat generation of solid cylinder subjected to torsional oscillations with maximum angle of twist of θ_0=3˚ at a) different constant frequencies with linear and nonlinear viscoelastic material behaviors and b) frequency of 0.383cps with linear, nonlinear, TSM, stress and temperature dependent viscoelastic material behaviors.

For a linear material, there is a linear temperature increase observed for both frequencies because of the constant rate of heat generation. For a given nonlinear material, the heat generation rate is affected by the nonlinear stress and temperature dependent material parameters and gradually decreases to produce less temperature change as compare to a linear viscoelastic material. Next, the effects of stress and temperature dependent parameters are examined for twisting of a specimen with a constant frequency of 0.3833 cycles per second (cps) and shear strain amplitude of 1.0%, as shown in Figure 2.10(b). It has been found that the given stress dependent material parameters decrease the rate of heat generation but still constant temperature rise per

cycle is produced. However, the temperature dependent material parameters for a given material reduce the rate of heat generation as time progresses and consequently the rate of change of the temperature rise per cycle also decreases for the nonlinear viscoelastic material having stress and temperature dependent material properties.

Next, the significance of a conduction phenomenon during the non-uniform stress generation in a structure is presented. Both viscous dissipation and conduction is considered. The cyclic bending of a beam under a uniformly distributed load is presented. A cyclic load with amplitude of 1kN/m and $\omega = \pi/4$ is applied for duration of 2400 seconds (40 minutes). The schematic of a geometry of the beam and boundary conditions are given in Figure 2.11.

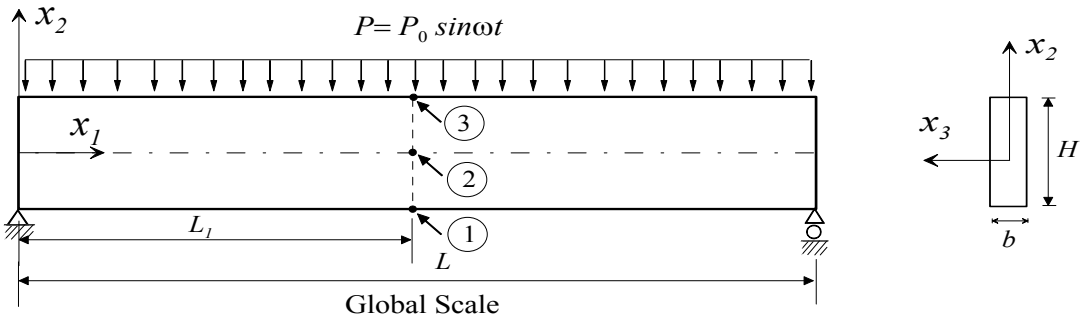

Length of the beam (D) = 100 mm Height of the beam (H) = 20mm

Thickness of the Beam (b) = 2mm L_1 = 50 mm

Figure 2.11 Geometry of the simply supported beam, loading, boundary conditions and locations at which the temperatures are measured.

The temperature generation at two different locations (see Figure 2.11) is shown in Figure 2.12. It is observed that the heat generation at point 2 is not affected by the conduction for the first few minutes of the analysis. However, due to the non-uniform stress generation (with alternating max./min. at top/bottom surface) the conduction

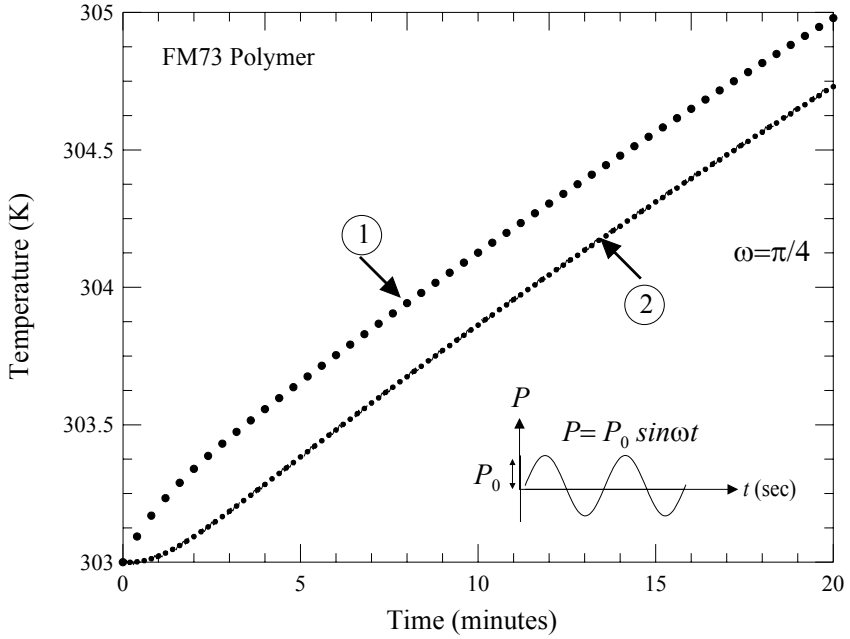

Figure 2.12 Temperature generations at point 1 and 2 during fully coupled thermoviscoelastic analysis of a homogeneous beam with conduction.

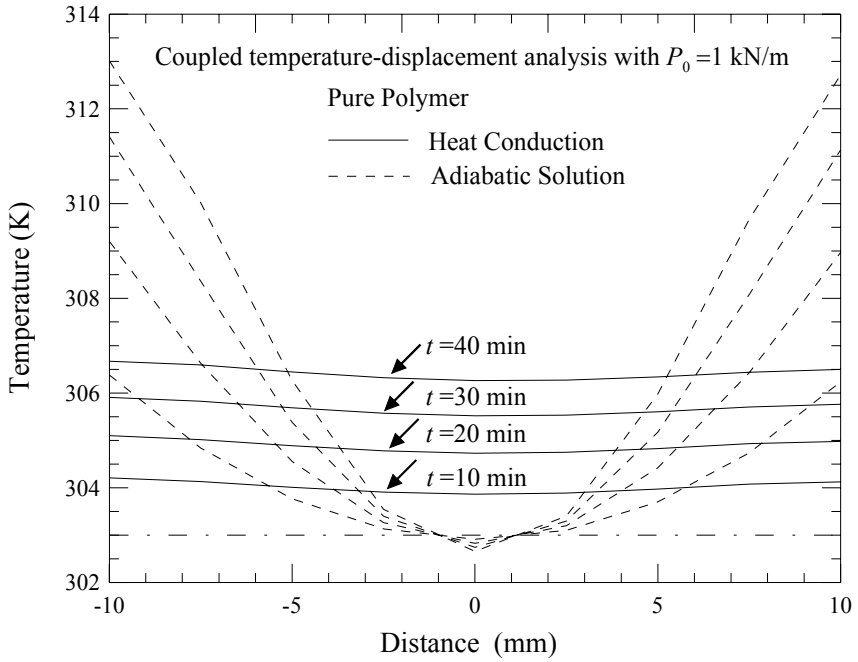

Figure 2.13 Temperature generation at the center of beam (i.e., $x_1=L_1$, $-10\leq x_2\leq 10$) during fully coupled thermoviscoelastic analysis of a homogeneous beam with adiabatic solution and heat conduction.

started to take place towards the centroidal axis of the beam and the temperature at point 2 increases. Figure 2.13 shows that if the conduction is neglected then the top/bottom surface temperature increases by a large number as compared to when a conduction is accounted for. This analysis shows the necessity of taking the conduction during coupled thermoviscoelastic response to realistically predict the temperature distribution within the structure.

Now the contribution of the thermoelastic coupling to the temperature generation is examined during cyclic loading at various stress amplitudes. The problem is discretized with one eight node linear brick element (ABAQUS generic name, C3D8T). The mechanical boundary conditions are shown in Figure 2.5 while for thermal boundary conditions all boundaries of the specimen are assumed to be insulated, i.e, no heat loss across the boundary. An axial cyclic load with $\omega = \pi/4$ is applied for duration of 2400 seconds (40 minutes). Figure 2.14 shows the temperature generation with and without taking into account the thermoelastic coupling. It has been observed that with the increase of stress amplitudes the thermoelastic coupling contribution increases. However, for the time period considered, the temperature increase with thermoelastic coupling is still insignificant as compare to the overall temperature increase when only viscous dissipation is considered. Therefore, for a given material, one can neglect the thermoelastic coupling while analyzing the fully-coupled thermoviscoelastic response of materials under a cyclic loading.

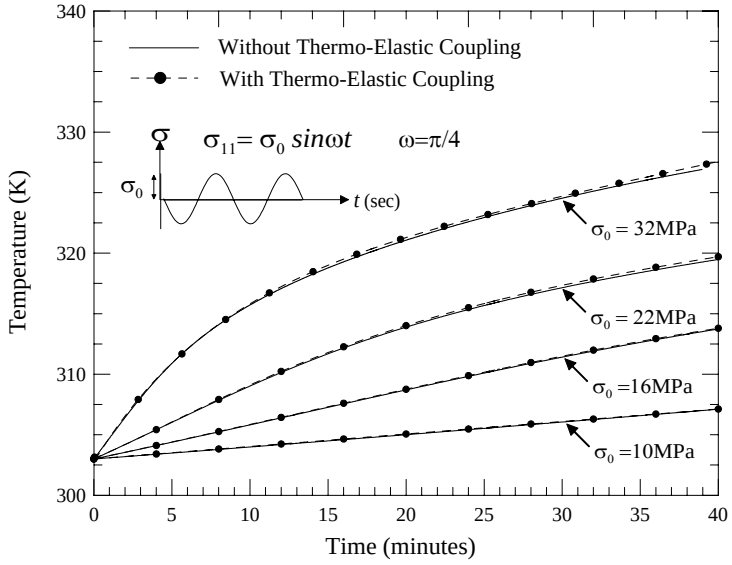

Figure 2.14 Temperature generations during the fully coupled thermoviscoelastic analysis of a homogeneous material with and without thermoelastic coupling effect.

2.4 CONVERGENCE BEHAVIOR OF COUPLED THERMOVISCOELASTIC RECURSIVE-ITERATIVE ALGORITHM

The proposed numerical scheme is implemented within a displacement-based FE code. The material subroutines (UMAT and UMATH) of the ABAQUS (2005) FE code are used for this purpose. The 3D nonlinear coupled thermo-viscoelastic response is generated at each material point (Gaussian integration point). For nonlinear response at a material level the recursive iterative algorithm with Newton-Raphson (NR) scheme is used. At the FE structural level, the default ABAQUS FE code (2005) iterative solver is used for the nonlinear analyses. Two criteria are checked in the ABAQUS iterative linear solver, which are force (flux) residual and displacement (temperature) corrections.

For nonlinear coupled thermoviscoelastic problems, an iterative scheme is generally employed to minimize the mechanical, R_i^U , and thermal, R_i^T , residual vectors

simultaneously, which can be expressed as:

$$\begin{Bmatrix} R_i^u \\ R_i^T \end{Bmatrix}^{t,(k)} = \begin{bmatrix} K_{ij}^{uu} & K_{ij}^{uT} \\ K_{ij}^{Tu} & K_{ij}^{TT} \end{bmatrix}^{t,(k)} \begin{Bmatrix} u_j^u \\ T_j^T \end{Bmatrix}^{t,(k)} - \begin{Bmatrix} F_i^u \\ F_i^T \end{Bmatrix}^{t,(k)} = \begin{Bmatrix} 0 \\ 0 \end{Bmatrix} \tag{2.90}$$

In a nonlinear problem, the residual vectors $\left\{R_i^u, R_i^T\right\}$ will only be approximating to zero and certain convergence criteria are set for residuals to achieve converged solutions. In addition to the residual vectors (thermal or mechanical), incremental displacement, du_j^t and temperature, dT_j^t correction criterion are also checked by the ABAQUS iterative solver. The displacement and temperature correction criteria are:

$$R_\delta^t = \frac{\delta du^t}{du^t}, \qquad R_T^{\mathrm{t}} = \frac{\delta dT^t}{dT^t} \tag{2.91}$$

where $\delta du^t, \delta dT^t$ and du^t, dT^t are the last displacement correction vector, last temperature correction, incremental displacement vectors and incremental temperature at current time *t*, respectively. Both convergence checks must be satisfied at the structural level before a solution is said to have converged for that time increment.

For nonlinear thermoviscoelastic behavior the convergence behaviors at the structural (element) and constituent (material) levels are examined. The convergence behavior is tested for various loading conditions. For both force and heat flux, the convergence criteria used at the element level follow the default criteria of the ABAQUS FE code (2005). The residual tolerance for force and flux is set to be $5\text{x}10^{-3}Q$, where Q is the average force or flux over time *t*. The default tolerance for the displacement and temperature corrections is 10^{-2}. The convergence criterion at the material level is described in Eq. (2.49) with tolerance of 10^{-6}. The following convergence studies are

performed for FM73 polymer. The Prony series coefficients, mechanical and thermal properties for FM73 adhesive polymer are already given in Table 2.4. The stress and temperature dependent parameters are expressed in Figure 2.7 (a)-(b).

2.4.1 PARAMETRIC STUDIES

In first parametric study the effect of an initial time increment on the structural and material response is determined. The Heaviside step function is simulated using different initial time ranging from 10^{-6} to 1 second with varying stress levels. Fully coupled thermo-viscoelastic material model is used. The instantaneous uni-axial strain values are reported for different time-increments and are compared with the analytical solution for load levels ranging from 10-40 MPa, as shown in Figure 2.15. The accuracy of the results strongly depends on the initial time increment size. A larger initial time increment and high stress values may lead to a diverged solution. From Figure 2.15 it is concluded that the initial time increment can be chosen in the range 10^{-6} to 10^{-3} seconds to better capture the instantaneous response for this material.

In the second parametric study the residual norms at structural and material level are monitored during the iterations process of a given time increment. The instantaneous load is applied with a time increment of 10^{-4}. Figures 2.16 (a)-(c) show the

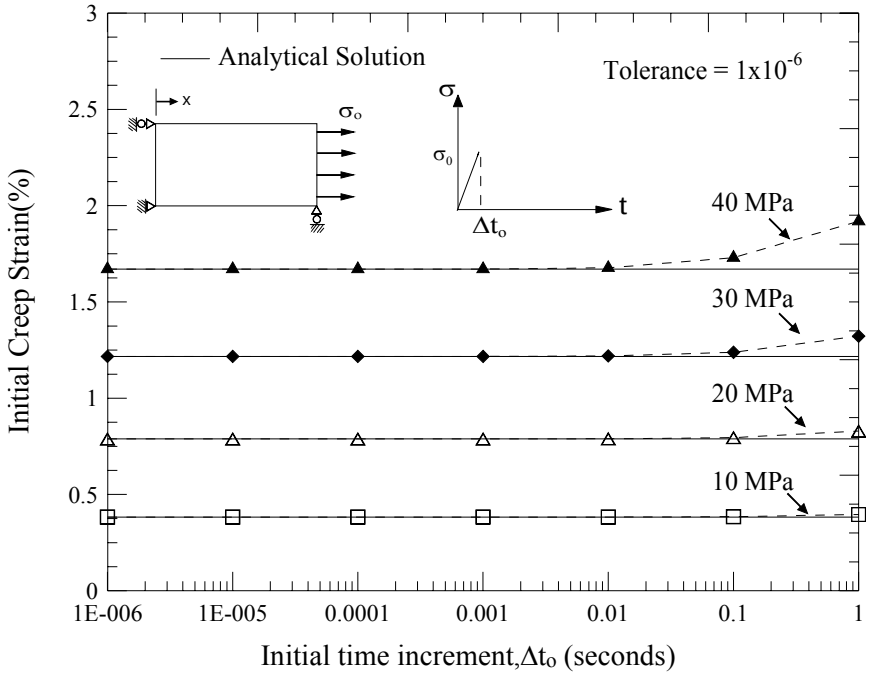

Figure 2.15 Effect of the time-increment size in the instantaneous static analysis for FM73 polymer.

convergence response under two applied stresses of 10 MPa and 40 MPa. The convergence at the structural level can be accelerated by incorporating an efficient iterative algorithm at the material level. The proposed iterative scheme shows quadratic convergence behavior at both stress level as shown Figure 2.16(c). It is noted that the convergence behavior at the material level are reported during the last iteration in the structural level. The residual behavior shows that a predictor-corrector scheme must be required at all levels to minimize the residuals. Table 2.5 shows the residual behavior at both element and material levels during the instantaneous loading step at various applied loads.

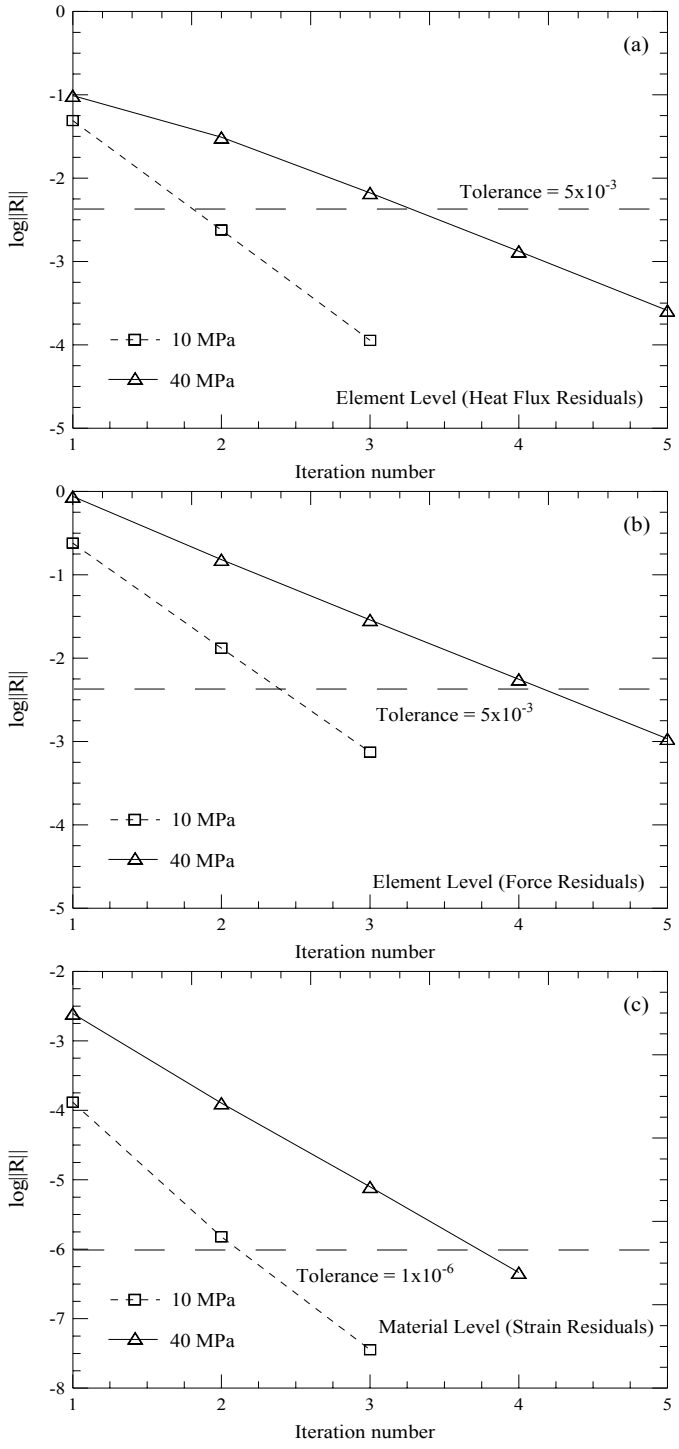

Figure 2.16 Residuals during iteration process for thermo-viscoelastic analyses under instantaneous mechanical load. (a) heat flux (b) force and (c) strain.

Table 2.5 Iteration process at element and material levels for coupled thermoviscoelastic recursive iterative numerical schemes during instantaneous "static" creep step loading ($\Delta t_0 = 10^{-4}$).

Load (MPa)	Time step (sec)	Element Level Residual			Material Level Residual	
		Iteration	Heat Flux(**)	Force(**)	# iteration	Strain(*)
10	10^{-4}	1	4.91×10^{-2}	2.40×10^{-1}	1	1.31×10^{-4}
		2	2.38×10^{-3}	1.32×10^{-2}	2	1.51×10^{-6}
		3	1.13×10^{-4}	7.45×10^{-4}	3	3.57×10^{-8}
20	10^{-4}	1	3.15×10^{-2}	4.63×10^{-1}	1	5.54×10^{-4}
		2	5.78×10^{-3}	4.69×10^{-2}	2	1.34×10^{-5}
		3	9.12×10^{-4}	4.99×10^{-3}	3	5.45×10^{-7}
30	10^{-4}	1	5.27×10^{-2}	6.73×10^{-1}	1	1.32×10^{-3}
		2	1.73×10^{-2}	9.47×10^{-2}	2	4.94×10^{-5}
		3	3.16×10^{-3}	1.42×10^{-2}	3	2.64×10^{-6}
		4	5.08×10^{-4}	2.17×10^{-3}	4	1.08×10^{-7}
40	10^{-4}	1	9.79×10^{-2}	8.71×10^{-1}	1	2.48×10^{-3}
		2	3.09×10^{-2}	1.52×10^{-1}	2	1.27×10^{-4}
		3	6.65×10^{-3}	2.88×10^{-2}	3	7.92×10^{-6}
		4	1.32×10^{-3}	5.58×10^{-3}	4	4.61×10^{-7}
		5	2.59×10^{-4}	1.08×10^{-3}		

* Strain residual at converged step in the material level. Convergence at material level set to be $||R|| < 10^{-6}$.
** Convergence at element level for both heat flux and force set to be $||R|| < 5 \times 10^{-3}$.

The convergence behavior is now examined during the coupled thermo-viscoelastic creep analysis. Loading is simulated in two steps. In the first step the instantaneous load of 40 MPa is applied with an initial time increment size of 10^{-4}. The second step simulated the viscoelastic analysis in which the constant load is held for 30 seconds with an initial time increment of 1.0 second. Two cases are studied. For the first one the mechanical load is applied in applied with no temperature boundary condition while in the second case a temperature of 313˚K is applied at one face of the cube during the second (viscoelastic) step to allow a conduction to take place in addition to the heat generation due to creep load. The geometry of the model and applied loading condition are shown in Figure 2.17.

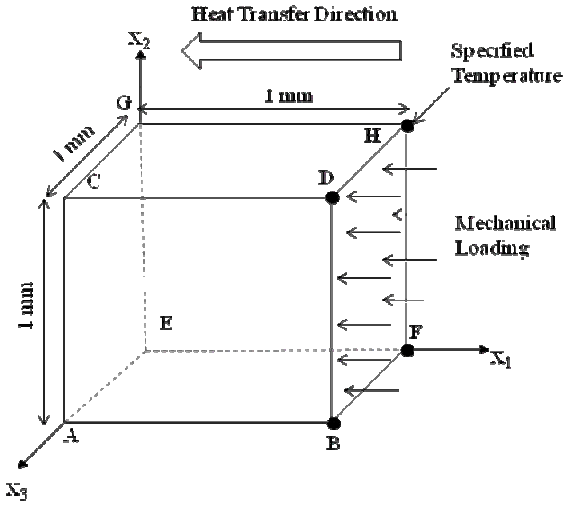

Figure 2.17 Three dimensional one element FE model for FM73 polymer.

The models were subjected to the following boundary conditions:

$$
\begin{aligned}
&T(x_1, x_2, x_3, 0) = 300K; && 0 \le x_1 \le 10, 0 \le x_2 \le 10,\ 0 \le x_3 \le 10 \\
&T(10, x_2, x_3, t) = 313K; && 0 \le x_2 \le 10,\ 0 \le x_3 \le 10,\ t \ge 0 \\
&\frac{\partial T(x_1, 0, x_3, t)}{\partial x_2} = \frac{\partial \bar{T}(x_1, 10, x_3, t)}{\partial x_2} = 0.0; && 0 \le x_1 \le 10,\ 0 \le x_3 \le 10,\ t \ge 0 \\
&\frac{\partial T(x_1, x_2, 0, t)}{\partial x_3} = \frac{\partial \bar{T}(x_1, x_2, 10, t)}{\partial x_3} = 0.0; && 0 \le x_1 \le 10,\ 0 \le x_2 \le 10,\ t \ge 0
\end{aligned}
\tag{2.92}
$$

$$
\begin{aligned}
&u_1(0, x_2, x_3, t) = 0.0; && 0 \le x_2 \le 10,\ 0 \le x_3 \le 10 \\
&u_2(x_1, 0, x_3, t) = 0.0; && 0 \le x_1 \le 10,\ 0 \le x_3 \le 10 \\
&u_3(x_1, x_2, 0, t) = 0.0; && 0 \le x_1 \le 10,\ 0 \le x_2 \le 10 \\
&t_1(10, x_2, x_3, t) = 40.0\,\text{MPa}; && 0 \le x_2 \le 10,\ 0 \le x_3 \le 10 \\
&t_2(x_1, 10, x_3, t) = 0.0\,\text{MPa}; && 0 \le x_1 \le 10,\ 0 \le x_3 \le 10 \\
&t_3(x_1, x_2, 10, t) = 0.0\,\text{MPa}; && 0 \le x_1 \le 10,\ 0 \le x_2 \le 10
\end{aligned}
\tag{2.93}
$$

where u_i and t_i (i=1,2,3) are the components of the displacements and the surface tractions, respectively.

The creep strains for both cases are shown in Figure 2.18(a). For the second case higher creep strains are observed due to the presence of temperature dependent material properties and thermal strain. The temperature increase is monitored at face ACGE. It is observed that when the temperature is specified on one face during the viscoelastic step then the temperature increase is due to two factors. The first one is from a conduction taking place between the two faces and the second factor is due to the heat generation during creep deformation. However, the rate of heat generation is relatively small during creep but it still affects the temperature change rate during the analysis.

Table 2.6 shows the force and heat flux residuals during the viscoelastic analysis when only stress is applied. The heat flux residuals are met for all stresses since very less temperature gradient is generated during the viscoelastic analysis. For force residuals the accelerated convergence rate in the proposed numerical method decreases the residual at the element level, especially in the case of highly nonlinear viscoelastic response. Table 2.7 is the same as Table 2.6 but with residuals for the viscoelastic analysis with specified temperature and mechanical loading. As expected, more iteration is required for these cases but the efficiency of the algorithm can be realized by examining the convergence of the first step in 40MPa loading. The efficiency of the algorithm is showed for other stresses in Table 2.7 by examining the number of iterations required for convergence with their decreasing residuals.

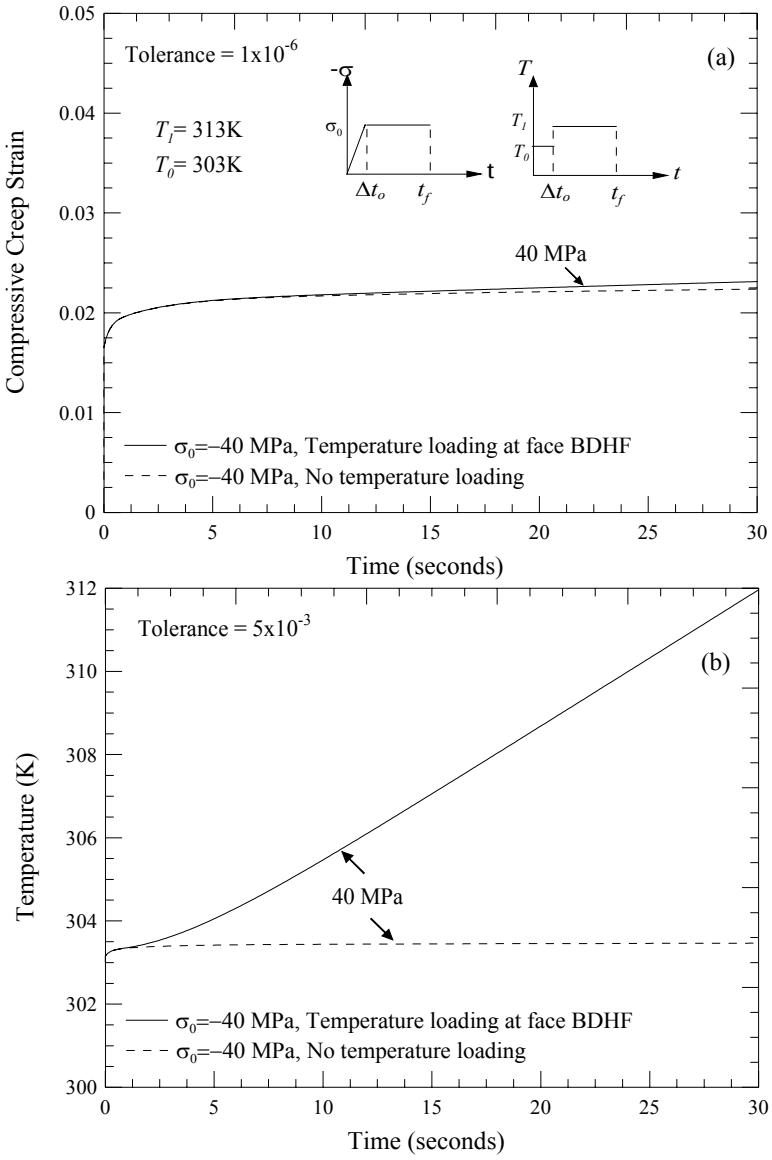

Figure 2.18 Thermo-viscoelastic creep analyses. (a) strain and (b) temperature increase during an applied stress of 40 MPa.

In the end the convergence behavior using the proposed algorithm is monitored at the structural and material level during a linear ramp loading. Three cases are studied. (1) A linear stress ramp is applied, (2) A linear temperature is applied and (3) Linear stress and temperature are applied. Figure 2.19 showed the geometry of the model and boundary conditions. Figure 2.19(a) illustrates the nonlinear creep strain for all three cases.

Table 2.6 Iteration process at element and material levels for coupled thermoviscoelastic recursive iterative numerical schemes during creep analysis (mechanical loading) at different times.

Load (MPa)	Time step (sec)	Element Level Residual			Material Level Residual		Material Level Residual (Last converged time step)	
		Iter.	Heat Flux(**)	Force(**)	# Iter.	Strain(*)	Iter.	Strain(*)
10	1.0	1	$7.58\text{x}10^{-7}$	$5.95\text{x}10^{-3}$	1	$2.02\ \text{x}10^{-7}$	1	$1.99\ \text{x}10^{-7}$
		2	$7.18\ \text{x}10^{-8}$	$2.54\ \text{x}10^{-4}$	1	$1.99\ \text{x}10^{-7}$		
	30.	1	$5.23\text{x}10^{-10}$	$3.89\ \text{x}10^{-7}$	1	$1.15\ \text{x}10^{-10}$	1	$1.15\ \text{x}10^{-10}$
20	1.0	1	$2.45\ \text{x}10^{-7}$	$2.23\ \text{x}10^{-2}$	2	$1.29\ \text{x}10^{-7}$	1	$1.43\ \text{x}10^{-6}$
		2	$3.25\ \text{x}10^{-9}$	$1.78\ \text{x}10^{-3}$	2	$4.01\ \text{x}10^{-8}$	2	$4.01\ \text{x}10^{-8}$
	25.0	1	$1.20\ \text{x}10^{-9}$	$2.83\ \text{x}10^{-7}$	1	$9.12\ \text{x}10^{-10}$	1	$9.12\text{x}10^{-10}$
30	1.0	1	$6.80\ \text{x}10^{-6}$	$1.05\ \text{x}10^{-1}$	3	$3.05\ \text{x}10^{-7}$	1	$1.02\ \text{x}10^{-5}$
		2	$2.00\ \text{x}10^{-6}$	$7.88\ \text{x}10^{-3}$	2	$1.02\ \text{x}10^{-7}$	2	$5.05\ \text{x}10^{-7}$
		3	$4.20\ \text{x}10^{-7}$	$1.42\ \text{x}10^{-3}$	2	$5.05\ \text{x}10^{-7}$		
	20.0	1	$6.88\ \text{x}10^{-10}$	$1.04\ \text{x}10^{-6}$	1	$9.71\ \text{x}10^{-9}$	1	$9.71\text{x}10^{-10}$
40	1.0	1	$3.08\ \text{x}10^{-5}$	$2.66\ \text{x}10^{-1}$	4	$4.47\ \text{x}10^{-7}$	1	$4.68\ \text{x}10^{-5}$
		2	$1.70\ \text{x}10^{-5}$	$5.04\ \text{x}10^{-2}$	3	$8.18\ \text{x}10^{-7}$	2	$3.76\ \text{x}10^{-6}$
		3	$6.04\ \text{x}10^{-6}$	$1.11\ \text{x}10^{-2}$	3	$5.02\ \text{x}10^{-7}$	3	$8.88\ \text{x}10^{-7}$
		4	$1.94\ \text{x}10^{-6}$	$3.23\ \text{x}10^{-3}$	3	$8.88\ \text{x}10^{-7}$		
	3.0	1	$3.97\ \text{x}10^{-7}$	$7.13\ \text{x}10^{-3}$	2	$2.39\ \text{x}10^{-7}$	1	$1.23\text{x}10^{-6}$
		2	$8.04\ \text{x}10^{-8}$	$1.04\ \text{x}10^{-4}$	2	$1.01\ \text{x}10^{-7}$	2	$1.01\text{x}10^{-7}$

* Strain residual at converged step in the material level. Convergence at material level set to be $||R||<10^{-6}$.
** Convergence at element level for both heat flux and force set to be $||R|| < 5\text{x}10^{-3}$.

Negligible creep strain is observed for linear thermal loading while for case 3 maximum creep strains are obtained. The temperature rises during all three cases are also shown in Figure 2.14(b). In absence of the mechanical load (case 2) the heat transfer equation is solved separately while for the cases 2 and 3 the fully coupled thermoviscoelastic model yields temperature rise by solving the heat conduction and deformation equations simultaneously. Thus, lower temperature is generated for the case 3 than the case 1

Table 2.7 Iteration process at element and material levels for coupled thermoviscoelastic recursive iterative numerical schemes during creep analysis (mechanical and temperature loading) at different times.

Load (MP)	Time step (sec)	Element Level Residual			Material Level Residual		Material Level Residual (Last converged time step)	
		Iter.	Heat Flux(**)	Force(**)	# Iter.	Strain(*)	Iter.	Strain(*)
10	1.0	1	1.77×10^{-1}	2.00×10^{-2}	2	2.99×10^{-8}	1	2.95×10^{-6}
		2	8.04×10^{-3}	6.24×10^{-4}	2	3.03×10^{-8}	2	3.04×10^{-8}
		3	3.62×10^{-4}	2.77×10^{-5}	2	3.04×10^{-8}		
	3.0	1	2.41×10^{-2}	7.04×10^{-4}	2	2.62×10^{-8}	1	2.61×10^{-6}
		2	9.67×10^{-4}	9.38×10^{-6}	2	2.67×10^{-8}	2	2.67×10^{-8}
20	1.0	1	1.62×10^{-1}	4.82×10^{-2}	2	3.01×10^{-9}	1	7.21×10^{-6}
		2	4.64×10^{-3}	3.63×10^{-3}	2	1.82×10^{-7}	2	1.82×10^{-7}
	7.0	1	6.03×10^{-3}	1.63×10^{-4}	2	1.46×10^{-7}	1	5.61×10^{-6}
		2	2.52×10^{-4}	3.79×10^{-6}	2	1.48×10^{-7}	2	1.48×10^{-7}
30	1.0	1	4.28×10^{-1}	1.28×10^{-1}	3	2.57×10^{-7}		
		2	1.58×10^{-1}	1.53×10^{-2}	2	5.01×10^{-7}	1	2.11×10^{-5}
		3	3.35×10^{-2}	2.80×10^{-3}	2	9.31×10^{-7}	2	1.02×10^{-6}
		4	6.19×10^{-3}	4.87×10^{-4}	3	1.48×10^{-7}	3	1.51×10^{-7}
		5	1.13×10^{-3}	8.97×10^{-5}	3	1.51×10^{-7}		
	5.0	1	1.19×10^{-2}	1.78×10^{-4}	2	4.85×10^{-8}	1	1.03×10^{-5}
		2	6.32×10^{-4}	1.60×10^{-5}	2	5.04×10^{-8}	2	5.04×10^{-7}
40	1.0	1	2.91×10^{0}	2.68×10^{-1}	4	4.44×10^{-7}		
		2	1.45×10^{0}	4.47×10^{-2}	3	7.32×10^{-7}	1	6.45×10^{-5}
		3	5.19×10^{-1}	1.56×10^{-2}	3	6.41×10^{-7}	2	5.20×10^{-6}
		4	1.66×10^{-1}	4.39×10^{-3}	4	1.06×10^{-7}	3	1.22×10^{-6}
		5	5.09×10^{-2}	1.30×10^{-3}	4	1.18×10^{-7}	4	1.24×10^{-7}
		6	1.53×10^{-2}	3.85×10^{-4}	4	1.22×10^{-7}		
		7	4.55×10^{-3}	1.14×10^{-4}	4	1.24×10^{-7}		
	3.0	1	5.97×10^{-2}	9.55×10^{-4}	3	3.31×10^{-7}	1	2.22×10^{-5}
		2	5.44×10^{-3}	1.78×10^{-4}	3	4.33×10^{-7}	2	1.78×10^{-6}
		3	2.35×10^{-4}	3.51×10^{-6}	3	4.42×10^{-7}	3	4.42×10^{-7}

* Strain residual at converged step in the material level. Convergence at material level set to be $||R|| < 10^{-6}$.
** Convergence at element level for both heat flux and force set to be $||R|| < 5 \times 10^{-3}$.

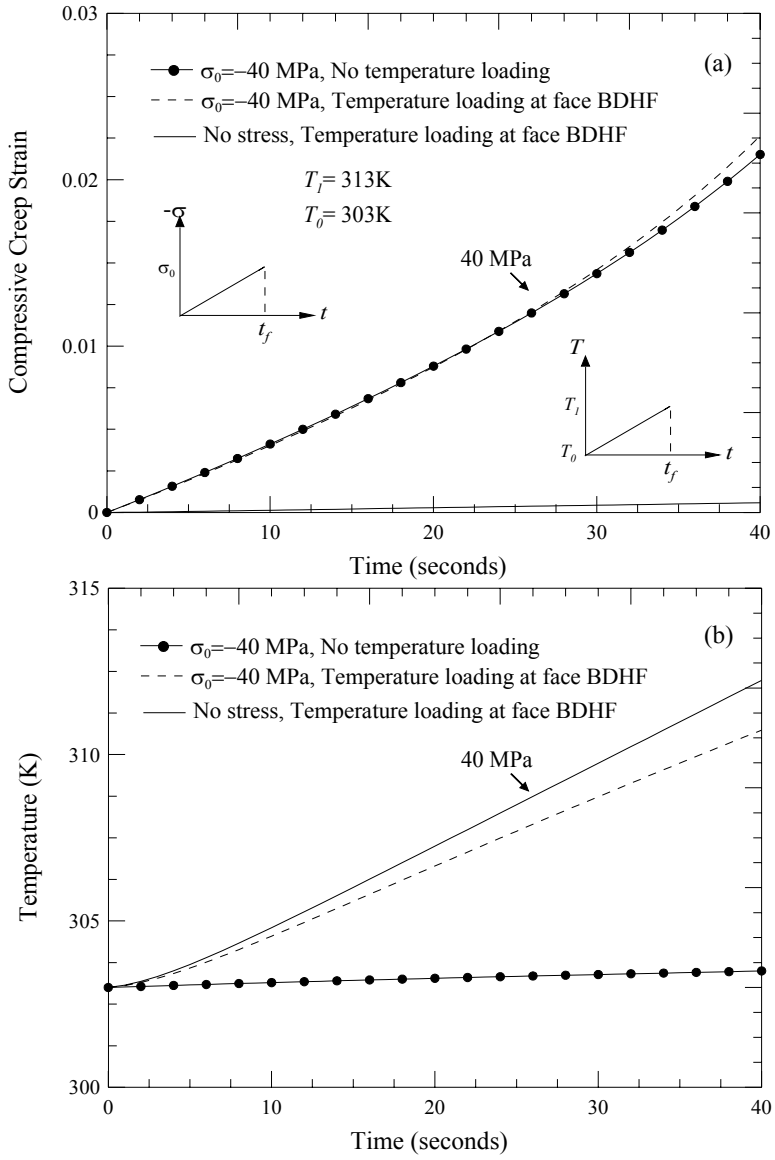

Figure 2.19 Thermo-viscoelastic analyses under linear stress and temperature ramp loadings. (a) strain and (b) temperature increase.

because the temperature generation due to the mechanical load lowers the temperature gradient and thus, the heat conduction takes place slowly.

The convergence behavior at the element and material levels for the case 3 is shown in Figure 2.20. The residuals behavior during iteration process at initial time

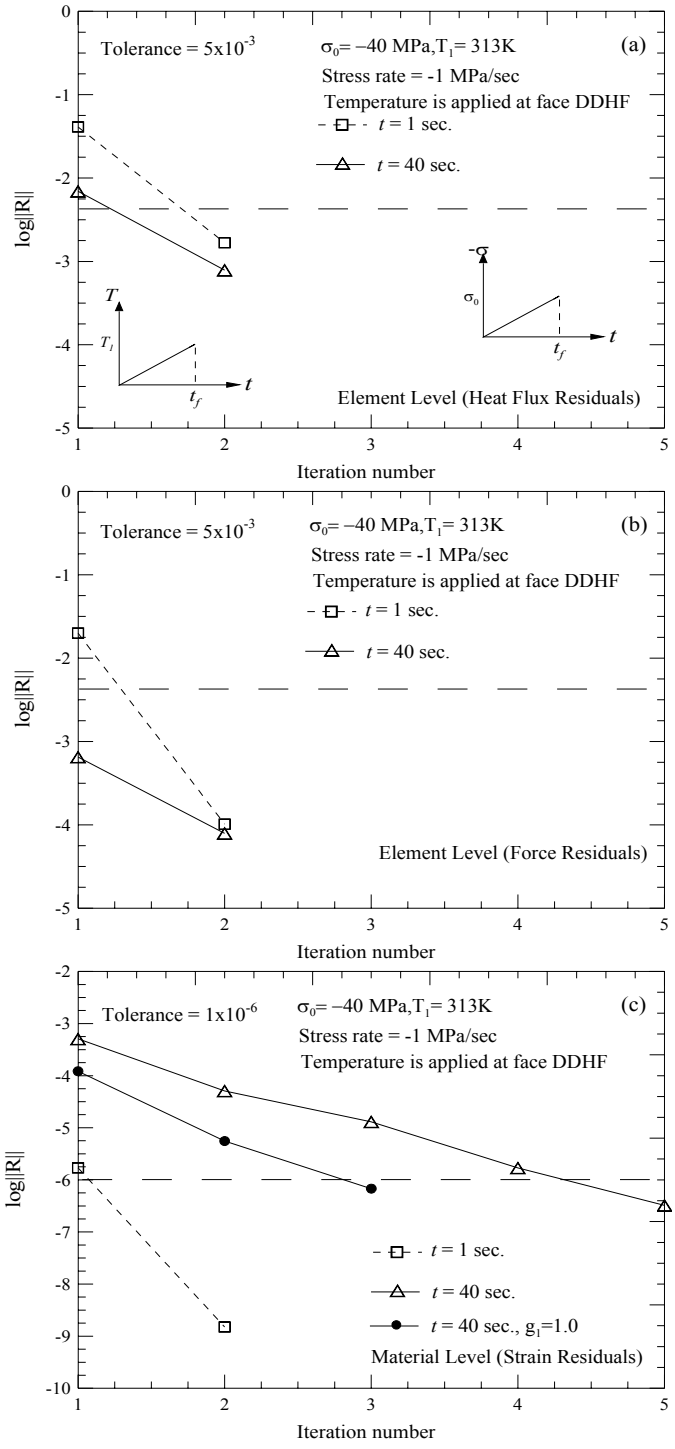

Figure 2.20 Residuals during iteration process for thermo-viscoelastic analyses under linear stress and temperature ramp loadings. (a) heat flux (b) force and (c) strain.

increment size of t=1sec. and at final step time of t=40 sec. are plotted. The fast convergence rate is observed at both levels. The nonlinear parameters, especially $g_1\left(\bar{\sigma}^t\right)$ near 40MPa stress, increase drastically and therefore more iterations are required for convergence at the material level. Figure 2.20 (c) shows that the number of iterations can be reduced for the same time increment if $g_1\left(\bar{\sigma}^t\right)$ is considered to be equal to 1.

In summary, the numerical algorithm is developed to predict the fully coupled nonlinear thermoviscoelastic response of isotropic homogeneous materials. For linear viscoelastic materials, the proposed algorithm has been successfully verified with analytical solutions. The study of the convergence behavior for different types of loadings demonstrated the efficiency of the algorithm in predicting the coupled heat conduction and deformation of nonlinear isotropic homogeneous viscoelastic materials. The fully coupled thermoviscoelastic response is important for cases when structures made of polymers are subjected to cyclic loadings over a long period. The nonlinear stress and temperature dependent material parameters should be account for when analyzing response of polymeric materials under cyclic loadings at moderate amplitudes and frequencies over a relatively long period. Moreover, the conduction plays a considerable role in predicting the factual temperature fields within structures having a non-uniform heat generation under a cyclic loading; these temperature fields can significantly alter the properties of polymer structures, affecting their overall response.

CHAPTER III

A MICROMECHANICAL MODEL FOR PARTICULATE COMPOSITE*

This chapter presents a micromechanical model for predicting effective thermal properties (linear coefficient of thermal expansion and thermal conductivity) and mechanical properties of viscoelastic composites having solid spherical particle reinforcements. A representative volume element (RVE) of the composites is modeled by a single particle embedded in a cubic matrix. The micromechanical model consists of four particle and matrix subcells. The micromechanical relations are formulated in terms of incremental average field quantities, i.e., stress, strain, heat flux and temperature gradient, in the subcells. Stress and temperature dependent viscoelastic constitutive models are used for the isotropic constituents in the micromechanical model. The thermal properties of the particle and matrix constituents are temperature dependent. The effective mechanical properties and coefficient of thermal expansion are derived by satisfying displacement- and traction continuities at the interfaces during thermo-viscoelastic deformations. This formulation leads to an effective time-temperature-stress-dependent coefficient of thermal expansion of the particulate composite. The effective thermal conductivity is formulated by imposing heat flux- and temperature continuities at the subcells' interfaces. When a nonlinear and time-dependent response is

---

*Reprinted with permission from "Effective thermal properties of viscoelastic composites having field-dependent constituent properties" by Khan, K.A., Muliana, A.H., 2010. Acta Mech., 209(1-2), 153-178, DOI: 10.1007/s00707-009-0171-6, Copyright 2010 by Springer-Verlag.

considered, an incremental formulation consisting of a linearized prediction and an iterative scheme is derived to obtain the effective material properties and field variables of the composite. The effective thermal properties obtained from the micromechanical model are compared with the analytical solutions and experimental data available in the literature.

3.1 EFFECTIVE THERMAL AND MECHANICAL PROPERTIES OF A PARTICULATE COMPOSITE

A simplified micromechanical model is formulated to determine the effective thermal and mechanical properties of homogenized composites by incorporating microscopic characteristics. Muliana and Kim (2007) developed a simplified micromechanical model for determining the effective viscoelastic responses of a particle reinforced polymer composite. In this study, the above-mentioned micromechanical model is modified to determine the effective thermal properties and thermo-viscoelastic response of particle reinforced composites. Figure 3.1 illustrates the simplified micromechanical model for the composite with randomly distributed solid spherical particles in a homogeneous matrix. The solid spherical particulate composites are idealized with uniformly distributed arrays of cubic particles. The gradient of the volume contents of the particles is assumed zero. A representative volume element (RVE) is defined as a cubic particle

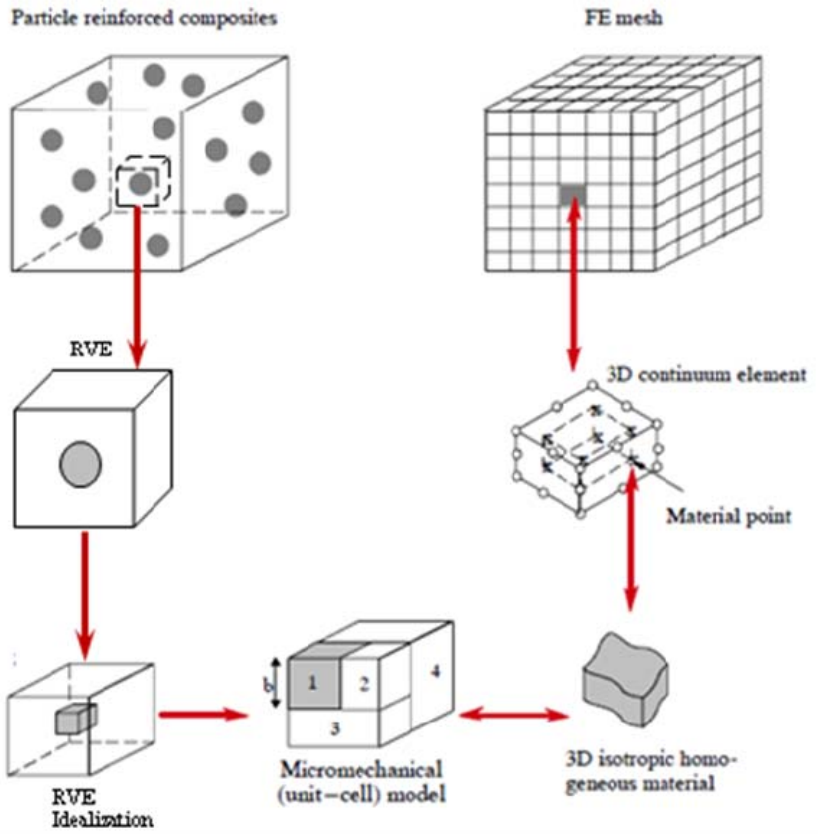

Figure 3.1 Representative unit-cell model for the particle reinforced composites.

embedded in the center of the matrix with cubic domain. Periodic boundary conditions are imposed to the RVE. A one eight unit-cell consisting of four subcells is modeled due to three-plane symmetry. The first subcell is a particle constituent, while the subcells 2, 3, and 4 represent the matrix constituents. The micromechanical relations provide equivalent homogeneous material responses from the heterogeneous microstructures and simultaneously recognize nonlinear behaviors of the individual constituents due to prescribed boundary conditions. The micromechanical formulations are designed to be compatible with general finite element structural analyses, i.e., ABAQUS in which the

effective responses from the micromechanical are implemented at each material point (Gaussian integration point) within the finite elements.

A percolation effect is primarily associated with the random or disordered media Stauffer (1985). In other words, this notion is more important in the modeling of the composite in which the dispersion of the inclusion is random in nature. Moreover, this issue is more important to examine whenever the distribution of the inclusion is describe using some probability distribution function. In the proposed micromechanical model, a statistically homogeneous distribution of inclusions is assumed. The micromechanical model is formulated by assuming all particles are fully surrounded by matrix and periodic boundary conditions are imposed to the selected unit-cell model. In reality, there often exists contact between particles. As the particle content in the composites increases contacts among particles become more pronounced and in some composites interpenetrating between the constituents (sometimes refer to as percolation) are also observed, making it difficult to distinguish the inclusion and matrix constituents. Interpenetrating between constituents and percolation can significantly alter the effective properties of composites (Torquato, 2002). Torquato (2002) has also discussed that a constituent/phase inversion in composites is another crucial microstructural feature in estimating the overall performance of composites. Thus, the present micromechanical model, which requires defining inclusion and matrix constituents, is not suitable to predict overall composite responses when the effect of percolation on the overall response of composite is significant.

3.1.1 FORMULATION OF THE EFFECTIVE COEFFICIENT OF THERMAL EXPANSION

The micromechanical relation for the effective CTE of the studied composite is derived in terms of the nonlinear time-stress-dependent moduli and temperature dependent CTE of each constituent. Each unit-cell is divided into a number of subcells and the spatial variation of the displacement field in each subcell is assumed such that the stresses and deformations are spatially uniform. The macroscopic effective properties of a heterogeneous medium are approximated using volume average of the properties of the individual constituents.

For the thermo-elastic problems, the scalar components of the effective stress ($\overline{\sigma}_{ij}$) and strain ($\overline{\varepsilon}_{ij}$) of the composites are related by the following constitutive equations:

$$\overline{\sigma}_{ij} = \overline{C}_{ijkl}\left[\overline{\varepsilon}_{kl} - \overline{\alpha}_{kl}\left(\overline{T} - \overline{T}_0\right)\right] \quad \text{or} \tag{3.1}$$

$$\overline{\varepsilon}_{ij} = \overline{S}_{ijkl}\overline{\sigma}_{kl} + \overline{\alpha}_{ij}\left(\overline{T} - \overline{T}_0\right) = \overline{\varepsilon}_{ij}^{M} + \overline{\varepsilon}_{ij}^{T} \tag{3.2}$$

where $\overline{C}_{ijkl}$ and $\overline{S}_{ijkl}$ are the components of the effective elastic stiffness and compliance tensors, respectively; and $\overline{\alpha}_{kl}$ are the components of the effective CTE. Variables $\overline{\varepsilon}_{ij}^{M}$ and $\overline{\varepsilon}_{ij}^{T}$ are the components of effective total mechanical and thermal strains, respectively. The parameters $\overline{T}$ and $\overline{T}_0$ are the effective current and reference temperatures, respectively. The elastic constants and CTEs of the particle and matrix are stress-temperature dependent, resulting in stress-temperature-dependent effective thermo-mechanical properties. The goal of the micromechanical model formulation is to obtain

$\overline{C}_{ijkl}$ or $\overline{S}_{ijkl}$ based on the constitutive relations in each constituents and microstructural geometry, i.e. RVE. The constitutive relations for a linear thermo-elastic problem in each constituent (m) are expressed by:

$$\sigma_{ij}^{(m)} = C_{ijkl}^{(m)} \left[\varepsilon_{kl}^{(m)} - \alpha_{kl}^{(m)} \left(T^{(m)} - T_0 \right) \right] \text{ or} \tag{3.3}$$

$$\varepsilon_{ij}^{(m)} = S_{ijkl}^{(m)} \sigma_{kl}^{(m)} + \alpha_{ij}^{(m)} \left(T^{(m)} - T_0 \right) = \varepsilon_{ij}^{M,(m)} + \varepsilon_{ij}^{T,(m)} \tag{3.4}$$

Due to the assumption that the RVE's length scale (micro-scale) is much smaller than the structural (macro) scale, the steady state condition within each unit-cell (material point of a composite) of the RVE is reached in a very short time period as compare to the overall time response. Therefore, the transient heat transfer analysis within a unit-cell can be ignored and temperatures are assumed to vary at the macroscopic (material) points. This assumption leads to the representation of the incremental and total temperature within each unit-cell of the RVE and their sub-cells at the steady state condition as:

$$dT^{t,(m)} = d\overline{T}^{t} \tag{3.5}$$

$$T^{t,(m)} = T^{t-dt,(m)} + dT^{t,(m)} \tag{3.6}$$

A volume averaging method is used to evaluate the effective response of a unit-cell (micromechanical model). The traction continuity at the interface between each sub-cells is satisfied in an average sense, which allows expressing the average stresses and strains by:

$$\bar{\sigma}_{ij} = \frac{1}{V}\sum_{m=1}^{N} \int_{V^{(m)}} \sigma_{ij}^{(m)}(x_k^{(m)})dV^{(m)} \approx \frac{1}{V}\sum_{m=1}^{N} V^{(m)}\sigma_{ij}^{(m)} \tag{3.7}$$

$$\bar{\varepsilon}_{ij} = \frac{1}{V}\sum_{m=1}^{N} \int_{V^{(m)}} \varepsilon_{ij}^{(m)}(x_k^{(m)})dV^{(m)} \approx \frac{1}{V}\sum_{m=1}^{N} V^{(m)}\varepsilon_{ij}^{(m)} \tag{3.8}$$

An overbar indicates effective field variables. The superscript (m) denotes the subcell's number and N is the number of subcells. The stress $\sigma_{ij}^{(m)}$ and strain $\varepsilon_{ij}^{(m)}$ are the average stress and strain in each subcell. The unit-cell volume V is:

$$V = \sum_{m=1}^{N} V^{(m)}, \text{ N} = 4 \tag{3.9}$$

The volume of the unit-cell is taken as one. The volume of the subcell 1 represents the volume content of the particle which is model as a cube of edge length b. Thus, the magnitude of b is always less than one. The volumes of the four subcells are then expressed as:

$$V^{(1)} = b^3,\ V^{(2)} = b^2(1-b),\ V^{(3)} = b(1-b),\ V^{(4)} = (1-b) \tag{3.10}$$

In this study, the elastic properties and CTE of the constituents are allowed to change with time, stress, and temperatures, which result in nonlinear stress-strain relations. To solve the nonlinear equations, linearized predictor and corrector schemes are formulated and Eqs. (3.1)-(3.4) are then satisfied in incremental relations. Within the FE analyses, the total stress, mechanical and thermal strains at current time *t* are defined by:

$$
\begin{aligned}
&\bar{\sigma}_{ij}^{t} = \bar{\sigma}_{ij}^{t\text{-}dt} + d\bar{\sigma}_{ij}^{t} \\
&\bar{\varepsilon}_{ij}^{M,t} = \bar{\varepsilon}_{ij}^{M,t\text{-}dt} + d\bar{\varepsilon}_{ij}^{M,t} \\
&\bar{\varepsilon}_{ij}^{T,t} = \bar{\varepsilon}_{ij}^{T,t\text{-}dt} + d\bar{\varepsilon}_{ij}^{T,t} \\
&\sigma_{ij}^{(m),t} = \sigma_{ij}^{(m),t\text{-}dt} + d\sigma_{ij}^{(m),t} \\
&\varepsilon_{ij}^{M(m),t} = \varepsilon_{ij}^{M(m),t\text{-}dt} + d\varepsilon_{ij}^{M(m),t} \\
&\varepsilon_{ij}^{T(m),t} = \varepsilon_{ij}^{T(m),t\text{-}dt} + d\varepsilon_{ij}^{T(m),t}
\end{aligned}
\tag{3.11}
$$

The superscript $t - dt$ indicates quantities at the previous converged time and prefix d denotes an incremental quantity at the current time increment. Due to the time-dependent and nonlinear response of the matrix sub-cells, the linearized micromechanical relations violate the constitutive relations. An iteration scheme is added to minimize the residuals aroused from the linearization. The converged solution satisfies both micromechanical relations and non-linear time-dependent constitutive equations.

In this study, the micromechanical model is designed to be compatible with displacement based FE structural analyses in which the effective mechanical strains ($\mathrm{d}\bar{\varepsilon}_{kl}^{M,t}$) are the independent variables. Following Hill (1965) method, the average stresses and strains in each subcell can be expressed in terms of the effective stress and strain by defining a concentration tensor. This study defines a strain interaction tensor ($\boldsymbol{B}^{(m),t}$), which relates the incremental average mechanical strains in each subcell, $d\varepsilon_{ij}^{M(m),t}$, to the effective incremental strain, $\mathrm{d}\bar{\varepsilon}_{kl}^{M,t}$:

$$
d\varepsilon_{ij}^{M,(m),t} = B_{ijkl}^{(m),t}\, d\bar{\varepsilon}_{kl}^{M,t} \tag{3.12}
$$

Using the incremental strain in Eq. (3.12), the incremental stress in the subcell (m) can be written as:

$$d\sigma_{ij}^{(m),t} = C_{ijkl}^{(m),t}\ B_{klrs}^{(m),t}\ d\bar{\varepsilon}_{rs}^{M,t} \tag{3.13}$$

Substituting Eq. (3.12) into the incremental form of Eq. (3.7) gives the effective incremental stresses:

$$d\bar{\sigma}_{ij}^{t} = \frac{1}{V}\sum_{m=1}^{N} V^{(m)}\ C_{ijkl}^{(m),t}\ B_{klrs}^{(m),t}\ d\bar{\varepsilon}_{rs}^{M,t} \tag{3.14}$$

The unit-cell effective tangent stiffness matrix $\bar{C}_{ijrs}^{\ t}$ is then determined by:

$$\bar{C}_{ijrs}^{t} = \frac{1}{V}\sum_{m=1}^{N} V^{(m)}\ C_{ijkl}^{(m),t}\ B_{klrs}^{(m),t} \tag{3.15}$$

The $B_{ijkl}^{(m),t}$ is the fourth order tensor, which can be obtained by satisfying the micromechanical relations and the constitutive equations. Detailed formulation of $B_{ijkl}^{(m),t}$ can be found in Muliana and Kim (2007).

The micromechanical relations within the four subcells are derived by assuming perfect bonds along the interfaces of the subcells. The homogenized incremental strain relations after imposing the displacement compatibility at the subcells' interfaces are given as:

$$\begin{aligned} d\bar{\varepsilon}_{ij}^{M,t} + d\bar{\varepsilon}_{ij}^{T,t} &= \frac{1}{V^{(1)}+V^{(2)}}\left[V^{(1)} d\varepsilon_{ij}^{M(1),t} + V^{(2)} d\varepsilon_{ij}^{M(2),t}\right] \\ &+ \frac{1}{V^{(1)}+V^{(2)}}\left[V^{(1)} d\varepsilon_{ij}^{T(1),t} + V^{(2)} d\varepsilon_{ij}^{T(2),t}\right] \\ &= d\varepsilon_{ij}^{M(3),t} + d\varepsilon_{ij}^{T(3),t} = d\varepsilon_{ij}^{M(4),t} + d\varepsilon_{ij}^{T(4),t} \quad for\ \ i = j;\ \ i,j = 1,2,3 \end{aligned} \tag{3.16}$$

$$d\bar{\gamma}_{ij}^{t} = V^{(1)} d\gamma_{ij}^{(1),t} + V^{(2)} d\gamma_{ij}^{(2),t} + V^{(3)} d\gamma_{ij}^{(3),t} + V^{(4)} d\gamma_{ij}^{(4),t} \quad for\ i \neq j \tag{3.17}$$

The homogenized stresses after imposing the traction continuity at the subcells' interface can be expressed as:

$$\begin{aligned} &d\bar{\sigma}_{ij}^{t} = V^{(A)} d\sigma_{ij}^{(A),t} + V^{(3)} d\sigma_{ij}^{(3),t} + V^{(4)} d\sigma_{ij}^{(4),t} \quad \text{for } i = j \\ &d\sigma_{ij}^{(A),t} = d\sigma_{ij}^{(1),t} = d\sigma_{ij}^{(2),t} \end{aligned} \tag{3.18}$$

$$d\bar{\sigma}_{ij}^{t} = d\sigma_{ij}^{(1),t} = d\sigma_{ij}^{(2),t} = d\sigma_{ij}^{(3),t} = d\sigma_{ij}^{(4),t} \quad \text{for } i \neq j \tag{3.19}$$

where the total volume of the subcells 1 and 2 in Eq. (3.18) is $V^{(A)} = V^{(1)} + V^{(2)}$

Using the micromechanical relations in Eq. (3.18) and thermo-elastic constitutive relations for the particle and matrix subcells, the incremental form of the effective stress-strain relations for the particle reinforced composite are:

$$\begin{aligned} d\bar{\sigma}_{ij}^{t} = {} & \frac{1}{V}\left[V^{(A)} C_{ijkl}^{(A),t} + V^{(3)} C_{ijkl}^{(3),t} + V^{(4)} C_{ijkl}^{(4),t} \right] d\bar{\varepsilon}_{kl}^{t} - \\ & \frac{dT}{V}\left[V^{(A)} C_{ijkl}^{(A),t} \alpha_{kl}^{(A),t} + V^{(3)} C_{ijkl}^{(3),t} \alpha_{kl}^{(3),t} + V^{(4)} C_{ijkl}^{(4),t} \alpha_{kl}^{(4),t} \right] \\ & \text{for } \; i = j \;\; \text{and} \;\; k = l \quad i, j, k, l = 1, 2, 3 \end{aligned} \tag{3.20}$$

Eq. (3.20) can be rewritten as:

$$\begin{aligned} d\bar{\sigma}_{ij}^{t} &= \bar{C}_{ijkl}^{t} d\bar{\varepsilon}_{kl}^{t} - \frac{dT}{V}\left[V^{(A)} C_{ijkl}^{(A),t} \alpha_{kl}^{(A),t} + V^{(3)} C_{ijkl}^{(3),t} \alpha_{kl}^{(3),t} + V^{(4)} C_{ijkl}^{(4),t} \alpha_{kl}^{(4),t} \right] \\ &= \bar{C}_{ijkl}^{t} \left[d\bar{\varepsilon}_{kl}^{t} - dT \bar{\alpha}_{kl}^{t} \right] \end{aligned} \tag{3.21}$$

The effective consistent tangent CTE in Eq. (3.21), for the isotropic nonlinear response, is then expressed as:

$$\bar{\alpha}_{ij}^{t} = \bar{\alpha}^{t} \delta_{ij} = \frac{\bar{C}_{ijkl}^{-1,t}}{V}\left[V^{(A)} C_{ijkl}^{(A),t} \alpha_{kl}^{(A),t} + V^{(3)} C_{ijkl}^{(3),t} \alpha_{kl}^{(3),t} + V^{(4)} C_{ijkl}^{(4),t} \alpha_{kl}^{(4),t} \right] \tag{3.22}$$

where $\alpha_{ij}^{(A),t}$ and $C_{ijkl}^{(A),t}$ in Eq. (3.21) are the effective thermal expansion and stiffness expressions for the subcells 1 and 2. The scalar components of $\alpha_{ij}^{(A),t}$ and $C_{ijkl}^{(A),t}$ can be expressed in the following equations:

$$\alpha_{ij}^{(A),t} = \alpha^{(A),t}\delta_{ij} = \frac{1}{V^A}\left[V^{(1)}\alpha_{ij}^{(1),t} + V^{(2)}\alpha_{ij}^{(2),t}\right], \text{ and} \tag{3.23}$$

$$C_{ijkl}^{(A),t} = X_{ijkl}^{-1,t} \tag{3.24}$$

$$\text{where } X_{ijkl}^{t} = \frac{1}{V^A}\left[V^{(1)}C_{ijkl}^{(1)-1,t} + V^{(2)}C_{ijkl}^{(2)-1,t}\right]. \tag{3.25}$$

It is seen that the effective tangent CTE in Eq. (3.22) within an incremental time step depends on the time-dependent moduli and CTE of each constituent. Thus, for the stress, temperature and time-dependent constituent mechanical and thermal properties, the effective CTE also varies with stress, temperature and time.

In order to formulate the strain interaction matrix ($\boldsymbol{B}^{(m),t}$) introduced in Eq. (3.12), the micromechanical relations and constitutive equations are imposed. The micromechanical model consists of four subcells with six components of strains need to be determined for every subcell. This requires forming 24 equations. The first sets of equations are determined from the strain compatibility equations which are given as:

$$\underset{(12x1)}{\{\boldsymbol{R}_{\varepsilon}\}} = \underset{(12x24)}{\left[\boldsymbol{A}_1^M\right]}\underset{(24x1)}{\left\{\begin{matrix}\boldsymbol{\varepsilon}^{(1)}\\ \boldsymbol{\varepsilon}^{(2)}\\ \boldsymbol{\varepsilon}^{(3)}\\ \boldsymbol{\varepsilon}^{(4)}\end{matrix}\right\}} - \underset{(12x6)}{\left[\boldsymbol{D}_1^M\right]}\underset{(6x1)}{\{\bar{\boldsymbol{\varepsilon}}\}} \tag{3.25}$$

where $\boldsymbol{R}_{\varepsilon}$ is the residual vector arising from imposing the strain compatibility relations. In the case of linear elastic response is exhibited for all subcells, the vector $\boldsymbol{R}_{\varepsilon}$ is zero. The second sets of equations are formed based on the traction continuity relations. The equations based on the traction continuity relations within subcells:

$$\underset{(12x1)}{\{\ \boldsymbol{R}_{\sigma}\ \}} = \underset{(12x24)}{\left[\ \boldsymbol{A}_2^{M,t}\ \right]} \begin{Bmatrix} \boldsymbol{\varepsilon}^{(1)} \\ \boldsymbol{\varepsilon}^{(2)} \\ \boldsymbol{\varepsilon}^{(3)} \\ \boldsymbol{\varepsilon}^{(4)} \end{Bmatrix}_{(24x1)} - \underset{(12x6)}{\left[\ \boldsymbol{O}\ \right]} \underset{(6x1)}{\{\ \bar{\boldsymbol{\varepsilon}}\ \}} \tag{3.26}$$

The residual vector $\boldsymbol{R}_{\sigma}$ results from satisfying the traction continuity relations. For linear elastic constituents, the components of $\boldsymbol{R}_{\sigma}$ are zero. The matrix $\boldsymbol{O}$ is the zero matrix and the components of matrix $\boldsymbol{A}_1^M$, $\boldsymbol{A}_2^{M,t}$ and $\boldsymbol{D}_1^M$ are given as follows:

$$\boldsymbol{A}_1^M = \begin{bmatrix} \underset{(3x3)}{\frac{V^{(1)}}{V^{(A)}}\boldsymbol{I}} & \underset{(3x3)}{\boldsymbol{0}} & \underset{(3x3)}{\frac{V^{(2)}}{V^{(A)}}\boldsymbol{I}} & \underset{(3x3)}{\boldsymbol{0}} & \underset{(3x3)}{\boldsymbol{0}} & \underset{(3x3)}{\boldsymbol{0}} & \underset{(3x3)}{\boldsymbol{0}} & \underset{(3x3)}{\boldsymbol{0}} \\ \underset{(3x3)}{\boldsymbol{0}} & \underset{(3x3)}{\boldsymbol{0}} & \underset{(3x3)}{\boldsymbol{0}} & \underset{(3x3)}{\boldsymbol{0}} & \underset{(3x3)}{\boldsymbol{I}} & \underset{(3x3)}{\boldsymbol{0}} & \underset{(3x3)}{\boldsymbol{0}} & \underset{(3x3)}{\boldsymbol{0}} \\ \underset{(3x3)}{\boldsymbol{0}} & \underset{(3x3)}{\boldsymbol{0}} & \underset{(3x3)}{\boldsymbol{0}} & \underset{(3x3)}{\boldsymbol{0}} & \underset{(3x3)}{\boldsymbol{0}} & \underset{(3x3)}{\boldsymbol{0}} & \underset{(3x3)}{\boldsymbol{I}} & \underset{(3x3)}{\boldsymbol{0}} \\ \underset{(3x3)}{\boldsymbol{0}} & \underset{(3x3)}{V^{(1)}\boldsymbol{I}} & \underset{(3x3)}{\boldsymbol{0}} & \underset{(3x3)}{V^{(2)}\boldsymbol{I}} & \underset{(3x3)}{\boldsymbol{0}} & \underset{(3x3)}{V^{(3)}\boldsymbol{I}} & \underset{(3x3)}{\boldsymbol{0}} & \underset{(3x3)}{V^{(4)}\boldsymbol{I}} \end{bmatrix} \tag{3.27}$$

$$\boldsymbol{A}_2^{M,t} = \begin{bmatrix} \underset{(3x3)}{-\boldsymbol{C}_{ax}^{(1)}} & \underset{(3x3)}{\boldsymbol{0}} & \underset{(3x3)}{\boldsymbol{C}_{ax}^{(2)}} & \underset{(3x3)}{\boldsymbol{0}} & \underset{(3x3)}{\boldsymbol{0}} & \underset{(3x3)}{\boldsymbol{0}} & \underset{(3x3)}{\boldsymbol{0}} & \underset{(3x3)}{\boldsymbol{0}} \\ \underset{(3x3)}{\boldsymbol{0}} & \underset{(3x3)}{-\boldsymbol{C}_{sh}^{(1)}} & \underset{(3x3)}{\boldsymbol{0}} & \underset{(3x3)}{-\boldsymbol{C}_{sh}^{(1)}} & \underset{(3x3)}{\boldsymbol{0}} & \underset{(3x3)}{\boldsymbol{0}} & \underset{(3x3)}{\boldsymbol{0}} & \underset{(3x3)}{\boldsymbol{0}} \\ \underset{(3x3)}{\boldsymbol{0}} & \underset{(3x3)}{-\boldsymbol{C}_{sh}^{(1)}} & \underset{(3x3)}{\boldsymbol{0}} & \underset{(3x3)}{\boldsymbol{0}} & \underset{(3x3)}{\boldsymbol{0}} & \underset{(3x3)}{\boldsymbol{C}_{sh}^{(3)}} & \underset{(3x3)}{\boldsymbol{0}} & \underset{(3x3)}{\boldsymbol{0}} \\ \underset{(3x3)}{\boldsymbol{0}} & \underset{(3x3)}{-\boldsymbol{C}_{sh}^{(1)}} & \underset{(3x3)}{\boldsymbol{0}} & \underset{(3x3)}{\boldsymbol{0}} & \underset{(3x3)}{\boldsymbol{0}} & \underset{(3x3)}{\boldsymbol{0}} & \underset{(3x3)}{\boldsymbol{0}} & \underset{(3x3)}{\boldsymbol{C}_{sh}^{(4)}} \end{bmatrix} \tag{3.28}$$

where:

$$\boldsymbol{C}_{ax} = \begin{bmatrix} C_{1111} & C_{1122} & C_{1133} \\ C_{2211} & C_{2222} & C_{2233} \\ C_{3311} & C_{3322} & C_{3333} \end{bmatrix}, \quad \boldsymbol{C}_{sh} = \begin{bmatrix} C_{1212} & 0 & 0 \\ 0 & C_{1212} & 0 \\ 0 & 0 & C_{1212} \end{bmatrix} \tag{3.29}$$

$$\boldsymbol{D}_1^{\mathrm{M}} = \begin{bmatrix} \underset{(3x3)}{\boldsymbol{I}} & \underset{(3x3)}{\boldsymbol{0}} \\ \underset{(3x3)}{\boldsymbol{I}} & \underset{(3x3)}{\boldsymbol{0}} \\ \underset{(3x3)}{\boldsymbol{I}} & \underset{(3x3)}{\boldsymbol{0}} \\ \underset{(3x3)}{\boldsymbol{0}} & \underset{(3x3)}{\boldsymbol{I}} \end{bmatrix} \tag{3.30}$$

The $\boldsymbol{B}^{(m),t}$ matrices in Eq. (3.12) are then formed using Eqs. (3.25) and (3.26), which in linearized relations are:

$$\underset{(24x6)}{\left[\boldsymbol{B}^{(m),t}\right]} = \underset{(24x24)}{\begin{bmatrix} \boldsymbol{A}_1^M \\ \boldsymbol{A}_2^{M,t} \end{bmatrix}^{-1}} \underset{(24x6)}{\begin{bmatrix} \boldsymbol{D}_1^M \\ \boldsymbol{O} \end{bmatrix}} \tag{3.31}$$

Once the $\boldsymbol{B}^{(m),t}$ matrices are determined, the effective homogenized stresses and stiffness matrix can be solved using Eqs. (3.14) and (3.15), respectively.

3.1.2 FORMULATION OF THE EFFECTIVE THERMAL CONDUCTIVITY

A volume averaging method based on a spatial variation of the temperature gradient in each subcell is adopted to determine the effective thermal conductivity of the particle reinforced composites. The average heat flux and temperature gradient are:

$$\bar{q}_i = \frac{1}{V}\sum_{m=1}^{N} \int_{V^{(m)}} q_i^{(m)}(x_k^{(m)})dV^{(m)} \approx \frac{1}{V}\sum_{m=1}^{N} V^{(m)} q_i^{(m)} \tag{3.32}$$

$$\bar{\varphi}_i = \frac{1}{V}\sum_{m=1}^{N} \int_{V^{(m)}} \varphi_i^{(m)}(x_k^{(m)})dV^{(m)} \approx \frac{1}{V}\sum_{m=1}^{N} V^{(m)} \varphi_i^{(m)} \tag{3.33}$$

The average heat flux equation for a homogeneous composite medium is expressed by the Fourier law of heat conduction as:

$$\bar{q}_i^t = -\bar{K}_{ij}^t \bar{\varphi}_j^t \quad where \ \bar{\varphi}_j^t = \frac{d\bar{T}^t}{dx_j} \tag{3.34}$$

It is noted that the components of the conductivity tensor, $\bar{K}_{ij}^t$, varies with temperature as the thermal conductivity for each constituent is allowed to vary with temperature. The heat flux at the current time within a FE scheme is solved numerically as:

$$\bar{q}_i^t = \bar{q}_i^{t-dt} + d\bar{q}_i^t \tag{3.35}$$

In uncoupled thermo-mechanical problems in which the dissipation of energy is neglected, the temperature field can be solved without the knowledge of the stress-strain fields. However, for fully coupled thermo-mechanical problems the temperature field must be obtained by taking into account the heat generation due to the dissipation of energy in viscoelastic bodies. The incremental heat flux can be written as

$$d\bar{q}_i^t = -\bar{K}_{ij}^t d\bar{\varphi}_j^t \tag{3.36}$$

The homogenized temperature gradient and heat flux relations are summarized as follows:

$$d\bar{\varphi}_i^t = \frac{1}{V^{(A)}}\left[V^{(1)} d\varphi_i^{(1),t} + V^{(2)} d\varphi_i^{(2),t}\right] = d\varphi_i^{(3),t} = d\varphi_i^{(4),t} \tag{3.37}$$

$$d\bar{q}_i^t = \frac{1}{V}\left[V^{(A)} dq_i^{(A),t} + V^{(3)} dq_i^{(3),t} + V^{(4)} dq_i^{(4),t}\right] \tag{3.38}$$

$$dq_i^{(A),t} = dq_i^{(1),t} = dq_i^{(2),t} \tag{3.39}$$

where the total volume of the subcells 1 and 2 in Eqs. (3.37) and (3.38) is

$V^{(A)} = V^{(1)} + V^{(2)}$.

We introduce a concentration tensor that relates the average temperature gradient of each subcell with the overall temperature gradient across the unit cell. Let $\boldsymbol{M}^{(m),t}$ be the concentration tensor of the temperature gradient. The temperature gradient in each subcell is given by

$$d\varphi_i^{(m),t} = M_{ij}^{(m),t} d\bar{\varphi}_j^t \tag{3.40}$$

and the incremental form of the heat flux in each subcell is expressed as:

$$dq_i^{(m),t} = -K_{ij}^{(m),t} M_{jk}^{(m),t} d\bar{\varphi}_k^t \tag{3.41}$$

The average heat flux in the unit-cell model is approximated as:

$$d\bar{q}_i^t = \frac{1}{V}\sum_{m=1}^{4} V^{(m)} dq_i^{(m),t} \tag{3.42}$$

Substituting Eq. (3.41) into (3.42) gives:

$$d\bar{q}_i^t = -\frac{1}{V}\sum_{m=1}^{4} V^{(m)} K_{ij}^{(m),t} M_{jk}^{(m),t} d\bar{\varphi}_k^t \tag{3.43}$$

Comparing the above equation with Eq. (3.36) gives the tangent effective thermal conductivity matrix of the composite, which is:

$$\bar{K}_{ik}^t = -\frac{1}{V}\sum_{m=1}^{4} V^{(m)} K_{ij}^{(m),t} M_{jk}^{(m),t} \tag{3.44}$$

To formulate the $\boldsymbol{M}^{(m),t}$ matrix that relates the average subcells temperature gradient with the overall temperature gradient across the unit cell, the micromechanical relations and the constitutive equations are imposed. The present micromechanical model consists of four (4) subcells with three (3) components of heat flux need to be determined for

every subcell. This requires forming twelve (12) equations. The first sets of equations are determined from the temperature continuity at the interface of each subcell in Eq. (3.37), which leads to the following equation:

$$\underset{(9\text{ x }12)}{\left[\boldsymbol{A}_1\right]}\underset{(12\text{x}1)}{\left\{\begin{matrix} d\varphi_i^{(1),t} \\ d\varphi_i^{(2),t} \\ d\varphi_i^{(3),t} \\ d\varphi_i^{(4),t} \end{matrix}\right\}} = \underset{(9\text{x}3)}{\left[\boldsymbol{D}_1\right]}\underset{(3\text{x}1)}{\{d\bar{\varphi}_i^{t}\}} \tag{3.45}$$

The second sets of equations are formed based on heat flux continuity relations, Eq. (3.38) which can be expressed as:

$$\underset{(3\text{x}12)}{\left[\boldsymbol{A}_2^t\right]}\underset{(12\text{x}1)}{\left\{\begin{matrix} d\varphi_i^{(1),t} \\ d\varphi_i^{(2),t} \\ d\varphi_i^{(3),t} \\ d\varphi_i^{(4),t} \end{matrix}\right\}} = \underset{(3\text{x}3)}{\left[\boldsymbol{O}\right]}\underset{(3\text{x}1)}{\{d\bar{\varphi}_i^{t}\}} \tag{3.46}$$

By substituting Eq. (3.40) to Eqs. (3.45) and (3.46), the $\boldsymbol{M}^{(m),t}$ matrix can be determined, which is:

$$\underset{(12\text{x}3)}{\left[\boldsymbol{M}^{(m),t}\right]} = \underset{(12\text{x}12)}{\begin{bmatrix} \boldsymbol{A}_1 \\ \boldsymbol{A}_2^t \end{bmatrix}^{-1}}\underset{(12\text{x}3)}{\begin{bmatrix} \boldsymbol{D}_1 \\ \boldsymbol{O} \end{bmatrix}} \tag{3.47}$$

The matrix $\boldsymbol{O}$ is the zero matrix and the components of matrix $\boldsymbol{A}_1$, $\boldsymbol{A}_2^t$ and $\boldsymbol{D}_1$ are given as follows:

$$\boldsymbol{A}_1 = \begin{bmatrix} \frac{V^{(1)}}{V^{(A)}}\underset{(3x3)}{\boldsymbol{I}} & \frac{V^{(2)}}{V^{(A)}}\underset{(3x3)}{\boldsymbol{I}} & \underset{(3x3)}{\boldsymbol{0}} & \underset{(3x3)}{\boldsymbol{0}} \\ \underset{(3x3)}{\boldsymbol{0}} & \underset{(3x3)}{\boldsymbol{0}} & \underset{(3x3)}{\boldsymbol{I}} & \underset{(3x3)}{\boldsymbol{0}} \\ \underset{(3x3)}{\boldsymbol{0}} & \underset{(3x3)}{\boldsymbol{0}} & \underset{(3x3)}{\boldsymbol{0}} & \underset{(3x3)}{\boldsymbol{I}} \end{bmatrix} \tag{3.48}$$

$$\boldsymbol{A}_2^t = \begin{bmatrix} K^{(1),t}\underset{(3x3)}{\boldsymbol{I}} & -K^{(2),t}\underset{(3x3)}{\boldsymbol{I}} & \underset{(3x3)}{\boldsymbol{0}} & \underset{(3x3)}{\boldsymbol{0}} \end{bmatrix} \tag{3.49}$$

$$\boldsymbol{D}_1 = \begin{bmatrix} \underset{(3x3)}{\boldsymbol{I}} \\ \underset{(3x3)}{\boldsymbol{I}} \\ \underset{(3x3)}{\boldsymbol{I}} \end{bmatrix} \tag{3.50}$$

3.1.3 FORMULATION OF THE EFFECTIVE ENERGY EQUATION

In this section, the effective coupled energy equation for the thermoviscoelastic composite materials is presented. The expression for the effective heat flux, temperature gradient and thermal conductivity were already obtained in section 3.1.2 through the micromechanical modeling approach. The effective heat capacity is defined by volume average of the constituents.

The energy equation for an isotropic homogeneous material was derived in Chapter II, which can be written as follows:

$$\rho c_\sigma \dot{T} + \dot{w}_{dis}^{E,t} = kT_{,ii} + \dot{w}_{dis}^{t} \tag{3.51}$$

where $\dot{w}_{dis}^{E,t}$ and $\dot{w}_{dis}^{t}$ are the thermo-elastic and viscous energy dissipation, respectively, and expressed as

$$\dot{w}_{dis}^{E,t} = \frac{\partial \alpha(T)}{\partial T} T\dot{T}\sigma_{kk} + \frac{\partial \alpha(T)}{\partial T} T\theta\dot{\sigma}_{kk} + T\alpha(T)\dot{\sigma}_{kk} + T\frac{\partial g_0(\bar{\sigma}, T)}{\partial T} D_{ijkl}^{e}\dot{\sigma}_{ij}\sigma_{kl}$$
$$\dot{w}_{dis}^{t} = g_1(\bar{\sigma}^t, T^t)\sigma_{ij}^{vis,t}\frac{d}{dt}\int_0^{\psi} dD\left(\psi^t - \psi^\tau\right)\frac{d}{d\tau}\left(g_2(\bar{\sigma}^\tau, T^\tau)\sigma_{ij}\right)d\tau \tag{3.52}$$

Taking the volume average of Eq. (3.51) over the volume V of the unit cell, the following energy equation results

$$\overline{\rho c}_\sigma \dot{\bar{T}} + \bar{\dot{w}}_{dis}^{E,t} = \overline{kT}_{,ii} + \bar{\dot{w}}_{dis}^{t} \tag{3.53}$$

The effective density and specific heat at a constant stress can be expressed as

$$\bar{\rho} \approx \frac{1}{V}\sum_{m=1}^{N} V^{(m)}\rho^{(m)} \tag{3.54}$$

$$\bar{c}_\sigma \approx \frac{1}{V}\sum_{m=1}^{N} V^{(m)} c_\sigma^{(m)} \tag{3.55}$$

The two effective heat generations terms can be expressed in a similar way as

$$\bar{\dot{w}}_{dis}^{E,t} \approx \frac{1}{V}\sum_{m=1}^{N} V^{(m)}\dot{w}_{dis}^{E,t(m)} \tag{3.56}$$

$$\bar{\dot{w}}_{dis}^{t} \approx \frac{1}{V}\sum_{m=1}^{N} V^{(m)}\dot{w}_{dis}^{t\ (m)} \tag{3.57}$$

In addition to these effective field variables we also need to find out the effective Jacobians, i.e., $\bar{C}_{ijkl}^{t}$, $\overline{\partial\sigma_{ij}^{t}/\partial T^{t}}$, $\overline{\partial\dot{w}_{dis}^{t}/\partial\varepsilon_{ij}^{t}}$, $\overline{\partial\dot{w}_{dis}^{t}/\partial T^{t}}$ etc. The effective stiffness matrix $\bar{C}_{ijkl}^{t}$ is given in Eq. (3.15) while the other effective Jacobians are simply the volume averages of the subcell's Jacobians.

The numerical algorithm for the nonlinear coupled thermoviscoelastic behavior of the particulate composite under general mechanical and temperature loading histories is

presented. The algorithm is implemented in displacement based FE structural analyses. Linearized solutions of the nonlinear constitutive equations and iterative schemes are performed at the macro (structural), micro and constituent levels. At the structural level, the default, the default ABAQUS (2005) iterative solver is used for the solution of nonlinear equations. At the micro level the micromechanical relations along with the nonlinear thermoviscoelastic constitutive equations at each subcells must be satisfied simultaneously. Therefore, an iterative scheme is added at the micro and material levels to minimize errors arising from the linearization of nonlinear response and/or time-dependent constituent at the subcells. The linearized micromechanical relations are satisfied only when all subcells exhibit linear elastic response. The numerical algorithm for fully coupled thermoviscoelastic analyses of particulate composite is summarized in Figure. 3.2.

The numerical algorithm to analyze coupled thermoviscoelastic response is integrated with the ABAQUS/standard FE code. At each integration point in the FE mesh, the user subroutines UMATH and UMAT are called. Within UMAT, the numerical algorithm to obtain the effective nonlinear thermo-viscoelastic response of the particulate composite is defined, which is used to provide the effective stresses, consistent tangent stiffness matrix $\overline{C}_{ijkl}^{t,(k)}$, stress variation with respect to strain ($\overline{\partial \sigma_{ij}^{t} / \partial T^{t}}$), heat generated rate ($\overline{\dot{w}}_{dis}^{t}$), variation of heat generation with respect to strain ($\overline{\partial \dot{w}_{dis}^{t} / \partial \varepsilon_{ij}^{t}}$) and temperature ($\overline{\partial \dot{w}_{dis}^{t} / \partial T^{t}}$). The effective thermal constitutive behavior is defined within UMATH which is used to define and update the effective internal

energy $\bar{\mathcal{E}}^{\mathrm{t,(k)}}$, variation of internal energy with respect to temperature $\overline{\left(\mathrm{d}\mathcal{E}/\mathrm{dT}\right)^{\mathrm{t,(k)}}}$ and temperature gradient $\overline{\left(\mathrm{d}\mathcal{E}/\mathrm{dg}\right)^{\mathrm{t,(k)}}}$, heat flux $\bar{q}_i^{\mathrm{t,(k)}}$, heat flux variation with respect to temperature $\overline{\left(\mathrm{d}q_i/\mathrm{dT}\right)^{\mathrm{t,(k)}}}$ and temperature gradient $\overline{\left(\mathrm{d}q_i/\mathrm{dg}\right)^{\mathrm{t,(k)}}}$.

Now, the numerical algorithm within the UMAT subroutine is described in detail. Let the superscript (k) denotes the global iteration counter within the current incremental time step. At each global iteration within the incremental time-step $dt^{(k)}$, trial incremental effective strain tensor $d\bar{\varepsilon}_{ij}^{t,(k)}$ and temperature $d\bar{T}^{t,(k)}$ are obtained, as illustrated in Figure 3.1. The goal is to calculate the effective stresses and Jacobians from given current variables and history variables stored from the previous converged solution at time $(t-dt)$. The converged $\bar{\sigma}_{ij}^{t}$ and effective Jacobians after K global iteration at the current time *t* will be used to provide incremental trial strains for the next time step $(t+dt)$. Due to the coupled thermo-mechanical problems, the trial incremental temperature $dT^{t,(k)}$ is directly linked to the incremental time step. However, for each global iteration, the temperature is obtained from solving the effective energy equation (3.53).

In this study the solution for the thermal and deformation fields are done incrementally due to the nonlinear and time-dependent constitutive response in the

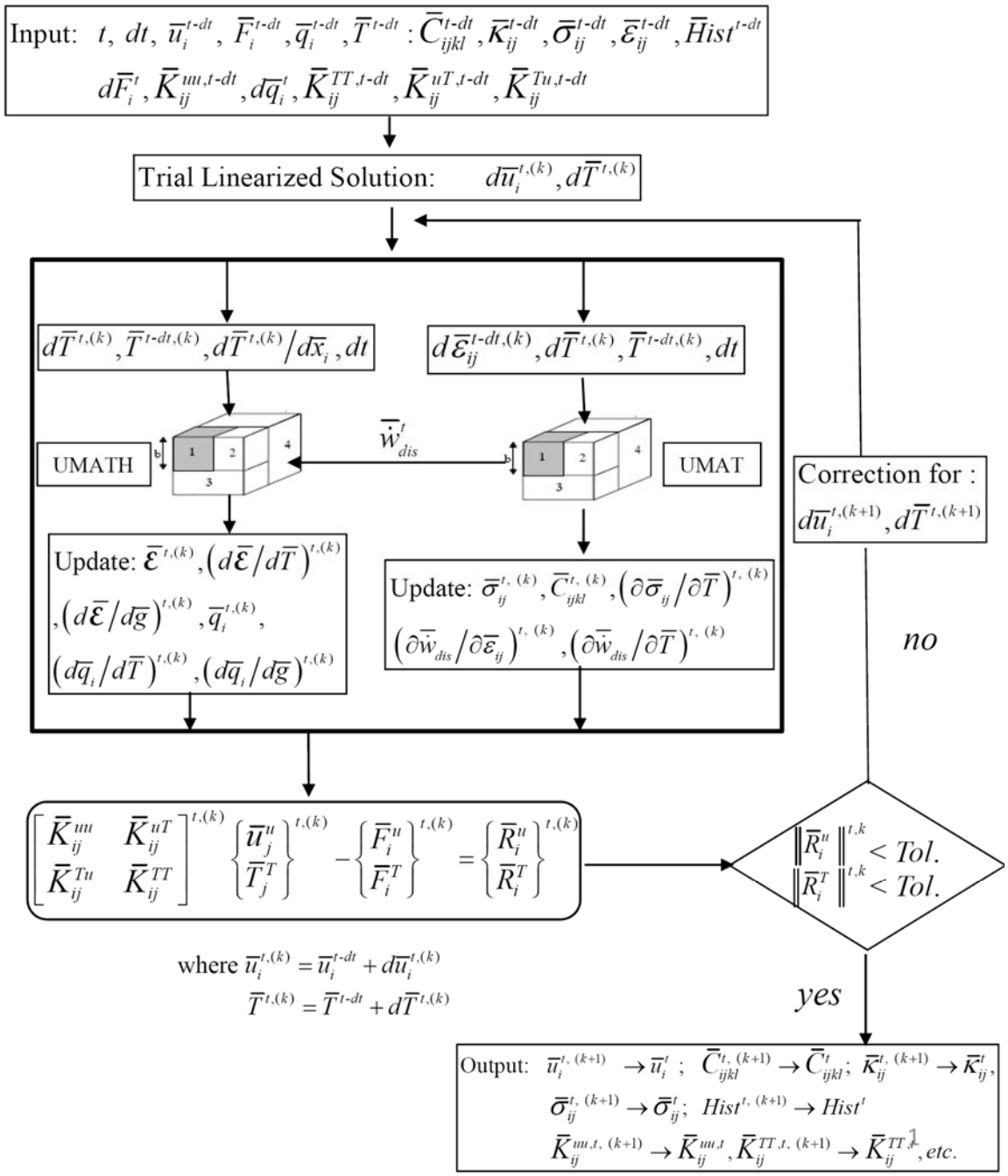

Figure 3.2 Numerical algorithm for the coupled thermo-viscoelastic behavior of particulate composite.

constituents. At the beginning of time increment using the backward Euler method, the linearized micromechanical relations are used to define the trial stresses and strains for each sub-cell. Due to the nonlinear and viscoelastic response in the matrix subcells, the linearized micromechanical relations result in non-zero residual vectors when the traction continuity and displacement compatibility at the subcells inter-faces are imposed. The strain-stress correction algorithm is needed to minimize the residual vectors. Since the stress and strain in each sub-cell are related through the constitutive relations, the correction is performed only for 24 independent variables. To minimize the residual the Newton–Raphson (NR) typed iterative method is used. In this study, the corrections are done for the strain and therefore the components of total strains in each sub-cell $\varepsilon_{ij}^{(\alpha),t} = \varepsilon_{ij}^{(\alpha),t-\Delta t} + d\varepsilon_{ij}^{(\alpha),t}$ are chosen as independent variables, which are

$$X^T = \left\{ \varepsilon^{(1),t} \quad \varepsilon^{(2),t} \quad \varepsilon^{(3),t} \quad \varepsilon^{(4),t} \right\}_{(1x24)} \tag{3-58}$$

The stress components in the sub-cells depend on the independent variables X_{ij}. The residual vector $\boldsymbol{R} = \left\{ \boldsymbol{R}_\sigma, \boldsymbol{R}_\varepsilon \right\}$ given in Eqs. (3-25) and (3-26) are used to correct for the trial solution. This requires defining the Jacobian tensor, which is given by

$$\left[\frac{\partial R_{ij}}{\partial X_{kl}} \right] = \begin{bmatrix} C_{ax}^{(1)} & 0 & -C_{ax}^{(2)} & 0 & 0 & 0 & 0 & 0 \\ 0 & C_{sh}^{(1)} & 0 & C_{sh}^{(2)} & 0 & 0 & 0 & 0 \\ 0 & C_{sh}^{(1)} & 0 & 0 & 0 & -C_{sh}^{(3)} & 0 & 0 \\ 0 & C_{sh}^{(1)} & 0 & 0 & 0 & 0 & 0 & -C_{sh}^{(4)} \\ f_1 I & 0 & f_2 I & 0 & 0 & 0 & 0 & 0 \\ 0 & 0 & 0 & 0 & I & 0 & 0 & 0 \\ 0 & 0 & 0 & 0 & 0 & 0 & I & 0 \\ 0 & V^{(1)} I & 0 & V^{(2)} I & 0 & V^{(3)} I & 0 & V^{(4)} I \end{bmatrix}_{(24\ x\ 24)} \tag{3-59}$$

$$f_1 = \frac{V^{(1)}}{V^{(1)} + V^{(2)}}, \qquad f_2 = \frac{V^{(2)}}{V^{(1)} + V^{(2)}} \tag{3-60}$$

where ***I*** and ***O*** are the 3x3 identity and zero matrices, respectively. A solution is said to be converged when all residual vectors defined using the micromechanical relations and for the time-dependent constitutive equations are diminished. The following procedure is performed at every material (Gaussian) integration point within elements at each structural iteration to achieve convergence at the structural, micromechanical and material levels simultaneously.

1. Input variables: (At the k^{th} global iteration)
   $d\bar{\varepsilon}_{ij}^{t,(k)}$, $dt^{(k)}$, $d\bar{T}^{t,(k)}$
   $\bar{\varepsilon}_{ij}^{t-\Delta t}, \bar{\sigma}_{ij}^{t-\Delta t}, \bar{T}^{t-\Delta t}, Hist^{t-\Delta t}$

   1.1 Calculate: $\bar{\varepsilon}_{ij}^{t,(k)} = \bar{\varepsilon}_{ij}^{t-\Delta t} + d\bar{\varepsilon}_{ij}^{t,(k)}$, $\bar{T}^{t,(k)} = \bar{T}^{t-\Delta t} + d\bar{T}^{t,(k)}$

2. Initial linearized approximation variables:

   $B_{ijkl}^{(\alpha),t,tr}(\ C_{ijkl}^{(\alpha),t-dt}, V),\ \ \alpha = 1,2,3,4$
   $d\varepsilon_{ij}^{(\alpha),t,tr,M} = B_{ijkl}^{(\alpha),t,tr} d\bar{\varepsilon}_{kl}^{t,(k),M}, \quad d\sigma_{ij}^{(\alpha),t,tr} = C_{ijkl}^{(\alpha),t}\ d\varepsilon_{ij}^{(\alpha),t,tr,M}$
   $\varepsilon_{ij}^{(\alpha),t,tr} = \varepsilon_{ij}^{(\alpha),t-\Delta t} + d\varepsilon_{ij}^{(\alpha),t,tr}, \sigma_{ij}^{(\alpha),t,tr} = \sigma_{ij}^{(\alpha),t-\Delta t} + d\sigma_{ij}^{(\alpha),t,tr}$

3. Iterate for m = 1, 2, 3. . . (m = local iteration counter at the micro level)

   3.1 Evaluate stresses at all subcells to obtain $\sigma_{ij}^{(\alpha),t,(m+1)}, C_{ijkl}^{(\alpha),t,(m)}$ (recursive iterative algorithm, Chapter II)

   3.2 Compute the strain correction at all subcells:
   Define: $X_{ij}^{t,(m+1)} = X_{ij}^{t,(m)} + \left[\frac{\partial R_{ij}^{t,(m)}}{\partial X_{kl}}\right]^{-1} R_{kl}^{t,(m)}$ for the total strain correction

   3.3 Evaluate residual vector: $R_{ij}^{t,(k+1)} = \left\{(R_{ij}^{t,(k+1)})_{\sigma}, (R_{ij}^{t,(k+1)})_{\varepsilon}\right\}$
   IF $\left\|R_{ij}^{t,(k+1)}\right\| \le Tol$ THEN GOTO 4 and EXIT

ENDIF GOTO 3

4. Update: $\bar{\sigma}_{ij}^{t,(k+1)} \to \sigma_{ij}^{t,k}, \bar{C}_{ijkl}^{t,(k+1)} \to \bar{C}_{ijkl}^{t,(k)}, Hist^t$

$\dot{w}_{dis}^t, \overline{\partial \sigma_{ij}^t / \partial T^t}, \overline{\partial \dot{w}_{dis}^t / \partial \varepsilon_{ij}^t}, \overline{\partial \dot{w}_{dis}^t / \partial T^t}$

3.2 NUMERICAL IMPLEMENTATION AND VERIFICATION

The proposed micromechanical model is implemented in a 3D continuum element using subroutines UMAT, UEXPAN and UMATH of ABAQUS FE code. The capability of the proposed micromechanical model in predicting the effective mechanical, thermal and viscoelastic response of a particulate composite is presented. Available analytical and experimental works reported in the literature are used for comparisons. The convergence study of fully coupled thermoviscoelastic analyses is also presented.

3.2.1. ELASTIC RESPONSE

The effective linear elastic properties of composites obtained from the proposed micromechanical model are compared with the micromechanical models of Dvorak and Srinivas (1999), Mori and Tanaka (1973) and self consistent model. These verifications have been done by Muliana and Kim (2007). A composite system made of silicon carbide particles embedded in the aluminum matrix is considered. Both particle and matrix are modeled as isotropic linear elastic. The elastic material properties of both constituents are taken from Eroshkin and Tsukrov (1995), which are given in Table 3.1. The effective shear and Young's moduli for several composite volume fractions are shown in Figures 3.3(a)-(b). The effective properties calculated from the proposed micromechanical model are comparable with other micromechanical models.

Table 3.1 Elastic properties of silicon carbide particle and aluminum matrix (Eroshkin and Tsukrov, 1995).

Constituents	Young modulus, (E) (MPa)	Poisson ratio, (v)
Silicon carbide	450000	0.17
Aluminum	70000	0.30

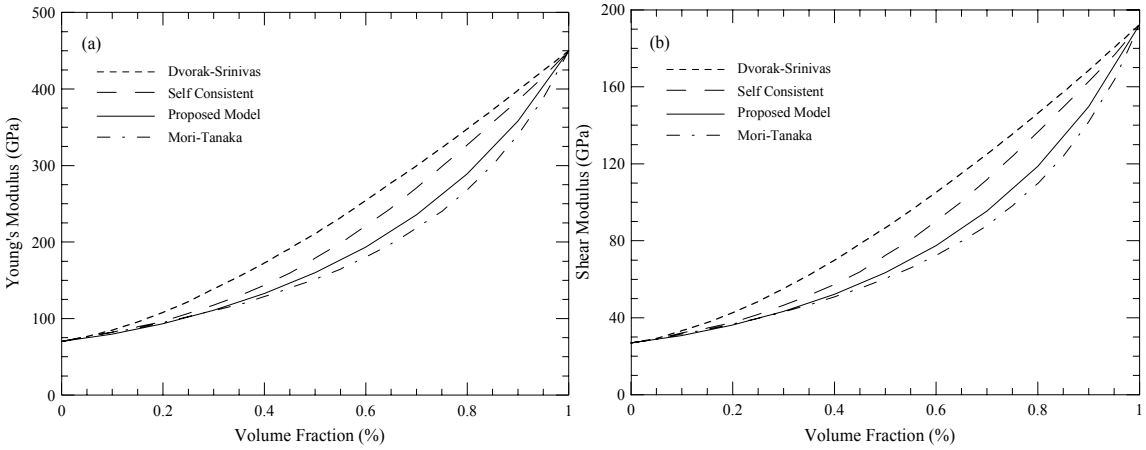

Figure 3.3 Effective composite (a) Young's and (b) Shear moduli.

Next, the nonlinear elastic response of composite is compared with available experimental data of Cho et al. (2006). These verifications are done by Muliana and Kim (2007).The experiments were performed for 5% volume fraction of glass beads embedded in vinylester resin. Four different diameters of particles were considered, i.e., 6, 70, 200 and 500 μm. The nonlinear stress dependent elastic modulus of the unreinforced vinylester resin is modeled using parameter g_0 (see Eq. (2.32)-(2.33)), which is fitted using a power law function, i.e., $g_0 = 1 + C\sigma^n$. The calibrated nonlinear parameters (C and n) for the vinylester resin and elastic properties of both constituents are given in Table 3.2. The effective nonlinear responses for the 5% composite volume

fraction are then given in Figure. 3.4. Good prediction is shown by the proposed micromechanical model.

Table 3.2 Elastic properties and nonlinear parameters of glass beads and vinylester resin (Cho et al., 2006).

Constituents	Young modulus, (E) (MPa)	Poisson ratio, (v)	C	n
Glass bead	10500	0.25	-	-
Vinyester	600	0.30	0.00029	1.603

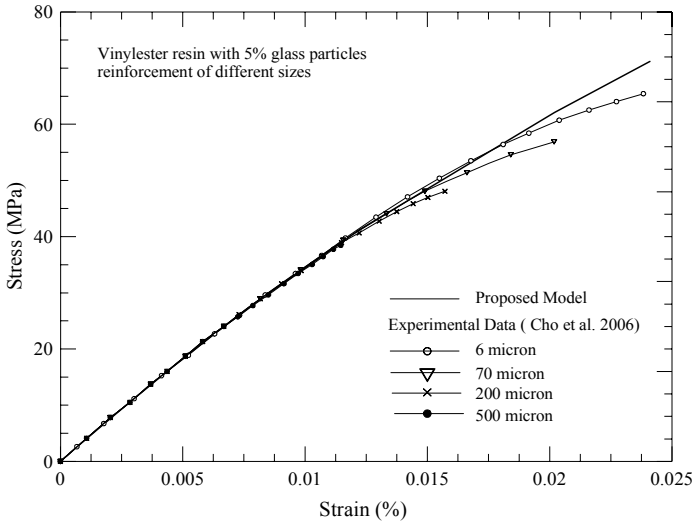

Figure 3.4 Nonlinear stress-strain relations for glass/vinylester composites.

3.2.2 VISCOELASTIC BEHAVIOR

The experimental creep compliance data reported by Aniskevich and Hristova (2000) are used to validate the accuracy of the proposed micromechanical model in predicting the effective viscoelastic responses of particulate composites (Muliana and Kim, 2007). Aniskevich and Hristova (2000) reported the long term creep data (4.1 months) of a polyester resin reinforced with diabase and marble spherical particles. The diabase and

marble reinforcements are assumed as linear elastic materials and the polyester resin follows a linear viscoelastic response. The linear elastic properties of the constituents and calibrated Prony parameters for linear viscoelastic behavior of the unreinforced polyester resin are given in Table 3.3.

The micromechanical model predictions of the composite's long-term transient compliances are illustrated in Figure. 3.5. The volume fractions of 0.36 and 0.2 are used

Table 3.3 Elastic Properties of diabase, marble and polyester resin and Prony series coefficients for polyester resin (Aniskevich and Hristova, 2000).

Constituents	Young modulus, (E) (MPa)	Poisson ratio, (v)
Glass	8800	0.26
Marble	440000	0.25
Polyester resin	5800	0.35
Prony series coefficients for polyester resin.		
n	$\lambda_n(\text{sec}^{-1})$	$D_n \times 10^{-6}(\text{MPa}^{-1})$
1	1.	4.50
2	10^{-1}	3.00
3	10^{-2}	5.40
4	10^{-3}	7.60
5	10^{-4}	16.0
6	10^{-5}	22.0
7	10^{-6}	25.0

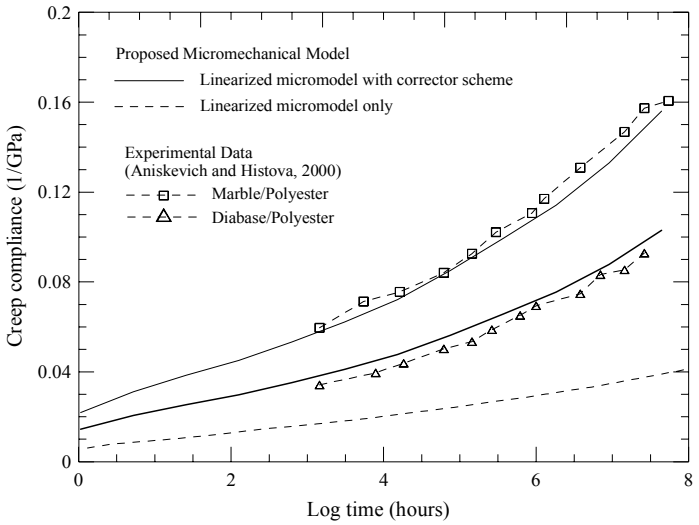

Figure 3.5 Long term creep compliance for polyester reinforced composites.

for diabase/polyester and marble/polyester composites, respectively. Good agreement with the experimental tests of Aniskevich and Hristova (2000) is shown for both diabase/polyester and marble/polyester systems. Figure 3.5 also presents the long-term responses of diabase/polyester from the proposed micromechanical model without the iterative correction scheme at the micro level. It is seen that using only linearized micromechanical relations lead to significant mismatch in predicting long-term material responses.

3.2.3 VERIFICATION OF THE EFFECTIVE CTE

The averaging procedure in the micromechanical model satisfies the traction continuity and displacement compatibility of the combined thermal and mechanical responses. Thus, the overall CTE of composites having viscoelastic matrix may indeed exhibit time-dependent behaviors. Furthermore, temperature changes in composites develop thermal stresses at each constituent due to different CTEs in the inclusion and

matrix. The existence of the thermal stresses can increase time-dependent deformations in the viscoelastic constituents. Under a constant temperature change, the overall time-dependent deformation is attributed to the constant thermal stress, which is a creep problem. If the strain is fixed, the stress in the viscoelastic constituent can relax with time and reduce the overall composite modulus. The viscoelastic characteristic may cause thermal stresses to relax, which may reduce the rate of creep deformations over longer time period.

The effective CTE obtained from the presented micromodel is compared with available analytical models. Figure 3.6 shows the effective CTE having linear thermo-elastic responses of the constituents. The studied composite material consists of glass beads as inclusions and FM73 polymer as matrix. The mechanical and thermal properties of the constituents are given in Table 3.4. The proposed model is compared with analytical

Table 3.4 Material properties used for CTE verification.

Material	Young Modulus (E), MPa	Poisson ratio (v)	Linear Thermal Expansion (α) 10^{-6}, 1/ K
Glass Bead	69000	0.3	8.5
FM73	2700	0.35	75
Zirconia	192000	0.23	9.40
Tin	42000	0.36	23.5
Glass	43000	0.13	6.45
Aluminum	69000	0.33	24
Silicon	107000	0.17	3.2
Ciba Geigy Epoxy Resin	3380	0.39	81
Silica Flour	95700	0.0775	10.5
Solid Glass	74000	0.24	6.9
Copper Powder	127050	0.346	16.5

models of Levin (1967), Wakashima (1974), Fahmy and Ragai (1970), which are obtained from the exact solutions. The present micromodel is a result of a numerical approximation following micromechanical averaging scheme. It is shown that the proposed model lies between the upper and lower bound which is acceptable as far as the effective properties are concerned. The results of the proposed micro-models are comparable to the ones reported by Levin (1967) and Fahmy and Ragai (1970).

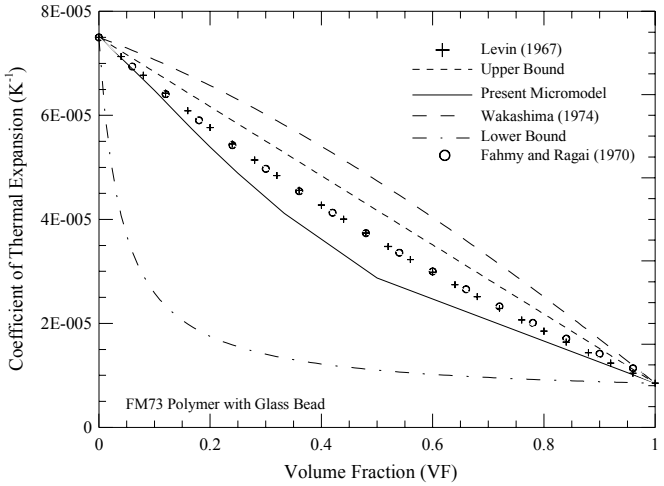

Figure 3.6 Comparison of the effective CTE with analytical models.

The effective CTEs of various composites are also compared with experimental data available in literature. Composite systems consisting of glass, zirconia and tin constituents are studied. The thermal and elastic properties of the glass, zirconia and tin constituents are taken from Tummala and Friedberg (1970), shown in Table 3.4. The material properties are assumed to be independent of temperature. Figure 3.7 illustrates the effective CTE at various volume fractions of the inclusions for two composite systems. In both cases, the micromodel shows good prediction. The experimental data of

Fahmy and Ragai (1970) is also used for verification. Figure 3.8 shows the comparison of the effective CTE of composites having aluminum and silicon constituents. The effective CTEs of the composite are plotted as a function of silicon contents. The experiments were conducted for two temperature ranges, i.e., at low temperature (between -196 C and 20 C) and at high temperature (between 20 C and 400 C). The temperature independent mechanical properties and thermal expansions of the silicon and aluminum are shown in Table 3.4. In both cases, the results of the proposed models are found in good agreement with the experimental data.

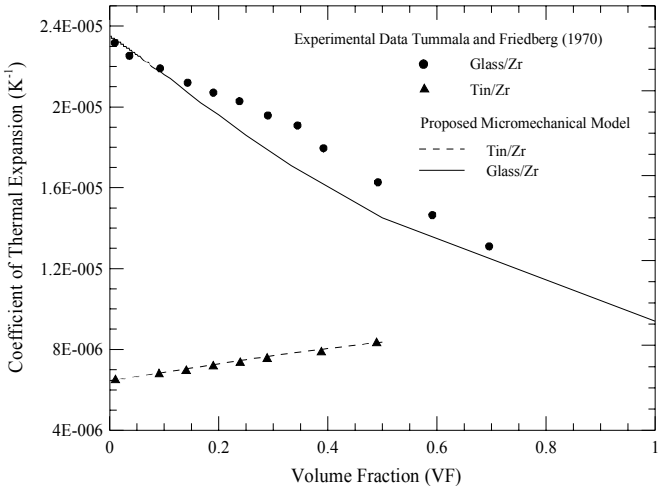

Figure 3.7 Comparisons of the effective CTE with the experimental data of Tummala and Friedberg (1970).

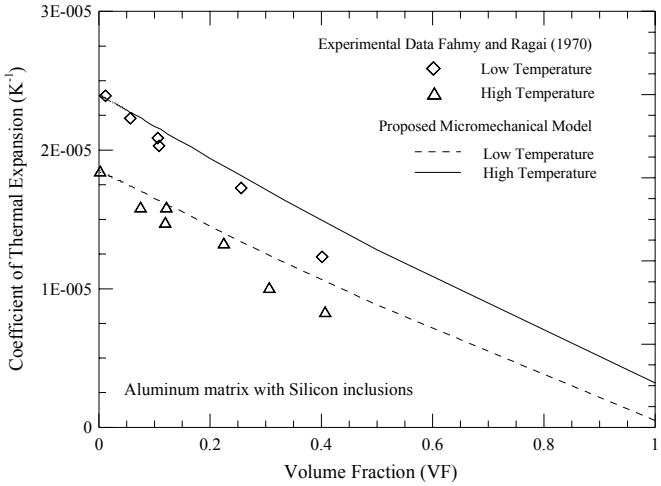

Figure 3.8 Comparisons of the effective CTE with the experimental data of Fahmy and Ragai (1970).

Feltham and Martin (1982) have experimentally studied the effects of temperatures on the effective CTE of the particle reinforced epoxy composites. The capability of the presented micromodel to predict the temperature dependent effective CTE is evaluated using Feltham and Martin (1982) experimental data. The effective CTEs of three composite systems, i.e., silica flour/epoxy, glass/epoxy and copper/epoxy, were measured for a temperature range of 100°K to 300°K and with particle volume fractions of 10%, 20%, 30 % and 40%. The elastic modulus of the epoxy resin at room temperature are taken from Feltham and Martin (1982), while the temperature dependent elastic modulus of the epoxy resin are obtained from Hartwig and Wuchner (1975). The temperature dependent CTEs of the epoxy resin and solid glass are taken from Feltham and Martin (1982) while the one for the silica flour is given in Touloukian et. al (1977). The elastic moduli of the particles are assumed to be independent of temperature and taken from Simmons and Wang (1971). The temperature dependent properties of the

constituents are shown in Figure 3.9, while the properties at the reference temperature (300 K) are given in Table 3.4.

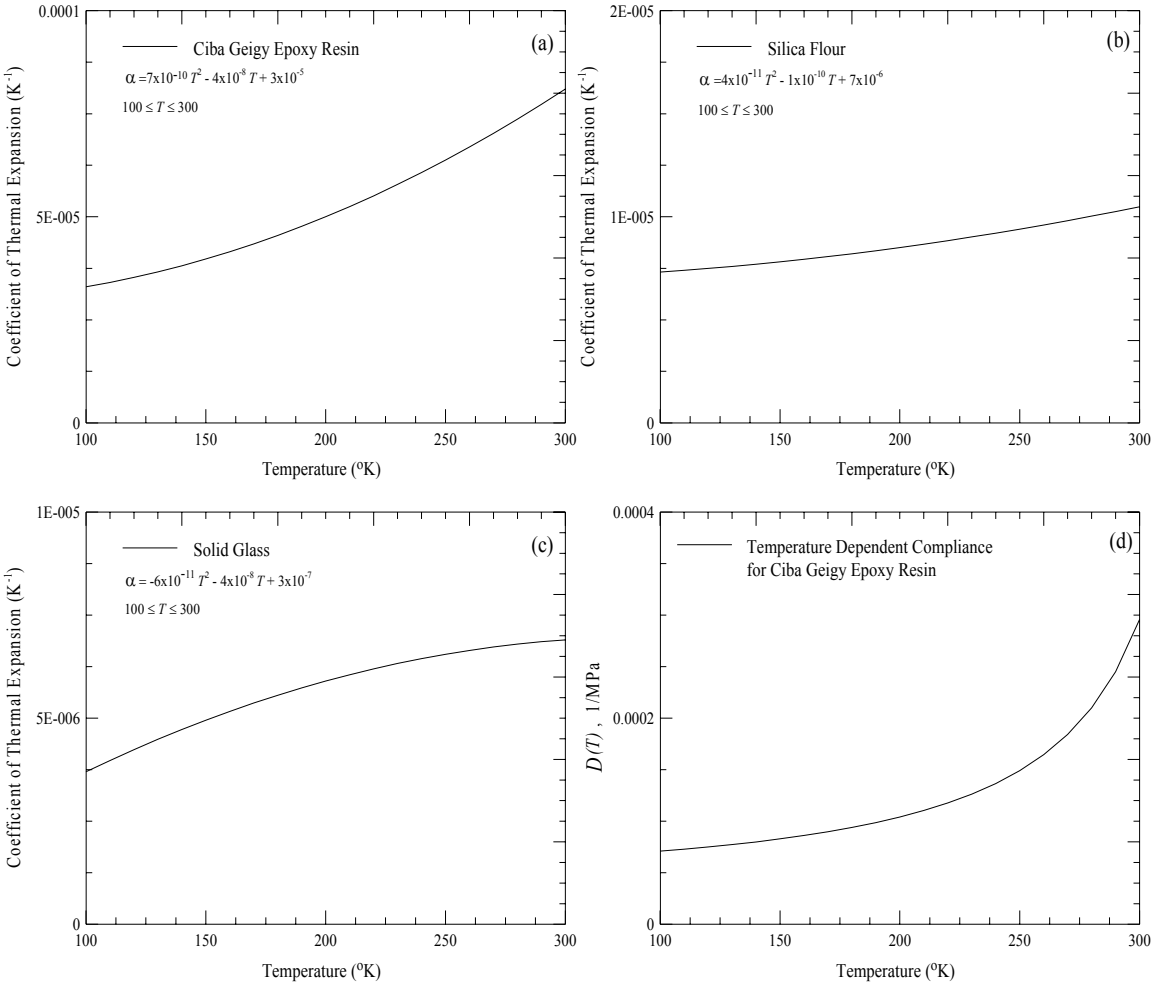

Figure 3.9 Non linear temperature dependent constituents properties a) CTE for Ciba Geigy epoxy resin, b) CTE for silica flour c) CTE for solid glass and d) temperature dependent compliance for Ciba Geigy epoxy resin.

Figure 3.10 shows predictions of the effective CTE of the silica flour/epoxy composites. Analytical models of Fahmy and Ragai (1970) and Turner (1946) are also reported. It is observed that the present micromodel predicts the experimental data very well and also comparable to the Fahmy and Ragai (1970) model. Figure 3.11 (a) shows a

CTE of a composite system consists of Ciba-Geigy epoxy resin with solid glass microspheres, while Figure 3.11 (b) illustrates a CTE for copper powder particles dispersed in epoxy resin. In both composites, response obtained from the micromechanical model is in good agreement with the experimental data.

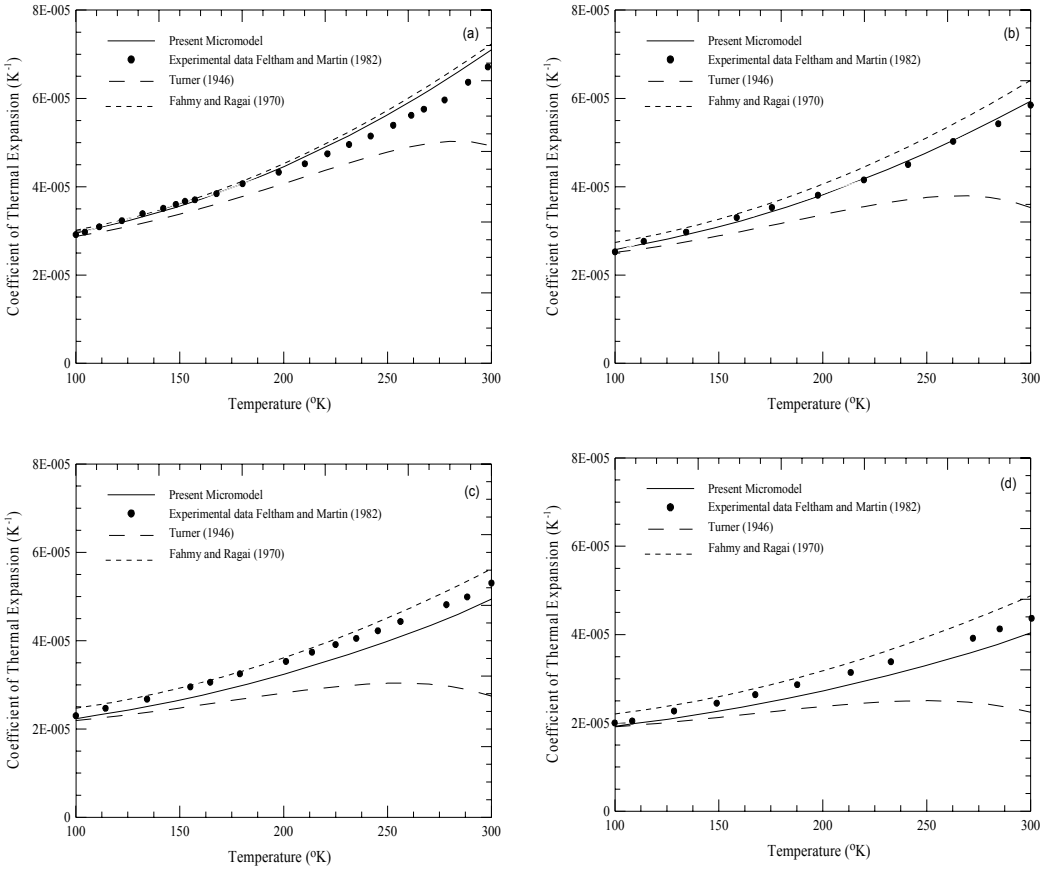

Figure 3.10 Temperature dependent effective CTE of Ciba-Geigy epoxy resin containing silica flour at different volume fraction (a) 10%, (b) 20% (c) 30% and (d) 40%.

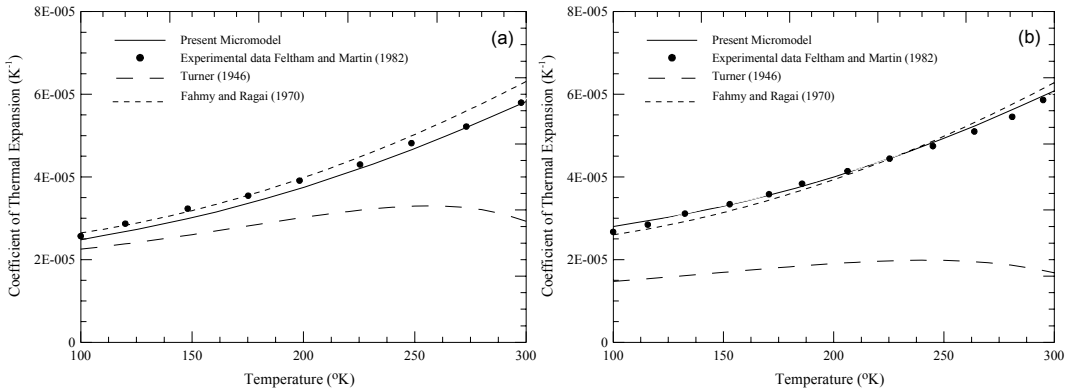

Figure 3.11 Temperature dependent effective CTE of Ciba-Geigy epoxy resin containing (a) solid glass microspheres and (b) copper powder at volume fraction of 20%.

The present micromodel is derived for predicting the effective CTE of composites having nonlinear thermo-viscoelastic responses. Several numerical simulations have been performed to analyze the time-dependent effective CTEs of the composite. The time-dependent behavior of the effective CTE is found to be dependent on the elastic moduli and the coefficient of thermal expansion of the constituents and the roles of the constituents as inclusion and matrix, i.e., stiffer inclusions dispersed in a softer matrix or softer inclusion in a stiffer matrix. Four parametric studies have been done to determine the effects of the particle and matrix thermal expansion and instantaneous elastic moduli on the overall time-dependent CTE of the particulate composite. In all studies, the matrix modulus follows a nonlinear viscoelastic model, while the particle has linear elastic behavior. The nonlinear and time-dependent properties of the epoxy matrix can be found in Khan (2006). A temperature loading with a constant rate is applied. In the first two studies, both constituents have the thermal properties independent on temperature, but due to the temperature dependent viscoelastic behavior of the matrix the overall CTE

shows time-dependent behaviors. In the third and fourth studies, a temperature dependent CTE of particle and/or matrix is considered and their effects on the overall CTE of the composites are examined.

Let *Ep* be the elastic modulus of the particle, *Em* be the elastic modulus of the matrix and α_m and α_p be the linear thermal expansion coefficients of the matrix and particle, respectively. In the first study, the ratio of α_p / α_m=0.5 is considered and the time-dependent effective CTE are determined for composites having 10%, 25% and 50% volume fractions, as shown in Figure 3.12. It is shown that for *Ep*<*Em* (softer inclusions dispersed in a stiffer matrix), the effective CTE decreases tremendously with time as compared to the case when *Ep*>*Em* (stiffer inclusions dispersed in a softer matrix). In the second study, when α_p / α_m=5, the time-dependent effective CTE increases prominently for the case when *Ep*<*Em* as illustrated in Figure 3.13. The percentage changes in the value of the effective CTE after 1800 seconds is shown in Tables 3.5 and 3.6. In both cases, for *Ep*<*Em*, a large amount of changes in the effective CTE is observed with the increase in the volume fraction of particles. It is noted that in all cases, the particle response is assumed linear elastic, while the matrix exhibits temperature dependent viscoelastic behaviors. Softer particles result in less resistance to the microstructural changes, which make matrix and the micro-constituents easier to deforms, while stiffer inclusions provide better resistance to deformations. Furthermore, adding softer inclusions increases ductility of the composite.

Table 3.5 Changes in effective CTE (%) after 1800 seconds with α_p / α_m =0.5.

VF (%)	*Ep<Em*	*Ep>Em*
10	4.0	0.3
25	10.4	0.9
50	19.7	1.4

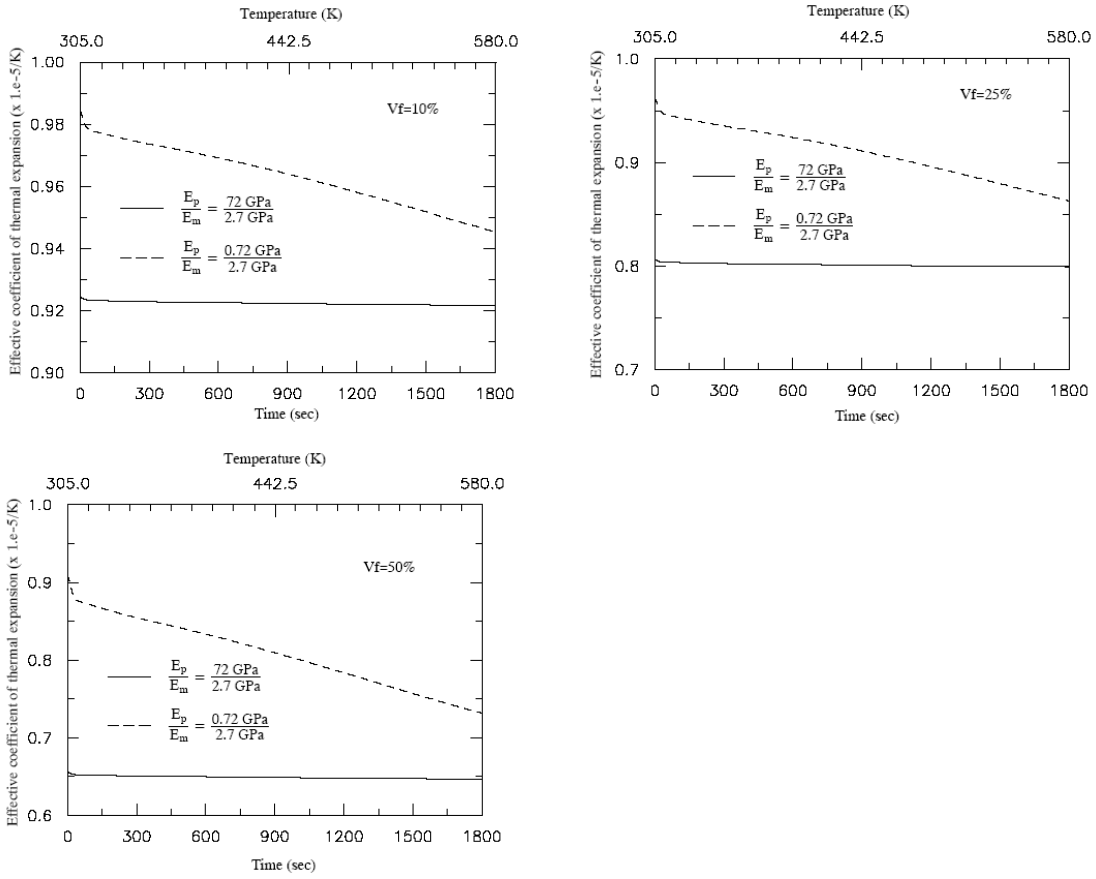

Figure 3.12 Time-dependent effective CTE at different volume fraction with thermal expansion ratio is less than one ($\alpha_p < \alpha_m$).

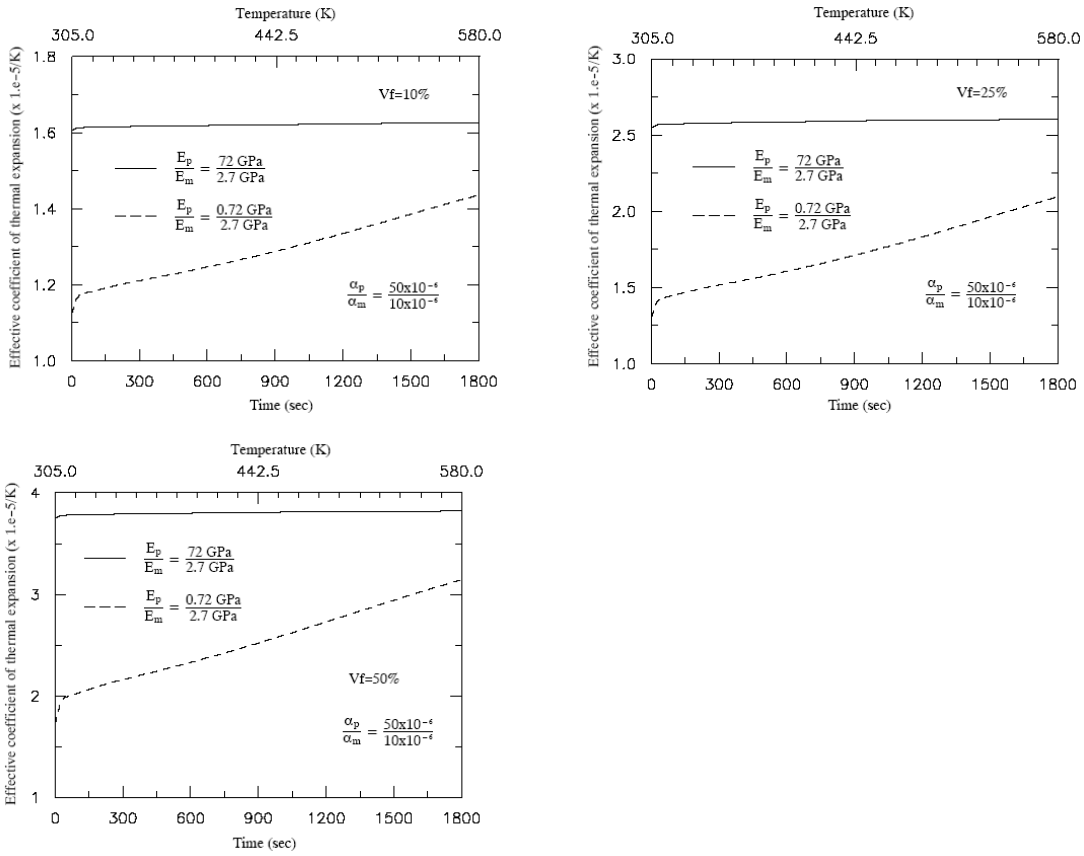

Figure 3.13 Time-dependent effective CTE at different volume fraction with thermal expansion ratio is greater than one ($\alpha_p > \alpha_m$).

Table 3.6 Changes in effective CTE (%)after 1800 seconds with α_p / α_m =5.0.

VF (%)	*Ep<Em*	*Ep>Em*
10	28	1.3
25	61	2.3
50	83	1.9

The last two studies deal with the cases when the CTEs of the matrix and particle are temperature dependent. The following cases are considered for each of the parametric studies: a) α_p is a linear function of temperature, $\alpha_p(T)$, and α_m is constant; (b) α_m is a

linear function of temperature, $\alpha_m(T)$, and α_p is constant; and (c) Both α_p and α_m are linear functions of temperature. Figures 3.14(a)-(d) show the variation of time-dependent CTEs of the composite under a linear temperature loading from reference temperature (300˚K) to 600˚K at different volume fractions with the ratio of α_p/α_m=0.5. Composites having *Ep>Em* and *Ep<Em* are studied. It is found that with the increase in volume fractions the change in the effective CTE after 1800 seconds increases for the composites having temperature dependent CTE of the particle. For the composites with $\alpha_m(T)$ and both $\alpha_m(T)$ and $\alpha_p(T)$ the percent change in the effective CTE decreases after 1800 seconds with increasing volume contents of the inclusion. Figures 3.15(a)-(d) show the time-dependent CTEs of the composite subject to a linear temperature loading from reference temperature (300˚K) to 600˚K at different volume fractions with the ratio of α_p/α_m=5. The results follow a similar trend as observed in the previous study. Tables 3.7 and 3.8 show the percent changes in the effective CTE for all cases described earlier.

Table 3.7 Changes in effective CTE (%) with α_p / α_m =0.5.

VF(%)	*Ep<Em*			*Ep>Em*		
	α_p *(T)*	$\alpha_m(T)$	$\alpha_p(T)$ and $\alpha_m(T)$	$\alpha_p(T)$	$\alpha_m(T)$	$\alpha_p(T)$ and $\alpha_m(T)$
10	2.66	51.64	51.74	1.52	113.71	114.29
50	16.35	31.20	32.40	5.22	59.36	63.55

Table 3.8. Changes in effective CTE (%) with α_p/α_m=5.0.

VF (%)	*Ep<Em*			*Ep>Em*		
	$\alpha_p(T)$	$\alpha_m(T)$	$\alpha_p(T)$ and $\alpha_m(T)$	$\alpha_p(T)$	$\alpha_m(T)$	$\alpha_p(T)$ and $\alpha_m(T)$
10	18.18	52.38	52.46	3.90	60.02	60.36
50	36.36	43.51	43.83	0.55	8.53	9.25

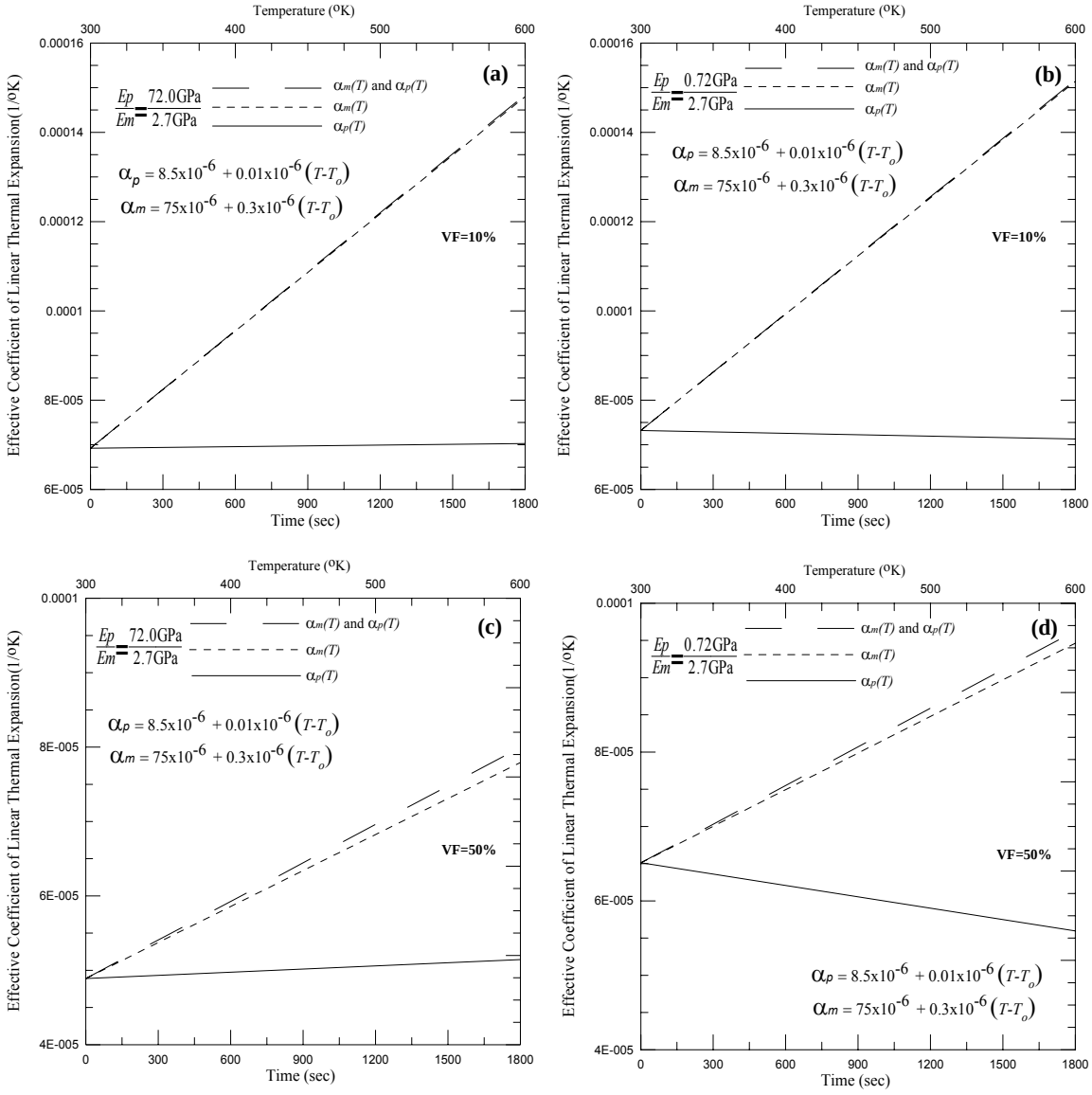

Figure 3.14 Time-dependent effective CTE at different volume fraction for CTE ratios is less than one, i.e., $\alpha_p < \alpha_m$, with and/or without linear temperature dependent CTE of each constituent.

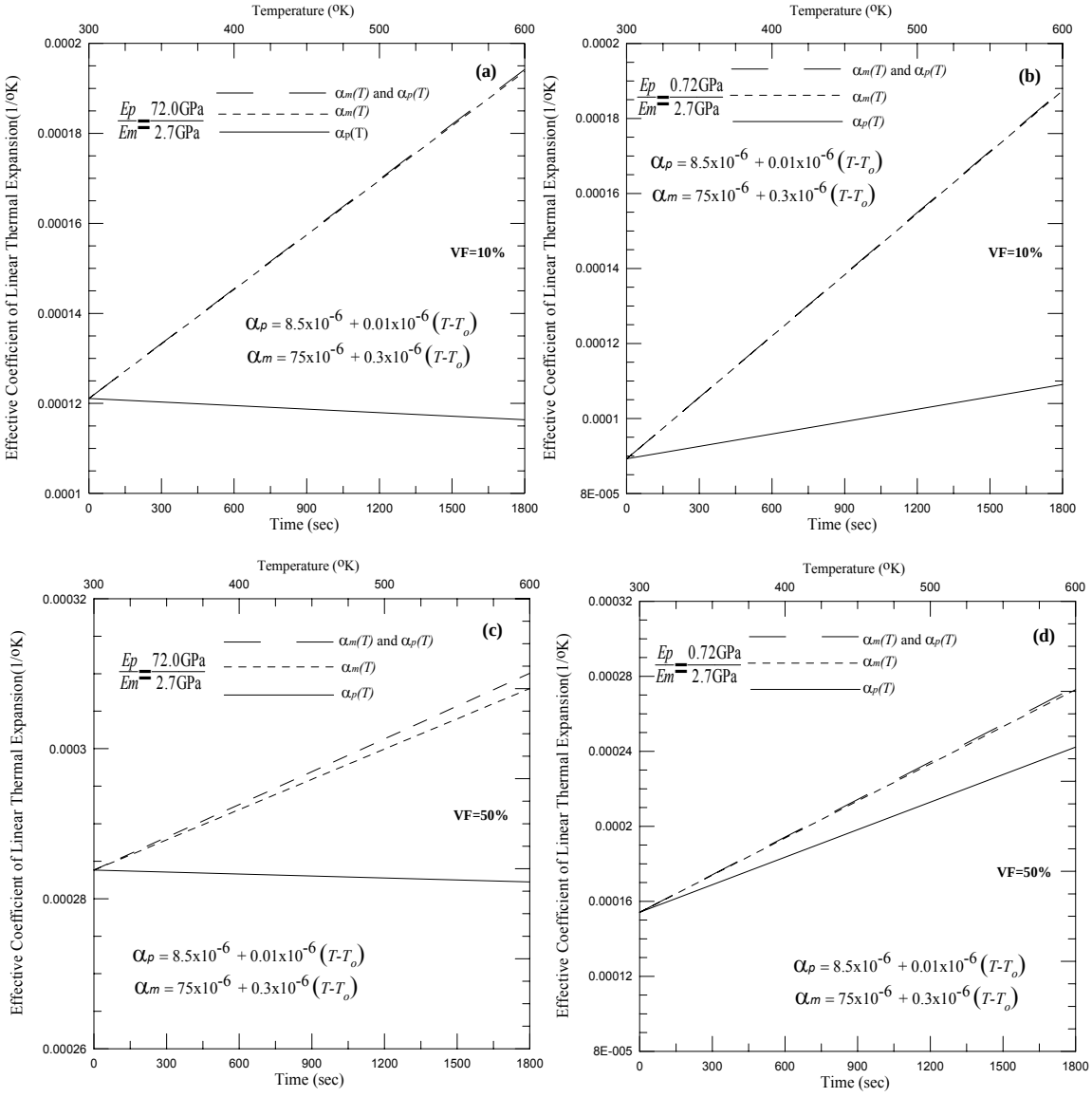

Figure 3.15 Time-dependent effective CTE at different volume fraction for CTE ratios is greater than one, i.e., $\alpha_p > \alpha_m$, with and/or without linear temperature dependent CTE of each constituent.

It is therefore concluded that for the temperature independent thermal and mechanical properties, the effective CTE is strongly dependent on the elastic moduli of the constituents. With any ratio of the CTE of the constituents, the softer inclusion allows the composite to deform easily under temperature changes as compare to the ones

with the stiffer inclusion. Changes in the effective CTE with time increases with the increase in volume contents. When temperature dependent properties are considered, with the increase in volume fractions of the softer inclusion, the effective CTE is strongly dependent on $\alpha_p(T)$. This is valid only for the case when $\alpha_p > \alpha_m$. For all other cases, the effective CTE of the composite is strongly dependent on the function of the temperature dependent CTE of the matrix, i.e., $\alpha_m(T)$.

3.2.4 VERIFICATION OF THE ETC

The ETC obtained from the micromechanical formulation is verified using analytical models and experimental data available in the literature. Figure 3.16 shows the ETC obtained from the present micromodel at various volume fractions. High density polyethylene (HDPE) based composite systems with tin particles as inclusion is used. The thermal conductivities for all constituents are constant and given in Table 3.9.

Table 3.9. Material properties used for ETC verification.

Material	Thermal Conductivity (K), W/m/ K
Air	0.02
Sandstone	1.6
Firebrick	1.2
High Density Polyethylene	0.532
Polyethylene	0.29
Polystyrene	0.14
Polyvinyl Chloride	0.17
Polyamide	0.19
Tin	64
Graphite	209

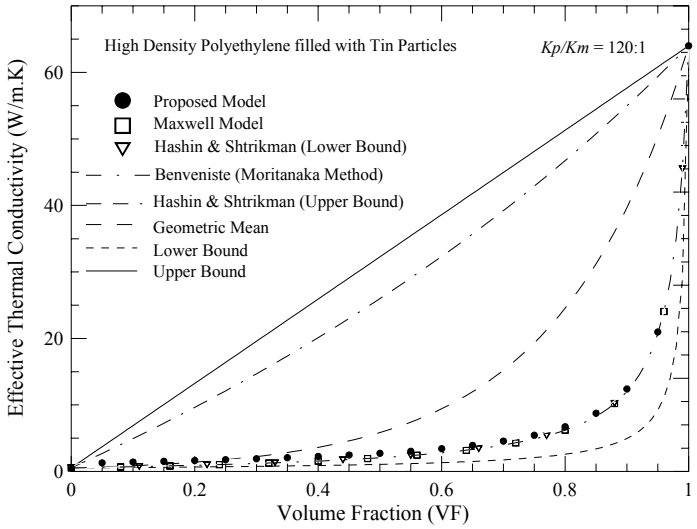

Figure 3.16 Comparison of the ETC with different analytical models.

It is shown that the ETC obtained from the present micromodel is comparable to the results obtained by Maxwell (1954), Hashin and Shtrikman (1962) and Benveniste (1986) and is closer to the lower bound. The experimental data of Sugawara and Yoshizawa is also considered to validate the ETC.

Figure 3.17 shows the ETC of the air saturated sandstone with porosity. Thermal conductivities of the studied materials are given in Table 3.9. The porous sandstone is assumed containing macroscopically series of consolidated spheres of pores and the air in the pores is considered as the inclusions. In this case, the conductivity of the inclusion is less than the matrix with a ratio of *Kp/Km* is equal to 1:80. The ETC determined from the present micromodel agrees well with the experimental data.

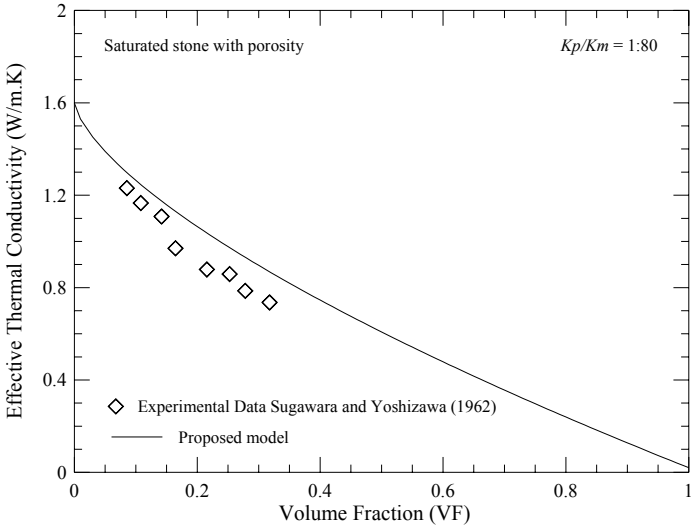

Figure 3.17 Comparisons of the ETC with the experimental data of Sugawara and Yoshizawa (1962).

Highly conductive materials have been added as fillers to the polymeric based matrix composites to increase the overall thermal conductivity of the composites. In most cases, fillers have less than 15% volume fractions. It has been observed that with the increase in the inclusion volume fractions and the ratios of the thermal conductivity of inclusions to the ones of the matrix are high, the ETC of the composites increases tremendously. Tavman (1998) experimentally investigated the ETC of tin powder filled high density polyethylene composites. Figure 3.18 shows the comparison of the present micromodel and Maxwell model (1954) with the experimental data. Thermal properties of tin and polyethylene are given in Table 3.9. Good predictions are shown for composites with volume content less than 10%. The results of the proposed model deviate from the experimental data as the volume fraction of tin particle increases as the present micromodel does not account for the conductive chain mechanism.

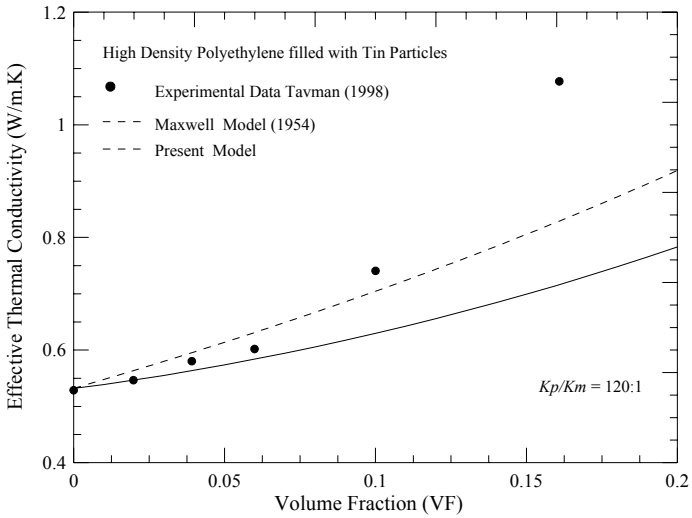

Figure 3.18 Comparison of the ETC with the experimental data of Tavman (1998).

Next, the experimental data of Zhang et al. (2005) on composites with various ratios of *Kp/Km* is also used in this study, as illustrated in Figure 3.19. It is seen that the micromechanical model predictions are in good agreement with the experimental data for composites with low values of *Kp/Km*. As *Kp/Km* increases, the micromechanical model shows good predictions only for lower volume contents (less than 15%). To better predict the ETC at higher volume fractions, there is a need to develop a micromodel that incorporate the chain conductive mechanism of the particles. Nevertheless, the present micromechanical model is suitable for predicting the ETC for filler composite or for composite with low *Kp/Km* (thermal conductivity of the particle is comparable to the one of the matrix).

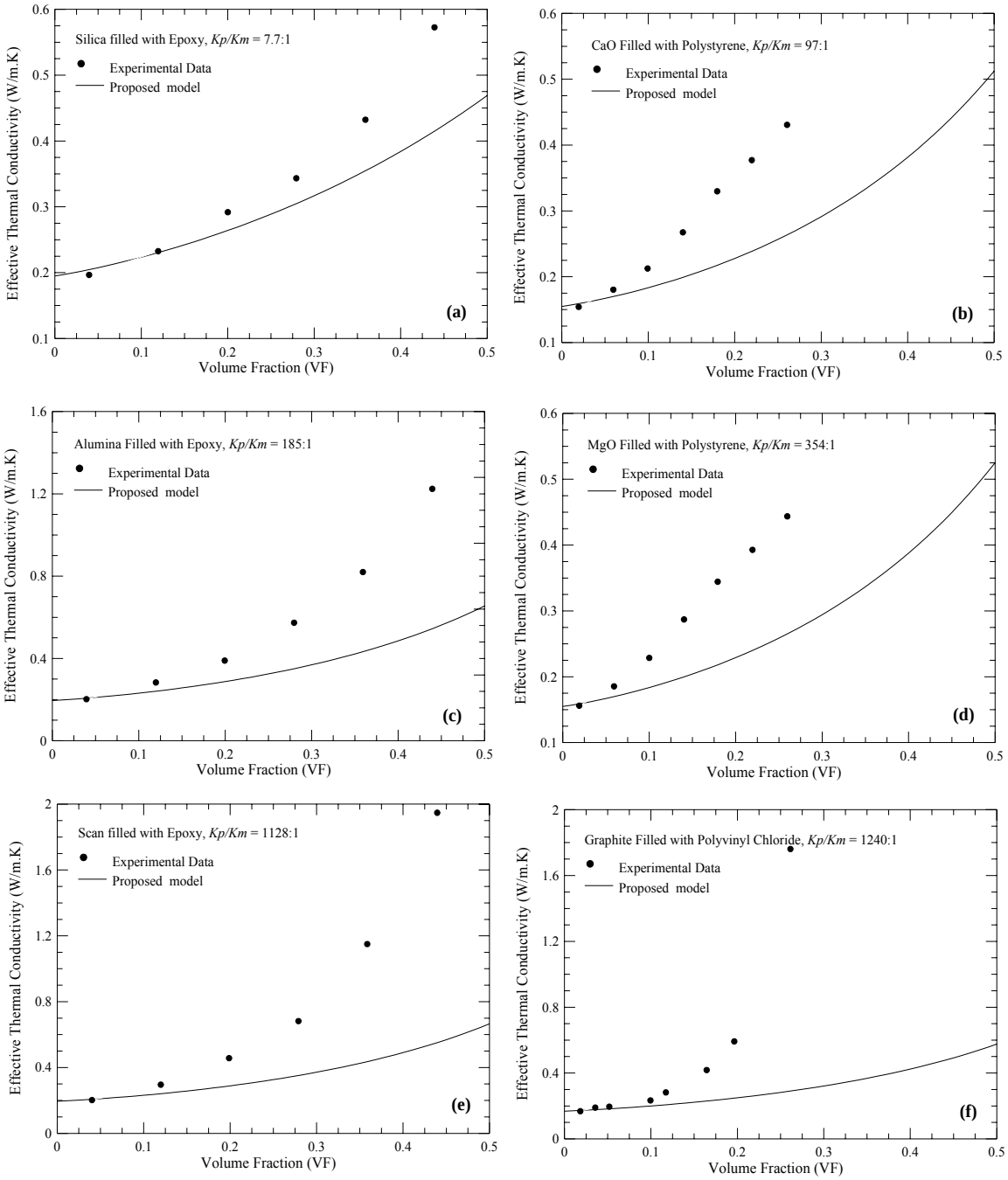

Figure 3.19 Comparisons of the ETC with the experimental data of Zhang et. al. (2005).

As mentioned earlier, the proposed model is developed for the class of particulate composite materials consisting of equi-sized spheres of one phase arranged in a simple

cubic array throughout a continuous second phase. Therefore the effect of percolation (the formation of thermal conductive strings of the particles) cannot be considered in the present study. It is shown by Zhang et al.(2005) that the larger *Kp/Km* gives the larger ETC/ *Km* for a certain volume fraction (VF), the increase of ETC is not significant when *VF* < 0.3. According to the percolation theory (1985), the exact value of the threshold for cubic percolation, *VFc*, is 0.3117–0.3333. When *VF* < *VFc*, the conductive particles are mainly dispersed, so the effect of the conductive chain mechanism on the ETC is small. When *VF* goes up to *VFc*, the connections of the particles increase exponentially and the formations of the conductive chains dominate the change of the ETC. Yin et al (2005) mentioned that the threshold limit of the percolation can go as high as 78%. It is observed that for the present model, the threshold limit is found to be near 80 %, as shown in Figure 3.20.

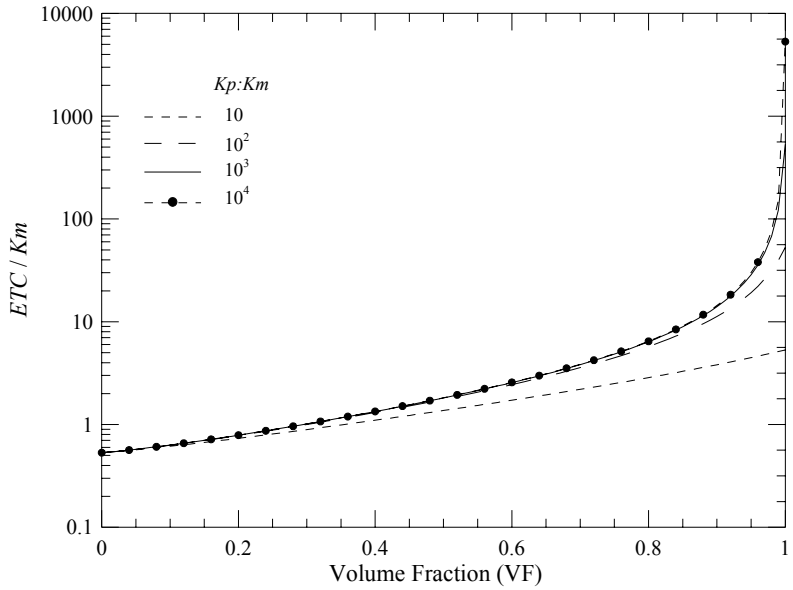

Figure 3.20 Numerical results of *ETC/Km* for different volume fraction and *Kp/Km*.

The parametric studies are done to determine the variations in the ETC of the composite when the particle and/or matrix conductivities are temperature dependent. The thermal conductivities of the particle and matrix are assumed to vary linearly with temperatures. Consider the thermal conductivities of the particle and matrix as *Kp* and *Km*, respectively. Three cases have been considered: a) *Kp* is a linear function of temperature and *Km* is constant; (b) *Kp* is constant and *Km* is a linear function of temperature; and (c) Both *Kp* and *Km* are linear functions of temperature. Since the present micromodel does not incorporate the chain conductive mechanism, the ETC is analyzed for a low ratio of thermal conductivities, i.e, *Kp/Km*=7.7:1. Figure 3.21 shows the variation of the ETC with temperatures for composites with 5%, 15% and 50% volume fractions. For low volume contents (<15%), with only temperature dependent *Kp(T)*, the ETC insignificantly varies with temperatures. For composites with 50% volume contents, the ETC with the temperature dependent *Kp(T)* shows significant variations with temperatures, although the changes are less than the ones with the temperature dependent *Km(T)*. It is noted that the rate of change of the thermal conductivity with temperatures for the particle is higher than the one of the matrix. It is observed that the ETC is strongly depend on the rate of change in the thermal conductivity of the matrix with temperature, i.e., with only temperature dependent *Kp(T)*, less variations of ETC at all volume contents are shown, while higher variations of the ETC with temperatures are shown for temperature dependent *Km(T)*. These parametric studies indicate that the ETC depends on the microstructural constituents (inclusion and matrix) and also on the properties of the constituents. To better

understand the effects of temperature dependent thermal conductivities and their variations on ETC with the increase of volume fraction, it is required to analyze the ETC of the composites with the micromodel that incorporate the chain conductive mechanism.

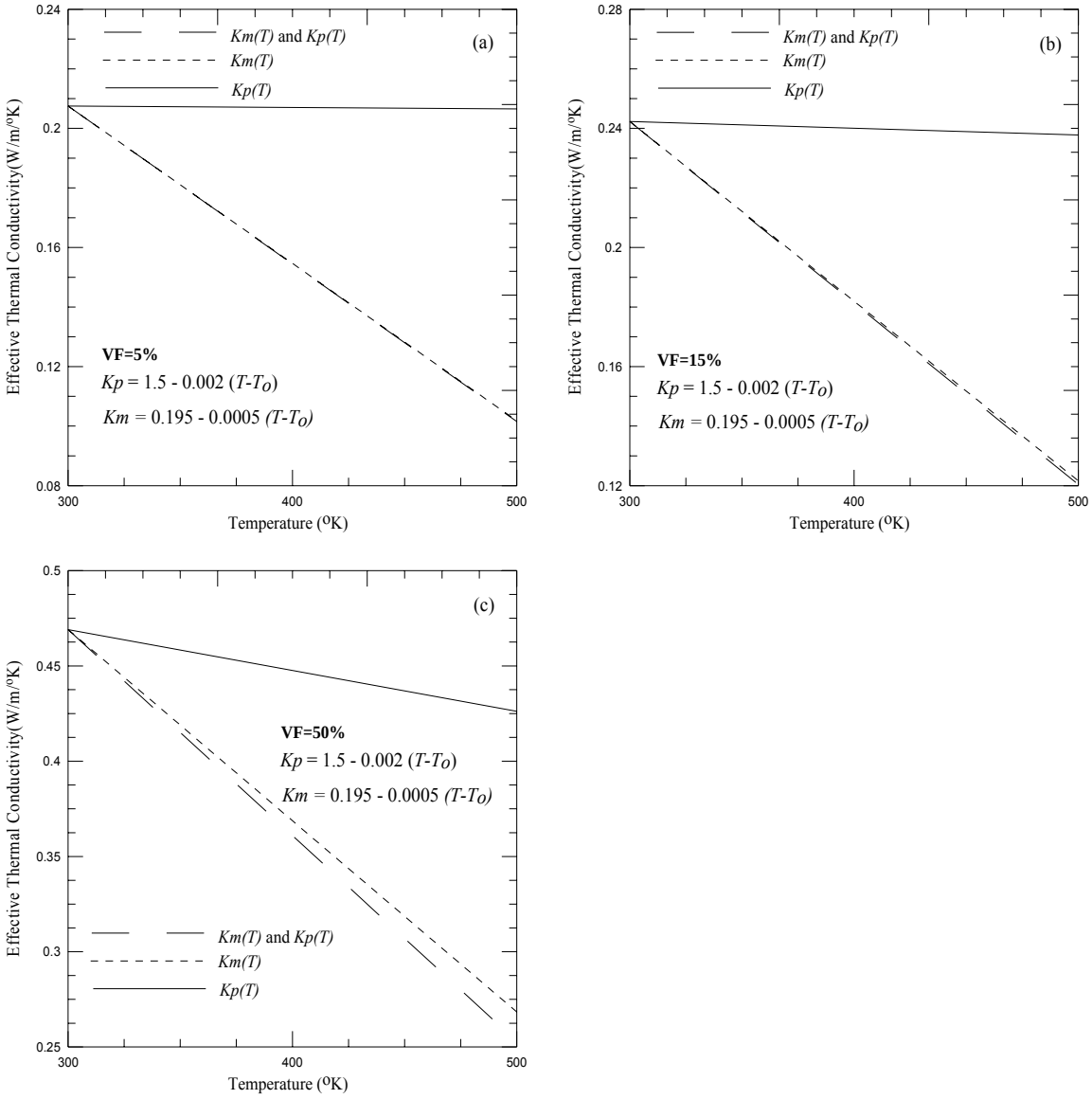

Figure 3.21 ETC with and/or without linear temperature variation of the thermal conductivities of each constituent for a ratio of *Kp/Km*=7.7:1.

3.3 CONVERGENCE BEHAVIOR OF THE COUPLED THERMOVISCOELASTIC RESPONSE OF PARTICULATE COMPOSITE

The proposed numerical scheme is integrated within the ABAQUS (FE code). The material subroutines UMAT, UMATH and UEXPAN are used to compute the effective thermo-mechanical response of a particulate composite. The effective nonlinear coupled thermo-viscoelastic response is calculated at each integration point of a FE mesh. At the FE structural level, the default ABAQUS FE code (2005) iterative solver is used for the nonlinear analyses. Two criteria are checked in the ABAQUS iterative linear solver, which are force (flux) residual and displacement (temperature) corrections. The residual force (heat flux) tolerance is set to be 0.5% times the average force (heat flux) over time t. The default tolerance for the displacement correction is 10^{-2}. At the micro level an iterative algorithm with the Newton-Raphson (NR) scheme is used to compute the strain/stress correction while the recursive-iterative algorithm (Chapter II) is used to compute the nonlinear thermoviscoelastic response of the matrix constituents in the sub-cells. The convergence criteria at both micromechanical (Eq.3.25-3.26) and material (Eq.2.49) levels are used with a tolerance of 10^{-6}. These residuals are defined in terms of strain components and the given tolerances allow for a maximum error to be 1 micro-strain. These tolerances are set as the limits within our numerical values of interests. Tightening the tolerances below these values does not significantly change overall response while relaxing at any level beyond these values might cause deviations in the responses and accumulate errors which leads to divergence (Haj-Ali and Muliana 2004; Muliana and Kim 2007).

The convergence study is presented for a linear stress ramp loading. The composite consisting of HDPE matrix reinforced with TiC+HDPE particle is used. The nonlinear stress and temperature dependent properties of the HDPE are given in Figure 3.22. The properties are taken from Lai and Bakker (1995) and Dorigato et al., 2009. The Prony series coefficients, thermal and mechanical properties of the HDPE matrix and TiC+HDPE particle are given in Tables 3.10 and 3.11. The thermal and mechanical properties of the TiC and HDPE particles are taken from available literature. For the HDPE, the specific heat and thermal conductivity are taken from Ghazanfari et al. (2008), the CTE is from Dzenis and Ponomarev (1989) and Young's Modulus are taken from Yuan et al. (2003). For the TiC, the specific heat, thermal conductivity and CTE are taken from Pierson (1996) and Young's Modulus are taken from Hannink and Murray (1974). In this study the HDPE particle size of 200 μm coated with 2 μm TiC is considered as a spherical particle (Inhance/Fluoro-Seal Ltd.).

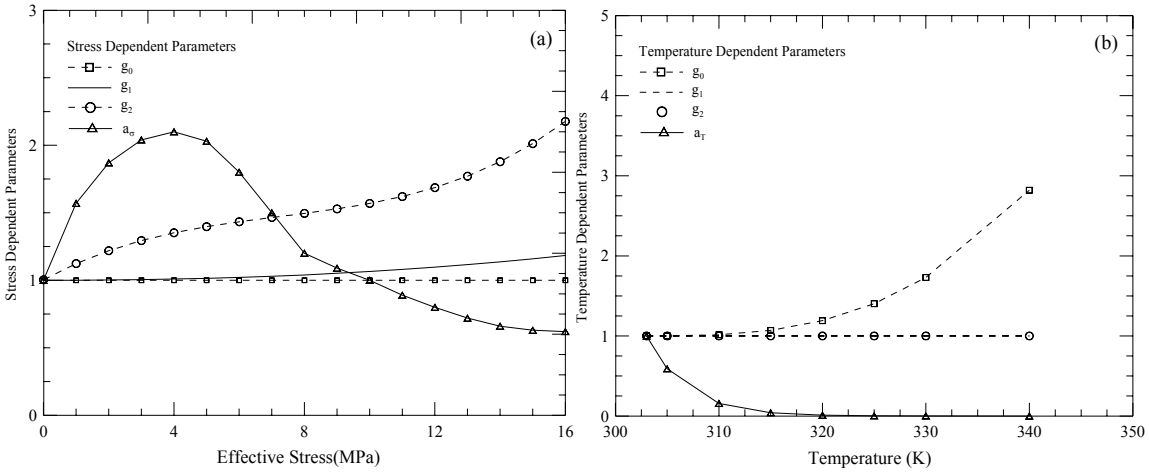

Figure.3.22 Nonlinear material parameters for HDPE. a) stress dependent and b) temperature dependent (Lai and Bakker, 1995; Dorigato et al., 2009).

Table 3.10 Prony series coefficients for HDPE polymer.

n	λ_n (sec^{-1})	$D_n \times 10^{-4}$ (MPa^{-1})
1	1.0	2.23
2	10^{-1}	2.27
3	10^{-2}	1.95
4	10^{-3}	3.5
5	10^{-4}	5.5
6	10^{-5}	5.5

The strain response and temperature increases of the composite with different volume fractions of particle at a rate of 1MPa/s are given in Figures 3.23(a)-(b). As expected, with the addition of stiff thermoelastic particles lower strain and temperature increase are shown.

Table 3.11 Temperature dependent mechanical and physical properties of materials of HDPE (polymer) and TiC+HDPE (particle) used in coupled thermo-viscoelastic FE analyses.

Property	HDPE	TiC+HDPE
Elastic Compliance, (D_0) (1/MPa)	$2.21\text{x}10^{-4}$	$7.9181\text{x}10^{-5}$
Poisson ratio,(υ)	0.3	0.297
Coefficient of Thermal Expansion, (α)10-6, 1/ K	$6.9\text{x}10^{-5} - 4.8\text{x}10^{-7}\ T + 3.0\text{x}10^{-9}\ T^2$	$7.0\text{x}10^{-5}\text{-}5.0\text{x}10^{-7}\ T + 3.0\text{x}10^{-9}\ T^2$
Thermal Conductivity, (K), W/m/ K	$1.223\text{-}5.963\text{x}10^{-3}\ T + 1.14\text{x}10^{-5} T^2$	$1.7 - 4.90\text{x}10^{-3}\ T + 1.02\text{x}10^{-5}\ T^2$
Specific heat,(c) , J/Kg.K	$18535 - 119.7\ T + 0.2055 T^2$	$17865 - 116.2\ T + 0.2 T^2$
Density, (ρ) , Kg/m3	958.0	965.1

* T is temperature in °K.

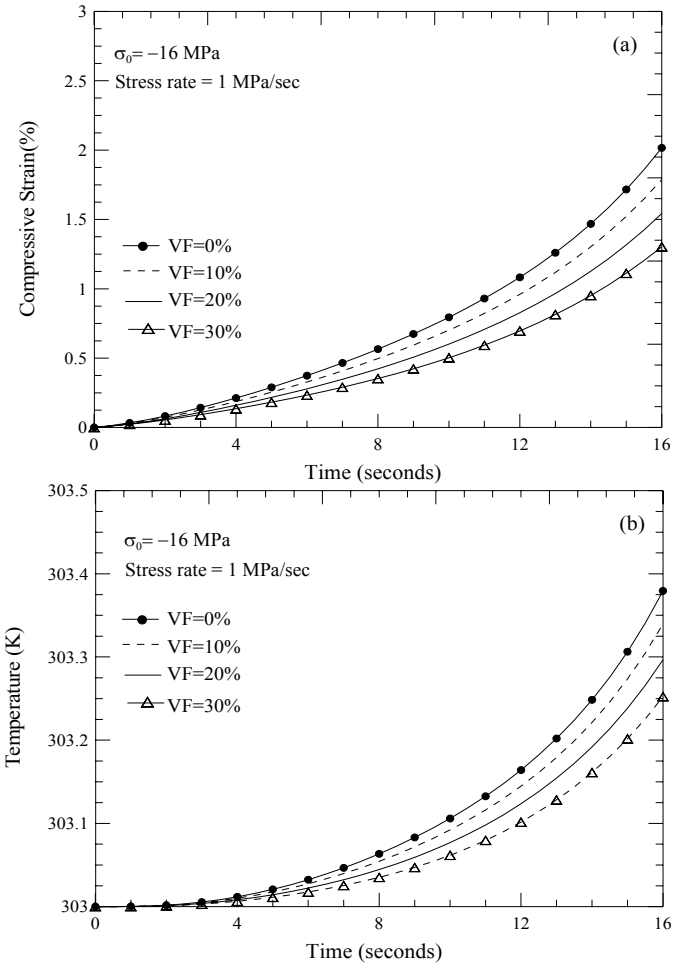

Figure 3.23 Coupled thermo-viscoelastic analyses of HDPE/TiC+HDPE composite under linear stress ramp loading with different volume fractions of TiC+HDPE particle. (a) strain and (b) temperature increase.

The multi-level convergence behavior is studied for the composite with a volume fraction of 10%. The residuals norm, in a logarithmic scale, at two stress levels: 6 and 12MPa is illustrated in Figures 3.24(a)-(d). The analysis is performed with a constant time increment of 1 second which is comparable to an incremental stress of 1 MPa. More iterations are required at the higher stress level to minimize the residuals of both force and heat flux. However, most of the time the force residuals meet the convergence

criterion in less iterations than the heat flux, as shown in Figures 3.24 (a)-(b). The residual norm at the micro level is shown in Figure 3.24 (c) during the last iteration at

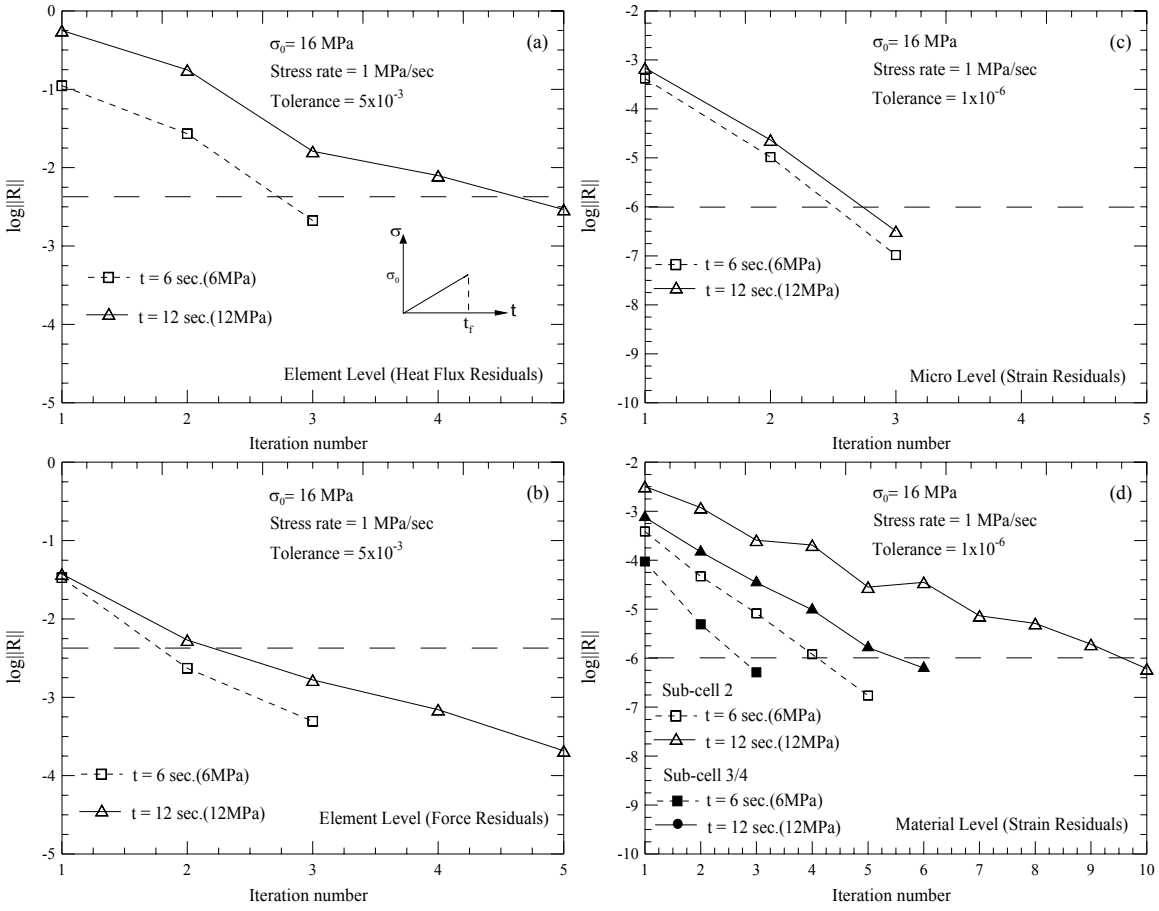

Figure 3.24 Multi-level convergence behaviors at two stresses during the nonlinear analyses of HDPE/TiC+HDPE composites (VF = 10%): (a) macro heat flux (b) macro force (c) micro (d) constituent (polymer) levels.

the macro level, which are iteration numbers 3 and 5 for stress levels 6 and 12 MPa, respectively. At the material levels the convergence behavior is reported at the last converged step at the micro level. Figure 3.24 (d) shows the residual norm for the matrix sub-cell numbers 2, 3 and 4. For the sub-cell numbers 3 and 4 the same convergence behavior is observed while more iterations are needed for the subcell number 2 to meet

the convergence criterion. The behaviors of these norms explain the needs of correction algorithm at each level. Otherwise large residual strains at the lower level may cause a divergence of the solutions at the upper level.

In summary, the proposed model is capable in predicting the effective elastic, viscoelastic, coefficient of thermal expansion and coupled thermo-viscoelastic response of particulate composites. The proposed model capability for predicting the elastic, viscoelastic and temperature dependent CTE of particulate composite is also presented by showing excellent agreement with the available experimental data. For composites having viscoelastic constituents, the expression of the effective CTE is also found to be strongly dependent on time-dependent moduli and CTE of each constituent. It is also found that the proposed model is not capable to predict the effective thermal conductivity quite well for the composite having high particle to matrix thermal conductivity ratio. With the increase in VF, the connections of the particles increase exponentially and as *Kp/Km* increases the formations of the conductive chains govern the change of the ETC. The present micromechanical model has not incorporated the conductive chain mechanism of the particles. Nonetheless, the proposed model is suitable for predicting ETC for filler composite (*VF*~15%) or for composite with low *Kp/Km*. Regardless of few limitations, the proposed micromechanical model provides the effective coupled response of particulate composites and simultaneously recognizes time-temperature-stress dependent behaviors of the individual constituents.

CHAPTER IV

A MULTISCALE MODEL FOR COUPLED HEAT CONDUCTION AND DEFORMATIONS OF VISCOELASTIC COMPOSITES

This study presents an integrated micromechanical model-FE framework for analyzing coupled heat conduction and deformations of particulate composites. Thermo-mechanical properties of the constituents in the particulate composites depend on time, temperature and stress. The integrated micromechanical model-FE framework is illustrated in Figure 4.1. The micromechanical model treats the composites as homogenized bodies. This micromechanical model is implemented at each material point within finite elements. This study uses a three dimensional (3D) continuum element. Therefore, the effective response evaluated at each integration (material) point represents homogenized composite response.

Two types of field-coupling (FC) between the mechanical and thermal effects are considered. The first type of FC is referred to sequentially coupled thermomechanical analysis. In this case, the heat generation due to the dissipation of viscoelastic effects is neglected and the conduction of heat is assumed to be independent of the deformation; however, the deformation in the viscoelastic composites is influenced by temperature changes in the composite bodies. This allows to separately solve the equations that govern heat conduction and deformation in the composites. The temperature profiles are used as inputs to analyze deformation in the viscoelastic composites. When the deformation of the composites is relatively small, the sequentially coupled analyses can still give reasonably good predictions of the field variables in the composites.

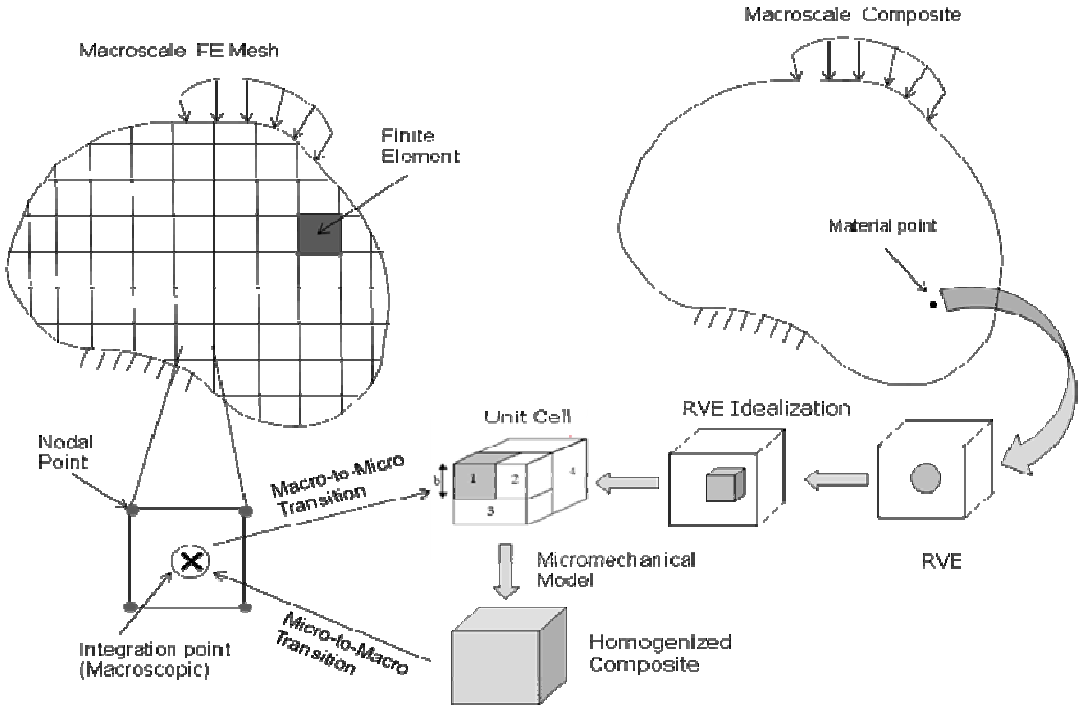

Figure 4.1 Schematic diagram of integration of micro-macro scale approach for particulate composites.

The second type of FC considers a fully coupled thermo-mechanical interaction. In this case, the heat generation due to the dissipation of energy during the deformation of viscoelastic bodies is considered. The heat conduction equation needs to be solved by incorporating the heat generation rate in addition to the existing prescribed thermal boundary conditions. The mechanical and thermal properties at each material point depend on the temperature which arises from both the prescribed thermal loads and heat generation during viscoelastic deformation. Therefore, one needs to solve simultaneously the equations governing the heat conduction and deformation in the composite bodies. In small deformation problems, the heat generation can be

pronounced when the viscoelastic composites undergoes a cyclic loading over a relatively long period of time.

4.1 SEQUENTIALLY COUPLED THERMOMECHANICAL ANALYSIS OF PARTICULATE COMPOSITES

The thermo-micromechanical analyses are performed to examine the effects of constituents' properties and microstructural details on the variation of field variables like stress, displacement and temperature within the homogenized and heterogeneous composites. The first type of FC is considered in this study. Two micromechanical modeling approaches are used to analyze spatial variations of these field variables in particulate composites during the transient heat conduction. In the first approach, a simple micromechanical model based on the first order homogenization scheme is adopted to obtain the effective mechanical and thermal properties, i.e., coefficient of linear thermal expansion, thermal conductivity, and elastic constants, of a particulate composite. These effective properties are evaluated at each material (integration) point in three dimensional (3D) finite element (FE) models that represent homogenized composite media. The second approach treats a heterogeneous composite explicitly. Heterogeneous composites that consist of solid spherical particles randomly distributed in homogeneous matrix are generated using 3D continuum elements in FE framework. For each volume fraction (VF) of particles, the FE models of heterogeneous composites with different particle sizes and arrangements are generated such that these models represent realistic volume elements "cut out" from a particulate composite. An extended definition of a RVE for heterogeneous composite is introduced, i.e., the number of

heterogeneities in a fixed volume that yield the same expected effective response for the quantity of interest when subjected to similar loading and boundary conditions. Thermal and mechanical properties of both particle and matrix constituents are temperature dependent. The effects of particle distributions and sizes on the variations of temperature, stress and displacement fields are examined. The predictions of field variables from the homogenized micromechanical model are compared with those of the heterogeneous composites.

This section focuses on understanding the effects of constituents' properties and microstructural details on the variation of stress, displacement and temperature in composites. The micromechanical model is called at each integration point in a FE mesh to calculate the local effective properties of the composite. The responses thus obtained are then compared to FE simulations of composites using the meshes of Barello and Lévesque (2008). The results are used to justify the capability of micromechanical models to analyze the overall response of composites subjected to simultaneous mechanical and thermal stimuli, within a certain degree of accuracy. A sequentially thermo-mechanical coupled problem, i.e., the temperature field influences the deformation field, is considered. The effects of particle volume contents and temperature dependent constituent properties on the overall thermo-elastic behavior of the composites are examined. An example of homogeneous composite and heterogeneous composites is shown in Figure 4.2.

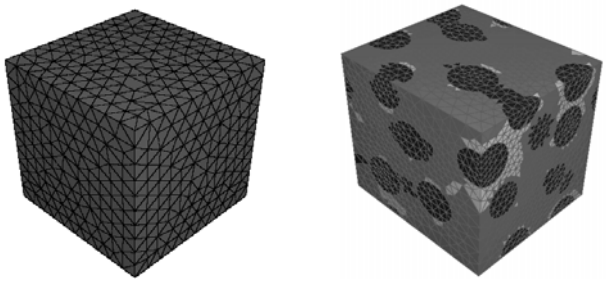

(a) (b)

Figure 4.2 3D FE models of (a) homogenized and (b) heterogeneous composites.

It should be emphasized here that the present micromechanical model idealizes the particles as cubes arranged uniformly in a homogeneous matrix. But the particles arrangement in realistic microstructures may not be statistically homogeneous and therefore composites are considered as heterogeneous materials that exhibit discontinuities in the field variables at the inter-phases of the different constituents and large variations in the field variables. These variations and discontinuities at the micro-scale cannot be captured if one treats the composites as homogenous (homogenized) body. The main advantage of the micromechanical model is that it predicts the overall response of composites with capabilities of incorporating field dependent thermo-mechanical properties of the constituents. As a result, large-scale structural analyses can be carried out under complex thermo-mechanical loadings.

The first micromechanical modeling approach is describes as follows. The micro-mechanical model of Chapter III has been integrated into a multi-scale FE framework in order to compute the field variables of a real-size composite. Boundary conditions are imposed on the real-size composite model and initial values of the field variables are

assumed. Local effective properties (thermal, mechanical) are computed at each integration point using the micro-mechanical model. The evaluation of the effective properties is based on the assumption that the each integration point is associated with a much smaller volume than that of the whole composite. As a result, we assumed that each volume associated with each integration point was at a uniform temperature. Therefore, at the micro-scale, both the matrix and reinforcement were assumed to be at the same temperature. This allows determining temperature-dependent thermal conductivities for the particle and matrix constituents and calculating the effective thermal conductivities of the composite at that instant of time in each material point. Therefore, in this context, the periodic boundary conditions are fully justified for obtaining the effective properties. At the macroscopic scale during the transient heat conduction, the temperature-dependent properties of the constituents lead to a spatially dependent ETC.

To simulate the effective thermo-mechanical response of the particulate composite, the micromechanical model is integrated with ABAQUS/standard FE code. At each integration point in the FE mesh, the user subroutine UMATH is first called to evaluate the effective thermal conductivity, heat fluxes, and temperature gradient for solving the equation that governs the conduction of heat in the composite body. The temperature distributions obtained from the heat transfer analyses at various instants of time in the composites are used as an input transient thermal load to determine the deformation in the composite body. UMAT and UEXPAN subroutines were used to evaluate the

effective mechanical response and CTE, respectively. Figure 4.1 illustrates the multi-scale framework.

The second micromechanical modeling approach is explained as follows. The multi-scale model of Chapter III can be considered as an approximation to a complicated thermo-mechanical problem: the problem of computing the temperature and stresses inside a heterogeneous material subjected to both thermal and mechanical loads. In order to evaluate the reliability of the micro-mechanical model, it is therefore required to compare its predictions against the "numerically exact solution". The objective of this section is to generate this so called numerically exact solution.

When dealing with effective properties, one of the key issues is the definition of the RVE. A RVE can be seen as a volume of material having the same behavior as any larger volume of the same material. The size of the RVE is measured in terms of inhomogeneities it contains (e.g. the number of particles meshed, like 5, 10, 15, etc., particles). One of the techniques used for obtaining the RVE size is to use a numerical homogenization based on FE. The method consists in generating many FE meshes of the composite microstructure with a fixed number of reinforcements (10, 15, 50, etc.). Since the particles are distributed according to a statistical distribution, each mesh, or *realization*, will be different. Therefore, each realization should lead to different (within certain accuracy) effective properties. For the same number of reinforcements and load history, the effective responses are computed for each realization and then averaged. Computing a confidence interval (for example a two-tail 95% confidence interval) on this data could give an estimation of the composite's effective properties and its

precision for a given number of reinforcements. The relative precision (for example the Young's modulus is estimated to be $x \pm y\%$) can be adjusted by varying the number of realizations. If many realizations are performed, the confidence interval can be adjusted to the desired width. Kanit et al. (2003) mentioned that for microstructures containing numerous reinforcements, smaller numbers of realizations are required to estimate the wanted overall property within desired precision. For relatively small number of particles, the homogenized properties vary statistically until a certain number of particles are meshed. The number of particles after which the effective response does not change anymore is called the representative volume element.

The FE meshes used in this study are those of Barello and Lévesque (2008). Their generation is recalled here. The detailed composite consists of a randomly distributed identical spherical particles reinforced matrix. The microstructures were generated using the Random Sequential Algorithm (Segurado and Llorca, 2002). The algorithm consists in generating the position of a first spherical particle center into a cubic volume using a uniform random number generator. Then, the center position of a second sphere is generated. If the distance between the centers of the first two particles and the distance from the particle center from the cube's faces is smaller than a preset value, then the second particle is rejected and a new center position is generated until the minimum distance criterion mentioned above is met. The other particles are sequentially added, following the same process where the distance criteria are checked with all the existing particles. The particles are added until the desired volume fraction is reached.

The particles were allowed to cut the edges and the faces of the cube. When this happened, the particles were completed periodically on the corresponding faces and edges. The realizations thus obtained were therefore periodic and always had an integer number of "complete" spheres. The minimum distance between two particles centers was set to $2.07r$, where r is the particle radius while the minimum distance from a particle center to a cube's face was set to $0.1r$. These distance criteria were obtained through trial and errors with the meshing software until elements of acceptable aspect ratios were obtained.

A Matlab program was used for generating the particles centers. This program wrote an ANSYS command file for generating the FE mesh of the microstructure*. Finally, a Matlab program was used for converting the ANSYS model to ABAQUS. The mesh consisted of 10-noded tetrahedra.

4.1.1 THERMOELASTIC ANALYSIS OF PARTICULATE COMPOSITES

For both the multi-scale framework and the detailed models of Barello and Lévesque (2008), cubic models of dimensions 10 x 10 x 10mm were used. Figure 4.3 shows these models as well as the axes used for defining the boundary conditions below. The studied composite is a ZrO_2 matrix reinforced by randomly distributed Ti-6Al-4V spherical particles. The heterogeneous composites directly incorporate nonlinear thermo-elastic behaviors for the particle and matrix regions. The thermal as well as the mechanical

* All the FE meshes, having microstructural details, used in this study are generated by Barello and Lévesque (2008).

properties used in the simulations can be found in Khan and Muliana (2010) and are given in Table 4.1. Two volume fractions of reinforcements were studied, namely 20% and 30%. For the detailed FE meshes, cubes containing 15, 20, 30, 40 and 45 spheres were generated. The transient thermal analysis consisted in a problem where a composite was initially at 300°K, except for one face that was at 600°K. This transient heat transfer problem was solved until a steady state was reached. A uniform stress of 10 MPa was applied on the face that was at 600°K in order to simulate the effective transient thermal stresses. The models were subjected to the following boundary conditions:

$$
\begin{aligned}
&T(x_1,x_2,x_3,0)=300°K; && 0\le x_1\le 10, 0\le x_2\le 10,\ 0\le x_3\le 10\\
&T(10,x_2,x_3,t)=600°K; && 0\le x_2\le 10,\ 0\le x_3\le 10,\ t\ge 0\\
&\frac{\partial T(x_1,0,x_3,t)}{\partial x_2}=\frac{\partial \overline{T}(x_1,10,x_3,t)}{\partial x_2}=0.0; && 0\le x_1\le 10,\ 0\le x_3\le 10,\ t\ge 0\\
&\frac{\partial T(x_1,x_2,0,t)}{\partial x_3}=\frac{\partial \overline{T}(x_1,x_2,10,t)}{\partial x_3}=0.0; && 0\le x_1\le 10,\ 0\le x_2\le 10,\ t\ge 0
\end{aligned}
\tag{4.1}
$$

$$
\begin{aligned}
&u_1(0,x_2,x_3,t)=0.0; && 0\le x_2\le 10,\ 0\le x_3\le 10\\
&u_2(x_1,0,x_3,t)=0.0; && 0\le x_1\le 10,\ 0\le x_3\le 10\\
&u_3(x_1,x_2,0,t)=0.0; && 0\le x_1\le 10,\ 0\le x_2\le 10\\
&t_1(10,x_2,x_3,t)=10.0\,\text{MPa}; && 0\le x_2\le 10,\ 0\le x_3\le 10\\
&t_2(x_1,10,x_3,t)=0.0\,\text{MPa}; && 0\le x_1\le 10,\ 0\le x_3\le 10\\
&t_3(x_1,x_2,10,t)=0.0\,\text{MPa}; && 0\le x_1\le 10,\ 0\le x_2\le 10
\end{aligned}
\tag{4.2}
$$

where u_i and t_i (i=1,2,3) are the components of the displacements and the surface tractions, respectively.

In the following subsections, the field variables distributions predicted from the multi-scale framework are compared to those of the detailed FE meshes of Barello and Lévesque (2008). We used an extended definition of the RVE in the sense that the

'effective properties' studied are in fact the field variables distributions. The averaged field variables distributions (within a prescribed confidence interval) predicted from the detailed models should converge as the number of spheres meshed is increased. It should be noted, as exemplified by Kanit et al. (2003), RVE sizes can vary from one property to the other (e.g. thermal vs. elastic properties) and from one set of constituent property to the other. Once converged, the field variables distributions predicted from the RVEs could be compared to those predicted by the multi-scale framework in order to evaluate its accuracy.

Due to the boundary conditions, the field variables distribution on the four cube segments oriented along x_1 (see Figure 4.3) should be identical for a large number of spheres. For the detailed models, the field variables were extracted at identical x_1 coordinates and then averaged. At each x_1 coordinate, 95% confidence intervals on the

Table 4.1 Temperature dependent mechanical and physical properties of materials of Ti-6Al-4V and $Zr0_2$ used in 3D FE analyses.

Property	Ti-6Al-4V	Zirconia ($Zr0_2$)
Young modulus, (E) (Pa)	$1.23\text{x}10^{11}$-$56.457\text{x}10^{6}\ T$	$2.44\text{x}10^{11}$-$334.28\text{x}10^{6}T$+$295.24\text{x}10^{3}T^2$-$89.79T^3$
Poisson ratio,(υ)	0.3	0.3
Coefficient of Thermal Expansion, (α)10-6, 1/°K	$7.58\text{x}10^{-6} + 4.927\text{x}10^{-9}\ T + 2.388\text{x}10^{-12}\ T^2$	$1.28\text{x}10^{-5}$-$19.07\text{x}10^{-9}\ T + 1.28\text{x}10^{-11}\ T^2$-$8.67\text{x}10^{-17}T^3$
Thermal Conductivity, (K), W/m/°K	$1.2095 + 0.01686\ T$	$1.7 + 2.17\text{x}10^{-4}\ T + 1.13\text{x}10^{-5}\ T^2$
Specific heat,(c), J/Kg. °K	$625.2969 - 0.264\ T + 4.49\text{x}10^{-4}\ T^2$	$487.3427 + 0.149\ T - 2.94\text{x}10^{-5}\ T^2$
Density, (ρ) , Kg/m3	4429	5700

* T is temperature in °K.

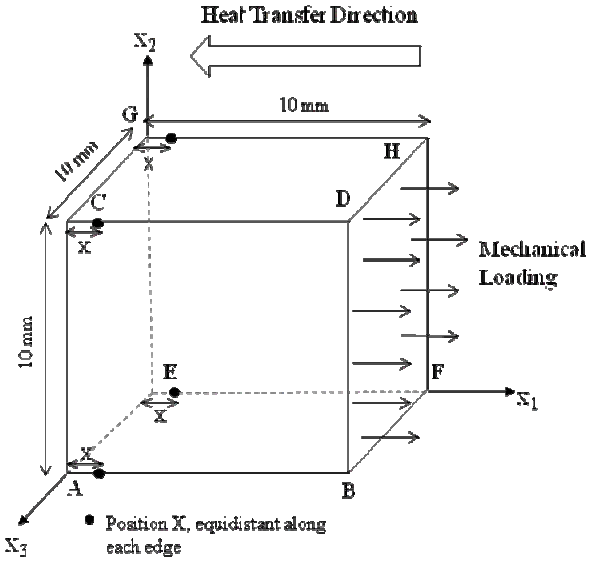

Figure 4.3 Schematic of thermal and mechanical loading directions and profiles along which field variables are evaluated, i.e., *AB*, *CD*, *EF* and *GH*.

mean value were computed. Finally, the averaged distributions of the detailed models were compared to the distributions of the multi-scale model.

4.1.1.1 TEMPERATURE DISTRIBUTION

Figures 4.4(a) and 4.4(b) show the temperature distributions obtained from the homogenized model as well as from the heterogeneous composite reinforced by 20% of Ti-6Al-4V particles for model sizes of 20 and 40 particles, respectively, for different times. Figures 4.4(c) and 4.4(d) show the mean responses of the various realizations, along with 95% confidence intervals for models of 20 and 40 particles, respectively. For the 20 particle model, the largest width of the confidence interval is 1.74% of the mean value while it is of 3.42% for the 40 particles model. The width of the confidence interval decreases as the time increases. Figures 4.5(a)-(f) show the temperature profiles

from a similar type of analyses but for a composite reinforced by 30% of Ti-6Al-4V particles and for models containing 15, 30 and 45 particles. The largest widths of the confidence intervals are of 3.25%, 1.88% and 3.7% for the 15, 30 and 45 particle models, respectively.

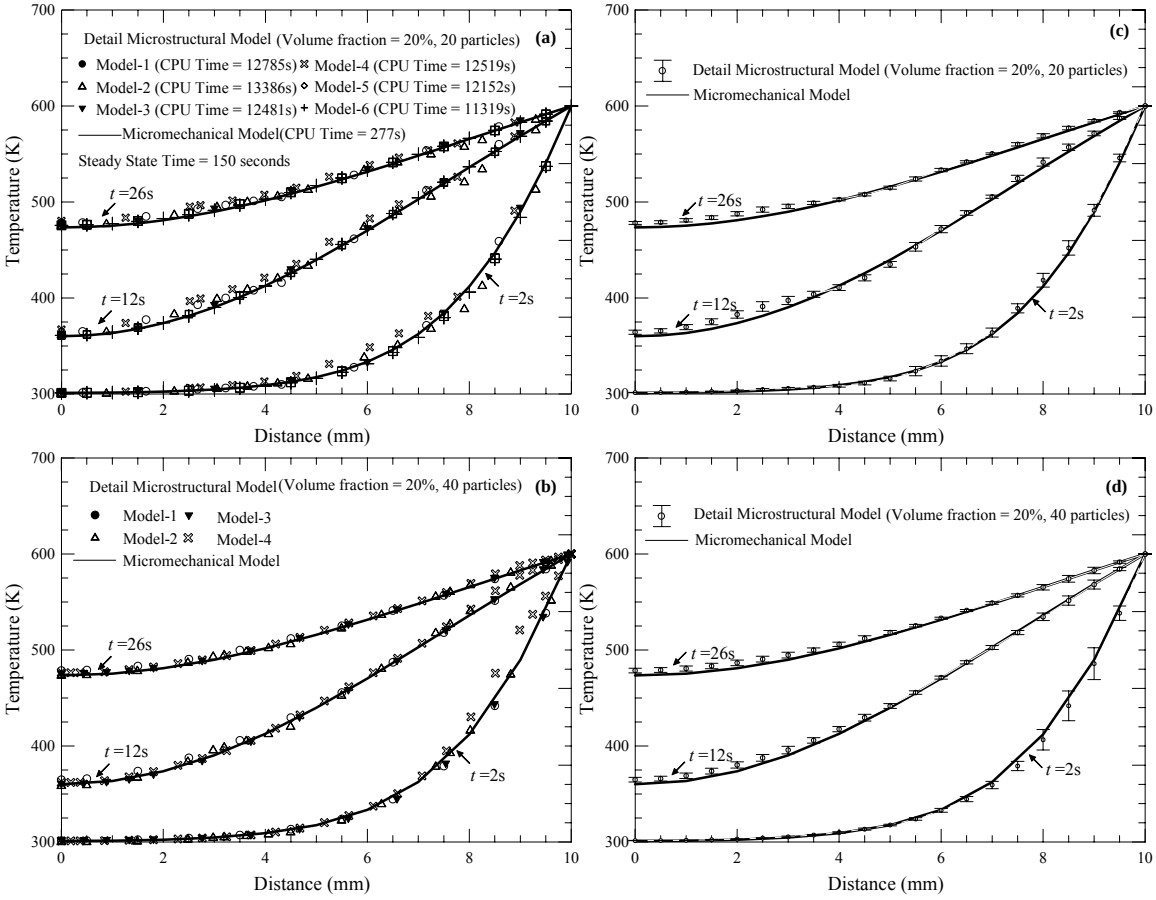

Figure 4.4 Comparison of temperature profiles for FE models with the unit cell (micromechanical model) at each integration point (solid line) and the FE models with 3D microstructural detail (symbols) for volume fraction of 20%. (a) and (b) are actual values of temperature at top (corner) edge $\{(X_1,10,10);\ 0 \leq X_1 \leq 10\}$, (c) and (d), mean value of temperatures of different FE models measured at extreme top and bottom (corner) edges of the cubes along the temperature gradient direction.

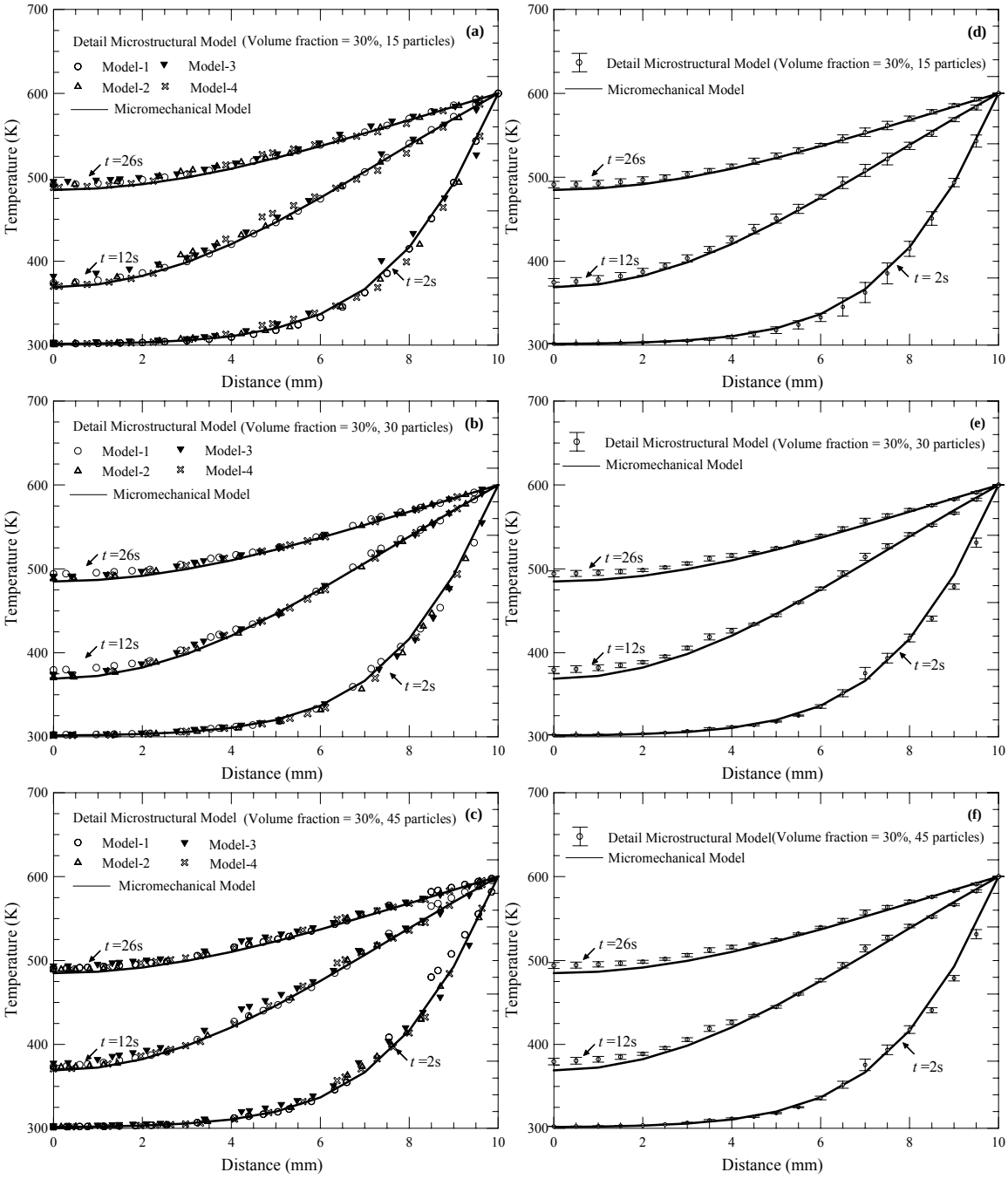

Figure 4.5 Comparison of temperature profiles for FE models with the unit cell (micromechanical model) at each integration point (solid line) and the FE models with 3D microstructural detail (symbols) for volume fraction of 30%. (a), (b) and (c) are actual values of temperature at top (corner) edge{(X_1,10,10); $0 \leq X_1 \leq 10$}, (d), (e) and (f), mean value of temperatures of different FE models measured at extreme top and bottom (corner) edges of the cubes along the temperature gradient direction.

Figure 4.6 (a) shows the mean temperature curves for a composite with 20% of Ti-6Al-4V particle volume content and for models containing 20 and 40 particles. Considering their relatively narrow confidence intervals, it can be seen that the RVE has been reached for these microstructures since both the 20 and 40 particle models lead to very similar results. Figure 4.6 (b) shows the mean temperature curves for the 15, 30 and 45 particle models for composites with 30% particle volume content. It can also be

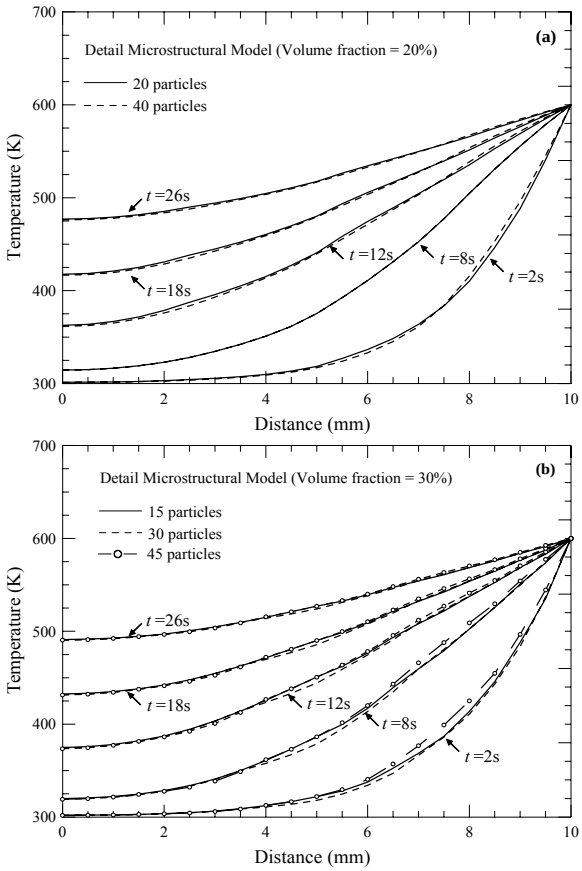

Figure 4.6 Mean temperature profiles for FE models with the unit cell (micromechanical model) at each integration point (solid line) and the FE models with 3D microstructural detail (symbols) for volume fraction of (a) 20% and (b) 30%.

concluded that the RVE size has been reached and overcame. Figures 3.4 and 3.5 show that the micromechanical model predicts fairly well the temperature profiles for the range of material properties simulated.

4.1.1.2 DISPLACEMENT DISTRIBUTION

Figures 4.7(a) and 4.7(b) show the displacement distributions obtained from the homogeneous and heterogeneous models for a composite containing 20% of Ti-6Al-4V particles for models having 20 and 40 particles, respectively. Figures 4.7(c) and 4.7(d) show the average response of the various realizations, along with 95% confidence intervals on the mean value for models containing 20 and 40 particles, respectively. For the 20 particles model, the largest width of the confidence interval is 96% of the mean value while it is of 52% for the 40 particles model.

Figures 4.8(a)-(f) show displacements from similar analyses but for a composite reinforced by 30% of Ti-6Al-4V particles for models containing 15, 30 and 45 particles. The largest widths of the confidence intervals were of 30%, 65% and 143% for the 15, 30 and 45 particle models, respectively.

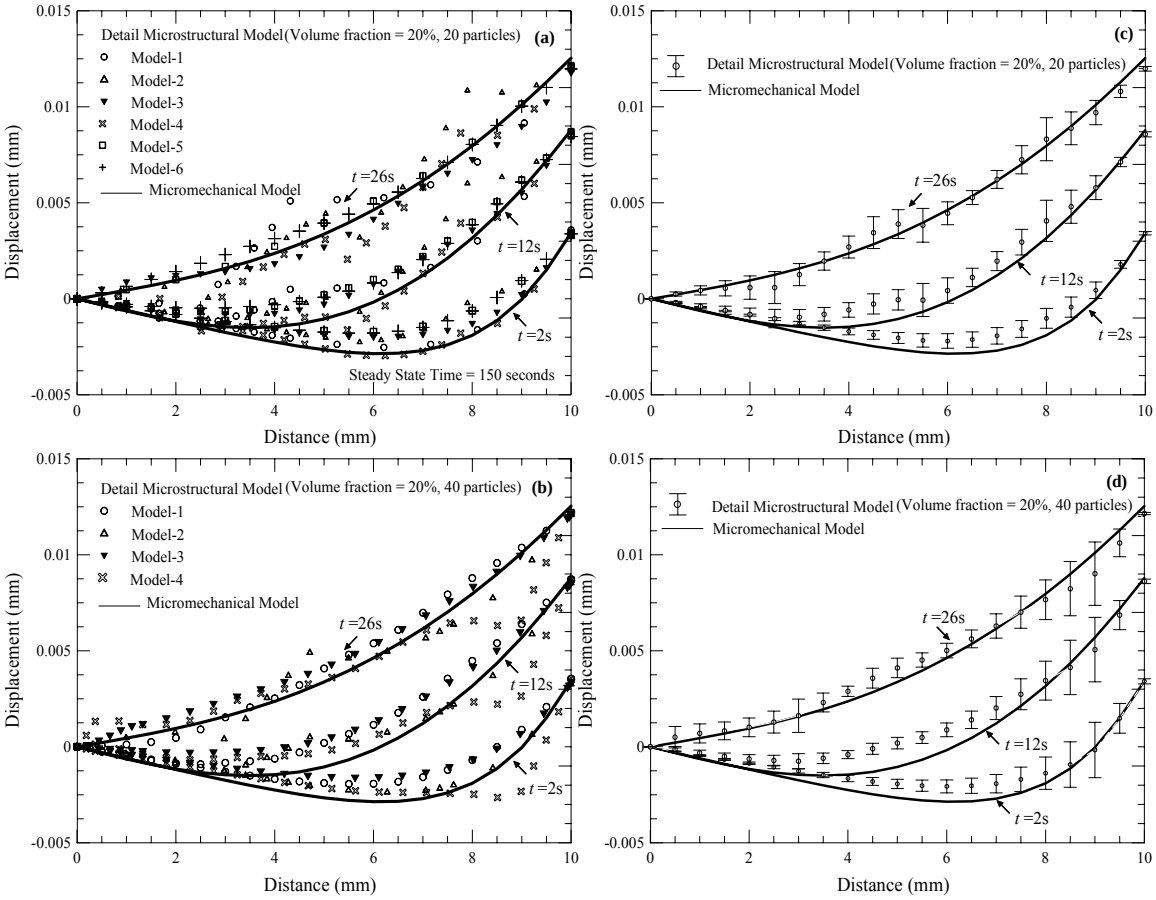

Figure 4.7 Comparison of axial displacements for FE models with the unit cell (micromechanical model) at each integration point (solid line) and the FE models with 3D microstructural detail (symbols) for volume fraction of 20%.(a) and (b) are actual values of displacements at top (corner) edge $\{(X_1,10,10);\ 0 \leq X_1 \leq 10\}$, (c) and (d), mean value of displacements of different FE models measured at extreme top and bottom (corner) edges of the cubes along the temperature gradient direction.

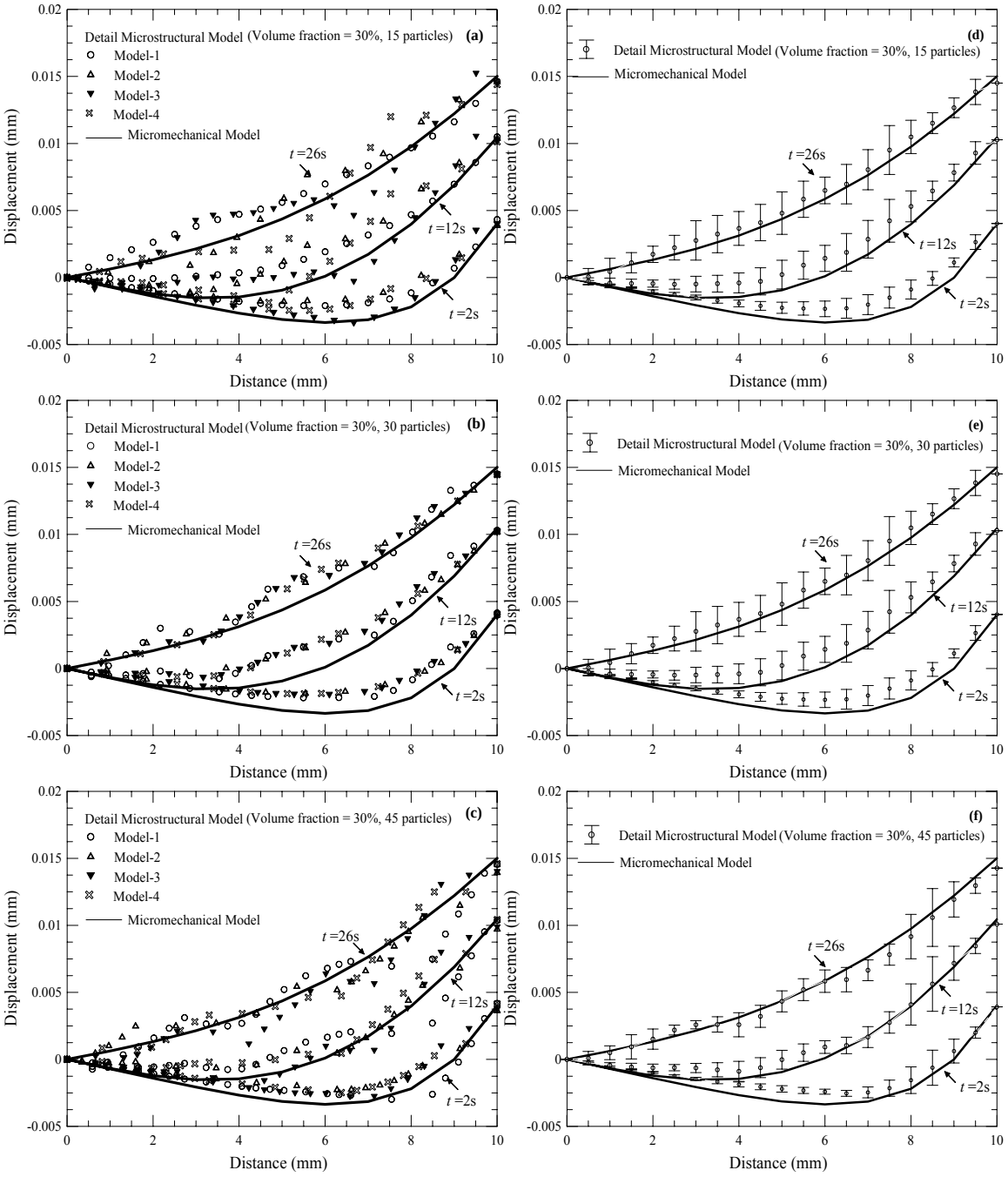

Figure 4.8 Comparison of axial displacements for FE models with the unit cell (micromechanical model) at each integration point (solid line) and the FE models with 3D microstructural detail (symbols) for volume fraction of 30%. %.(a), (b) and (c) are actual values of displacements at top (corner) edge $\{(X_1,10,10);\ 0 \le X_1 \le 10\}$, (d), (e) and (f), mean value of displacements of different FE models measured at extreme top and bottom (corner) edges of the cubes along the temperature gradient direction.

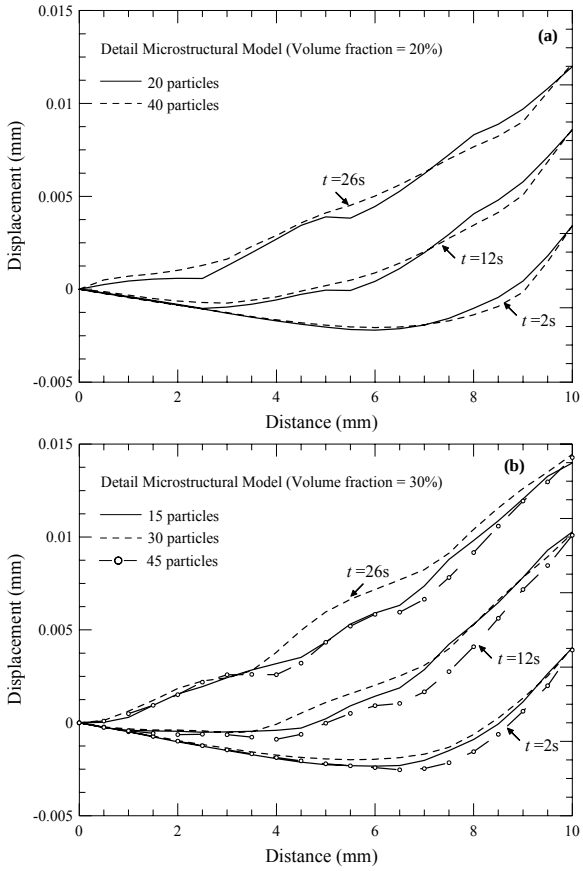

Figure 4.9 Mean displacement profiles for FE models with the unit cell (micromechanical model) at each integration point (solid line) and the FE models with 3D microstructural detail (symbols) for volume fraction of (a) 20% and (b) 30%.

Figure 4.9(a) shows the superimposed curves for 20 and 40 particles model for a sphere volume fraction of 20%. Considering the width of the confidence intervals of Figure 4.7, it can be seen that the average responses are reasonably close and hence that the RVE has been reached. These observations allow to conclude that the micro-mechanical model predicts relatively well the macroscopic response of the composite for this specific microstructure. Figure 4.9(b) shows the superimposed curves for 15, 30 and 45 particles model for a sphere volume fraction of 30%. For times t=12 and t=26

seconds, the huge widths of the confidence intervals (see Figures 4.8(d)-(f)) do not allow to conclude whether the size of the RVE has been reached or not within a reasonable precision and hence render these RVE analyses meaningless. However, for t=2 sec, the confidence intervals are relatively narrow and it is possible to conclude from Figure 4.9(b) that for this time, the RVE size has been reached. For t=2 sec, it seems that the micro-mechanical model predicts relatively well the homogenized displacement distribution, although it is less accurate than the microstructure having 20% of reinforcements. Moreover, it seems that performing simulations with more than 45 reinforcements might lead to narrower confidence intervals for a better assessment of the RVE size. Finally, it can be observed that the micro-mechanical model predicts with more accuracy the temperature distribution than the displacement field, for the cases studied here.

4.1.1.3 THERMAL STRESSES DISTRIBUTIONS

The contrast in the CTEs values of the constituents and high temperature gradient are the main cause for the generation of high thermal stresses. Figures 4.10 to 4.13 show the variation of thermal stresses for spheres volume fractions of 20% and 30% at different times for the homogenized and heterogeneous composites, respectively. For all the figures, except for t=2 sec over a certain distance, the width of the confidence intervals cannot be used to determine if the RVE size has been reached with a high degree of

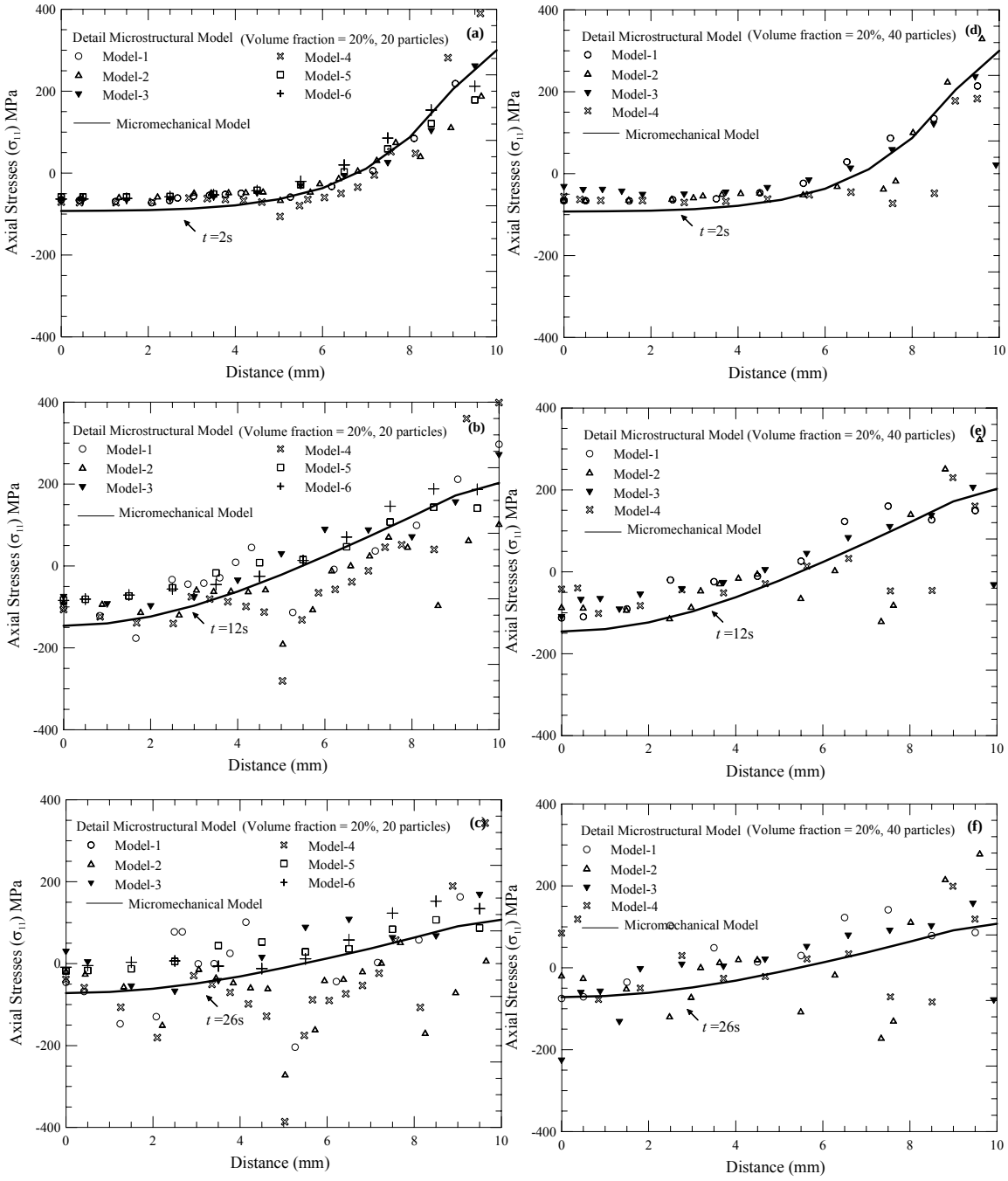

Figure 4.10 Axial thermal stresses for FE models with the unit cell (micromechanical model) at each integration point (solid line) and the FE models with 3D microstructural detail (symbols) for volume fraction of 20% at different times.

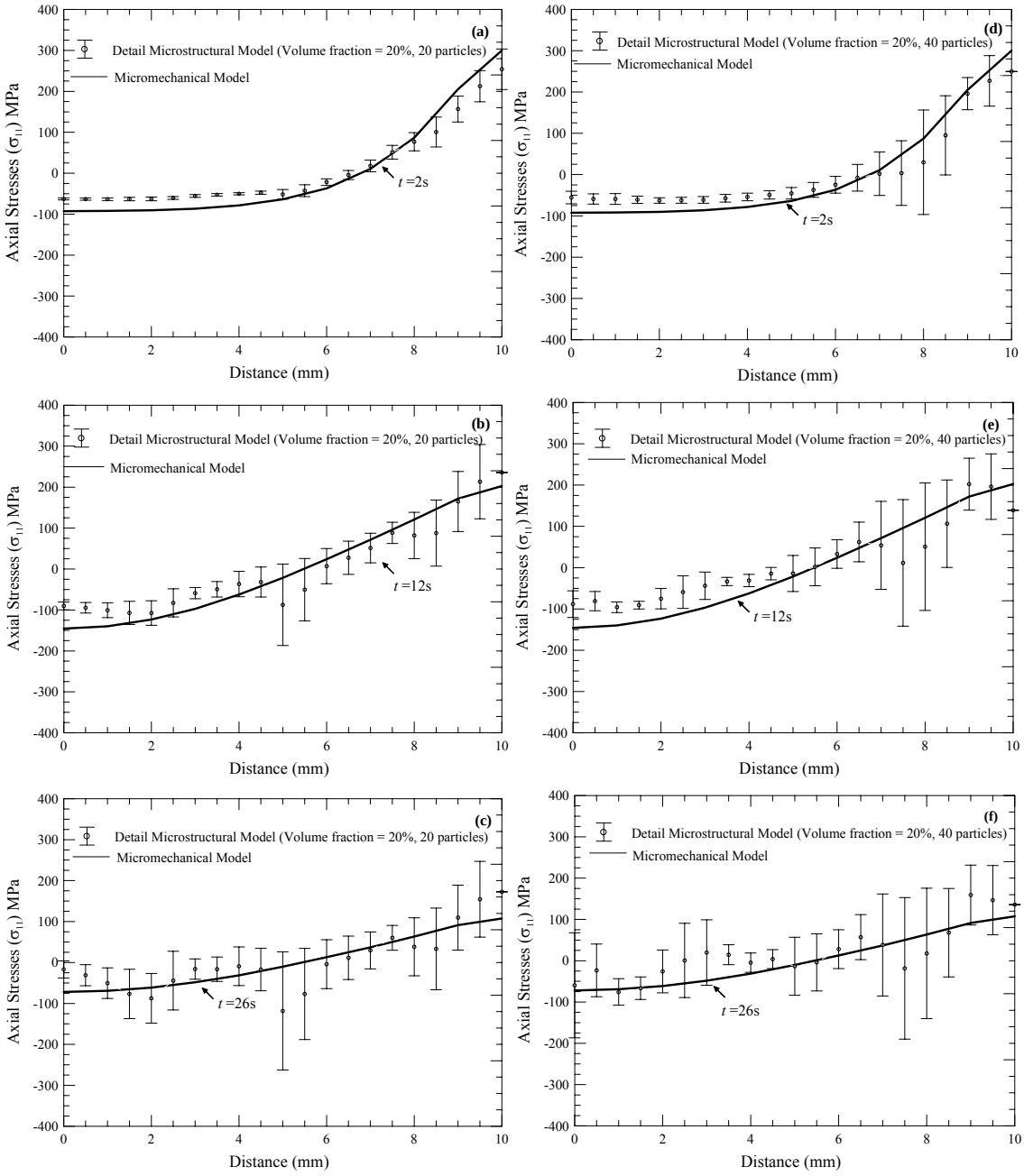

Figure 4.11 Axial thermal stresses for FE models with the unit cell (micromechanical model) at each integration point (solid line) and the FE models with 3D microstructural detail (symbols) for volume fraction of 20% at different times with C.I of 95%. (a), (b) and (c) are mean value of stresses of different FE models with 20 particles and (d), (e) and (f) with 40 particles, measured at extreme top and bottom (corner) edges of the cubes along the temperature gradient direction.

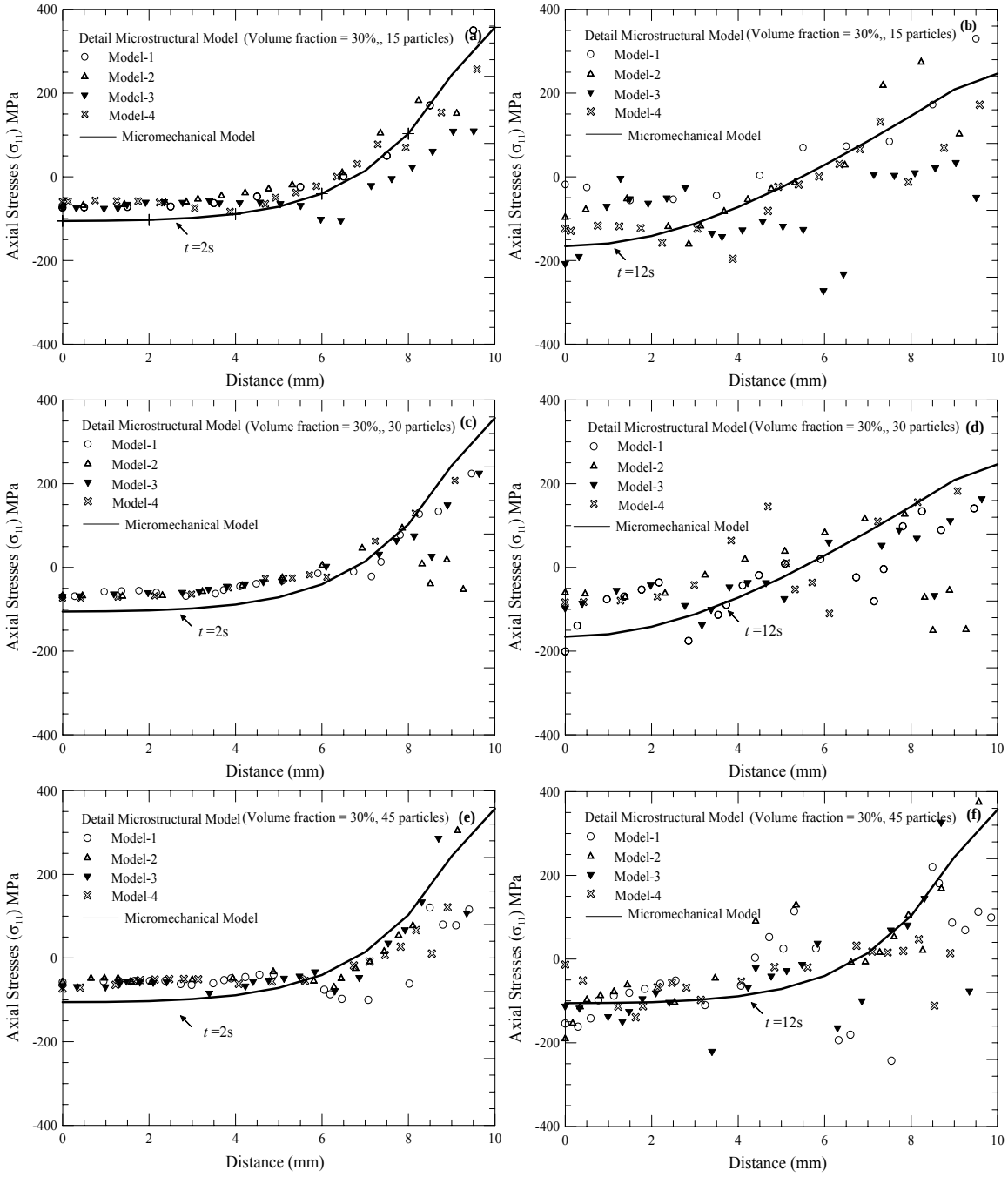

Figure 4.12 Axial thermal stresses for FE models with the unit cell (micromechanical model) at each integration point (solid line) and the FE models with 3D microstructural detail (symbols) for volume fraction of 30% at different times.

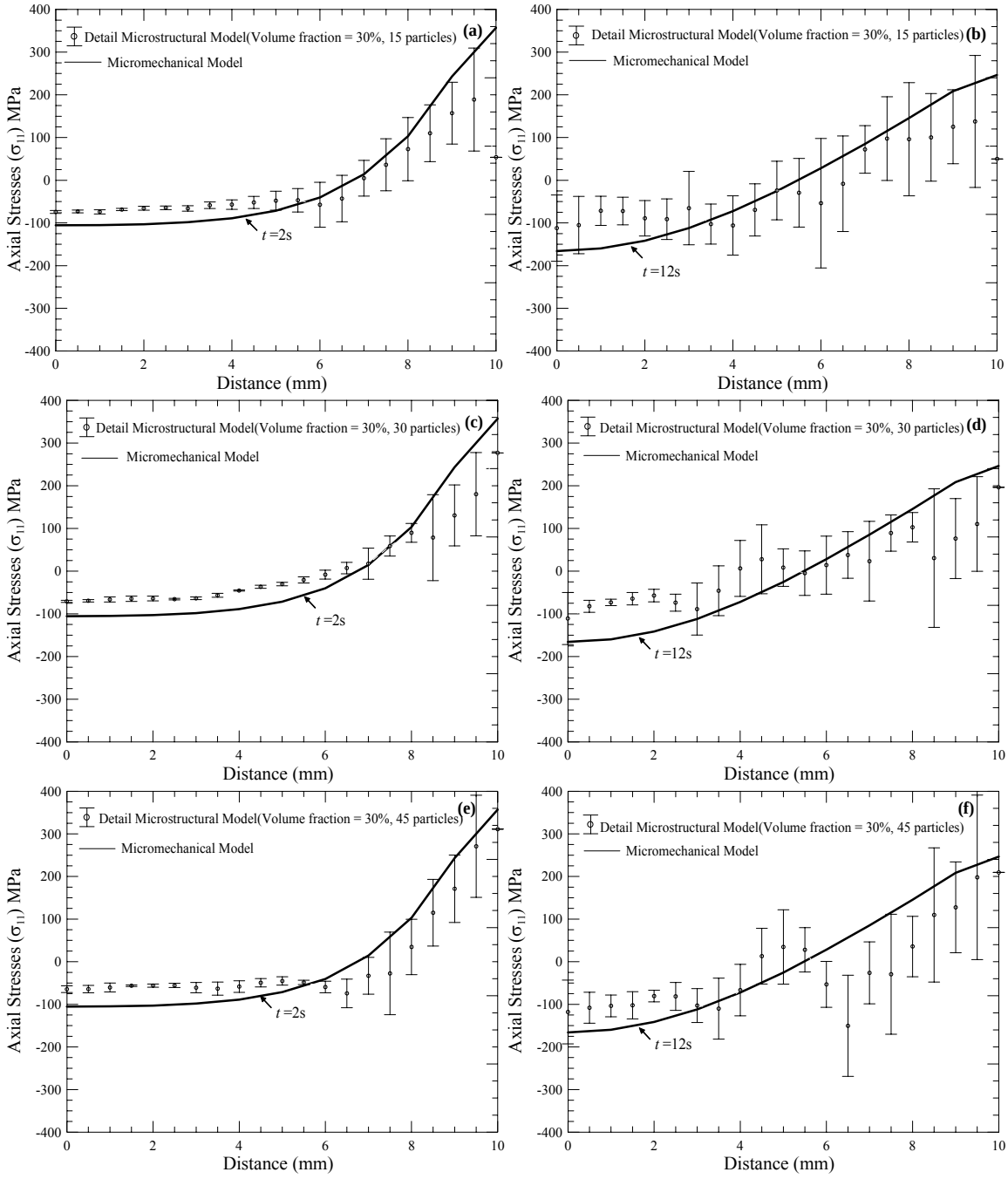

Figure 4.13 Axial thermal stresses for FE models with the unit cell (micromechanical model) at each integration point (solid line) and the FE models with 3D microstructural detail (symbols) for volume fraction of 30% at different times with C.I of 95%. (a), (b) and (c) are mean value of stresses of different FE models with 15 particles and (d), (e) and (f) with 30 particles, (g), (h) and (i) with 45 particles, measured at extreme top and bottom (corner) edges of the cubes along the temperature gradient direction.

confidence. For t=2 sec, it seems that the micro-mechanical model can predict reasonably well the thermal stresses distribution. However, for all the other cases, the results suggest that the micro-mechanical is not capable of capturing the thermal stresses with good accuracy. To corroborate the above-mentioned hypothesis, the mean values of axial thermal stress at different times are shown in Figures 4.14(a)-(c) for the microstructures having 20% of reinforcements. More realizations, and possibly with models having more reinforcements, are required for confirming this hypothesis with more confidence.

The localized stresses are found in some models which are generally due to the specific micro-geometrical features and the high fluctuation about the mean stress profile is due to the presence or absence of the particle along the profile where the stresses are computed. These high compressive stresses are found in those matrix elements which surrounds the particle region. In this study the thermal expansion of the particle is higher than the surrounding matrix at all temperatures. Therefore, during the transient heat conduction the free expansions of the particle are restrained by the surrounding matrix elements. The larger CTE mismatch of particle/matrix elements results in such high values of compressive stresses in the neighboring elements of particle.

For example, consider model-2 shown in Figure 4.15(a) for which the high compressive stresses are found in the matrix region that restraint the free expansion of two particle regions. A similar behavior is found for the elements neighboring the particle region approximately at 2.5mm and 8.3mm, respectively. For the same

temperature difference the particle expands more than the matrix but the surrounding restraints

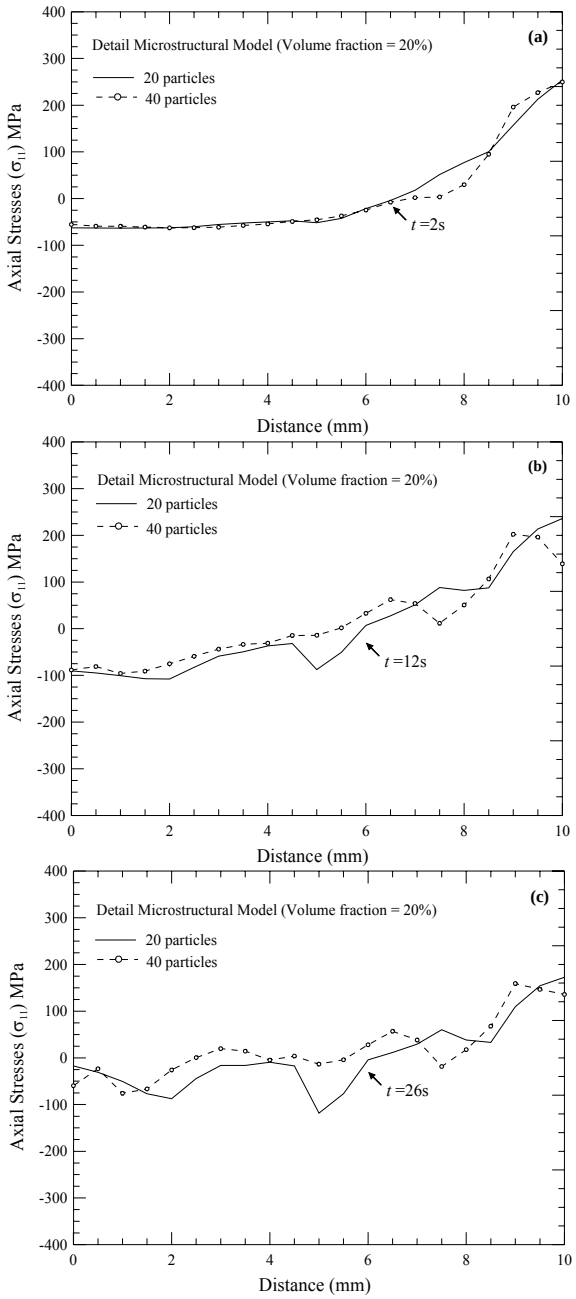

Figure 4.14 Mean stress profiles for FE models with the unit cell (micromechanical model) at each integration point (solid line) and the FE models with 3D microstructural detail (symbols) for volume fraction of (a) 20% at different times.

provided by the matrix elements are the main cause for the generation of such high values of compressive stresses. The same description is applicable to other models where such micro-geometrical features are found; for example, see below Figure 4.15(b) of model-1.

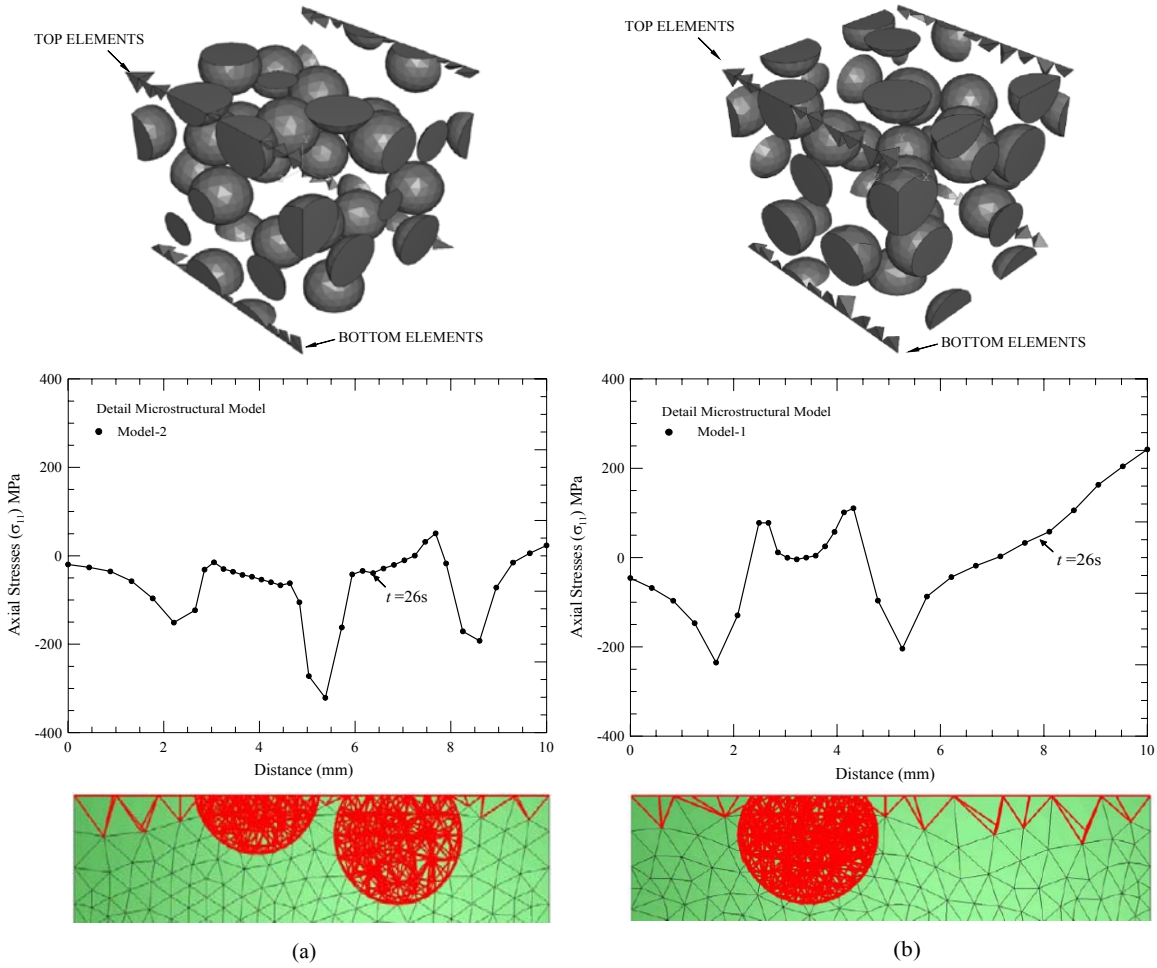

Figure 4.15 Axial thermal stresses for FE models with 3D microstructural detail for volume fraction of 20% at t=26 sec. (a) and (b) are actual values of stresses at top (corner) edge $\{(X_1,10,10);\ 0 \leq X_1 \leq 10\}$ for model-2 and model-1, respectively.

4.1.1.4 EFFECTIVE THERMOELASTIC DISPLACEMENT

The effective displacement, ($\overline{\delta_1}$), is defined as $\overline{\delta_1} = \overline{\varepsilon}_{11} L$, where $\overline{\varepsilon}_{11}$ is the volume average of the strains in x_1 direction and L is the length of the cube. For both the multi-scale and the detailed models, ($\overline{\delta_1}$) was computed at the face of loading (BDHF in Figure 4.3) for composites having a sphere volume fraction of 20% and 30%, respectively. The $\overline{\delta_1}$ as a function of time is plotted in Figure 4.16 (a)-(b). The mean values of effective displacements (along with 95% confidence intervals) for

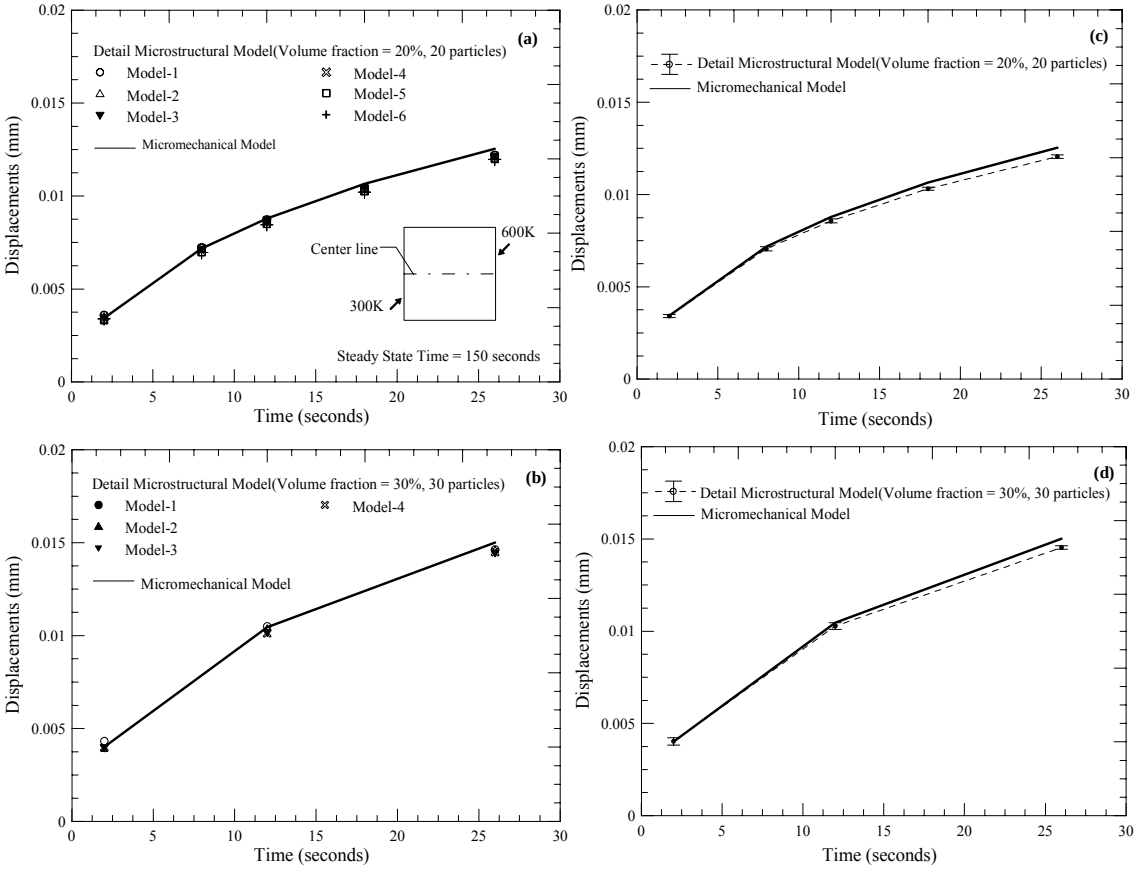

Figure 4.16 Effective axial displacements for FE models with the unit cell (micromechanical model) at each integration point (solid line) and the FE models with 3D microstructural detail (symbols) for volume fraction of (a) 20% and (b) 30%. Mean values of effective displacements for (c) 20% and (d) 30% with C.I of 95%.

heterogeneous composite models having 20% and 30% reinforced particles are shown in Figures 4.16(c)-(d). Agreement of these results corroborate that the present micromechanical formulation is suitable for the prediction of effective responses of composites through the incorporation of a nonlinear thermo-elastic constitutive material model.

4.1.2 THERMOVISCOELASTIC ANALYSES

Next, the sequentially coupled thermo-viscoelastic analyses are performed. Both micromechanical approaches of Section 4.1, cubic models of dimensions 10 x 10 x 10mm, were used. The studied composite is a Hercules epoxy matrix reinforced by randomly distributed TiC+HDPE spherical particles. Two volume fractions of reinforcements were studied, namely 20% and 30%. For the detailed FE meshes, cubes containing 20 and 30 spheres are considered. The matrix follows non-linear thermo-viscoelastic behavior while particle is considered to be thermoelastic. The heterogeneous composites directly incorporate nonlinear thermo-viscoelastic behaviors for the particle and matrix regions. The thermal as well as the mechanical properties used in the simulations given in Table 4.2. The thermal, mechanical and Prony series coefficients for Hercules epoxy are taken from Khan (2006). The thermal and mechanical properties for TiC and HDPE particles are taken from available literature. The details of references are given in Section 3.3 of Chapter III.

Table 4.2. Temperature dependent mechanical and physical properties of materials of Hercules 3502 epoxy (polymer) and TiC+HDPE (particle) used in thermo-viscoelastic FE analyses.

Property	Hercules Epoxy	TiC+HDPE
Young modulus, (E) (MPa)	$4291.85\exp\left[-0.675\left(\frac{T-303}{303}\right)^{0.787}\right]$	$-6\times10^{6}+84074T-527.32T^{2}+1.7504T^{3}-0.0032\,T^{4}+3\times10^{-6}\,T^{5}-1\times10^{-9}\,T^{6}$
Poisson ratio,(υ)	0.36	0.297
Coefficient of Thermal Expansion, (α)10-6, 1/°K	$30\times10^{-6}\,T+2.67\times10^{-7}\,(T-273)$	$7.0\times10^{-5}-5.0\times10^{-7}\,T+3.0\times10^{-9}\,T^{2}$
Thermal Conductivity, (K), W/m/°K	$0.202+6.12\times10^{-3}\,T-4.81\times10^{-5}\,T^{2}+1.25\times10^{-7}T^{3}-1.04\times10^{-10}T^{4}$	$1.7-4.90\times10^{-3}\,T+1.02\times10^{-5}\,T^{2}$
Specific heat,(c) , J/Kg. °K	$5.347\,T-456.9$	$17865-116.2\,T+0.2T^{2}$
Density, (ρ) , Kg/m3	1260	965.1

* T is temperature in °K.

The transient creep thermal analysis consisted in a problem where a composite was initially at 300°K, except for one face that was at 400°K. This transient heat transfer problem was solved until a steady state was reached. A uniform stress of 10 MPa was applied on the face that was at 400°K in order to simulate effective transient creep response. The models were subjected to the following boundary conditions:

$$
\begin{aligned}
&T(x_1,x_2,x_3,0)=300K; && 0\le x_1\le 10, 0\le x_2\le 10,\ 0\le x_3\le 10\\
&T(10,x_2,x_3,t)=400K; && 0\le x_2\le 10,\ 0\le x_3\le 10,\ t\ge 0\\
&\frac{\partial T(x_1,0,x_3,t)}{\partial x_2}=\frac{\partial \overline{T}(x_1,10,x_3,t)}{\partial x_2}=0.0; && 0\le x_1\le 10,\ 0\le x_3\le 10,\ t\ge 0\\
&\frac{\partial T(x_1,x_2,0,t)}{\partial x_3}=\frac{\partial \overline{T}(x_1,x_2,10,t)}{\partial x_3}=0.0; && 0\le x_1\le 10,\ 0\le x_2\le 10,\ t\ge 0
\end{aligned}
\qquad (4.3)
$$

$$
\begin{aligned}
&u_1(0,x_2,x_3,t)=0.0; && 0\le x_2\le 10,\ 0\le x_3\le 10\\
&u_2(x_1,0,x_3,t)=0.0; && 0\le x_1\le 10,\ 0\le x_3\le 10\\
&u_3(x_1,x_2,0,t)=0.0; && 0\le x_1\le 10,\ 0\le x_2\le 10\\
&t_1(10,x_2,x_3,t)=10.0\,\text{MPa}; && 0\le x_2\le 10,\ 0\le x_3\le 10\\
&t_2(x_1,10,x_3,t)=0.0\,\text{MPa}; && 0\le x_1\le 10,\ 0\le x_3\le 10\\
&t_3(x_1,x_2,10,t)=0.0\,\text{MPa}; && 0\le x_1\le 10,\ 0\le x_2\le 10
\end{aligned}
\tag{4.4}
$$

where u_i and t_i (i=1,2,3) are the components of the displacements and the surface tractions, respectively. In the following subsections, the field variables variations during transient creep forecasted from the multi-scale framework are compared to those of the detailed FE meshes of Section 4.1.

4.1.2.1 TEMPERATURE DISTRIBUTION

Figure 4.17(a) shows the temperature distributions obtained from the homogenized model as well as from the heterogeneous composite reinforced by 20% of TiC+HDPE particles for model size of 20 particles, for different times. Figure 4.17(b) shows the mean responses of the various realizations, along with 95% confidence intervals for models of 20 particles. The largest width of the confidence interval was found to be 1.36% of the mean value. The width of the confidence interval decreases as the time increases. Figures 4.18(a)-(b) shows temperature profiles from a similar type of analyses but for a composite reinforced by 30% of TiC+HDPE particles and for model containing 30 particles. The largest width of the confidence intervals is 1.52% of the mean value. Figures 4.17 and 4.18 show that the micromechanical model predicts fairly well the temperature profiles for the range of material properties simulated.

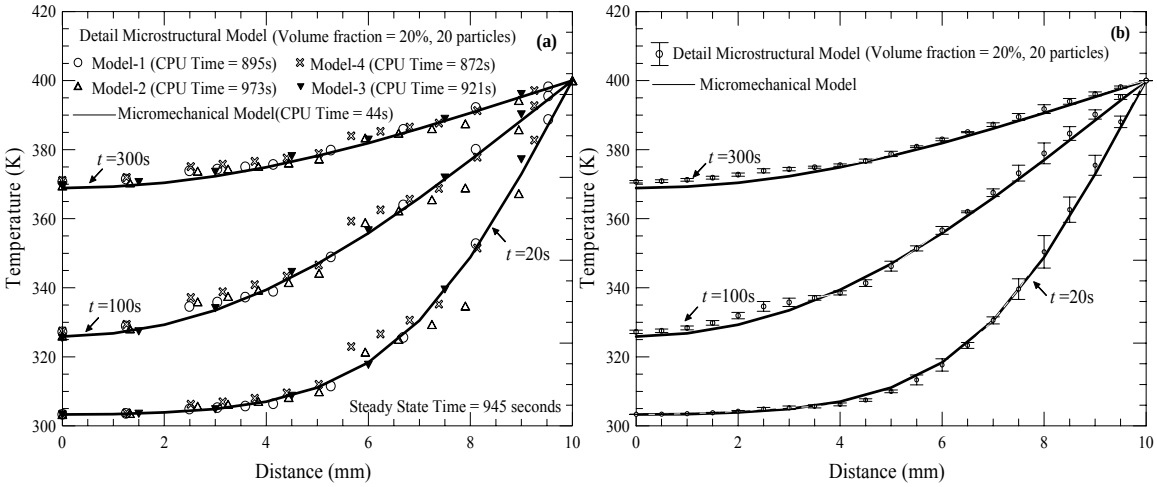

Figure 4.17 Comparison of temperature profiles for FE models with the unit cell (micromechanical model) at each integration point (solid line) and the FE models with 3D microstructural detail (symbols) for volume fraction of 20% at different times. (a) average values of temperature at top and bottom (4-corners) edges {(X_1,0,0); (X_1,0,10); (X_1,10,0); (X_1,10,10); $0 \leq X_1 \leq 10$} (b) mean values of temperature of different FE models with C.I of 95% along the temperature gradient direction.

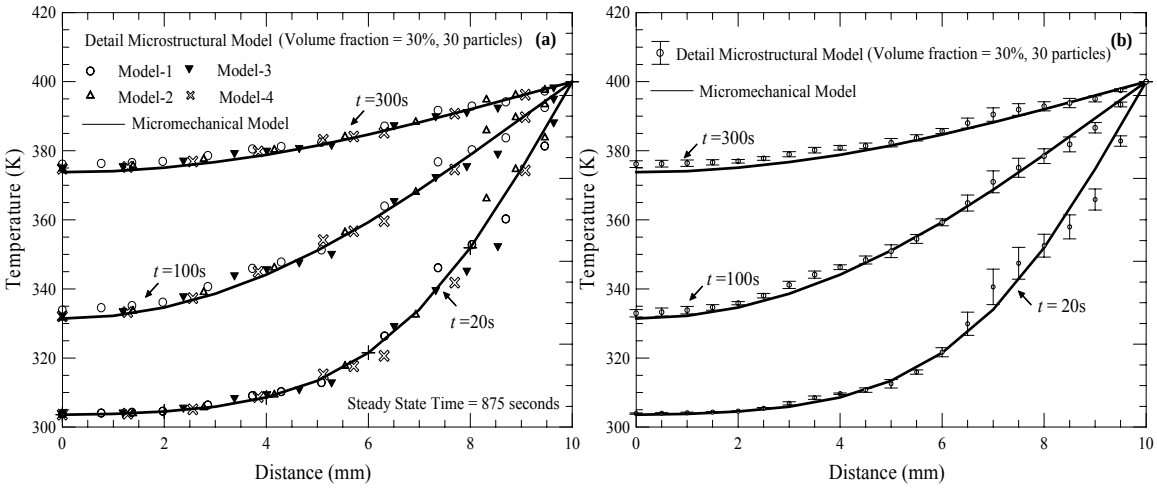

Figure 4.18 Comparison of temperature profiles for FE models with the unit cell (micromechanical model) at each integration point (solid line) and the FE models with 3D microstructural detail (symbols) for volume fraction of 30% at different times. (a) average values of temperature at top and bottom (4-corners) edges {(X_1,0, 0); (X_1,0,10); (X_1,10,0); (X_1,10,10); $0 \leq X_1 \leq 10$} (b) mean values of temperature of different FE models with C.I of 95% along the temperature gradient direction.

Table 4.3 Prony series coefficients for the Hercules 3502 polymer.

n	$\lambda_n(\text{sec}^{-1})$	$D_n \times 10^{-6}(\text{MPa}^{-1})$
1	1	176.0
2	10^{-1}	5.0
3	10^{-2}	29.0
4	10^{-3}	25.0
5	10^{-4}	35.0
6	10^{-5}	6.80

4.1.2.2 DISPLACEMENT DISTRIBUTION

Figure 4.19(a) shows the displacement distributions obtained from the homogeneous and heterogeneous models for a composite containing 20% of TiC+HDPE particles for model having 20 particles. Figure 4.19(b) shows the average response of the various realizations, along with 95% confidence intervals on the mean value. The largest width of the confidence interval was found to be 156% of the mean value. Figures 4.20(a)-(b) show displacements from similar analyses but for a composite reinforced by 30% of TiC+HDPE particles for models containing 30 particles. The largest width of the confidence interval was of 160%. It can be observed that the similar trends are found in the thermoviscoelastic analyses as were observed for the thermoelastic analyses. The micro-mechanical model predicts with more accuracy the temperature distribution than the displacement field, for the cases studied here. Nevertheless, it still gives average displacement response of the composite.

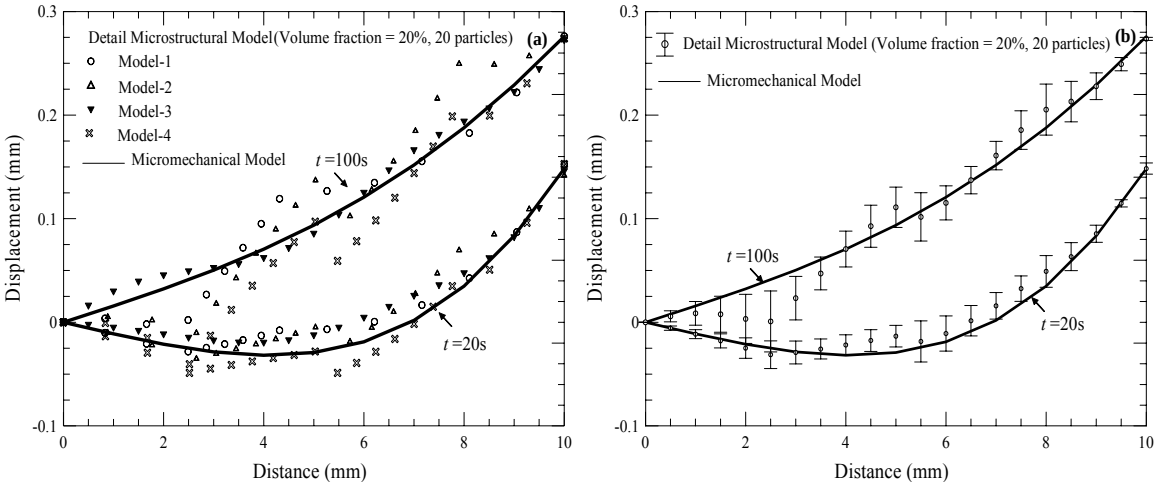

Figure 4.19 Comparison of axial displacements for FE models with the unit cell (micromechanical model) at each integration point (solid line) and the FE models with 3D microstructural detail (symbols) for volume fraction of 20% at different times. (a) average values of displacements at top and bottom (4-corners) edges {(X_1,0,0); (X_1,0,10); (X_1,10,0); (X_1,10,10); $0 \leq X_1 \leq 10$} (b) mean values of displacements of different FE models with C.I of 95% along the temperature gradient direction.

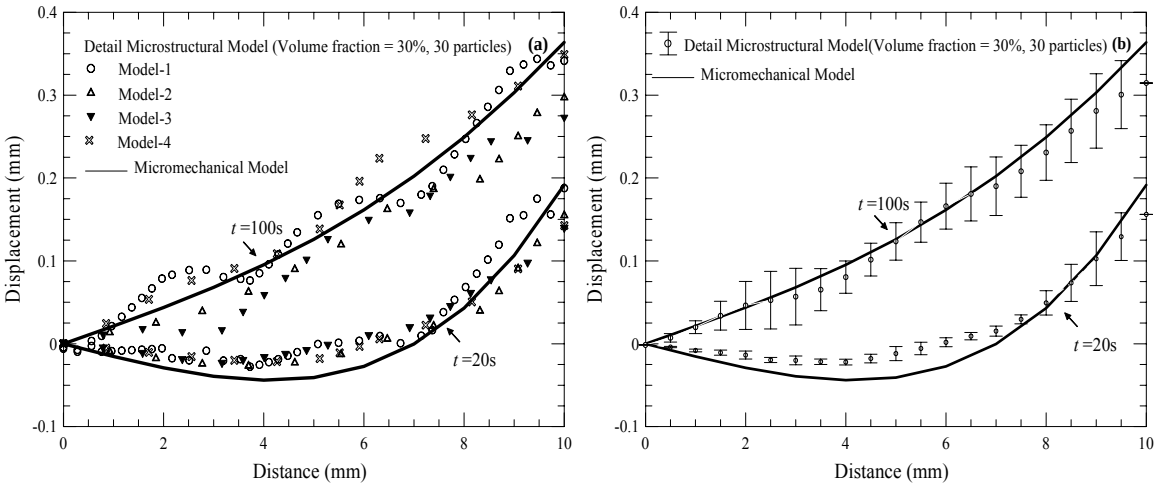

Figure 4.20 Comparison of axial displacements for FE models with the unit cell (micromechanical model) at each integration point (solid line) and the FE models with 3D microstructural detail (symbols) for volume fraction of 30% at different times. (a) average values of displacements at top and bottom (4-corners) edges {(X_1,0,0); (X_1,0,10); (X_1,10,0); (X_1,10,10); $0 \leq X_1 \leq 10$} (b) mean values of displacements of different FE models with C.I of 95% along the temperature gradient direction.

4.1.2.3 THERMAL STRESSES DISTRIBUTIONS

Figures 4.21 to 4.22 show the variation of thermal stresses for spheres volume fractions of 20% and 30% at different times for the homogenized and heterogeneous composites, respectively. For all the figures, the widths of the confidence intervals are very high. The results show that the micromechanical model only gives average responses of the overall thermal stresses. This approach is useful for designing composite structures in which the structures are designed with the maximum load carrying capacity below the threshold of failure/damage. However the simplified micromechanical model is limited in obtaining detailed field variables such as discontinuities of stress at the interfaces of the constituents and therefore it is not capable of incorporating failure mechanism such as de-bonding, damage, crack propagation etc.

4.1.2.4 EFFECTIVE THERMOVISCOELASTIC DISPLACEMENT

For both the multi-scale and the detailed models, ($\overline{\delta_1}$,effective far field displacement) was computed at the face of loading (BDHF in Figure 4.3) for composites having a sphere volume fraction of 20% and 30%, respectively. The $\overline{\delta_1}$ is plotted as a function of time in Figures 4.23 (a)-(b). The mean values of effective displacements (along with 95% confidence intervals) for heterogeneous composite models having 20% and 30% reinforced particles are shown in Figures 4.23 (c)-(d). Good agreements are observed for the sphere volume fraction of 20% while for the particle VF of 30% the present micromechanical predictions for effective displacements are higher than those of the heterogeneous composite. One of the reasons for the higher values of displacements for 30% VF is that the CTE for particles are approximately 7 times more than the matrix that

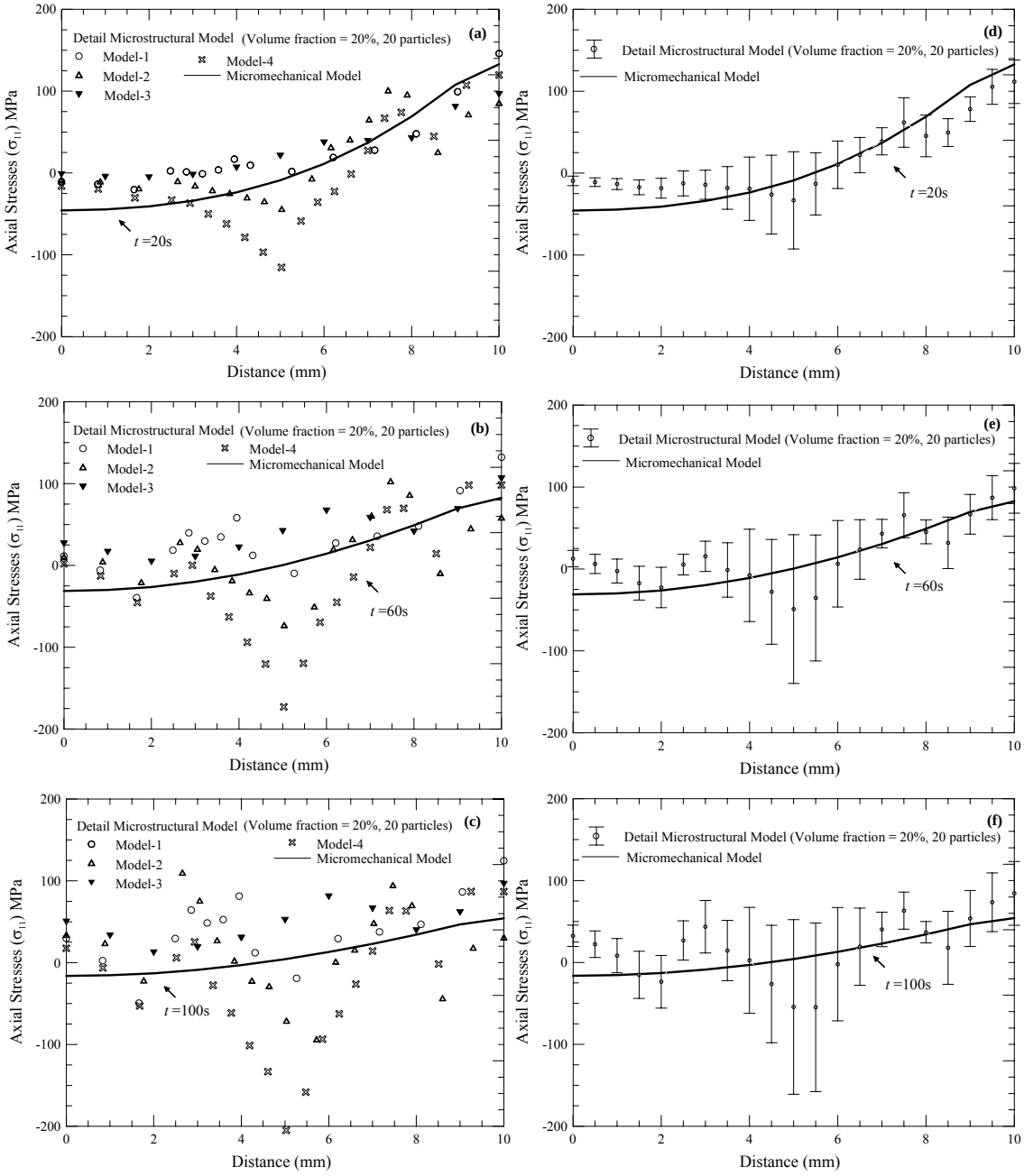

Figure 4.21 Comparison of axial thermal stresses for FE models with the unit cell (micromechanical model) at each integration point (solid line) and the FE models with 3D microstructural detail (symbols) for volume fraction of 20% at different times. (a) average values of stresses at top and bottom (4-corners) edges {(X_1,0,0); (X_1,0,10); (X_1,10,0); (X_1,10,10); $0 \leq X_1 \leq 10$} (b) mean values of stresses of different FE models with C.I of 95% along the temperature gradient direction.

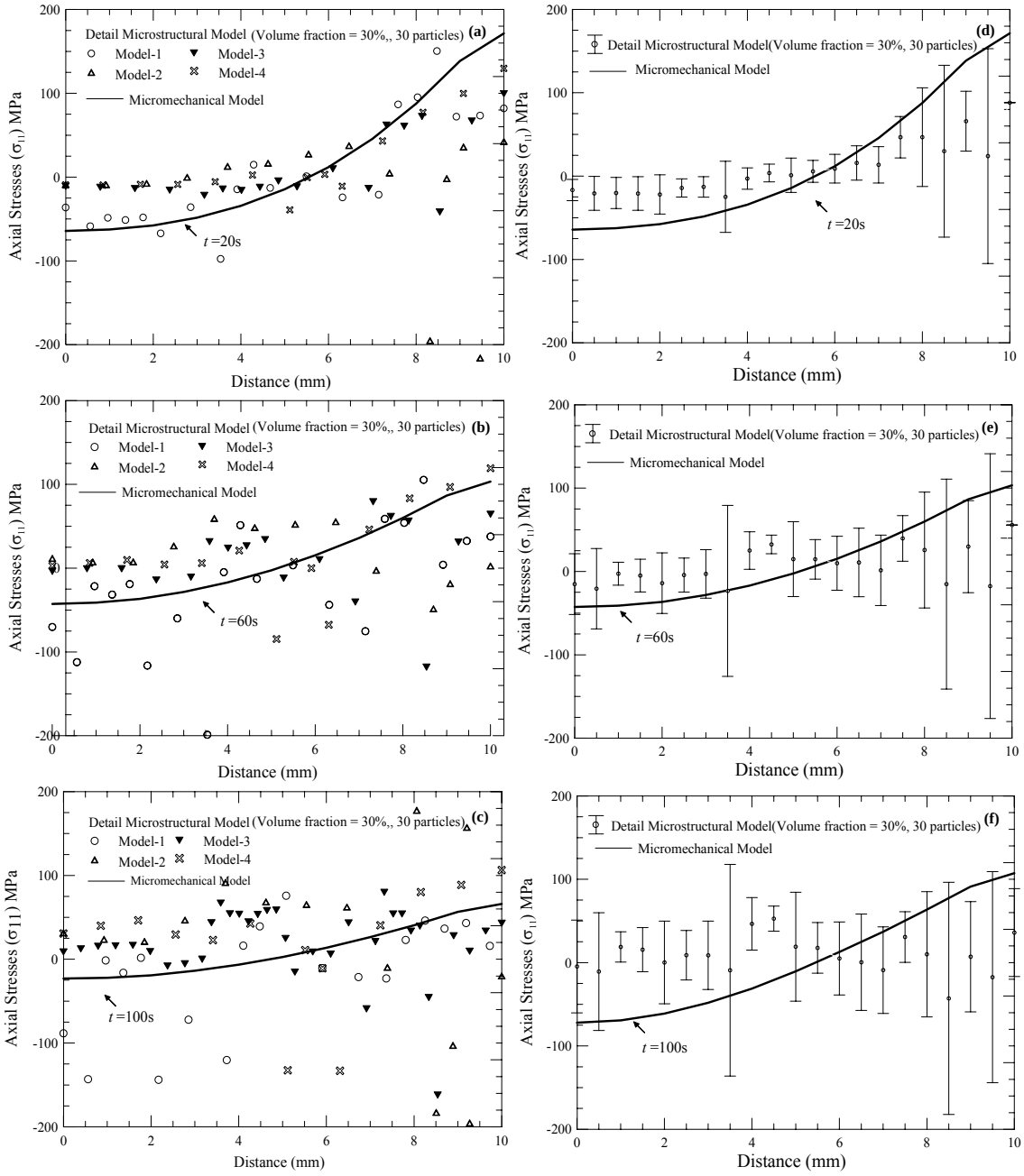

Figure 4.22 Comparison of axial thermal stresses for FE models with the unit cell (micromechanical model) at each integration point (solid line) and the FE models with 3D microstructural detail (symbols) for volume fraction of 30% at different times. (a) average values of stresses at top and bottom (4-corners) edges {(X_1,0,0); (X_1,0,10); (X_1,10,0); (X_1,10,10); $0 \leq X_1 \leq 10$} (b) mean values of stresses of different FE models with C.I of 95% along the temperature gradient direction.

raised the effective CTE of the homogenized composite. However, for detailed microstructural FE models the expansion of the particles are restrained causing in high compressive thermal stresses but lesser displacement values than the homogenized ones. Moreover, this is expected because of the increase of the volume content of stiffer inclusion.

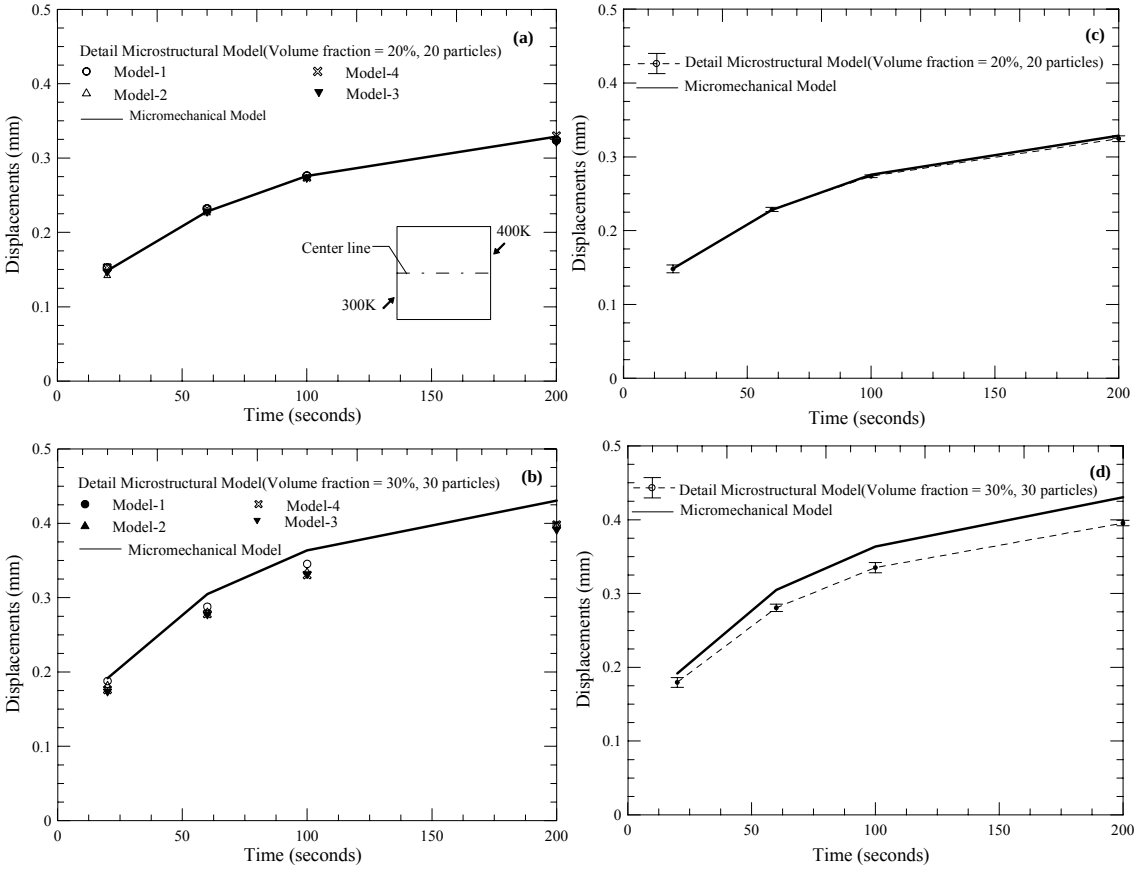

Figure 4.23 Effective axial displacements for FE models with the unit cell (micromechanical model) at each integration point (solid line) and the FE models with 3D microstructural detail (symbols) for volume fraction of (a) 20% and (b) 30%. Mean values of effective displacements for (c) 20% and (d) 30% with C.I of 95%.

The comparisons of transient responses of the homogenized and heterogeneous composites due to coupled heat conduction and mechanical loading have been studied.

For the temperature response, the RVE size was reached for both models having 20% and 30% reinforcements. It was found that the temperature distribution is relatively well predicted by the multi-scale model. The width of the confidence intervals for the displacements were larger than those for the temperature but allowed nevertheless to conclude that the multi-scale framework can also predict with a reasonable accuracy the displacement field inside the composite. The RVE size was not reached for the thermal stresses and it is not possible to conclude that the multi-scale framework is suitable for representing accurately these stresses. Larger RVEs or many more simulations for the same RVE sizes would be required in order to narrow the confidence intervals. However, the mean results obtained are encouraging and running more simulations might reveal that the multi-scale framework is also suitable for evaluating the overall (average) thermal stresses. Finally, the multi-scale model predicted with reasonable accuracy the effective displacement. Therefore, the main contribution of this work was the development and the partial validation of a multi-scale framework that allows predicting the effective field variables of composite undergoing coupled thermo-mechanical loadings.

4.2 FULLY COUPLED THERMOMECHANICAL ANALYSIS OF PARTICULATE COMPOSITES

The proposed multiscale framework is used to analyze fully coupled thermo-viscoelastic response of composite structural components under multi-axial stresses. A square composite plate with dimensions of 200mm x 200mm x1 mm having a hole of a diameter 10 mm is considered (see Figure 4.24(a)). A multi-axial state of stress exists around the hole for a uniaxial load prescribed at the two opposite surfaces. Due to a double symmetric condition, only a quarter of the plate is modeled. FE mesh with 8-node linear brick element (C3D8T) is generated to perform the coupled temperature-displacement analysis. One element is used through the thickness of 1 mm. A total of 463 nodes and 269 elements are generated.

The studied composite is a FM73 matrix reinforced by TiC+HDPE particles. The Prony series coefficients, nonlinear stress and temperature dependent parameters, thermal and mechanical properties used in the simulations are already given in section 2.3 of Chapter II and section 3.3 of Chapter III. The schematic of the geometry of the plate and boundary conditions are given in Figure 4.24(a)-(c). A cyclic stress of $\sigma_{11} = \sigma_0 \sin \omega t$ along x_1 direction is applied at the far ends of the plate for duration of 2400 seconds (40 minutes). A composite was initially at 303°K. The following case studies are considered:

Case 1: The cyclic stress of amplitude (σ_0) 10MPa and frequency (ω) $\pi/4$ is applied with no heat flux across prescribed at all faces of the plate including the surface of a

hole. As a result, the evolution of temperature is only due to the energy dissipation of a viscoelastic body during the deformation.

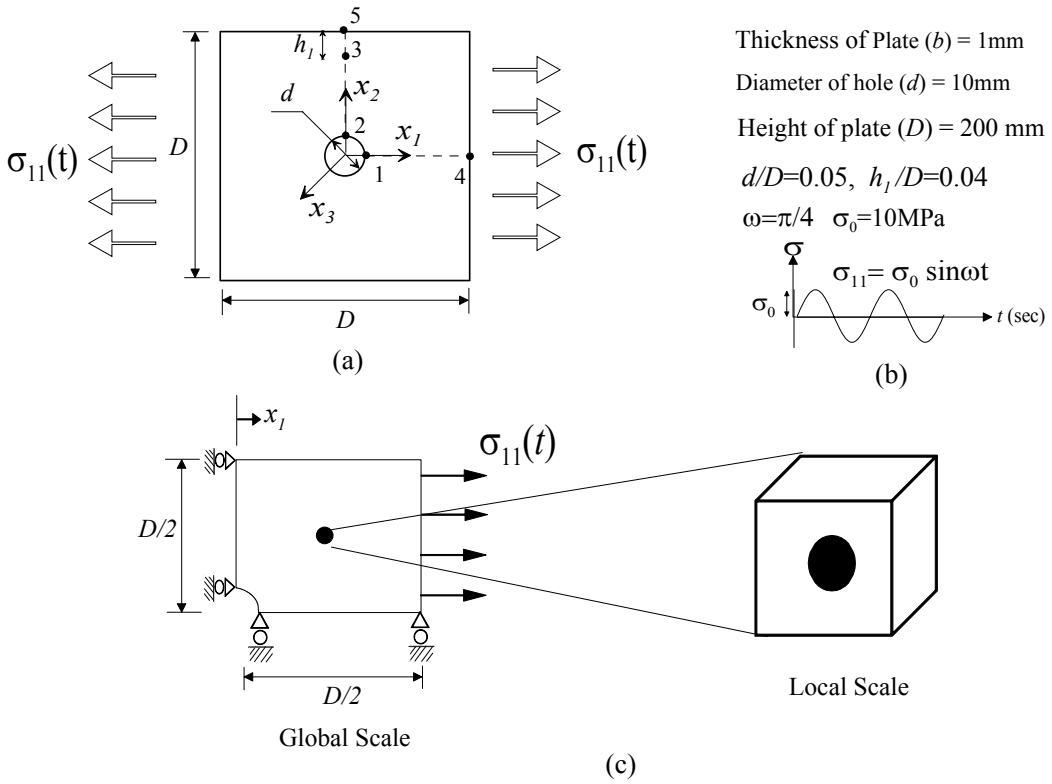

Figure 4.24 a) Geometry of the plate, loading direction and locations at which the temperatures are measured. (b) plate dimensions and loading type (c) representation of multiscale models along with geometry, loading and boundary conditions of the FE model.

Case 2: The cyclic stress of amplitude (σ_0) 10MPa and frequency (ω) $\pi/4$ is applied with no heat flux across prescribed at all faces of the plate except the face where the axial load is applied. The temperature of 313°K is specified on the face at which the load is applied. This allows us to analyze the heat conduction along axial direction (x_1 axis) along with the dissipation of energy due to the viscoelastic deformation.

The temperature generation at three different locations (see Figure 4.24a) is shown in Figure 4.25 for the case 2 with VF of 0% and 10%. It is observed that the heat generation at these points is not affected by the conduction for the given duration of the analysis. The maximum heat is generated at point 2 where the maximum stresses are present. At these three points the conduction due to the prescribed temperature at the boundary is taking place very slowly as compare to the heat generation due to the dissipation. Lower heat is generated for the composite as compared to the unreinforced material resulting in lower temperature increase.

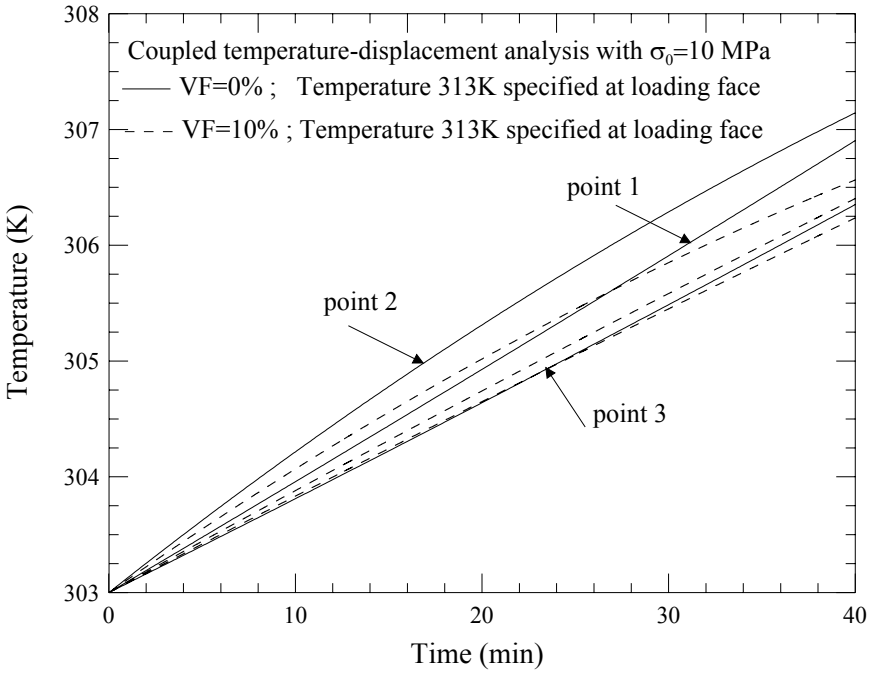

Figure 4.25 Temperature increase due to temperature and cyclic stress loading at locations 1, 2 and 3 for composites having TiC+HDPE particle volume fractions of 0% and 10%.

The temperature increase along the line joining points 1 and 4 (see Figure 4.24a) in the x_1 direction is reported in Figure 4.26. During the entire cyclic loading the

temperature boundary condition is specified at the right face. Figure 4.26(a) shows the conduction behavior for the neat FM73 matrix along with the heat generation during the viscoelastic deformation. The conduction is taking place so slowly such that the

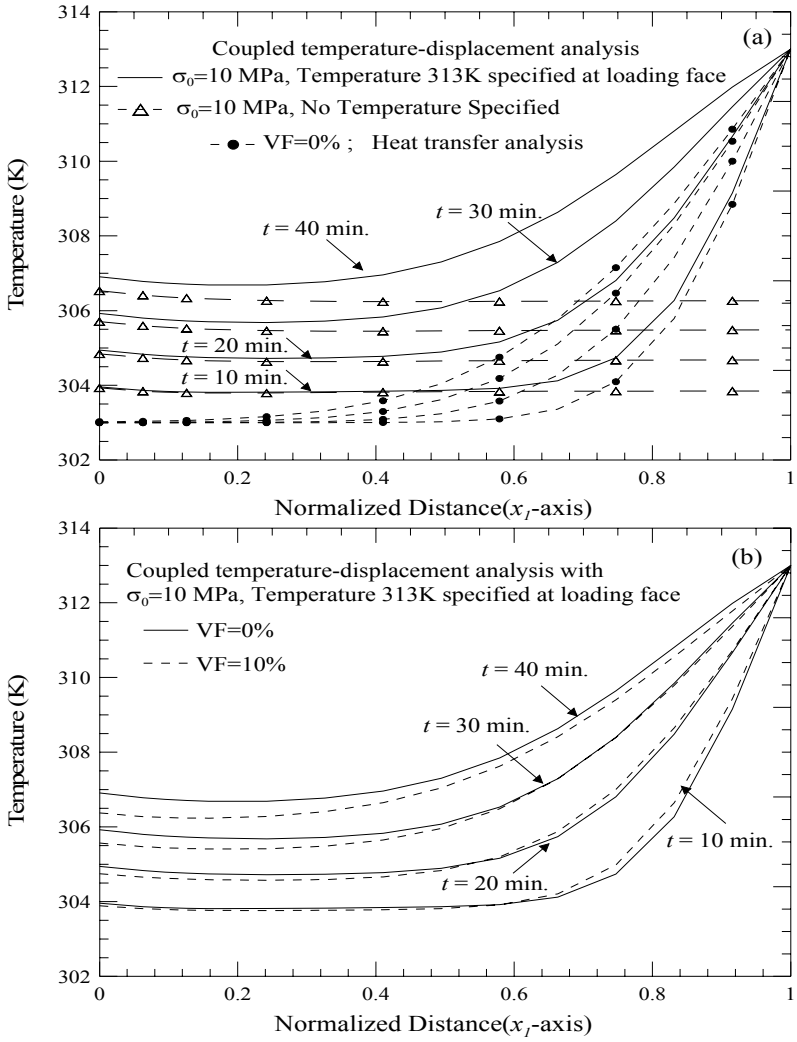

Figure 4.26 Temperature profile along the x_1-axis (line joining point 1-4) for composites. a) heat transfer vs. coupled temperature displacement analysis for pure FM73 polymer. b) coupled temperature displacement analysis for composites having 0% and 10% VF of TiC+HDPE particles.

temperature rise due to the dissipation overcomes the propagation of the temperature due to conduction along the axial direction. The heat generation rate increases with time,

accelerating the temperature increase, as shown in Figure 4.26(b) and 4.27. As expected less temperature rise is obtained for the composite reinforced with particle VF of 10% as compared to the neat matrix.

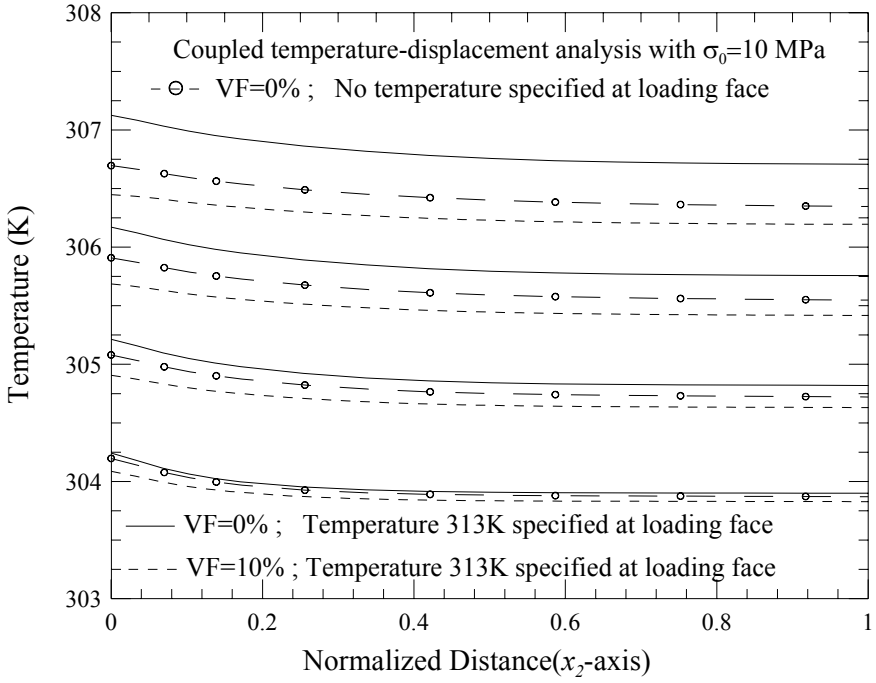

Figure 4.27 Temperature profile along the x_2-axis (line joining point 2-5) for FM73/TiC+HDPE composites during coupled temperature displacement analysis.

Next, bending of a cantilever beam under a cyclic load is studied. The beam with dimensions of 100mm x 20mm x2 mm is considered. FE mesh with 8-node linear brick element (C3D8T) is generated to perform the coupled temperature-displacement analysis. One element is used through the thickness of 2 mm. A total of 198 nodes and 80 elements are generated.

The studied composite is a FM73 matrix reinforced by TiC+HDPE particles. The schematic of the geometry of the beam and boundary conditions are shown in Figure

4.28. All boundaries of the specimen are assumed to be insulated, i.e, no heat lost across the boundary. The cyclic transverse load of different amplitudes is applied at the free end of the beam for duration of 1200 seconds (20 minutes). The beam made of a composite material with particle VF of 0%, 12.5% and 25% is studied. The temperature is measured at a point located on the top surface of the beam at a distance of h_1 from the fixed end. Figure 4.29 shows the temperature generation for homogeneous and composite beams. It is found that the temperature generation greatly influenced by the magnitude of the applied load however the temperature increase is slightly lowered by adding some amount of particles.

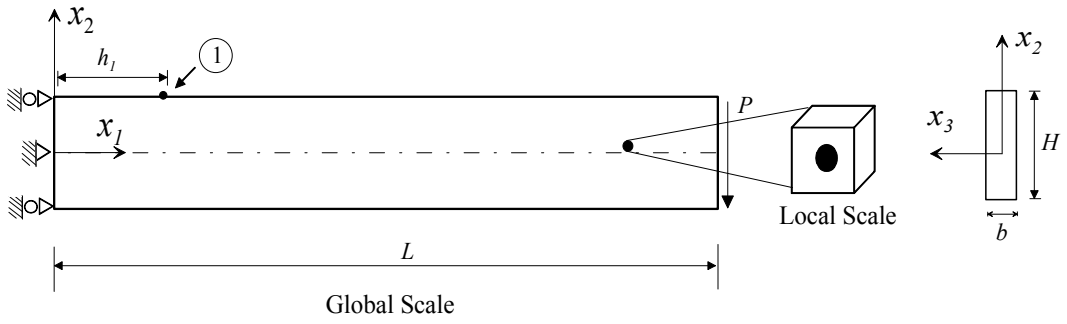

Figure 4.28 Illustration of a multiscale modeling approach for analyzing fully coupled thermoviscoelastic bending analysis of a composite cantilever beam.

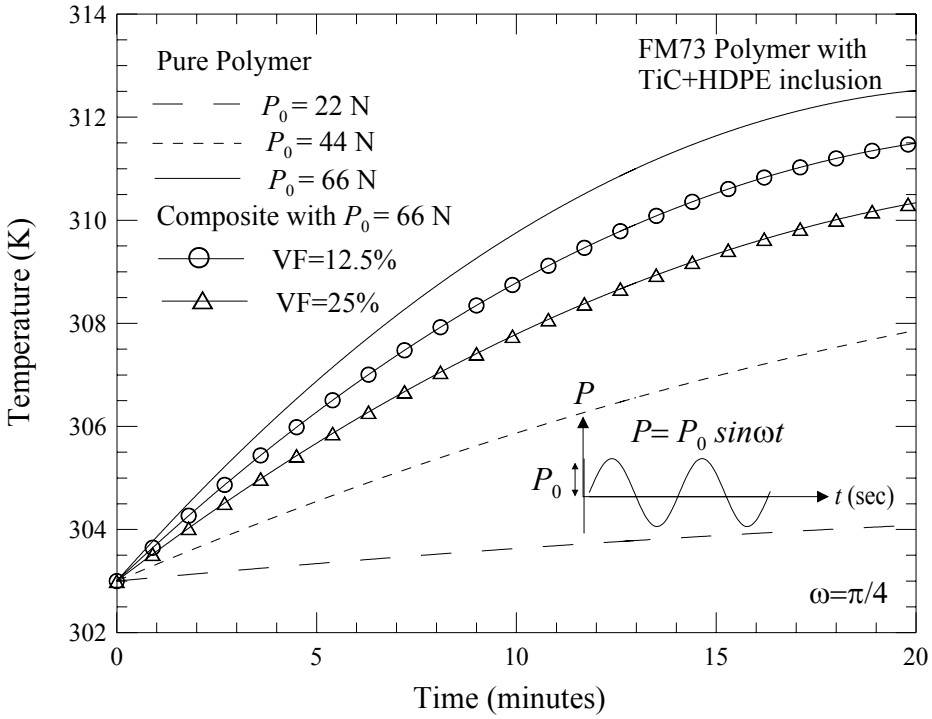

Figure 4.29 Temperature generations at point 1 during fully coupled thermoviscoelastic analysis of a homogeneous and composite cantilever beam.

These analyses show a successful integration of the multiscale micromechanical framework to perform structural analyses and incorporating the dissipation of energy on the deformation of viscoelastic structures.

In summary, the particulate composite having polymeric matrix can generate enormous amount of heat when subjected to cyclic loading for a long period of time. Primarily, the viscoelastic properties of the matrix dominate the overall heat generation rate of the composite. In addition to that, the heat generation rate also depends on the amplitude and frequency of the cyclic loading. The dissipation of energy in the viscoelastic bodies is important for polymer matrix composite structures in which non-uniform heat is generated under a cyclic loading where there is no such cooling

mechanism available that can lowered the localized temperature increase. Moreover, since polymeric based composites have low thermal conductivity, there is a possibility that conduction takes place so slowly such that the temperature continues to increase locally as time progresses. This local temperature increase degrades the material properties and could possibly affect the performance of the structure. If highly conductivity particles are added to the low thermal conductivity matrix then it might be possible that these localized temperature regions could possibly spread out and the overall performance of the composite can be slightly improved. In such cases, the heat generation due to viscoelastic deformation dominates and should be considered. In contrast to large structures conduction plays a very important role in lowering the temperature at the points of maximum stresses in small structures, even for composites having low thermal conductivity. For example, when a composite beam is subjected to a cyclic loading, the conduction takes place from highest temperature regions (due to the generation of high stresses) towards the lowest ones in the beam. As a result, the temperature is dispersed throughout the body of the beam and the values of temperature decreases at the point of maximum stresses. However, under a cyclic loading at high stress amplitudes and moderate frequencies (0.1-10 rad/sec.) for a long period of time the temperature generation is significant and therefore the dissipation of energy due to viscoelastic constituents in composites should be considered.

CHAPTER V

A MULTI-SCALE MODEL FOR COUPLED HEAT CONDUCTION AND DEFORMATIONS OF VISCOELASTIC FUNCTIONALLY GRADED MATERIALS*

An integrated micromechanical-structural framework is presented to analyze coupled heat conduction and deformations of functionally graded materials (FGM) having temperature and stress dependent viscoelastic constituents. A through-thickness continuous variation of the thermal and mechanical properties of the FGM is approximated as an assembly of homogeneous layers. Average thermo-mechanical properties in each homogeneous medium are computed using a simplified micromechanical model for particle reinforced composites described in Chapter III. This micromechanical model consists of two isotropic constituents. The mechanical properties of each constituent are time-stress-temperature dependent. The thermal properties (coefficient of thermal expansion and thermal conductivity) of each constituent are allowed to vary with temperature. Sequentially and fully coupled heat transfer and displacement analyses are performed, which allow analyzing stress/strain behaviors of FGM having time stress, and temperature dependent material properties. The thermo-mechanical responses of the homogenized FGM obtained from the

---

*Reprinted with permission from "A Multi-scale Model for Coupled Heat Conduction and Deformations in Functionally Graded Materials" by Khan, K.A., Muliana, A.H., 2009. Special Issue on Blast/impact on engineered (nano) composite materials Composites Part B: Engineering, 40(6), 511-521, Copyright 2009 by Elsevier Ltd.

multiscale framework are compared with experimental data and the results obtained from finite element (FE) analyses of FGMs having microstructural details. The present micromechanical modeling approach is computationally efficient and shows good agreement with experiments in predicting time-dependent response of FGMs. Our analysis forecasts a better design for creep resistant materials using FGMs.

FGMs are composite materials in which the physical and mechanical properties of the materials vary spatially along specific directions over the entire domain. Structures made of FGMs are often subjected to high temperature gradient loadings. Under such conditions, the properties of the constituents in FGM structure can vary significantly with temperatures accompanied by a non-negligible time-dependent response. For example, FGMs composed of metal and ceramic constituents tend to creep at high temperatures. In addition, non-uniform temperature fields and mismatch in the properties of the constituents in FGMs generate thermal/residual stresses that affect overall performance of FGMs. Therefore, understanding nonlinear thermo-viscoelastic behavior of FGMs plays a significant role in evaluating the performance of structures made from such materials.

Extensive numerical and analytical models have been developed to determine the macroscopic thermal, elastic and inelastic behaviors of FGMs. Noda (1991) and Tanigawa (1995) provided detailed reviews on thermoelastic and thermo-inelastic studies in FGMs having temperature dependent/independent material properties. Limited analytical models have been developed to study the linear viscoelastic macroscopic behavior of FGMs, e.g., Yang (2000), Paulino and Jin (2001) and Mukherjee and

Paulino (2003). Yang (2000) formulated analytical solutions of the time-temperature dependent behavior of joined cylinder having spatially gradation of the material properties. Paulino and Jin (2001) introduced the correspondence principle for non-homogeneous linearly isotropic viscoelastic materials whose relaxation (or moduli) functions can be uncoupled as functions of space and time. The principle is applied for the viscoelastic FGMs with spatially varying material properties but having time-independent coefficient of thermal expansion. The validity of the principle is presented by applying it on standard Maxwell and linear solid models. Later, Mukherjee and Paulino (2003) found that there are some material behaviors for which relaxation (or moduli) functions cannot be separated and thus for those class of materials, the correspondence principle is not valid.

FE formulations have also been developed to obtain solution for the thermo-mechanical behavior of cylinders and plates having graded material properties. The macroscopic properties are obtained using a rule of mixture approach and the effect of spatial variations of the properties on the overall response of FGM is examined. Examples are given in Reddy and Chin (1998), Praveen and Reddy (1998), Praveen et al. (1999), Reddy (2000) and Shabana and Noda (2008). Few experimental studies have been performed to determine the variation of the thermal as well as mechanical properties of FGMs and are mainly limited to thermo-elastic behavior, e.g., Zhai et al. (1993b) and Paramesvaran and Shukla (2000).

Simulating the microscopic responses of FGMs using detailed FE modeling of the graded microstructure with some idealized geometry is computationally expensive and

inadvisable for practical applications. Micromechanical models with simplified microstructural geometries have an advantage over other modeling techniques because they can give approximate macroscopic properties of non-homogeneous materials while recognizing the microscopic properties of each constituent. However, there are some limitations in the simplified micromechanical models which depend on the assumptions and simplifications made on deriving the micromechanical models. Thus, it cannot capture the detail discontinuities of the thermal stresses at the particle-matrix inter-phase regions and local variations of the field variables within the particle and matrix regions. Several micromechanical modeling approaches have been used to study the elastic behavior of composites including FGMs. Micromechanical models like the self-consistent method (SCM), Mori-Tanaka (MT), and Method of Cells (MOC) have been used for evaluating the properties of FGMs. The FGM was represented as a piece-wise layered material with uniform effective properties in each layer, which were evaluated using the micromechanical models. The self consistent scheme and Mori Tanaka method have been widely used by the authors to analyze the behavior of FGM, e.g., Zhai et al. (1993a), Reiter et al. (1997), Tsukamoto (2003) and Zhang et al. (2005). A detailed review of the micromechanical-modeling approaches used by the researchers to study the behavior of FGM can also be found in Gasik (1998). Aboudi et al. (1999) developed a generalized higher order micromechanical theory using MOC. The coupling effects at the micro and macro levels were considered to analyze the thermo-mechanical behavior of the FGM graded in three directions.

Another approach to idealize the graded microstructure of FGM is done by defining RVE, in which functional spatial variations of the inclusions are assumed, to analyze the thermo-mechanical behavior of the FGM. Grujicic and Zhang (1998) used the Voronoi cell FE method (VCFEM), and Yin et al. (2007) introduced pair wise particle interactions and Eshelby's equivalent inclusion solution to evaluate the effective thermo-elastic properties of graded RVE. Reiter et al. (1997) and Dao et al. (1997) performed thermo-elastic FE analysis of FGM models having linear gradation of an idealized geometry of inclusions. Available micromechanical and FE based studies on FGM are limited to thermo-elastic and linear viscoelastic behaviors. There is clearly a need to understand the non-linear thermo-viscoelastic behavior of FGMs with non-constant properties of the constituents. In this study, the proposed micromechanical model is applied to analyze the coupled thermoviscoelastic behavior of FGMs.

The present study addresses coupled heat conduction and deformation of viscoelastic FGM using a micromechanical modeling approach. A through-thickness continuous variation of the thermal and mechanical properties of the FGM is modeled as an assembly of homogeneous layers. Average thermo-mechanical properties in each homogeneous medium are defined using micromechanical model for particle reinforced composites developed at Chapter III. Experimental data available in the literature are used to verify the model. Numerical simulations are also performed to analyze non-linear thermo-viscoelastic responses of homogenized FGM using a micromechanical model and comparisons are made with the results obtained from FE analysis of two dimensional (2D) FGM models having microstructural details (i.e., heterogeneous

FGM). In the 2D FE model of heterogeneous FGM, the inclusions are idealized as circles and their volume fraction vary from one end of geometric model to the other. Comparisons of results show that the present micromechanical model is capable of predicting the non-linear viscoelastic responses of FGMs. In the end, fully coupled thermoviscoelastic behavior of functionally graded beam under cyclic loading is presented.

5.1 MODELING OF FUNCTIONALLY GRADED MATERIALS

In this study, a FGM consisting of two constituents whose material properties change with time, stress, and temperature, is considered. The FGM graded in one direction is idealized as a piece-wise homogeneous medium whose macroscopic properties are evaluated using a micromechanical model. The variation in properties from a series of homogeneous layers along the graded direction is shown in Figure 5.1(a). The FGM is approximated as an assembly of a fictitious layered medium to facilitate the process of integration of micromechanical model with FE package, i.e., ABAQUS. The variations in material properties with locations are incorporated by introducing the multiple integration points along the graded directions, i.e. thickness direction. Each integration point represents a material property of a discretized area. Thus, the overall through-thickness FGM responses show zigzag (discontinuous) variations. By increasing the number of integration points along the graded directions, the discontinuities in the FGM can be minimized.

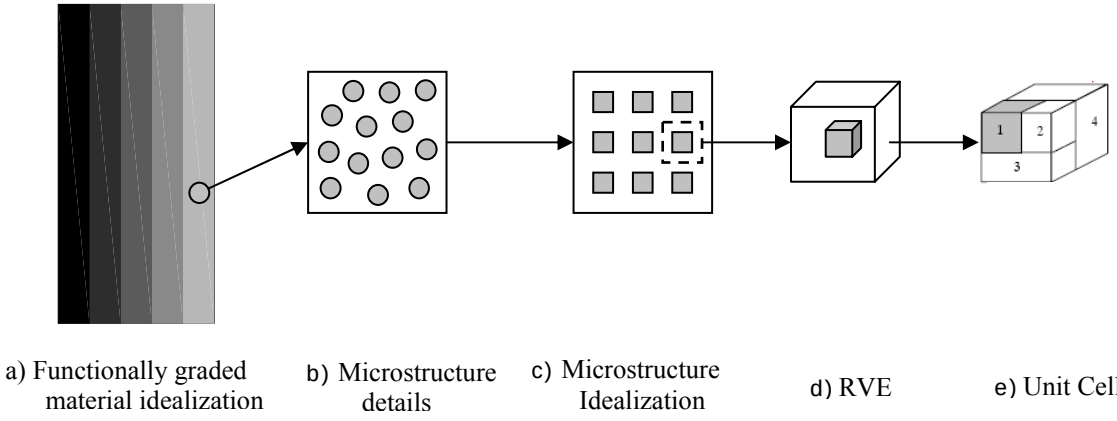

Figure 5.1 Illustration of modeling approach for FGM using a micromechanical model.

Each layer of the FGM is composed of a homogeneous matrix and spherical inclusion particles. The spherical particles are assumed to be uniformly distributed in each macroscopic layer. The particles in the microstructure are idealized as cubes and distributed uniformly in three dimensional periodic arrays. A representative volume element (RVE) consisting of one particle embedded in cubic matrix is considered. Due to the three plane symmetry, one-eight unit cell is assumed to consist of four sub cells. The first sub-cell contains a particle constituent, while the subcells 2, 3, and 4 represent the matrix constituents, as shown in Figure 5.1(e). Perfect bonds are assumed at the subcell's interfaces. Periodic boundary conditions are imposed on the RVE. Stress, temperature and time-dependent constitutive models are used for the isotropic constituents. Temperature dependent thermal properties are considered for particle and matrix constituents. The effective properties of the unit cell define the macroscopic properties at a material point in the homogeneous layer which in turn represents the effective response of each layer. The present micromechanical model is compatible with

general displacement based FE software to perform the thermo-mechanical analyses of FGM structures.

In the following sections, Eqs. (3.15), (3.22) and (3.44) are used to determine the variations of the effective time-dependent stiffness matrix, coefficient of linear thermal expansion, and thermal conductivity along the graded direction of FGMs.

5.2 EFFECTIVE THERMO-MECHANICAL PROPERTIES OF FGM

To demonstrate the capability of the proposed micromechanical model, the thermo-mechanical responses of FGM from the micromechanical model are compared with ones from existing experimental data, and FE model of FGMs having microstructural details.

The experimental data of Zhai et al. (1993b) is used to compare the variations of elastic modulus in the FGMs. TiC/Ni_3Al FGMs were prepared with Ni_3Al particles dispersed in the continuous TiC matrix. The elastic properties of the constituents are shown in Table 5.1. Comparisons of the predicted elastic modulus distribution along the gradation direction with the experimental data are shown in Figure 5.2. The proposed model provides relatively good agreement with the experimental data. The responses are characterized at fixed temperature.

Table 5.1 Mechanical and physical properties of materials used in FGM.

Material	Young Modulus (E), GPa	Poisson ratio (ν)	Linear Thermal Expansion (α) 10^{-6}, 1/°K	Thermal Conductivity (K), W/m/°K.
Ni_3Al	199	0.295	11.90	-
TiC	460	0.19	7.20	-
Al-6061 (T6)	70.3	0.34	23.40	173
SiC	400	0.20	3.4	120
Si	112.4	0.42	3.0	100
Al	72	0.33	23.6	234

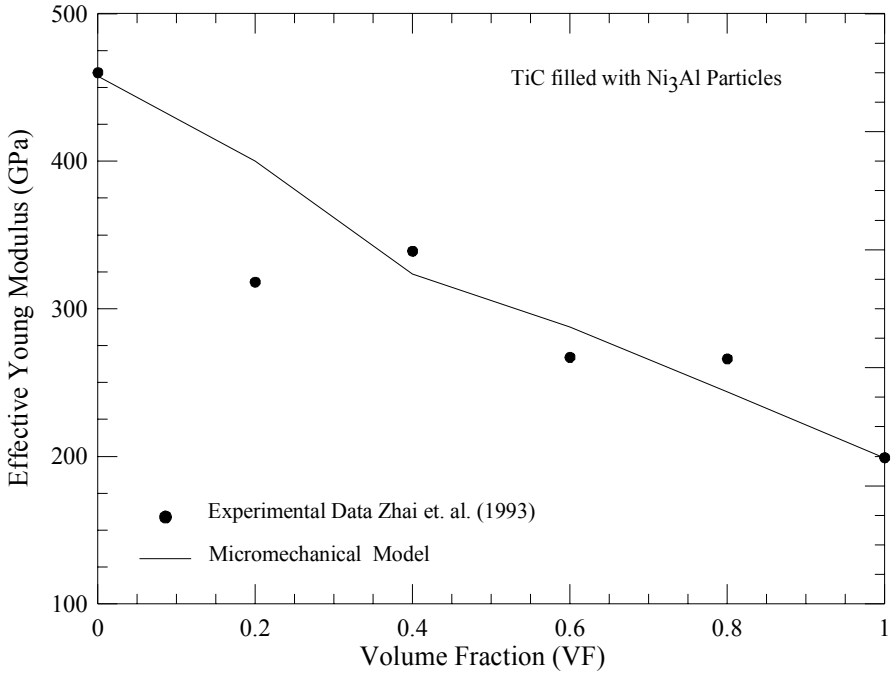

Figure 5.2 Comparison of Young's Modulus for FGM consisting of TiC and Ni_3Al.

The FGMs consisting of metal-matrix systems are widely used in high temperature applications. The metallic components having a high coefficient of thermal expansion (CTE) are generally doped with constituents having a low CTE to tailor the overall CTE. Thus, the FGM can be used in applications requiring low CTE and high thermal

conductivity. The CTE is one of the main features of FGM needed to be analyzed when designing FGM for high temperature applications. Geiger and Jackson (1989) measured the CTE distribution in Al/Si FGM with a volume fraction of Si particles that varies from 0 to 45%. The material properties of Al and Si are given in Table 5.1. Comparisons of the effective CTE obtained from the micromechanical model with the ones obtained from the experimental data are shown in Figure 5.3. The results are found to be in good agreement with the experimental data. Geiger and Jackson (1989) also measured the thermal conductivity of the Al-6061(T6) /SiC FGM with a SiC particle volume fraction varies from 0 to 60%. The material properties of Al-6061(T6) and SiC are given in Table 5.1. Figure 5.4 shows the comparison of experimental data and the results obtained from the micromechanical model for the thermal conductivity variations along the graded direction. Comparing the experimental data with the results obtained from the micromechanical model, as shown in Figures 5.2-5.4, it is suggested that the proposed micromechanical model is capable of predicting the thermo-mechanical behaviors of FGM along the graded direction.

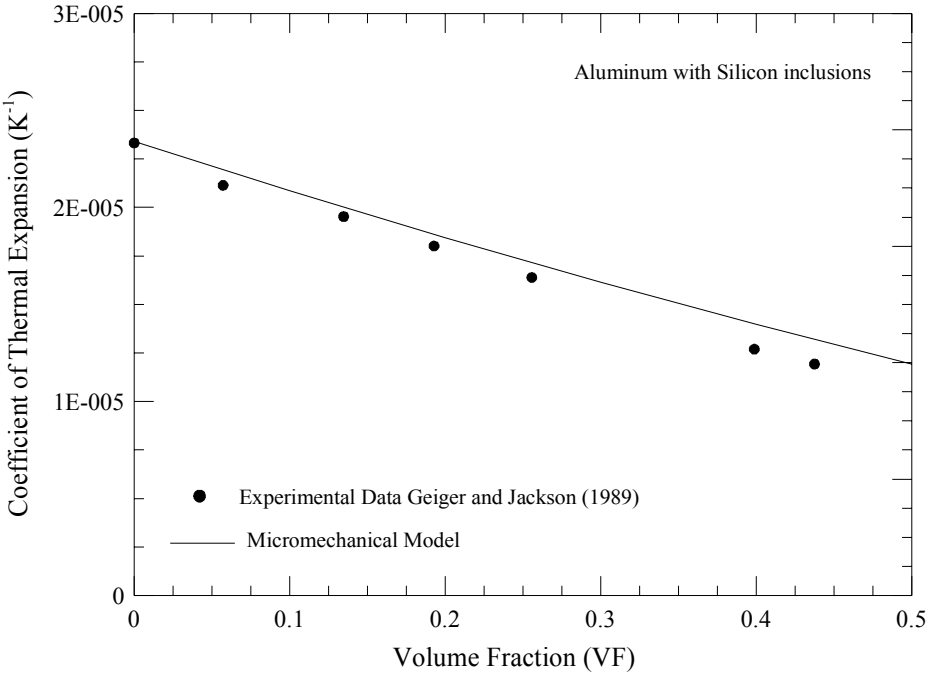

Figure 5.3 Comparison of the coefficient of thermal expansion for FGM consisting of Al with Si inclusions.

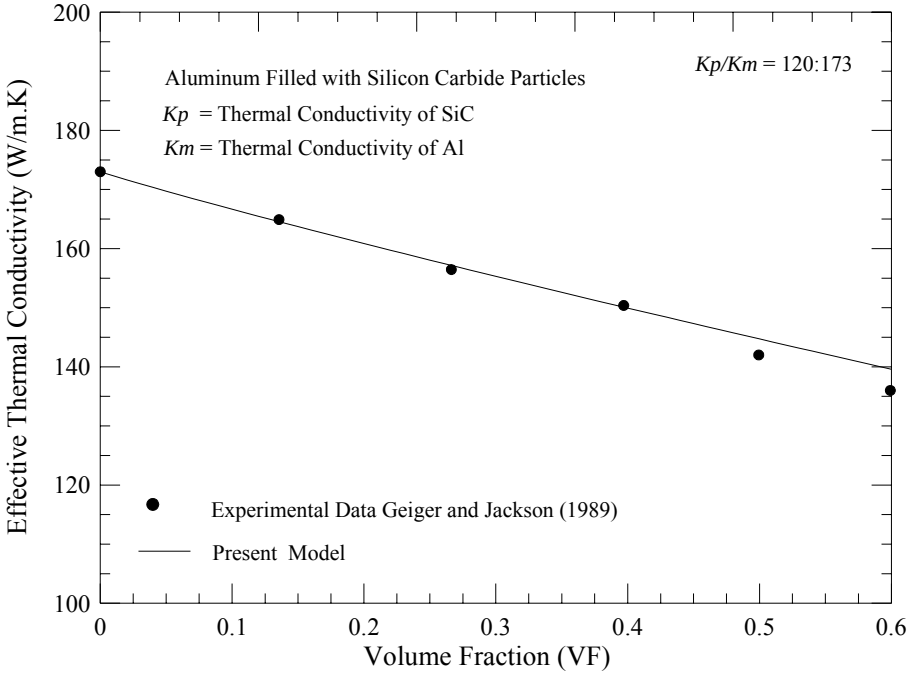

Figure 5.4 Comparison of the thermal conductivity of FGM consisting of Al and SiC particles.

5.3 SEQUENTIALLY COUPLED HEAT CONDUCTION AND DEFORMATIONS OF FGM

Experimental data of FGMs having time-temperature dependent behavior is currently not available. FE analysis is performed to determine the effects of time-temperature dependent constituent properties on the thermo-viscoelastic behaviors of FGMs. All simulations are performed using the ABAQUS FE software. The results obtained from the micromechanical model are compared with the ones from FE analysis of the FGM model having microstructural details. The FGM panel of 16mm length x 10mm height x 1mm depth is studied. The volume fraction of inclusions varies along the length direction. A 2D FE model of FGM having a gradation of the particle in one direction is shown in Figures 5.5 (a) and 5.5(b). The particles in the form of circles are dispersed randomly with a gradient of volume fractions of particle from 0 to 40%. In Figure 5.5(a), large diameter particles are distributed while Figure 5.5 (b) contains small size particles. Small size particles show more uniform distribution as compare to the ones with large size particle. Figure 5.5 (c) illustrates the simplified piece-wise homogenized model with sixteen (16) layers. Each layer represents the macroscopic material point with homogeneous properties varying with the gradient of volume fraction of the particles. The heat transfer analysis is first performed to obtain the temperature distribution along the graded direction. Using the temperature distribution, the stress analyses are carried out to determine the time-temperature dependent deformations of FGM along the graded directions. In order to obtain the temperature profiles, the equation governing the heat conduction in an FGM body needs to be solved. This equation is written as:

$$\overline{\rho c}(x_k)\dot{\bar{T}} = -\bar{q}_{i,i} \qquad i,k = 1,2,3 \tag{5.1}$$

where $\overline{\rho c}(x_k)$ is the effective heat capacity that depends on the composition, density, and specific heat of the two constituents in the FGM body. The effective heat capacity is obtained using a volume average method.

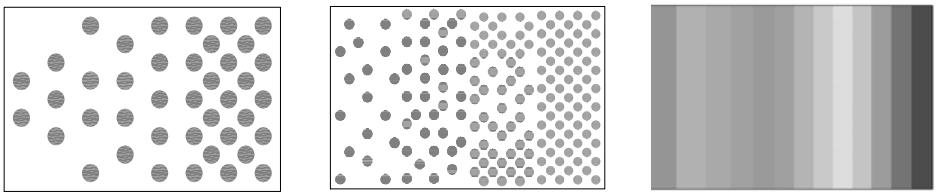

(a) (b) (c)

Figure 5.5 Illustration of the geometry of the finite element models for a volume fraction that varies from 0 to 40%. a) coarse and b) fine microstructural details c) piece wise homogeneous macroscopic layers.

The FGM consisting of Ti-6Al-4V and $Zr0_2$ is first considered. The temperature dependent mechanical and physical properties of these materials are given in Table 5.2. The properties are taken from Praveen et al. (1999). First, a transient heat transfer analysis is performed by applying a uniform temperature of 1000°K at one end. The entire FGM is initially at constant temperature of 300°K. After 159 seconds, the temperature distributions reach to steady state condition. Temperature profile is plotted along the graded direction. The results obtained from our micromechanical formulation are compared with the ones obtained from FE model having coarse and fine microstructural details. Comparison of the results in Figure 5.6 shows that profiles obtained from the fine microstructural details and micromechanical model are in good agreement, while results obtained from coarse microstructural details show some

deviations. The deviation is mainly due to uneven and sparse distribution of inclusions. In all further analyses, FE model having fine microstructural details will be considered. The computational (CPU) time taken to analyze the FE model of FGM having fine microstructural details is 118 seconds which is about 13 times higher than the one taken by the analysis using our micromechanical formulation.

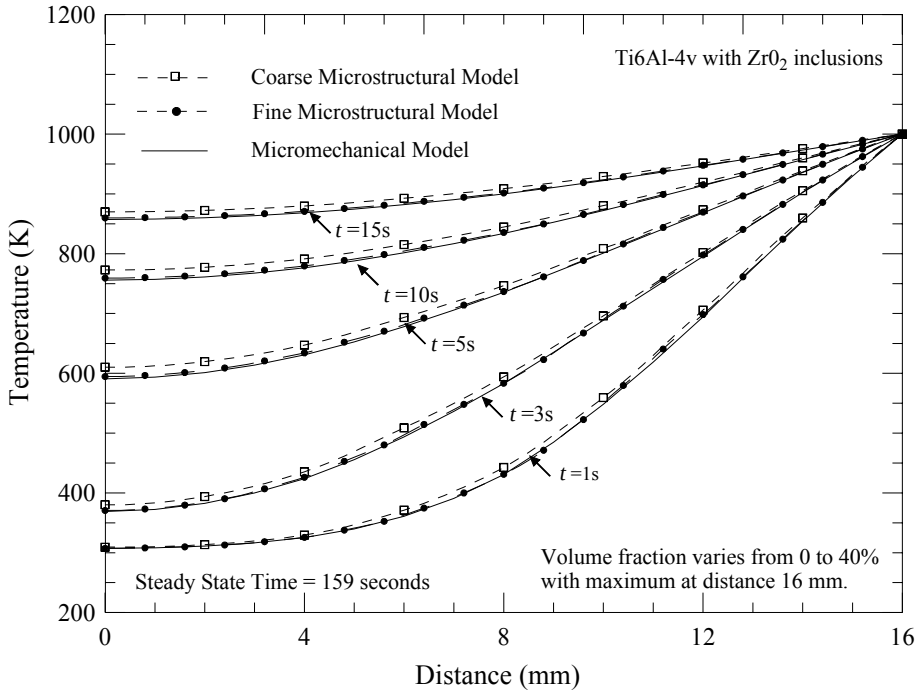

Figure 5.6 Temperature profiles at different times along the graded direction of FGM having constituents with temperature dependent thermal conductivities, for Ti6Al-4V/Zr0$_2$.

Next, the stress analyses are performed based on the temperature distribution obtained from the heat conduction analyses. A uniaxial stress of 10 MPa is applied along the graded direction. The temperature distribution obtained from transient heat transfer analysis is considered as a field dependent temperature loading. The elastic properties of

the constituents change with temperature as shown in Table 5.2. Figure 5.7 shows the profiles of the displacement fields. The results obtained from FE analysis of FGM models having fine microstructural details and the ones using a micromechanical model are in good agreement. In the above analyses, the effect of temperature on the deformation is incorporated through the temperature dependent elastic properties while the effect of thermal expansion is neglected. However, with such a high temperature changes, the effects of free thermal expansion of each constituents can be very significant. Mismatches in the thermal expansion coefficient of the constituents can generate thermal stresses. Figure 5.8 shows the results of variations of displacement along the graded direction with temperature dependent thermal expansion and elastic properties. The FE model with microstructural details incorporates thermal stresses due to mismatches in the thermal expansion coefficients. At the beginning of the heat transfer analysis, there is a high rate of change of the temperature gradient which causes generation of high thermal stresses at the interfaces of the constituents. These stress fields in turn affect the displacement fields of the entire FGM. The thermal stress effect is currently not being included in the present micromechanical model, which is shown by the deviation in the two responses in Figure 5.8. As time progresses, the temperature gradient decreases which reduces thermal stresses and for a zero temperature gradient both results agree quite well.

Table 5.2 Temperature dependent mechanical and physical properties of materials of Ti-6Al-4V and $Zr0_2$.

Property	Ti-6Al-4V	Zirconia ($Zr0_2$)
Young modulus, (E) (Pa)	$1.23\text{x}10^{11}$-$56.457\text{x}10^{6}\,T$	$2.44\text{x}10^{11}$-$334.28\text{x}10^{6}\,T$ $+295.24\text{x}10^{3}T^{2}$- $89.79T^{3}$
Poisson ratio, (ν)	0.3	0.3
Coefficient of Thermal Expansion, (α) 10^{-6}, 1/°K	$7.58\text{x}10^{-6}$ + $4.927\text{x}10^{-9}\,T$ + $2.388\text{x}10^{-12}\,T^{2}$	$1.28\text{x}10^{-5}$-$19.07\text{x}10^{-9}\,T$ + $1.28\text{x}10^{-11}\,T^{2}$- $8.67\text{x}10^{-17}T^{3}$
Thermal Conductivity, (K), W/m/°K	$1.2095 + 0.01686\,T$	$1.7 + 2.17\text{x}10^{-4}\,T + 1.13\text{x}10^{-5}\,T^{2}$
Specific heat, (c), J/Kg. °K	$625.2969 - 0.264\,T$ $+ 4.49\text{x}10^{-4}\,T^{2}$	$487.3427 + 0.149\,T - 2.94\text{x}10^{-5}\,T^{2}$
Density, (ρ), Kg/m^3	4429	5700

* T is temperature in °K.

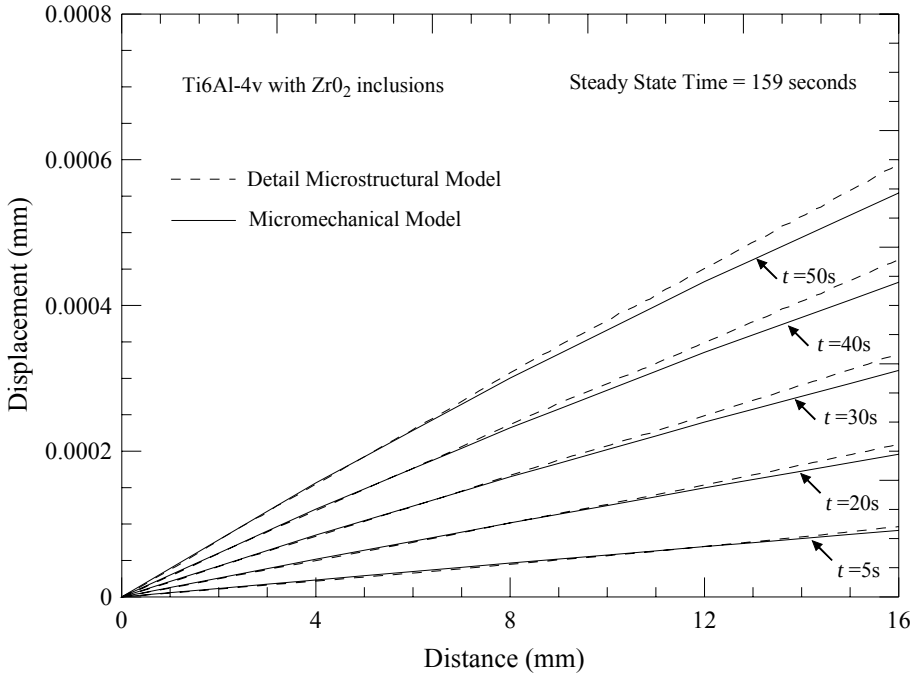

Figure 5.7 Variations of displacement field at different times along the graded direction of FGM having constituents with temperature dependent elastic properties, for Ti6Al-4V/$Zr0_2$.

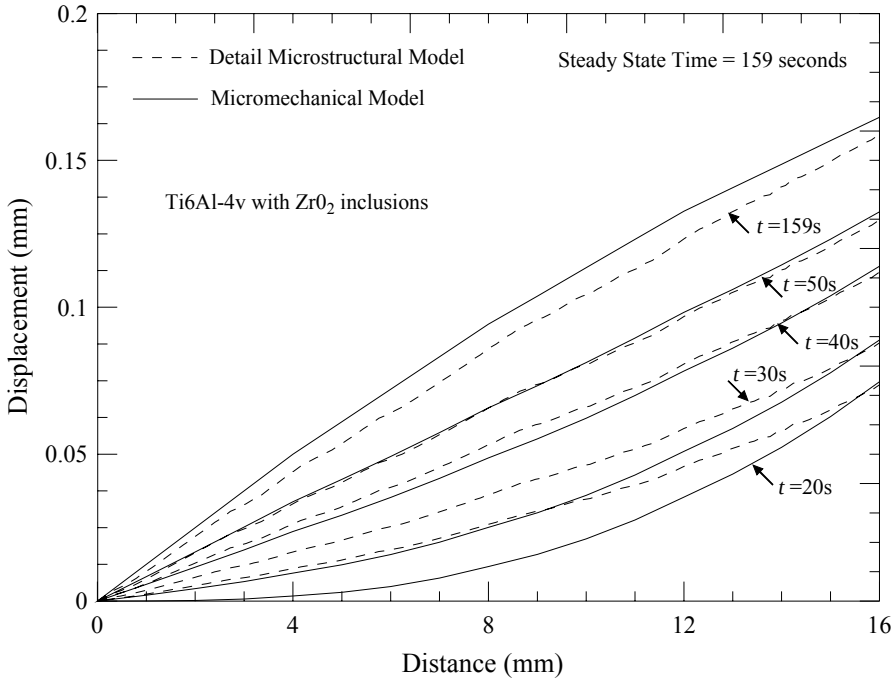

Figure 5.8 Variations of displacement field at different times along the graded direction of FGM having constituents with temperature dependent elastic and thermal properties, for Ti6Al-4V/$Zr0_2$.

Next, coupled heat-conduction and deformation analysis is performed to investigate the effect of viscoelastic constituents on the overall thermo-mechanical responses of FGMs. The time-dependent behavior of metal matrix composites is of importance at high temperatures. The creep behavior of Al with Silicon carbide inclusions is thus numerically studied as an example. The temperature dependent elastic modulus of aluminum is taken from Kaufman (2000). The properties of SiC are taken from Geiger and Jackson (1989). The temperature dependent mechanical and physical properties of Al and SiC are given in Table 5.3. The present model requires the creep parameters which can be obtained from a series of experimental data performed at constant stress and different temperatures. Because of the unavailability of such data, creep properties

of aluminum at 573°K and 28.5 MPa are taken from the experimental work of Tjong and Ma (1999). The time-dependent and non-linear temperature dependent parameters of Al are given in Table 5.4. Moreover, Dicarlo and Yun (2006) reported that the SiC does not show any creep up to 1073°K. This temperature is far above the temperatures considered in this study. Therefore, SiC is assumed to behave linearly elastic. The axial creep data of pure aluminum is shown in Figure 5.9. The axial creep of composites and FGMs consisting of aluminum and SiC is computed using the micromechanical model. A constant stress of 28.5 MPa and fixed temperature of 573°K are prescribed at one end for 12000 seconds. The boundary conditions of the specimens are shown in Figure 5.9. Composites having a uniform distribution and linear gradation of SiC along the graded direction are considered. The results of axial creep deformations (measured at point *B*) in Figure 5.9 show that, the graded material shows more creep resistance than the composites having uniform distribution of the SiC particles.

Table 5.3 Temperature dependent mechanical and physical properties of materials of Al and SiC.

Property	Aluminum (Al)	Silicon carbide (SiC)
Young modulus, (E) (MPa)	$65144 + 73.432\,T - 0.1618\,T^2$	$406783 - 22.61T$
Poisson ratio, (ν)	0.33	0.2
Thermal Conductivity, (K), W/m/°K	$235 - 0.0305\,T + 0.0003\,T^2 - 6\times10^{-7}\,T^3 + 3\times10^{-10}\,T^4$	$183.78 - 0.1569\,T$
Specific heat, (c), J/Kg. °K	900	750
Density, (ρ), Kg/m^3	2700	3210
Coefficient of Thermal Expansion, (α) 10^{-6}, 1/°K	$2\times10^{-5} + 6\times10^{-9}\,T + 3\times10^{-12}\,T^2 + 1\times10^{-14}\,T^3$	$3\times10^{-6} + 3\times10^{-9}\,T - 6\times10^{-13}\,T^2$

* T is temperature in °K.

Table 5.4 Prony series coefficients and temperature dependent parameters for Al.

n	$\lambda_n(\text{sec}^{-1})$	$D_n \times 10^{-6}(\text{MPa}^{-1})$
1	1	0.1
2	10^{-1}	0.15
3	10^{-2}	20
4	10^{-3}	30
5	10^{-4}	160
6	10^{-5}	1100
$g_0^T = \exp\left[0.36\left(\frac{T-T_0}{T_0}\right)^2\right]$, $g_1^T = g_2^T = a_T = 1$		

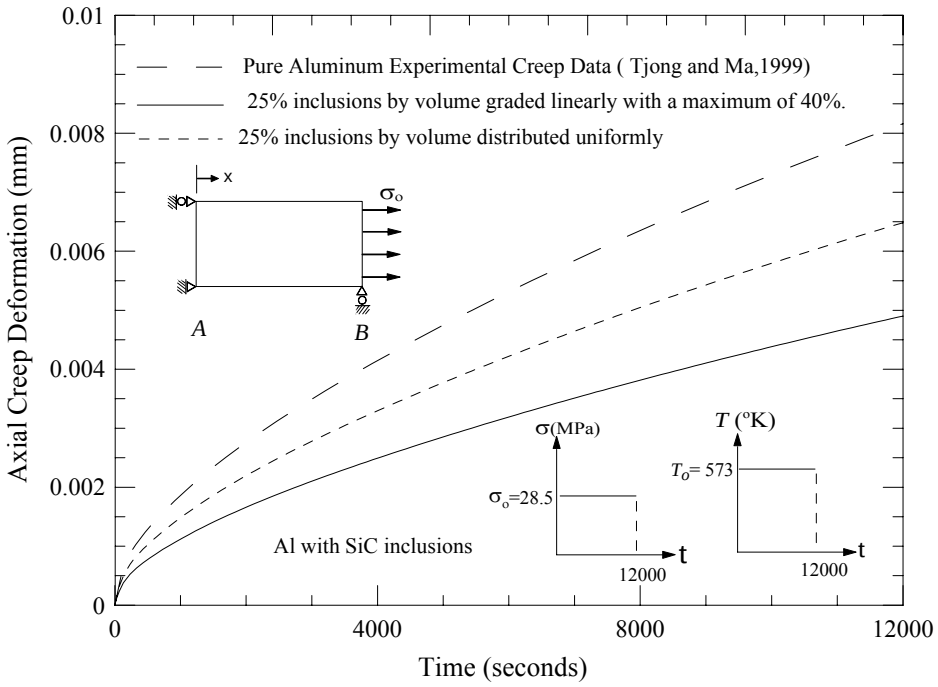

Figure 5.9 Comparison of axial creep deformations for Al, Al/SiC composite and FGM.

A sequentially coupled analysis of Al/SiC FGM is then performed to analyze its time-temperature dependent behavior. The Al is assumed to have time-temperature

dependent properties while SiC behaves linearly elastic. Initially the entire FGM is assumed to be at 300˚K. Transient heat transfer analysis is performed by applying a constant temperature of 573˚K at one end. The temperature reached steady state after 14.8 seconds. Figure 5.10 shows the temperature profile at different times along the graded direction. The results obtained from heat transfer analyses of the FGM models having fine microstructural details and the ones using micromechanical model are in good agreement. Next, the stress analyses are performed based on the temperature distribution obtained from the thermal analyses. A constant stress of 28.5 MPa is applied in the graded direction. The stress is held constant for up to 2000 seconds. Creep deformations at different times are plotted along the graded direction. Though, steady state time is reached after 14.8 seconds, because of the presence of the viscoelastic Al, the deformation continues to grow under a constant stress of 28.5 MPa at a temperature of 573˚K. Figure 5.11 shows that the results obtained from FE analysis of FGM models having fine microstructural details and the ones using a micromechanical model are in good agreement. The comparisons of these results are strong evidence that the present micromechanical model is capable of predicting non-linear viscoelastic behavior of FGM with a reasonable level of uncertainty (±10%).

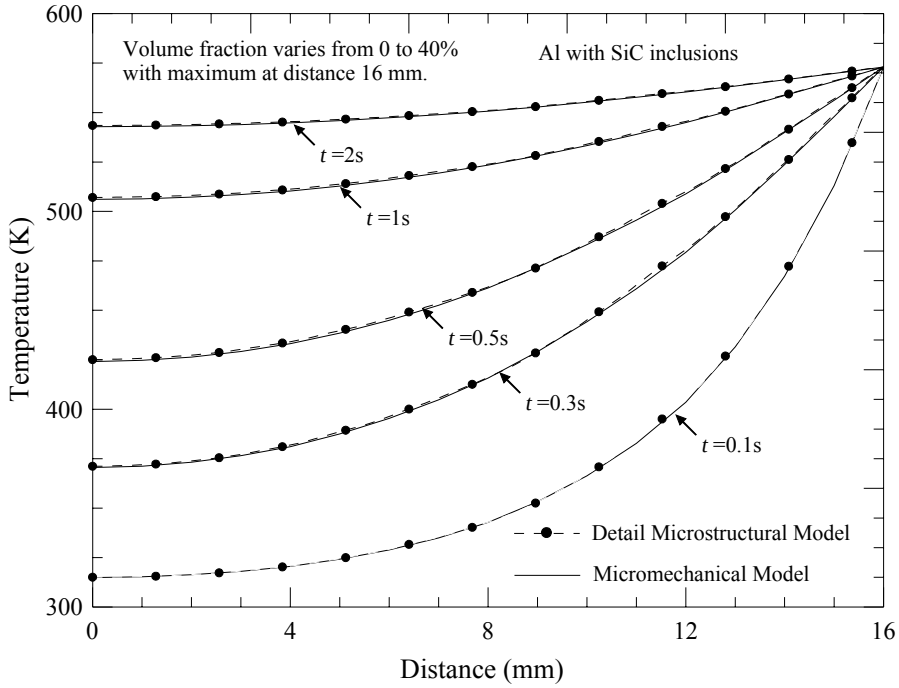

Figure 5.10 Temperature profiles at different times along the graded direction of FGM having constituents with temperature dependent thermal conductivities, for Al/SiC.

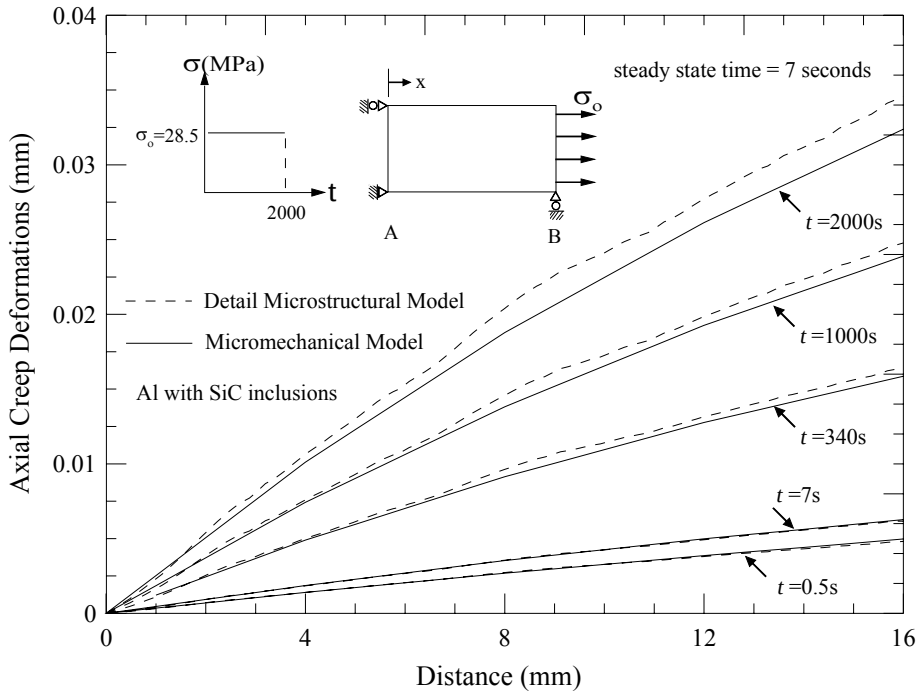

Figure 5.11 Variations of axial creep deformations of FGM having constituents with temperature dependent elastic and thermal properties, for Al/SiC.

5.4 FULLY COUPLED HEAT CONDUCTION AND DEFORMATIONS OF FGM BEAM

The proposed multiscale framework is implemented in the ABAQUS to analyze the fully coupled thermo-viscoelastic behavior of structural components. A cyclic bending of a functionally graded beam under uniformly distributed load is studied. An FGM beam with dimensions of 100mm x 20mm x1 mm is considered. FE mesh with 20-node quadratic brick element (C3D20T) is generated to perform a coupled temperature-displacement analysis. One element is used through the thickness of 2 mm. A total of 653 nodes and 64 elements are generated.

The studied composite is a FM73 matrix reinforced by TiC+HDPE particles. The Prony series coefficients, nonlinear stress and temperature dependent parameters, thermal and mechanical properties used in the simulations are already given in section 2.3 of Chapter II and section 3.3 of Chapter III. The schematic of geometry of the beam and boundary conditions are shown in Figure 5.12. All boundaries of the specimen are assumed to be insulated, i.e, no heat lost across the boundary. The cyclic distributed load of 1 kN/m along x_2 direction is applied at the top surface of a beam for duration of 2400 seconds (40 minutes). The simplified piece-wise homogenized model of beam with eight (8) layers along the height of the beam is also shown in Figure 5.12. Each layer represents the macroscopic material point with homogeneous properties. The beam made of composite material with particle VF of 0%, 12.5% and step-wise varying the gradient of volume fraction from 0 to 25% through-height of the beam on both side of x_1 axis.

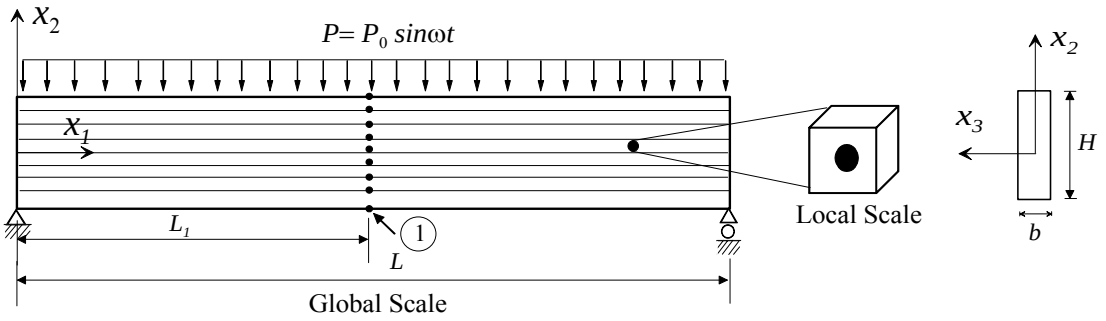

Length of the beam (D) = 100 mm Height of the beam (H) = 20mm

Thickness of the Beam (b) = 2mm L_1 = 50 mm

Figure 5.12 Illustration of multiscale modeling approach for analyzing fully coupled thermoviscoelastic bending analysis of a functionally graded simply supported beam under cyclic distributed load.

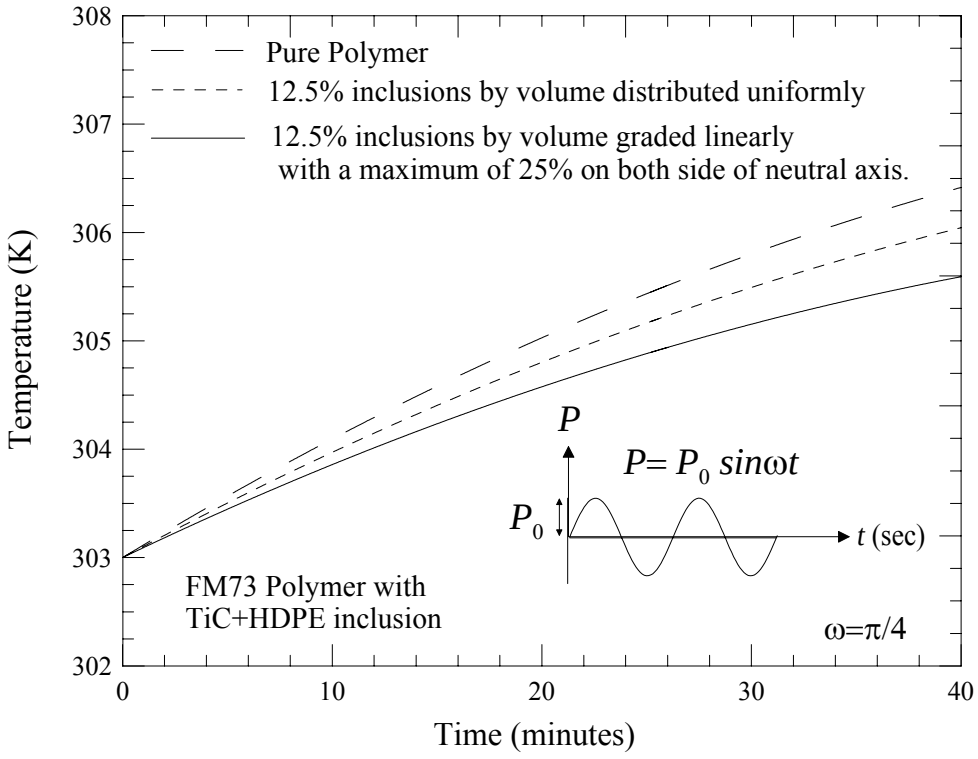

Figure 5.13 Temperature generation at point 1 during fully coupled thermoviscoelastic analysis of a homogeneous, composite and functionally graded beam.

The comparison of temperature generation for homogeneous, composite and functionally graded beam at point 1 on the bottom surface and through-height of the beam are shown in Figures 5.13 and 5.14. It is found that the lowest temperature is generated for the beam consisting of FGMs while the maximum temperature is generated in the case of beam made of homogeneous material.

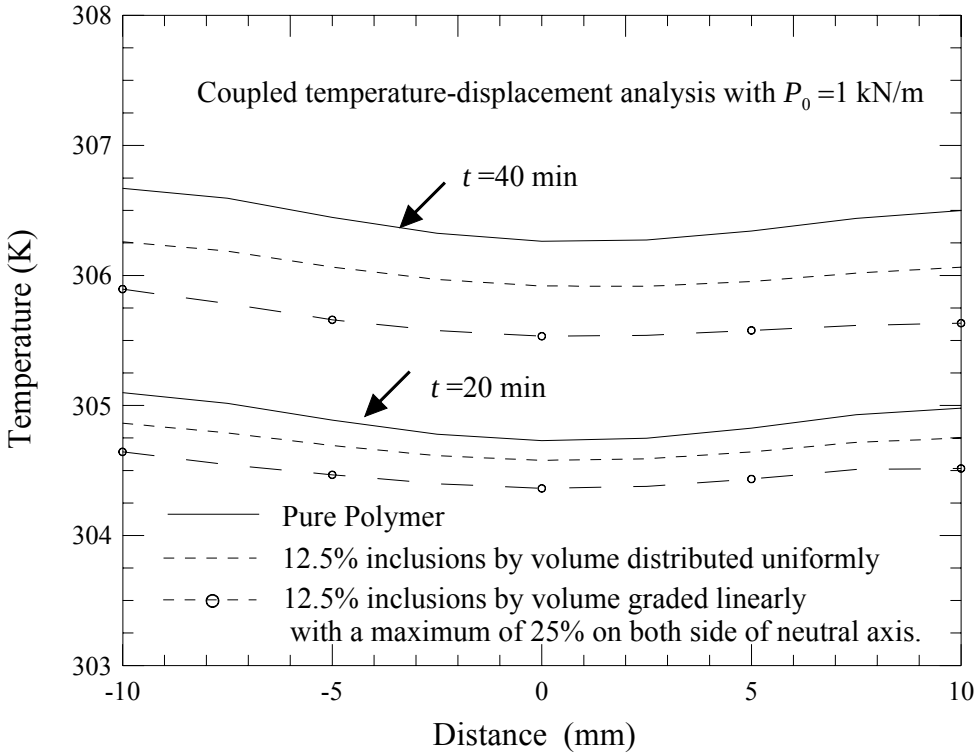

Figure 5.14 Temperature generation at the center of beam (i.e., x_1=L_1, -10≤x_2≤10) during fully coupled thermoviscoelastic analysis of a homogeneous, composite and functionally graded beam.

In summary, the coupled thermo-viscoelastic analysis of FGM is performed using a multiscale modeling approach. The proposed model has a capability to analyze the coupled heat conduction and thermo-viscoelastic deformations of FGMs having time-temperature and stress dependent field dependent properties. When the gradients of

temperature in the FGM are relatively large, the effect of thermal stresses due to the mismatch in the coefficient of thermal expansions of the constituents on the overall mechanical responses of FGM is significant. The thermal stresses are localized at the interface between the inclusion and matrix, which can potentially cause debonding. In the present micromechanical model, the effect of stress concentration is not incorporated, which is shown to be a limitation of the current model. Based on the creep analysis of Al/SiC, it is concluded that better creep resistant material for high temperature applications can be obtained by proper distribution of the SiC particles along the graded direction of the composites. The fully coupled analyses of a functionally graded beam also showed that lower temperature generation at the point of maximum stress can be achieved by using the composite or graded materials while maintaining the structural flexibility. The present micromechanical modeling approach is computationally efficient and reasonable in predicting time-dependent response of FGMs.

CHAPTER VI

CONCLUSIONS AND FUTURE RESEARCH

Polymeric based structural components are currently used in many applications. Experimental results show that the polymers are dissipative in nature and under cyclic loading for a long time the heat generation is significant; thus increasing the temperature of the materials (Schapery and Cantey 1966a; Huang and Lee 1967; Tauchert 1967a, b, c). In this study, the following hypotheses have been made for polymeric based structural components undergoing small deformations and subjected to cyclic loadings for a relatively longer time. 1) The dissipation effect is affected due to the stress and temperature dependent parameters that material possessed. 2) The conduction plays a vital role during the coupled heat conduction and deformations. 3) The dissipation effect can be minimized and creep resistant materials can be obtained by adding particle to polymer matrix. 4) In general, the effective thermal and mechanical properties of the composites can be tailored by adding the particles into the homogeneous matrix. For this purpose, the effect of uniform spatial distribution and functional gradation of the particles in the polymeric matrix are examined on the heat generation rate and overall performance of the composite. Several numerical simulations have been performed under various loadings to examine the above-mentioned hypothesis and then numerous conclusions are drawn.

6.1 CONCLUSIONS

An integrated micromechanical FE framework for analyzing fully coupled nonlinear thermoviscoelastic response of particulate composite structures has been developed. A

simplified micromechanical model consisting of four sub-cells, i.e., one particle and three matrix sub-cells is formulated. The highest scale represents the homogenized continuum elements within the finite element (FE) structural analyses. The lowest scale represents three dimensional nonlinear thermoviscoelastic constitutive material models of each constituent having stress and temperature dependent material parameters. The proposed simplified micromechanical model is capable of predicting the effective thermal and mechanical properties and effective nonlinear thermoviscoelastic response of particulate composites. The proposed model has also been used to analyze response of coupled heat conduction and deformation of viscoelastic composites and structures made of particulate composite. The thermo mechanical coupling is due to the viscous dissipation of the constituents and temperature dependent material parameters in the viscoelastic constitutive model. A recursive-iterative algorithm for simultaneously solving the equations that govern heat conduction and thermoviscoelastic deformations of isotropic homogeneous materials is developed. The algorithm is then incorporated within each sub-cell of the micromechanical model together with the macroscopic energy equation to determine the effective coupled thermoviscoelastic response of the particulate composite. The micromechanical modeling framework is implemented within the ABAQUS to perform coupled heat conduction and deformations of composite structures. The research summary, findings and conclusions are discussed as follows:

1) A numerical algorithm is formulated for solving nonlinear coupled thermo mechanical constitutive equations of homogeneous isotropic viscoelastic materials (Chapter II). The Schapery (1969) single integral model is used for a 3D isotropic

nonlinear thermoviscoelastic response while the Fourier law of conduction is used to represent the thermal constitutive behavior. An energy equation along with a nonlinear dissipation function is derived using the Gibbs free energy expression introduced by Schapery (1997). A recursive-iterative time integration algorithm is employed to integrate the time-dependent dissipation function in the energy equation and nonlinear thermoviscoelastic integral model of the Schapery (1969). An iterative scheme is added to minimize errors arising from the linearization of the nonlinear viscoelastic constitutive equations. The numerical formulation and constitutive material model are suitable only for small deformation gradient problems under a quasi-static loading.

For linear viscoelastic materials, the capability of the algorithm is justified by showing excellent agreement with the analytical solutions. It is established that the fully coupled thermoviscoelastic analyses should be performed when analyzing the viscoelastic materials under cyclic loading for a longer period of time. The temperature increases were found to be accelerated with the increase of frequency and amplitudes of the cyclic load. It is concluded that the linear viscoelastic behavior with temperature independent material properties generates linear temperature increase. The nonlinear stress and temperature dependent material parameters were found to have a significant effect on the heat generation and should be accounted for in designing the components made of viscoelastic materials. The nature of the effect of these parameters on temperature generation depends on the type of nonlinearity that the material possessed. Moreover, including the conduction behavior shows

more realistic temperature fields due to the non-uniform heat generation during the cyclic loading.

2) A micromechanical model has been developed for predicting the effective CTE, ETC and mechanical properties of composites having solid spherical reinforcements. A representative volume element (RVE) of the composites is modeled by a single particle embedded in the cubic matrix. A one eighth unit-cell model consisting of four sub-cells is generated. A perfect bond is assumed along the sub-cell's interfaces. The effective mechanical properties and coefficient of thermal expansion are derived by satisfying the displacement- and traction continuities at the interfaces during thermo-viscoelastic deformations. The effective thermal conductivity is formulated by imposing the heat flux- and temperature continuities at the subcells' interfaces. When a nonlinear and time-dependent response is considered, an incremental formulation consisting of linearized prediction and iterative scheme is derived to obtain effective material properties and field variables of the composite. The macroscopic energy equation is also derived in terms of the effective thermal and mechanical properties and dissipation function. In this study, the coefficient of thermal expansion is assumed to be time-independent at the constituents' level. However, the formulation of the effective CTE leads to time-dependent because of the time-dependence of the matrix moduli. The effect of the dissipation of energy due to the transient component of the effective CTE is shown negligible for small deformation problems. The proposed homogenization scheme is compatible with a displacement based FE framework, i.e., ABAQUS and used to predict the effective

coupled heat conduction and thermoviscoelastic deformations of particle reinforced composites.

The capability of the proposed micromechanical model in predicting the effective mechanical, thermal and viscoelastic responses of particulate composites is validated by comparing these properties with analytical and experimental works reported in the literature. The proposed model is not suitable to predict the overall composite mechanical response when the effects of percolation, particle size and interfacial properties on the overall response of the composites are significant. The proposed model is also not suitable to predict the ETC for composites having high particle volume fractions (VF>15%) and high ratios (*Kp/Km>100*) of the particle to matrix thermal conductivity. However, the model is found to be good for predicting the ETC of the composites with low ratios of the particle to matrix thermal conductivity and for filler composites.

3) An integrated micromechanical model-FE framework has been successfully employed for analyzing the coupled heat conduction and deformations of particulate composite structures. Sequentially coupled and fully coupled thermomechanical behaviors of particulate composites are studied. The latter requires simultaneous solution while the former allows independent solutions of the equations that govern the heat conduction and deformation in the composites.

When the duration of loading is relatively short and thermomechanical coupling effects are negligible, the sequentially coupled analyses can give reasonably good predictions of the field variables in the composites. It is found that the multiscale

model predicts the microscopic temperature and displacements fields with a reasonable accuracy. Based on the sequentially coupled analyses, it is conclude that the multiscale framework is not suitable to represent accurately the discontinuities at the interfaces within the composite. However, it is concluded that the miltiscale framework predicts the effective displacements with relatively better accuracy.

For fully coupled thermo-mechanical analyses, under mechanical loadings only, FE simulations show that an addition of the thermo-elastic particles can help to reduce the temperature generation during the cyclic thermoviscoelastic deformations. It is concluded that the temperature generation is governed by the matrix constituents. A better creep resistant matrix material can lower the temperature generation. Higher temperature generations would deteriorate the material properties of the composite and thus affects its load bearing capacity and furthermore its functionality.

For fully coupled thermo-mechanical analyses, under simultaneous thermal and mechanical boundary conditions, FE simulation shows that the heat generation due to mechanical loads dominates the temperature generation at a farthest distance from the boundary because the heat conduction due to the prescribed temperature at the boundary takes place very slowly due to the low thermal conductivity of the polymeric based composites. This leads to local deterioration of the material properties and thus affecting the overall response of the composite structure.

4) An integrated micromechanical-FE framework was successfully implemented within ABAQUS to analyze coupled heat conduction and deformations of

functionally graded materials (FGM). A through-thickness continuous variation of the thermal and mechanical properties of the FGM is approximated as an assembly of homogenized particulate composite layers. The proposed model has a capability to analyze the heat conduction and thermo-viscoelastic deformations of FGMs having time-temperature and stress dependent field dependent properties. The thermo-mechanical responses of the homogenized FGM obtained from the micromechanical model are compared with experimental data and the results obtained from finite element (FE) analysis of FGMs having microstructural details. The present micromechanical modeling approach is computationally efficient and shows good agreement with experiments in predicting time-dependent responses of FGMs. Our analysis forecasts a better design for creep resistant and less dissipative materials using particulate FGM composites while maintaining the structural flexibility.

6.1.1 COMPUTATIONAL EXPENSE

The proposed integrated micromechanical FE framework is computationally efficient in solving various difficult thermo-mechanical problems of composites. The efficiency of the proposed miltiscale model in terms of computational time has been shown in Chapter IV for heat transfer and stress analysis of homogeneous and heterogeneous composites. It was noticed that the proposed model is approximately 20 times faster than the FE analysis of heterogeneous composites.

For cyclic loadings under specific loading and boundary conditions, the computational time to obtain coupled linear viscoelastic response is often reduced by

taking average dissipation per cycle. For generalized nonlinear case, the analyses are performed by taking complete cyclic loading to capture the factual coupled thermoviscoelastic response of a material. Nevertheless, the proposed model is found to be efficient as compared to the FE simulations based on heterogeneous composites having microstructural details. As the computational capability continues to advances, it is possible to incorporate more complicated micromechanical models within the proposed multiscale framework.

6.2 FUTURE RESEARCH

The current study can be extended as follows:

1) The time-dependent constitutive models can be modified to include the effects of environmental condition, such as moisture diffusion etc. A general integral form of the time-dependent constitutive material model can be extended to include time dependent coefficient of thermal expansion. The effect of time dependent specific heat on the evolution of dissipation function and temperature can also be studied.

2) Damage and plasticity are also the most vital behaviors in composites. The time dependent constitutive model can also be extended to incorporate the dissipation of energy due to combined viscoelastic-viscoplastic-damage behavior of the materials and its effect on the degradation on the material properties.

3) Interphase subcells can be added to the micromechanical model to simulate a traction separation type damage between the particle and matrix subcells.

4) Conduction in inhomogeneous materials is strongly influenced by the conductance at the interfaces between phases. The simplified micromechanical model with four subcells in its present condition is not capable of incorporating the effect of the conductance at the interface on the overall conduction process in heterogeneous materials. It might be possible to incorporate the interface effect by adding more subcells that represent interphase constituents.

5) The procedure for the characterization of the effective nonlinear properties from the micromechanical model can be established.

A multiscale framework that has all the above features would be an ideal framework to analyze the thermomechanical responses of composite structures made of polymer, metal and ceramic based composites under variety of loading conditions.

REFERENCES

ABAQUS: User's Manual, Version 6.5. Hibbitt, Karlsson and Sorensen Inc., Providence, RI (2005)

Aboudi, J.: Micromechanical characterization of the non-linear viscoelastic behavior of resin matrix composites. Composites Science and Technology **38**, 371-386 (1990)

Aboudi, J.: Mechanics of Composite Materials: A Unified Micromechanical Approach. Elsevier, Amsterdam (1991)

Aboudi, J., Pindera, M.J., Arnold, S.M.: Higher-order theory for functionally graded materials. Composites: Part B **30**, 777-832 (1999)

Aboudi, J.: Micromechanically established constitutive equations for multiphase materials with viscoelastic-viscoplastic phases. Mechanics of Time-Dependent Materials **9**, 121-145 (2005)

Aboudi, J.: Thermomechanically coupled micromechanical analysis of multiphase composites. J. Eng Math. **61**(2-4), 111-132 (2008)

Agri, Y., Uno, T.: Thermal conductivity of polymer filled with carbon materials: Effect of conductive particle chains on thermal conductivity. Journal of Applied Polymer Science **30**, 2225-2235 (1985)

Agri, Y., Uno, T.: Estimation on thermal conductivities of filled polymers. Journal of Applied Polymer Science **32**, 5705-5712 (1986)

Allen, D.H.: Homogenization principles and their application to continuum damage mechanics. Composites Science and Technology **61**, 2223-2230 (2001)

Ali, M.Y., Nusier, S. Q, Newaz, G. M.: Creep effects on early damage initiation in a TBC system. Journal of Materials Science **39**, 3383–3390 (2004)

Aniskevich, K., Hristova, J.: Creep of polyester resin filled with mineral. J. Applied Polymers Sci. **77**, 45-52 (2000)

Augusto V.: Homogenization of the nonlinear Kelvin-Voigt model of viscoelasticity and of the Prager model of plasticity. Continuum Mechanics and Thermodynamics **18**(3-4), 223-252 (2006)

Augusto V.: Homogenization of nonlinear visco-elastic composites. Journal de Mathématiques Pures et Appliqués **89**(5), 477-504 (2008)

Auriault, J.L.: Heterogeneous medium is an equivalent macroscopic description possible. International Journal of Science **29**(7), 785-795 (1991)

Babuska, I.: Homogenization approach in engineering. In: Proc. 2nd Int. Symposium on Comp. Meth. in App. Science and Eng. 137-153. Springer, New York (1976)

Barello, R.B., Lévesque, M.: Comparison between relaxation spectra obtained from homogenization model and FE simulation. Int. J. Solids and Structures **45**, 850-867 (2008)

Bakhvalov N.S., Panasenko G.P.: Homogenization: Averaging Process in Periodic Media. Kluwer, Dordrecht (1989)

Baschirow, A. B., Selenew, J.W.: Thermal conductivity of composites. Plaste Kaut 23, 656 (1976)

Bassiouny, E., Ghaleb, A.F., Maugin, G.A.: Thermodynamical formulation for coupled electromechanical hysteresis effects-I: Basic equations. International Journal of Engineering Science **26**(12), 1279-1295 (1988)

Bensoussan, A., Lions, J., Papanicolaou, G.: Asymptotic Analysis for Periodic Structures. North-Holland, Amsterdam (1978)

Benvensite, Y.: On the effective thermal conductivity of multiphase composites. Journal of Applied Mathematics and Physics **37**, 696-713 (1986)

Biot, M.A: Linear thermodynamics and the mechanics of solids. In: Proc. 3rd. U.S. National Congress of Applied Mechanics, 1 (1958)

Brinson, L.C., Knauss, W.G.: Thermo-rheologically complex behavior of multi-phase viscoelastic materials. J. Mech. Phys. Solids. **39**(7), 859-880 (1991)

Brinson, L.C., Lin, W.S.: Comparison of micromechanics methods for effective properties of multiphase viscoelastic composites. Compos. Struct. **41**, 353–367 (1998)

Brockenbrough, J.R., Suresh, S., Wienecke, H.A.: Deformation of metal matrix composites with continuous fibers: geometrical effect of fiber distribution and shape. Acta Metall. Mater. **39**(5), 735–752 (1991)

Budiansky, B.: On the elastic moduli of some heteorogeneous materials. J. Mech. Phys. Solids **13**, 223-227 (1965)

Butt, D.P., Korzekwa, D.A., Maloy, S.A., Kung, H., Petrovic, J.J.: Impression creep behavior of SiC particle-MoSi2 composites. J. Mater. Res. **11**, 1528–1536 (1996)

Chawla, N., Andres, C., Jones, J.W., Allison, J.E.: Effect of sic volume fraction and prticle size on the fatigue resistance of a 2080 Al/SiC composite. Metallurgical and Materials Transactions A, Physical Metallurgy and Materials Science **29**(11), 2843–2854 (1998)

Chazal, C., Arfaoui, M.: Further development in thermodynamic approach for thermoviscoelastic materials. Mechanics of Time-Dependent Materials **5**, 177–198 (2001)

Chen, H.S., Acrivos, A.: The effective elastic moduli of composite materials containing spherical inclusions at non-dilute concentrations. International Journal of Solids and Structures **14**(5), 349-364 (1978)

Cheng, S.C., Vachon, R. I.: The prediction of the thermal conductivity of two and three phase solid heterogeneous mixtures. Int. J. Heat Mass Transfer **12**, 249-264 (1969)

Cho, J., Joshi, M.S., Sun, C.T.: Effects of inclusion size of mechanical properties of polymeric composites with micro and nano particles. Composite Sci. Technol. **66**, 1941-1952 (2006)

Christensen, R.M.: Viscoelastic properties of heterogeneous media. Journal of the Mechanics and Physics of Solids. **17**(1), 23-41 (1969)

Christensen, R.M., Lo, K.H.: Solutions for effective shear properties in three phase sphere and cylinder models. J. Mech. Phys. Solids **27**, 315–330 (1979)

Christensen, R.M., Lo, K.H.: Erratum solutions for effective shear properties in three phase sphere and cylinder models. J. Mech. Phys. Solids **34**(6), 639-640 (1986)

Christensen, R.M., Naghdi, P.M.: Linear non-isothermal viscoelastic solids. Acta Mechanic **3**, 1-12 (1967)

Christman, T., Needleman, A., Suresh, S.: An experimental and numerical study of deformation in metal-ceramic composites. Acta Metall. Mater. **37**, 3029-3050 (1989)

Chung, P.W., Tamma, K.K., Namburu, R.R.: A micro/macro homogenization approach for viscoelastic creep analysis with dissipative correctors for heterogeneous woven-fabric layered media. Composites Science and Technology **60**(12-13), 2233-2253 (2000)

Clausius, R.: Über die Wärmeleitung gasförmiger Körper. Annalen der Physik **115**, 1–57 (1862)

Coleman, B.D.: Thermodynamics of materials with memory. Arch. Rational Mech. Anal. **17**, 1 (1964)

Cost, T.L.: Dissipation of mechanical energy in viscoelastic materials viscoelastic solids. Bulletin of 8th JANNAF Mechanical Behavior Working Group Meeting, CPIA Publication **193**(1), 113 (1969a)

Cost, T.L.: Thermomechanical coupling phenomena in non-isothermal viscoelastic solids. Rohm and Haas Company, Huntsville, Alabama. Technical Report. S-226 (1969b)

Cost, T.L.: Thermomechanical coupling phenomena in non-isothermal viscoelastic solids. Ph.D. Thesis, University of Alabama (1969c)

Daneshjo, K., Ramezani, M.: Classical coupled thermoelasticity in laminated composite plates based on third-order shear deformation theory. Composite Structures **64**(3-4), 369-375 (2004)

Dao, M., Gu, P., Maewal, A., Asaro, R.J.: A micromechal study of residual stress in functionally graded materials. Acta Materials **45**(8), 3265-3276 (1997)

Devries, F., Dumontet, H., Duvaut, G., Lene, F.: Homogenization and damage for composite structures. Int. J. Numer. Meth. Engrg. **27**, 285–298 (1989)

Dillon, 0.W.Jr.: An experimental study of the heat generation during torsional oscillations. J. Mech. Phys. Solids **10**, 235-244 (1962)

Dillon, 0.W.Jr., Coupled thermoplasticity. J. Mech. Phys. Solids **11**, 21 (1963)

Doncel, G.G., Sherby, O.D.: High temperature creep behavior of metal matrix Aluminum-SiC composites. Acta Metallurgica et Materialia **41**(10), 2797-2805 (1993)

Dorigato, A., Pegoretti, A., Messori, M., Fabbri, P.: Viscoelastic and fracture behaviour of HDPE–TiO2 micro and nanocomposites. VII Convegno Nazionale Instm Sulla Scienza E Tecnologia Dei Materiali, Tirrenia (Italy), University of Trento (2009)

Drugan, W.J., Willis, J.R.: A micromechanics-based non-local constitutive equation and estimates of representative volume element size for elastic composites, Journal of the Mechanics and Physics of Solids **4**(44), 497-524 (1996)

Duvaut, G.: Homogeneization et materiaux composite. In: Ciarlet, P.; Rouseau, M. (eds): Theoretical and Applied Mechanics. Amsterdam, North-Holland (1976)

Dvorak, G.J., Srinivas, M.V.: New estimates of overall properties of heterogeneous solids. J. Mech. Phys. Solids. **47**, 899–920 (1999)

Dzenis, Yu. A., Ponomarev, V. M.: Thermal expansion of a polymer composite with an aggregating disperse filler. Institute of Polymer Mechanics, Academy of Sciences of the Latvian SSR, Riga. Translated from Mekhanika Kompozitnykh Materialov **1**, 70-77 (1989)

Ene, H.I.: On linear thermoelasticity of composite materials. International Journal of Engineering Science **21**(5), 443-448 (1983)

Eroshkin, O., Tsukrov, I.: On micromechanical modeling of particulate composites with inclusions of various shapes. Int. J. Solids Struct. **42**, 409–427 (1995)

Eshelby, J.D.: The determination of the elastic fieid of an ellipsoidal inclusion and related problems. Proc. R. Soc. London. A241, 376-396 (1957)

Fahmy, A.A., Ragai, A.N.: Thermal expansion behavior of two phase solids. Journal of Applied Physics **41**(13), 5108-5111 (1970)

Feltham, S.J , Yates, B., Martin, R.J.: The thermal expansion of particulate-reinforced composites, Journal of Material Science **17**, 2309-2323 (1982)

Feng, Y.P., Cui, J.Z.: Multi-scale analysis and FE computation for the structure of composite materials with small periodic configuration under condition of coupled thermoelasticity. International Journal for Numerical Methods in Engineering **60**(11), 1879–1910 (2004)

Fish, J., Shek, K.: Computational plasticity and viscoplasticity for composite materials and structures. Compos Part B: Engng. **29**(5), 613–619 (1998)

Fish, J., Yu, Q., Shek, K.: Computational damage mechanics for composite materials based on mathematical homogenisation. Int. J. Numer. Meth. Engrg. **45**, 1657–1679 (1999)

Flugge, W.: Viscoelasticity. Springer-Verlag, New York (1975)

Francfort, G.A.: Homogenization and linear thermoelasticity. SIAM J. Math. Anal. **14**, 696-708 (1983)

Francfort, G.A., Suquet, P.M.: Homogenization and mechanical dissipation in thermoelasticity. Archives for Rational Mechanics and Analysis **96**, 265-293 (1986)

Gasik, M.M.: Micromechanical modeling of functionally graded materials. Computational Materials Sciences **13**, 42-55 (1998)

Ghazanfari, A.: Thermal and mechanical properties of blends and composites from HDPE and date pits particles. Journal of Composite Materials **42**(1) (2008)

Ghosh, S., Lee, K., Moorthy, S.: Multiple scale analysis of heterogeneous elastic structures using homogenization theory and voronoi cell finite element method. International Journal of Solids and Structures **32**(1), 27–62 (1995)

Ghosh, S., Lee, K., Moorthy, S.: Two scale analysis of heterogeneous elastic–plastic materials with asymptotic homogenisation and voronoi cell finite element model. Computer Methods in Applied Mechanics and Engineering **132**, 63–116 (1996)

Gibbs, J.W.: A method of geometrical representation of the thermodynamic properties of substances by means of surfaces. Transactions of the Connecticut Academy II, 382-404 (1873)

Grujicic, G., Zhang, Y.: Determination of effective elastic properties of functionally graded materials using voronoi cell finite element method. Material Science and Engineering A251, 64-76 (1998)

Guedes, J. M., Kikuchi, N.: Preprocessing and postprocessing for materials based on the homogenization method with adaptive finite element methods. Comput. Methods Appl. Mech. Engrg. **83**, 143–198 (1990)

Haj-Ali, R.M., Muliana, A.H.: Micromechanical models for the nonlinear viscoelastic behavior of pultruded composite materials. Int. J. Solids and Structures **40**, 1037-1057 (2003)

Haj-Ali, R.M., Muliana, A.H.: A multi-scale constitutive framework for the nonlinear analysis of laminated composite materials and structures. Int. J. Solids and Struc. **41**, 3461-3490 (2004)

Haj-Ali, R.M., Pecknold, D.A.: Hierarchical material models with microstructure for nonlinear analysis of progressive damage in laminated composite structures. Struct. Res. Ser. No. 611, UILU-ENG-96-2007, Department of Civil Engineering, University of Illinois at Urbana-Champaign, (1996)

Hannink , R.H.J., Murray¸ M.J.: Elastic moduli measurements of some cubic transition metal carbides and alloyed carbides. Journal of Materials Science **9**, 223-228 (1974)

Hartwig, G., Wuchner, F.: Low temperature mechanical testing machine, Rev. Sci. Instrum. **46**(4), 481-485 (1975)

Hashin, Z., Shtrikman, S.: A variational approach to the theory of the elastic behavior of potycrystals. J. Mech. Phys.Solids **10**, 343-352 (1962)

Hashin, Z.; Shtrikman, S.: A variational approach to the theory of the elastic behavior of multiphase materials. J. Mech.Phys. Solids. **11**, 127-140 (1963)

Helmholtz, H.: On the thermodynamics of chemical processes. In: Physical Memoirs Selected and Translated from Foreign Sources **1**, 43-97 (1882). Physical Society of London, Taylor and Francis, (1888)

Hill, R.: The elastic behaviour of a crystalline aggregate. Proc. Phys. Soc. London. A65, 349-354 (1952)

Hill, R.: Elastic properties of reinforced solids: some theoretical principles. J. Mech. Phys. Solids **11**, 357-372 (1963)

Hill, R.: A self consistent mechanics of composite materials. J. Mech. Phys. Solids **13**, 213-222 (1965)

Hollister, S.J., Kikuchi, N.: A comparison of homogenization and standard mechanics analyses for periodic porous composites. Computational Mechanics **10**, 73-95 (1992)

Holzapfel, G.A., Reiter, G.: Fully coupled thermomechanical behaviour of viscoelastic solids treated with finite elements. Int. J. Engng Sci. **33**(7), 1037-1058 (1995)

Hsieh, C.L., Tuan, W.H.: Elastic and thermal expansion behavior of two-phase composites. Material Science and Engineering A425, 349–360 (2006)

Huang, N.C., Lee, E.H.: Thermomechanieal coupling behavior of viscoelastic rods subjected to cyclic loads. J. Appl. Mech. **34**, 127-132 (1967)

Huang, N.C.: Dissipation function in thermomechanical phenomena of viscoelastic solids. ZAMP **19**, 492-501 (1968)

Hunter, S.C.: Tentative equations for the propagation of stress, strain, and temperatare fields in viscoelastic solids. J. Mech. Phys. Solids **9**, 39 (1961)

Jansson, S.: Homogenized nonlinear constitutive properties and local stress concentrations for composites with periodic internal structure. Int. J. Solids Struct. **29**(17), 2181–2200 (1992)

Kanit, T., Forest, S., Galliet, I., Mounoury, V., Jeulin, D.: Determination of the size of the representative volume element for random composites: statistical and numerical approach. International Journal of Solids and Structures **40**, 3647–3679, (2003)

Kasti, N.A., Lubliner, J., Taylor, R.L.: A numerical solution for the coupled quasi-static linera thermoelastic problem. J. of Thermal Stresses. **14**(3), 333-349 (1991)

Keller, J.B.: Effective behavior of heterogeneous media. In: Proc., Symposium on Statistical Mechanics and Statistical Methods, Plenum Press, 631-644 (1977)

Kerner, E.H.: Elastic and thermoelastic properties of composite media, Proc. Phys. Soc. London B69, 808 (1956)

Khan, K.A., Muliana, A.H.: Effective thermal properties of viscoelastic composites having field-dependent constituent properties. Acta Mech. **209**(1-2), 153-178 (2010)

Khan, K.A.: A time integration scheme for stress temperature dependent viscoelastic behaviors of adhesive polymers, M.S. Thesis, Texas A&M University (2006)

Knauss, W.G., Emri, I.: Volume change and the nonlinearly thermo-viscoelastic constitution of polymers. Polymer Engineering and Science **27**(1), 86–100 (1987)

Kouznetsova, V., Brekelmans, W.A.M., Baaijens, F.P.T.: An approach to micro–macro modeling of heterogeneous materials. Comput. Mech. **27**, 37–48 (2001)

Lai, J., Bakker, A.: An integral constitutive equation for nonlinear plasto-viscoelastic behavior of high-density polyethylene. Polymer Engr. Sci. **35**, 1339-1347 (1995)

Lai, J., Bakker, A.: 3-D Schapery representation for nonlinear viscoelasticity and finite element implementation. Computational Mechanics **18**, 182-191 (1996)

Li, J., Weng, G.J.: Stress-strain relations of a viscoelastic composite reinforced with elliptic cylinders. J. Thermoplastic Composite Materials **10**, 19-30 (1997)

Lianis, G.: Nonlinear thermorheologically simple materials. In: Fifth International Congress on Rheology, Kyoto, Japan (1968)

Lévesque, M., Derrien, K., Mishnaevski, L., Baptiste, D., Gilchrist, M. D.: A micromechanical model for nonlinear viscoelastic particle reinforced polymeric composite materials: undamaged state. Composites A35, 905-913 (2004)

Levin, V.M.: On the coefficients of thermal expansion of hetrerogeneous materials. Mechanics of Solids **2**, 58-61 (1967)

Lewis, T., Nielsen, L.: Dynamic mechanical properties of particulate-filled polymers. J. Appl. Polym. Sci. **14**, 1449-1471 (1970)

Lions, J.L.: Asymptotic expansions in perforated media with a periodic structure. J. Math. **10**, 125-140 (1980)

Lim, T.J., McDowell, D.L.: Cyclic thermomechanical behavior of a polycrystalline pseudoelastic shape memory alloy. Journal of the Mechanics and Physics of Solids **50**(3), 651-676 (2002)

Maghous, S., Creus, G.J.: Periodic homogenization in thermoviscoelasticity: case of multilayered media with ageing. International Journal of Solids and Structures **40**, 851-870 (2003)

Marias, C., Villoutreix, G.: Analysis and modeling of the creep behavior of the thermostable PMR-15 Polyimide. Journal of Applied Polymer Science **69**, 1983-1991 (1998)

Maxwell, J.C.: A Treatise on Electricity and Magnetism. Dover, 3rd Ed., New York (1954)

McHugh, P.E., Asaro, R.J., Shin, C.F.: Computational modeling of metal matrix composite materials-II. Isothermal stress-strain behaviour. Acta Metall. Mater. **41**(5), 1477–1488 (1993)

McLaughlin, R.: A study of the differential scheme for composite materials. International Journal of Engineering Science **15**(4), 237-244 (1977)

Medri, G.: Coupled thermoviscoelasticity: a way to the stress-strain analysis of polymeric industrial components. Meccanica **23**(4), 226-231 (1988)

Michel, J.C., Moulinec, H., Suquet, P.: Effective properties of composite materials with periodic microstructure: a computational approach. Comput. Methods Appl. Mech. Engrg. **172**, 109–143 (1999)

Miehe, C., Koch, A.: Computational micro-to-macro transition of discretized microstructures undergoing small strain. Arch. Appl. Mech. **72**, 300–317 (2002)

Mishra, R.S., Pandey, A.B.: Some observations on the high-temperature creep behavior of 6061 Al-SiC composites. Metallurgical and Materials Transactions A **21**(7), 2089-2090 (1990)

Mori, T., Tanaka, K.: Average stress in matrix and average elastic energy of materials with misfiting inclusions. Acta. Metallurgica **21**, 571-574 (1973)

Mukherjee, S., Paulino, G.H.: The elastic-viscoelastic correspondence principle for functionally graded materials, revisited. Journal of Applied Mechanics **70**, 359-363 (2003)

Muliana, A.H., Nair, A., Khan, K.A., Wagner, S.: Characterization of thermo-mechanical viscoelastic and long-term behaviors of multi-layered composite materials. Composite Sci. Tech. **66**, 2907-2924 (2006)

Muliana, A.H., Kim, J. S.: A concurrent micromechanical model for nonlinear viscoelastic behaviors of particle reinforced composites. International Journal of Solids and Structures **44**(21), 6891-6913 (2007)

Muliana, A.H., Khan, K.A.: A time-integration algorithm for thermorheologically complex polymers. Computational Materials Science **41**(4), 576-588 (2008)

Muliana, A.H., Multi-scale framework for the thermo-viscoelastic analyses of polymer composites. Mech. Res. Comm. **35**(1-2), 89-95 (2008)

Muliana, A.H., Sawant, S.A.: Responses of viscoelastic polymer composites with temperature and time-dependent constituents. Acta Mechanica **204**(3-4), 155-173 (2009)

Mura, T.: Micromechanics of Defects in Solids. Martinus Nijhoff, The Hague (1982)

Nakamura, T., Suresh, S.: Effect of thermal residual stress and fiber packing on deformation of metal-matrix composites. Acta Metall. Mater. **41**(6),1665–1681 (1993)

Nemat-Nasser, S., Hori, M.: Micromechanics: Overall Properties of Heterogeneous Materials, 2nd Ed., Elsevier, Amsterdam (1999)

Nguyen, H.V., Pastor, J., Muller, D.: A method for predicting linear viscoelastic mechanical behavior of composites, a comparison with other methods and experimental validation. European Journal of Mechanics, A/Solids **14**, 939-960 (1995)

Noda, N.: Thermal stresses in materials with temperature dependent properties. Applied Mechanics Reviews **44**, 383-397 (1991)

Noel, L., Suquet, P.: Effective behavior of linear viscoelastic composites: a time-integration approach. International Journal of Solids and Structures **44**(2), 507-529 (2007)

Nogales, S., Bohm, H.J., Modeling of the thermal conductivity and thermomechanical behavior of diamond reinforced composites. Int. J. Engng. Sci. **46**(6), 606–619 (2008)

Norris, A.N.: A differential scheme for the effective moduli of composites. Mechanics of Materials **4**(1), 1-16 (1985)

Odegard, G., Kumosa, M.: Elastic-plastic and failure properties of unidirectional graphite/PMR-15 composites at room and elevated temperature. Comp. Sci. Tech. **60**, 2979-2988 (2000)

Oden, J.T., Kauss, D.A.: Analysis of general coupled thermoelasticity problems by the finite element method. In: Proc., 2nd Conf: Matrix Methods in Structural Mechanics (edited by L. Berke et al.), AFFDL-TR-68-150, Wright-Patterson AFB, Ohio (1968)

Oden, J.T., Armstrong, W.H.: Analysis of nonlinear dynamics coupled thermoviscoelasticity problems by the finite element method. Compulers & Structures **1**, 603-621 (1971)

Oden, J.T.: Finite element analysis of nonlinear problems in the dynamical theory of coupled thermoelasticity. Nuclear Engng Design **10**,465-475(1969)

Oden, J.T., J. Poe, On the numerical solution of a class of problems in dynamic coupled thermoelasticity. In: Proc., 5th SECTAM, Developments in Theoretical and Applied Mechanics (edited by D. Frederick), Pergamon Press, Oxford (1970)

Oruganti, R.K., Ghosh, A.K.: Fabrication and creep properties of superalloy-zirconia composites. Metallurgical and Materials Transactions A, **34**(11), 2643-2653 (2003)

Özdemir, I., Brekelmansa, W.A.M., Geers, M.G.D.: FE2 computational homogenization for the thermo-mechanical analysis of heterogeneous solids. Computer Methods in Applied Mechanics and Engineering **198**(3-4), 602-613 (2008)

Parameswaran, V., Shukla, A.: Processing and characterization of a model functionally graded material. Journal of Material Science **33**, 21-29 (2000)

Parkus, H.: Grundlagen and probleme der thermo and thcrmoviskoelastizitat ZAMM 46, T16-T24 (1966)

Paulino, G.H., Jin. Z. H.: Correspondence principle in viscoelastic functionally graded materials. ASME Journal of Applied Mechanics **68**, 129-132 (2001)

Peretz, D., Weitsman, Y.: Nonlinear viscoelastic characterization of FM73 adhesives. Journal of Rheology **26**(3), 245-261 (1982)

Peretz, D., Weitsman, Y.: The nonlinear thermoviscoelastic characterization of FM73 adhesives. Journal of Rheology **27**(2), 97-114 (1983)

Pierson, H.O.: Handbook of Refractory Carbides & Nitrides: Properties, Characteristics, Processing and Apps.: Properties, Characteristics, Processing and Applications (Materials Science and Process Technology), Noyes Publications, Park Ridge, NJ (1996)

Praveen, G.N., Reddy, J.N.: Nonlinear transient thermoelastic analysis of functionally graded ceramic-metal plates. International Journal of Solid and Structures **37**(33), 4457-4476 (1998)

Praveen, G.N., Chin, C.D., Reddy, J.N.: Thermoelastic analysis of functionally graded ceramic-metal cylinder. Journal of Engineering Mechanics **125**(11), 1259-1267 (1999)

Rajagopal, K.R., Srinivasa, A.R.: A Gibbs-potential-based formulation for obtaining the response functions for a class of viscoelastic materials, Proc. R. Soc. A8, **467**(2125), 39-58 (2011)

Reddy, J.N., Chin, C.D.: Thermomechanical analysis of functionally graded cylinders and plates. Journal of Thermal Stresses **21**, 593-626 (1998)

Reddy, J.N.: Analysis of functionally graded plates. International Journal for Numerical Methods in Engineering **47**, 663-684 (2000)

Reddy, J.N.: An Introduction to Nonlinear Finite Element Analysis. Oxford University Press, New York (2004)

Reddy, J.N.: An Introduction to Continuum Mechanics: With Applications. Cambridge University Press, New York (2008)

Reiter, T., Dvorak, G.J., Tvergaard, V.: Micromechanical models for graded composite materials. J. Mech. Phys. Solids **45**(8), 1281-1302 (1997)

Reuss, A.: Berechnung der fliesgrenze von mischkristallen auf grund der plastizitatbedingung fur einkristalle. Z. Agnew. Math. Mech. **9**, 49-58 (1929)

Rice, J.R.: Inelastic constitutive relations for solids: an internal variable theory and its application to metal plasticity. J. Mech. Phys. Solids **19**, 433–455 (1971)

Rosen, B.W., Hashin, Z.: Effective thermal expansion coefficients and specific heats of composite materials. Int. J. Engng. Sci. **8**, 157-173 (1970)

Rougier, Y., Stolz, C., Zaoui, A.: Spectral analysis of linear viscoelastic inhomogeneous materials. Comptes rendus de l'Academie des sciences. Series 2, Mecanique, Physique, Chimie, Sciences de l'univers, Sciences de la Terre. 316(11), 1517-1522 (1993)

Rupnowski, P., Gentz, M., Kumosa, M.: Mechanical response of a unidirectional Graphite fiber/polyimide composite as a function of temperature, Composite Sci. Tech. **66**, 1045-1055 (2006)

Sanchez-Palencia, E.: Comportements local et macroscopique d'un type de milieux physiques heterogenes. Int. J. Eng. Sci. **12**, 331-351 (1974)

Sanchez-Palencia, E.: Non-Homogeneous Media and Vibration Theory. Springer, New York (1980)

Schapery, R.A.: Application of thermodynamics to thermomechanical, fracture, and birefringent phenomena in viscoelastic media. J. Appl. Phys. **35**(2), 1451–1465 (1964)

Schapery, R.A.: Thermomechanical behavior of viscoelastic media with variable properties subject to cyclic loading. J. Appl. Mech. **32**, 611-619 (1965)

Schapery, R.A., Cantey, D.E.: Thermomechanical response studies of solid propellants subjected to cyclic and random loadings. AIAA J. **4**(2), 255-264 (1966a)

Schapery, R.A.: A theory of non-linear thermoviscoelasticity based on irreversible thermodynamics. In: Proc., ASME, University of Minnesota, 511–530 (1966b)

Schapery, R.A.: Thermal expansion coefficients of composite materials based on energy principles, J. Comp. Mater., **2**, 380, (1968)

Schapery, R.A.: Further development of a thermodynamic constitutive theory: stress formulation, Purdue University Report No. AA & ES. 692 (1969)

Schapery, R.A.: Nonlinear viscoelastic and viscoplastic constitutive equations based on thermodynamics. Mechanics of Time-Dependent Materials **1**, 209–240 (1997)

Schwarzl, F., Staverman, A.J.: Time temperature dependence of linear viscoelastic behavior. J. Appl. Physics **23**, 838 (1952)

Segurado, J., Llorca, A.: Numerical approximation to the elastic properties of sphere-reinforced composites. Journal of the Mechanics and Physics of Solids **50**, 2107–2121 (2002)

Shabana, Y.M., Noda, N.: Numerical evaluation of the thermomechanical effective properties of a functionally graded material using the homogenization method. International Journal of Solid and Structures **45**, 3494-3506 (2008)

Shibuya, Y.: Evaluation of creep compliance of carbon fiber reinforced composites by homogenization theory. JSME International Journal. Series A, Mechanics and Material Engineering **40**(3), 313-319 (1997)

Simmons, G., Wang, H.: Single Crystal Elastic Constants and Calculated Aggregate Properties: A Handbook. MIT Press, Cambridge, MA (1971)

Smit, R.J.M., Brekelmans, W.A.M., Meijer, H.E.H.: Prediction of the mechanical behaviour of non-linear heterogeneous systems by multi-level finite element modeling. Comput. Methods Appl. Mech. Engg. **155**,181–192 (1998)

Smit, R.J.M., Brekelmans, W.A.M., Meijer, H.E.H.: Prediction of the large-strain mechanical response of heterogeneous polymer systems: local and global deformation behaviour of a representative volume element of voided polycarbonate. J. Mech. Phys. Solids **47**, 201–221 (1999)

Staverman, A.J., Schwarzl, F.: Thermodynamics of viscoelastic behavior. In: Prec., Nederlandse Akad. Van Wetensch. B55, 474-486 (1952)

Stauffer, D.: Introduction to Percolation Theory. Taylor & Francis, London (1985)

Sugawara, A, Yoshizawa, Y.: An experimental investigation on the thermal conductivity of consolidated porous materials. J. of Applied Physics **33**, 3135-3138 (1962)

Suquet, P.: Plasticité et homogénéisation (in French). Ph.D. Dissertation, UniversitéPierre-et-Marie Curie, Paris (1982)

Suquet, P.: Elements of homogenization for inelastic solid mechanics. In: Sanchez-Palencia, E., Zaoui, A. (Eds.), Homogenization Techniques for Composite Media. Lecture Notes in Physics 272, Springer-Verlag, Berlin (1985)

Suquet, P.: Elements of homogenization for inelastic solid mechanics. In: Sanchez-Palencia, E., Zaoui, A. (Eds.), Homogenization Techniques for Composite Media. Lecture Notes in Physics 272, Springer-Verlag, Berlin (1986)

Suquet, P.: Elements of homogenization theory for inelastic solid mechanics. In: Sanchez-Palencia, E.; Zaoui, A. (Eds.): Homogenization techniques for composite media. Lecture Notes in Physics 272, Springer-Verlag, Berlin (1987)

Torquato, S.: Random Heterogeneous Materials: Microstructure and Macroscopic Properties, Springer, New York (2002)

Tanigawa, Y.: Some basic thermoelastic problems for nonhomogeneous structural materials. Applied Mechanics Reviews **48**, 287-300 (1995)

Tartar, L.: Memory effects and homogenization. Archive for Rational Mechanics and Analysis **111**, 121-133 (1990)

Tauchert, T.R: The temperature generated during torsional oscillation of polyethylene rods. Int. J. Eng. Sci. **5**, 353-365 (1967a)

Tauchert, T.R., Afzal S.M.: Heat generated during torsional oscillations of polymethylmethacrylate tubes. J. Appl. Phys. **38**(12), 4568-4572 (1967b)

Tauchert, T.R.: Heat generation in a viscoelastic solid. Acta Mechanica **3**(4), 385-396 (1967c)

Tauchert, T.R.: Transient temperature distributions in viscoelastic solids subject to cyclic deformations. Acta Mechanica **6**, 239-252 (1968)

Tavman, I.H.: Effective thermal conductivity of isotropic polymer composites. Int. Comm. Heat Mass Transfer **25**(5), 723-732 (1998)

Terada, K., Kikuchi, N.: Nonlinear homogenization method for practical applications, in: S. Ghosh, M. Ostoja-Starzewski (Eds.). Computational Methods in Micromechanics. AMD-212/MD-62, ASME, 1–16 (1995)

Terada, K., Kikuchi, N.: A class of general algorithms for multi-scale analysis of heterogeneous media. Comput. Methods Appl. Mech. Engg. **190**, 5427–5464 (2001)

Tolenado, A., Murakami, H.: A high-order mixture model for periodic particulate composites. Int. J. Solids Structures **23**, 989–1002 (1987)

Touloukian, Y.S, Kirby, R.K., Taylor, R.E., Lee, T.Y.R.: Thermophysical properties of matter: thermal expansion. Non Metallic Solids. **13**, 350 (1977)

Turner, P.S.: Thermal expansion stresses in reinforced plastics. J. Res. NBS **37**, 239-250 (1946)

Truesdell, C., Noll, W. The Nonlinear Field Theories of Mechanics. Encyclopedia of Physics III/l (edited by S. Flugge). Springer-Verlag, New York (1965)

Tseng, K.K.: A statistical micromechanics based multi-scale framework for effective thermomechanical behaviours of particle reinforced composites. International Journal of Solids and Structures **41**, 295-304 (2004)

Tummala, R.R., Friedberg, A. L: Thermal expansion of composites as affected by the matrix. J. Am. Ceram. Soc. **53**, 376 (1970)

Tvergaard, V.: Analysis of tensile properties for wisker-reinforced metal-matrix composites. Acta Metall. Mater. **38**(2), 185–194 (1990)

Valanis, K.C.: Unified Theory of Thermomechanical Behavior of Viscoelastic Materials. Mechanical Behavior of Materials Under Dynamic Loads, Ulric S. Lindholm, ed., Springer-Verlag, New York (1968)

Verma, L.S., Shrotriya, A.K, Singh, R., Chaudhary, D.R.: Thermal conduction in two phase materials with spherical and non spherical inclusions. Journal of Applied Physics D24, 1729-1737 (1991)

Voigt, W.: Lehrbuch Der Kristallphysik, Teubner, B.G., Leipzig, Germany (1910)

Walpole, L.J.: On bounds for the overall elastic moduli of inhomogeneous systems-I. J. Mech. Phys. Solids **14**,151-162 (1966)

Wakashima, K., Otsuka, M., Umekawa, S.: Thermal expansion of heterogeneous solids containing aligned ellipsoidal inclusions, J. of Composite Mat. **8**, 391-404 (1974)

Watt, D.F., Xu, X.Q., Lloyd, D.J.: Effects of particle morphology and spacing on the strain fields in a plastically deforming matrix. Acta Mater. **44**(2), 789–799 (1996)

Williams, T.O., Aboudi, J.: A fully coupled thermo-mechanical micromechanics model. Journal of Thermal Stresses **22**(9), 841-873 (1999)

Wineman, A.S, Rajagopal, K.R.: Mechanical Responses of Polymers: An Introduction. Cambridge University Press, London, UK (2001)

Wolosewicakn, R.M., Gratch, J.: Transient response in a viscoelastic material with temperature dependent properties and thermomechanical coupling. Appl. Mech. **32**, 620-622 (1965)

Wu, X., Ohno, N.: A homogenization theory for time-dependent nonlinear composites with periodic internal structures. International Journal of Solids and Structures **36**(33), 4991-5012 (1999)

Yang, Y.Y.: Time-dependent stress analysis in functionally graded materials. International Journal of Solid and Structures **37**, 7593-7608 (2000)

Yi, Y.M., Park, S.H., Youn, S.K.: Asymptotic homogenization of viscoelastic composites with periodic microstructures. International Journal of Solids and Structures **17**, 2039-2055 (1998)

Yin, H.M., Paulino, G.H., Buttlar, W.G., Sun, L.Z.: Micromechanics based thermoelastic model for functionally graded particulate materials with particle interactions. Journal of Mechanics and Physics of Solids **55**, 132-160 (2007)

Yong, L., Langdon, T.G.: Creep behavior of an Al-6061 metal matrix composite reinforced with alumina particulates. Acta Materialia **45**(11), 4797-4806 (1997)

Yu, Q., Fish, J.: Multiscale asymptotic homogenization for multiphysics problems with multiple spatial and temporal scales: a coupled thermo-viscoelastic example problem. International Journal of Solids and Structures **39**(26), 6429-6452 (2002)

Yuan, Q., Jiang, W., Li, R.K.Y., Jiang, Z.: Mechanical and thermal properties of high-density polyethylene toughened with glass beads. Journal of Applied Polymer Science **89**, 2102–2107 (2003)

Zhai, P.C., Zhang, Q.J., Jiang, C.R.: Micromechanical design of ceramic/metal functionally gradient composite materials. In: Proc., ICCM-9, July12-16, Madrid, Spain, 95-102 (1993a)

Zhai, P.C., Zhang, Q.J., Jiang, C.R.: Application of three phase micromechanical theories to ceramic/metal functionally gradient materials. Ceramic Transactions **34**, 449 (1993b)

Zhang, M., Zhai, P.C., Zhang, Q.C.: Effective thermal conductivity of functionally graded composite with arbitrary geometry of particulate. Key Engineering Materials **297-300**, 1522-1528 (2005)

Zohdi, T.I., Wriggers, P.: Aspects of the computational testing of the mechanical properties of microheterogeneous material samples. International Journal for Numerical Methods in Engineering **50**, 2573-2599 (2001)

APPENDIX A

In this appendix, the Schapery's viscoelastic material model which was derived using the thermodynamics of irreversible processes (TIP) is revisited. Using the Gibbs free energy potential that was originally introduced by Schapery (1997) the energy equation capable to model temperature evolution in nonlinear coupled thermoviscoelastic materials is established. Explicit expressions are derived for mechanical dissipation rate, the rate of change of entropy and specific heat expressions, respectively.

The thermodynamic state of a material is fully characterized by the independent variables called as state variables. The choice of a state variable depends on the physical phenomena of the thermodynamic system. Under isothermal conditions, the free energy potentials can be expressed as a function of the strains or stresses and other possible internal state variables (ISVs). Schapery (1997) introduced Gibbs free energy in terms of stresses (σ_i) and internal state variables (ISVs) ζ_m and temperature *T*. The Gibbs free energy for a nonlinear thermoviscoelastic material can be expressed in the following form

$$G = G_0 - A_m\zeta_m + \frac{1}{2}B_{mn}\zeta_m\zeta_n \tag{A.1}$$

where G_0, A_m and B_{mn} are function of σ_i and *T*. The strain can be obtained from the following equation (Schapery, 1969)

$$\varepsilon_i = -\frac{\partial G}{\partial \sigma_i} \tag{A.2}$$

so that,

$$\varepsilon_i = -\frac{\partial G_0}{\partial \sigma_i} + d\varepsilon_i \tag{A.3}$$

where, $d\varepsilon_i = \frac{\partial A_m}{\partial \sigma_i}\zeta_m$ (A.4)

after neglecting terms of second order in ζ_m. The first and second law of thermodynamics leads to the expression for entropy production rate $\dot{\gamma}_{\text{int}}$ (e.g. Rice, 1971)

$$T\dot{\gamma}_{\text{int}} = f_m\dot{\zeta}_m \geq 0 \tag{A.5}$$

where $f_m = -\frac{\partial G}{\partial \zeta_m}$ (A.6)

The entropy production rate in Eq. (A.5) is always positive unless $\zeta_m = 0$. The expression for thermodynamic forces can be obtained using Eq. (A.1) and can be written as:

$$f_m = -\frac{\partial G}{\partial \zeta_m} = A_m - B_{mn}\zeta_n \tag{A.7}$$

The present model is equivalent to generalized nonlinear Voigt model. The ranges of *m* and *n* depend on number of dashpots. To obtain the expression that describes the changes in the ISVs, evolution equations are needed that relate the thermodynamic forces and ISVs, which can be written as.

$$\dot{\zeta}_m = \frac{c_{mn} f_n}{a_1} \tag{A.8}$$

where c_{mn} is a constant, positive definite, symmetric matrix and a_1 is a positive scalar quantity that may be a function of σ_i and *T*. At the reference state $a_1 = 1$.

The thermodynamic forces in Eq. (A.7) are combined with the inverse of Eq. (A.8), yields:

$$a_1 \tilde{c}_{mn} \dot{\zeta}_n + B_{mn} \zeta_n = A_m \tag{A.9}$$

where $\tilde{c}_{mn} = \left[c_{mn} \right]^{-1}$. Assuming $B_{mn} = a_2 C_{mn}$, the Eq. (A.9) can be expressed as

$$\tilde{c}_{mn} \frac{d\zeta_n}{d\psi} + C_{mn} \zeta_n = \frac{A_m}{a_2} \tag{A.10}$$

where a_2 is a positive scalar quantity that may be a function of σ_i and *T*, and

$$d\psi = \frac{a_2}{a_1} dt \text{ or } d\psi = \frac{dt}{a_\sigma} \text{ or } \psi = \int_0^t \frac{dt'}{a_\sigma} \tag{A.11}$$

is reduce time. The function a_σ is stress-dependent that is used to define a time scale shift factor for stress dependent behaviors. Since C_{mn} and c_{mn} are symmetric and positive definite matrices, it is always possible to diagonalize Eq. (A.10). Thus uncoupled set of equations in terms of the new principal ISVs can be written as (*m* not summed)

$$\frac{d\zeta_m}{d\psi} + c_m C_m \zeta_m = \frac{c_m A_m}{a_2} \tag{A.12}$$

where C_m and c_m replace C_{mn} and c_{mn}, respectively. The general solution of Eq. (A.12) is (*m* not summed)

$$\zeta_m = \frac{1}{C_m} \int_0^\psi \left[1 - \exp\left[-\left(\frac{\psi - \psi'}{\tau_m} \right) \right] \right] \frac{d}{d\psi'} \left(\frac{A_m}{a_2} \right) d\psi' \tag{A.13}$$

where, $\tau_m = \left(c_m C_m\right)^{-1}$ is positive retardation time. The term ψ' is a function of time t', time at which the input load is applied. To facilitate the characterization in terms of master creep functions through reduce time, let assume A_m as follows.

$$A_m = C_{mj}\hat{\sigma}_j + \alpha_m \hat{\phi} \tag{A.14}$$

where C_{mj} and α_m are constants. $\hat{\sigma}_j$ depend on σ_i and T and $\hat{\phi}$ may depend on temperature but not on stress. $\hat{\phi}$ accounts for thermal expansion effect; thus $\hat{\phi} = 0$ when $T=T_R$ (reference temperature). Substituting of A_m into Eq. (A.13) and after some simplification, we can write Eq. (A.4) as

$$d\varepsilon_i = \frac{\partial \hat{\sigma}_j}{\partial \sigma_i}\left[\int_0^{\psi} dD_{jk}\left(\psi - \psi'\right)\frac{d}{d\psi'}\left(\frac{\hat{\sigma}_k}{a_2}\right)d\psi' + \int_0^{\psi} d\alpha_j\left(\psi - \psi'\right)\frac{d}{d\psi'}\left(\frac{\hat{\phi}}{a_2}\right)d\psi'\right] \tag{A.15}$$

where $dD_{jk}\left(\psi\right)$ and $d\alpha_j\left(\psi\right)$ are the transient components of the mechanical and expansion creep compliances, respectively, which are given by

$$dD_{jk}\left(\psi\right) = \sum_m \frac{C_{mj}C_{mk}}{C_m}\left[1 - \exp^{-\frac{\psi}{\tau_m}}\right] \tag{A.16}$$

$$d\alpha_j\left(\psi\right) = \sum_m \frac{C_{mj}\alpha_m}{C_m}\left[1 - \exp^{-\frac{\psi}{\tau_m}}\right] \tag{A.17}$$

The total strain using Eq. (A.3) can be expressed as

$$\varepsilon_i = -\frac{\partial G_0}{\partial \sigma_i} + \frac{\partial \hat{\sigma}_j}{\partial \sigma_i}\left[\int_0^{\psi} dD_{jk}\left(\psi - \psi'\right)\frac{d}{d\psi'}\left(\frac{\hat{\sigma}_k}{a_2}\right)d\psi' + \int_0^{\psi} d\alpha_j\left(\psi - \psi'\right)\frac{d}{d\psi'}\left(\frac{\hat{\phi}}{a_2}\right)d\psi'\right] \tag{A.18}$$

Considering G_0 (the nonlinear thermo-elastic potential) such that it yields the following form of thermal strain and instantaneous nonlinear mechanical strain as:

$$-\frac{\partial G_0}{\partial \sigma_i} = \alpha_i^t \left(T^t - T_0\right) + g_0(\bar{\sigma}^t, T^t) D_0 \sigma_i^t \tag{A.19}$$

When only one component of stress or strain is considered the constitutive expression for strain can be simplified. Schapery (1969) derived an expression for strain response due to uniform uniaxial state of stress ($\hat{\sigma} = \sigma$) and introduce nonlinear parameters to incorporate the contribution of higher orders terms of the Gibb's free energy in terms of the applied stresses. Under isothermal conditions, the uniaxial strain in Eq. (A.18) can be rewritten in order to incorporate nonlinear effects as:

$$\varepsilon(\psi) = g_0(\sigma^{\psi}) D_0 \sigma^{\psi} + g_1(\sigma^{\psi}) \int_0^{\psi} dD\left(\psi - \psi'\right) \frac{d}{d\psi'} \left(g_2(\sigma^{\psi'}) \sigma^{\psi'}\right) d\psi' \tag{A.20}$$

where $g_0(\sigma^{\psi})$, $g_1(\sigma^{\psi})$ and $g_2(\sigma^{\psi})$ are the nonlinear parameters which represent the instantaneous nonlinearity in thermo-elastic strain, the nonlinearity in transient strain and the effect of loading rate of stress for viscoelastic strain, respectively. For uniaxial loading, Schapery (1969) defined these nonlinear parameters as follows:

$$g_0\left(\sigma\right) = -\frac{\partial G_0}{\partial \sigma} \cdot \frac{1}{D_0 \sigma} \tag{A.21}$$

$$g_1\left(\sigma\right) = \frac{\partial \hat{\sigma}}{\partial \sigma} \tag{A.22}$$

$$g_2\left(\sigma\right) = \frac{\hat{\sigma}}{a_2 \sigma} \tag{A.23}$$

The dependence of temperature on mechanical properties and thermal expansion history can be incorporated to yield expression for thermal and mechanical strain histories as follows:

$$\varepsilon(\psi) = g_0(\sigma^{\psi}, T^t)D_0\sigma^{\psi} + g_1(\sigma^{\psi}, T^t)\int_0^{\psi} dD(\psi - \psi')\frac{d}{d\psi'}\left(g_2(\sigma^{\psi'}, T^t)\sigma^{\psi'}\right)d\psi' + \varepsilon^T(\psi) \tag{A.24}$$

where the thermal strain history can be expressed using Eqs. (A.18) and (A.19) as

$$\varepsilon^T(\psi) = \alpha^{\psi}\phi^t + g_1(\sigma^{\psi}, T^t)\int_0^{\psi} d\alpha(\psi - \psi')\frac{d}{d\psi'}\left(\frac{\hat{\phi}}{a_2}\right)d\psi' \tag{A.25}$$

The expression for entropy can be found using Eq. (A.1), Schapery (1997)

$$\eta = -\frac{\partial G}{\partial T} = -\frac{\partial G_0}{\partial T} + \frac{\partial A_m}{\partial T}\zeta_m \tag{A.26}$$

Substituting A_m from Eq. (A.14), we get

$$\eta = -\frac{\partial G_0}{\partial T} + \alpha_m\frac{\partial \hat{\phi}}{\partial T}\zeta_m \tag{A.27}$$

Substituting ζ_m from Eq. (A.13) and after some simplification, we can write Eq. (A.27) as

$$\eta = -\frac{\partial G_0}{\partial T} + \frac{\partial \hat{\phi}}{\partial T}\int_0^{\psi} d\alpha_j(\psi - \psi')\frac{d}{d\psi'}\left(\frac{\hat{\sigma}_j^{\psi'}}{a_2}\right)d\psi' + \frac{\partial \hat{\phi}}{\partial T}\int_0^{\psi} dC(\psi - \psi')\frac{d}{d\psi'}\left(\frac{\hat{\phi}}{a_2}\right)d\psi' \tag{A.28}$$

where $d\alpha_j(\psi)$ is already defined in Eq. (A.17), while $dC(\psi)$ is the transient components of the specific heat at constant stress, which is given by

$$dC(\psi - \psi') = \sum_m \frac{\alpha_m\alpha_m}{C_m}\left[1 - \exp\left[-\left(\frac{\psi - \psi'}{\tau_m}\right)\right]\right] \tag{A.29}$$

The specific heat capacity is defined as

$$c_{\sigma} = -T\left(\frac{\partial^2 G}{\partial T^2}\right)\Bigg|_{\sigma} = T\left(\frac{\partial \eta}{\partial T}\right)\Bigg|_{\sigma} \tag{A.30}$$

The specific heat can also be defined using internal energy $\mathcal{E}$, i.e.,

$$c_\sigma = \frac{\partial \mathcal{E}}{\partial T} \tag{A.31}$$

Substituting Eq. (A.28) into Eq. (A.30), we get specific heat at constant stress

$$\begin{aligned} c_\sigma &= -T\frac{\partial^2 G_0}{\partial T^2} \\ &+T\frac{\partial}{\partial T}\left[\frac{\partial \hat{\phi}}{\partial T}\int_0^{\psi} d\alpha_j\left(\psi-\psi'\right)\frac{d}{d\psi'}\left(\frac{\hat{\sigma}_j^{\psi'}}{a_2}\right)d\psi' + \frac{\partial \hat{\phi}}{\partial T}\int_0^{\psi} dC\left(\psi-\psi'\right)\frac{d}{d\psi'}\left(\frac{\hat{\phi}}{a_2}\right)d\psi'\right] \end{aligned} \tag{A.32}$$

The similar form of specific heat given in Eq. (A.32) has been developed by Schapery (1964, 1966b) and Chazal and Arfaoui (2001) using Helmholtz free energy. Now the rate of internal entropy generation can be found using Eq. (A.5), which can be expressed using Eq. (A.7) and assuming $B_m = a_2 C_m$ as (m not summed):

$$T\dot{\gamma}_{\text{int}} = f_m\dot{\zeta}_m = \left(A_m - a_2 C_m \zeta_n\right)\dot{\zeta}_m \tag{A.33}$$

Substituting A_m and ζ_m from Eq. (A.13) and Eq. (A.14), we can write Eq. (A.33) as

$$\begin{aligned} T\dot{\gamma}_{\text{int}} = f_m\dot{\zeta}_m = &\left(\begin{array}{l} C_{mj}\left\{\hat{\sigma}_j^{\psi} - a_2\int_0^{\psi}\sum_m \left[1-\exp\left[-\left(\frac{\psi-\psi'}{\tau_m}\right)\right]\right]\frac{d}{d\psi'}\left(\frac{\hat{\sigma}_j^{\psi'}}{a_2}\right)d\psi'\right\} \\ -a_2\int_0^{\psi}\sum_m \left[1-\exp\left[-\left(\frac{\psi-\psi'}{\tau_m}\right)\right]\right]\frac{d}{d\psi'}\left(\frac{\alpha_m\hat{\phi}}{a_2}\right)d\psi' + \alpha_m\hat{\phi} \end{array}\right) \\ &\left(\frac{d}{dt}\frac{1}{C_m}\int_0^{\psi}\sum_m \left[1-\exp\left[-\left(\frac{\psi-\psi'}{\tau_m}\right)\right]\right]\frac{d}{d\psi'}\left(\frac{C_{mj}\hat{\sigma}_j^{\psi'} + \alpha_m\hat{\phi}}{a_2}\right)d\psi'\right) \end{aligned} \tag{A.34}$$

If dissipation due to transient components of thermal strain and specific heat is neglected then after some simplification, we can write Eq. (A.34) as

$$T\dot{\gamma}_{\text{int}} = a_2\left\{g_2(\bar{\sigma}^{\psi})\sigma_j^{\psi} - \int_0^{\psi}\sum_m \left[1-\exp\left[-\left(\frac{\psi-\psi'}{\tau_m}\right)\right]\right]\frac{d}{d\psi'}\left(g_2(\bar{\sigma}^{\psi'})\sigma_j^{\psi}\right)d\psi'\right\} \left(\frac{d}{dt}\int_0^{\psi} dD_{jk}(\psi-\psi')\frac{d}{d\psi'}\left(g_2(\bar{\sigma}^{\psi'})\sigma_k^{\psi'}\right)d\psi'\right) \tag{A.35}$$

The force f_m is acting on mth dashpot and ζ_m is proportional to the strain in the mth Voigt unit. The $a_2C_m\zeta_m$ in the expression of thermodynamic force $f_m = A_m - a_2C_m\zeta_m$ represent nonlinear back stress provide by the spring to resist the increment of ζ_m (m not summed). Thus, it is appropriate to assume that the a_2 can be approximately equivalent to the nonlinear parameter $g_1(\bar{\sigma}^{\psi})$ which measures the nonlinearity effect in the transient compliance. Thus, the mechanical dissipation expression becomes:

$$T\dot{\gamma}_{\text{int}} = g_1(\bar{\sigma}^{\psi})\left\{g_2(\bar{\sigma}^{\psi})\sigma_j^{\psi} - \int_0^{\psi}\sum_m \left[1-\exp\left[-\left(\frac{\psi-\psi'}{\tau_m}\right)\right]\right]\frac{d}{d\psi'}\left(g_2(\bar{\sigma}^{\psi'})\sigma_j^{\psi'}\right)d\psi'\right\} \left(\frac{d}{dt}\int_0^{\psi} dD_{jk}(\psi-\psi')\frac{d}{d\psi'}\left(g_2(\bar{\sigma}^{\psi'})\sigma_k^{\psi'}\right)d\psi'\right) \tag{A.36}$$

The expression for energy balance can be easily obtained from Gibbs potential energy given in Eq. (A.1). Combining the first and second law of thermodynamics, the following expression for the energy balance in thermoviscoelastic materials can be easily established (Valanis, 1968; Rajagopal and Srinivasa, 2011).

$$T\dot{\eta} = -T\frac{d}{dt}\left\{\frac{\partial G}{\partial T}\right\} = -q_{i,i} + T\dot{\gamma}_{\text{int}} \tag{A.37}$$

where entropy is given in Eq. (A.28). Assuming thermo-elastic Gibbs potential (G_0) in Eq. (A.28) of the following form:

$$G_0 = -C_{th} - \alpha_{ij}(T)\theta\sigma_{ij} - \frac{1}{2}D^e_{ijkl}(\bar{\sigma},T)\sigma_{ij}\sigma_{kl} \tag{A.38}$$

where C_{th} and D^e_{ijkl} are the thermal part of the Gibbs free energy (thermo-elastic) and elastic compliance respectively. The entropy of thermo-elastic material is

$$\eta_0 = -\frac{\partial G_0}{\partial T} = \frac{\partial C_{th}}{\partial T} + \frac{\partial \alpha_{ij}(T)}{\partial T}\theta\sigma_{ij} + \alpha_{ij}(T)\sigma_{ij} + \frac{1}{2}\frac{\partial D^e_{ijkl}(\bar{\sigma},T)}{\partial T}\sigma_{ij}\sigma_{kl} \tag{A.39}$$

and the rate of entropy generation can be expressed as

$$\begin{aligned}\dot{\eta}_0 = \frac{d}{dt}\left(-\frac{\partial G_0}{\partial T}\right) = \frac{d}{dt}\left(\frac{\partial C_{th}}{\partial T}\right) + \frac{\partial \alpha_{ij}(T)}{\partial T}\dot{\theta}\sigma_{ij} + \frac{\partial \alpha_{ij}(T)}{\partial T}\theta\dot{\sigma}_{ij} \\ + \alpha_{ij}(T)\dot{\sigma}_{ij} + \frac{\partial g_0(\bar{\sigma},T)}{\partial T}D^e_{ijkl}\dot{\sigma}_{ij}\sigma_{kl}\end{aligned} \tag{A.40}$$

Substituting Eq. (A.39) into Eq. (A.32), the specific heat expression can be obtained for infinitesimal theory and expressed as:

$$\begin{aligned}c_\sigma = T\frac{\partial^2 C_{th}}{\partial T^2} + T\frac{\partial^2 \alpha_{ij}(T)}{\partial T^2}\theta\sigma_{ij} + 2T\frac{\partial \alpha_{ij}(T)}{\partial T}\sigma_{ij} + \frac{1}{2}T\frac{\partial^2 g_0(\bar{\sigma},T)}{\partial T^2}D^e_{ijkl}\sigma_{ij}\sigma_{kl} \\ + T\frac{\partial}{\partial T}\left[\frac{\partial \hat{\phi}}{\partial T}\int_0^{\psi} d\alpha_j(\psi-\psi')\frac{d}{d\psi'}\left(\frac{\hat{\sigma}^{\psi'}_j}{a_2}\right)d\psi' + \frac{\partial \hat{\phi}}{\partial T}\int_0^{\psi} dC(\psi-\psi')\frac{d}{d\psi'}\left(\frac{\hat{\phi}}{a_2}\right)d\psi'\right]\end{aligned} \tag{A.41}$$

The total rate of change of entropy using Eq. (A.28) and Eq. (A.40) can be expressed as

$$\begin{aligned}T\dot{\eta} = T\frac{d}{dt}\left(\frac{\partial C_{th}}{\partial T}\right) + T\frac{\partial \alpha_{ij}(T)}{\partial T}\dot{\theta}\sigma_{ij} + T\frac{\partial \alpha_{ij}(T)}{\partial T}\theta\dot{\sigma}_{ij} \\ + T\frac{\partial g_0(\bar{\sigma},T)}{\partial T}D^e_{ijkl}\dot{\sigma}_{ij}\sigma_{kl} + T\alpha_{ij}(T)\dot{\sigma}_{ij} \\ + T\frac{\partial}{\partial t}\left\{\frac{\partial \hat{\phi}}{\partial T}\int_0^{\psi} d\alpha_j(\psi-\psi')\frac{d}{d\psi'}\left(\frac{\hat{\sigma}^{\psi'}_j}{a_2}\right)d\psi' + \frac{\partial \hat{\phi}}{\partial T}\int_0^{\psi} dC(\psi-\psi')\frac{d}{d\psi'}\left(\frac{\hat{\phi}}{a_2}\right)d\psi'\right\}\end{aligned} \tag{A.42}$$

The energy equation using Eq. (A.37) and Eq. (A.42) becomes

$$T\frac{d}{dt}\left(\frac{\partial C_{th}}{\partial T}\right)+T\frac{\partial \alpha_{ij}(T)}{\partial T}\dot{\theta}\sigma_{ij}+T\frac{\partial \alpha_{ij}(T)}{\partial T}\theta\dot{\sigma}_{ij}+T\frac{\partial g_0(\bar{\sigma},T)}{\partial T}D^{e}_{ijkl}\dot{\sigma}_{ij}\sigma_{kl}+T\alpha_{ij}(T)\dot{\sigma}_{ij}$$
$$+T\frac{\partial}{\partial t}\left\{\frac{\partial \hat{\phi}}{\partial T}\int_0^{\psi} d\alpha_j(\psi-\psi')\frac{d}{d\psi'}\left(\frac{\hat{\sigma}_j^{\psi'}}{a_2}\right)d\psi'+\frac{\partial \hat{\phi}}{\partial T}\int_0^{\psi} dC(\psi-\psi')\frac{d}{d\psi'}\left(\frac{\hat{\phi}}{a_2}\right)d\psi'\right\}$$
$$=-q_{i,i} \qquad \text{(A.43)}$$
$$+g_1(\bar{\sigma}^{\psi})\left\{g_2(\bar{\sigma}^{\psi})\sigma_j^{\psi}-\int_0^{\psi}\sum_m\left[1-\exp\left[-\left(\frac{\psi-\psi'}{\tau_m}\right)\right]\right]\frac{d}{d\psi'}\left(g_2(\bar{\sigma}^{\psi'})\sigma_j^{\psi'}\right)d\psi'\right\}$$
$$\left(\frac{d}{dt}\int_0^{\psi} dD_{jk}(\psi-\psi')\frac{d}{d\psi'}\left(g_2(\bar{\sigma}^{\psi'})\sigma_k^{\psi'}\right)d\psi'\right)$$

Let assume that the thermal part of thermoelastic Gibbs free energy C_{th} is same as used in linear thermoelasticity formulation, i.e,

$$C_{th}=\frac{1}{2}\frac{\rho c_{\sigma}^{0}}{T_0}\theta^2 \qquad \text{(A.44)}$$

where c_{σ}^{0} is the temperature independent specific heat at constant stress and reference temperature. Substituting Eq. (A.44) into Eq. (A.42) and neglecting terms containing transient specific heat, thermal expansion and temperature dependent properties, the Eq. (A.42) becomes,

$$T\dot{\eta}=\rho c_{\sigma}(T)\dot{T}+T\alpha_{ij}\dot{\sigma}_{ij} \qquad \text{(A.45)}$$

where $c_{\sigma}(T)$ is the linear dependence of the specific heat at constant stress on temperature. For isotropic materials, using Eq. (A.45), the energy equation considering nonlinearity only due to dissipation function, having both stress and temperature dependent parameters, can be expressed as

$$\rho c_\sigma(T)\dot{T} + T\alpha\dot{\sigma}_{kk} = -q_{i,i}$$
$$+ g_1(\bar{\sigma}^{\psi}, T^t)\left\{ g_2(\bar{\sigma}^{\psi}, T^t)\sigma_j^{\psi} - \int_0^{\psi} \sum_m \left[1 - \exp\left[-\left(\frac{\psi - \psi'}{\tau_m} \right) \right] \right] \frac{d}{d\psi'} \left(g_2(\bar{\sigma}^{\psi'}, T^t)\sigma_j^{\psi'} \right) d\psi' \right\} \quad \text{(A.46)}$$
$$\left(\frac{d}{dt} \int_0^{\psi} dD_{jk}(\psi - \psi') \frac{d}{d\psi'} \left(g_2(\bar{\sigma}^{\psi'}, T^t)\sigma_k^{\psi'} \right) d\psi' \right)$$

For linear viscoelastic material, the above equation can be written as

$$\rho c_\sigma(T)\dot{T} + T\alpha\dot{\sigma}_{kk} = -q_{i,i}$$
$$+ \left\{ \sigma_j - \int_0^{t} \sum_m \left[1 - \exp\left[-\left(\frac{t - t'}{\tau_m} \right) \right] \right] \frac{d}{dt'} \left(\sigma_j^{t'} \right) dt' \right\} \left(\frac{d}{dt} \int_0^{t} dD_{jk}(t - t') \frac{d}{dt'} \left(\sigma_k^{t'} \right) dt' \right) \quad \text{(A.47)}$$

APPENDIX B

This Appendix presents the analytical solutions for linear viscoelastic materials under various loadings.

1. STANDARD LINEAR SOLID (SLS) MODEL (See Reddy, 2008)

1.1 SHEAR CREEP LOADING

Under shear strain, the governing equation for SLS model can be written as:

$$\frac{\partial \varepsilon_{12}(t)}{\partial t} + \frac{\mu_2}{\eta}\varepsilon_{12}(t) = \frac{1}{\mu_1}\frac{\partial \sigma_{12}(t)}{\partial t} + \frac{(\mu_1+\mu_2)}{\eta\mu_1}\sigma_{12}(t) \tag{B.1}$$

Let an instantaneous constant shear stress of magnitude τ_1 is applied at time *t=0*.

$$\sigma_{12}(t) = \tau_1 H(t) \tag{B.2}$$

where *H(t)* is a Heaviside function. Substituting Eq. (B.2) into Eq. (B.1), taking Laplace transform and using initial condition $\varepsilon_{12}(0) = 0$, we get

$$\bar{\varepsilon}_{12}(s) = \frac{\tau_1(\eta s + \mu_1 + \mu_2)}{\mu_1 s(\eta + \mu_2)} \tag{B.3}$$

where bar shows the transformed variable. Taking inverse Laplace of Eq. (B.3), we get the expression for time-dependent strain as

$$\varepsilon_{12}(t) = \frac{\tau_1}{\mu_1} + \frac{\tau_1}{\mu_2}\left(1 - \exp[-\frac{\mu_2}{\eta}t]\right) \tag{B.4}$$

The energy equation, assuming an adiabatic process and no internal heating source, for an isotropic viscoelastic material can be expressed as:

$$\rho c_\sigma \dot{T} = \dot{w}_{dis}^t \tag{B.5}$$

For SLS model the energy equation becomes

$$\rho c_\sigma \frac{\partial T(t)}{\partial t} = \eta \left[\varepsilon_{12}(t) - \frac{1}{\mu_1} \frac{\partial \sigma_{12}(t)}{\partial t} \right]^2 \tag{B.6}$$

Substituting the expressions of $\varepsilon_{12}(t)$ and $\sigma_{12}(t)$ and solving the Eq. (B.6) using initial condition *T(0)=0*, we can obtained the expression for the evolution of temperature.

$$T(t) = \int_0^t \frac{{\tau_1}^2}{\eta \rho c_\sigma {\mu_1}^2} \left[\exp\left(-\frac{2\mu_2}{\eta} \psi \right) {\mu_1}^2 + 2 \exp\left(-\frac{\mu_2}{\eta} \psi \right) \eta \mu_1 \delta(\psi) - \delta^2(\psi) \eta^2 \right] d\psi \tag{B.7}$$

where $\delta(t)$ is the Dirac delta function. The integration is done using Maple 13 to obtain numerical values of the temperature.

1.2 CYCLIC STRESS LOADING

Now consider the oscillating shear stress

$$\sigma_{12}(t) = \tau_2 \sin(\omega t) \tag{B.8}$$

Substituting the Eq. (B.8) into Eq. (B.1), taking Laplace transform and using initial condition $\varepsilon_{12}(0) = 0$.

$$\bar{\varepsilon}_{12}(s) = \frac{\tau_2 \omega (\eta s + \mu_1 + \mu_2)}{\mu_1 (s^2 + \omega^2)(\eta s + \mu_2)} \tag{B.9}$$

Taking inverse Laplace of Eq. (B.9), we get expression for time-dependent strain as

$$\varepsilon_{12}(t) = \frac{\tau_2 \sin(\omega t)}{\mu_1} + \frac{\tau_2}{{\mu_2}^2 + \omega^2 \eta^2} \left[\sin(\omega t) \mu_2 + \omega \eta \left\{ \exp[-\frac{\mu_2}{\eta} t] - \cos(\omega t) \right\} \right] \tag{B.10}$$

Substituting the expressions of $\varepsilon_{12}(t)$ and $\sigma_{12}(t)$ and solving the Eq. (B.6) using initial condition *T(0) =0*, the expression for the evolution of temperature can be obtained.

$$T(t)=\frac{1}{4\rho c_\sigma \mu_2^{\,4}+8\rho c_\sigma \mu_2^{\,2}\omega^2\eta^2+4\rho c_\sigma \omega^4\eta^4}$$
$$\mathrm{X}\left[\begin{array}{l}-\dfrac{16\rho c_\sigma \mu_2 \tau_2^{\,2}\omega^6\eta^6}{4\rho c_\sigma \mu_2^{\,4}+8\rho c_\sigma \mu_2^{\,2}\omega^2\eta^2+4\rho c_\sigma \omega^4\eta^4}-\dfrac{32\rho c_\sigma \mu_2^{\,3}\tau_2^{\,2}\omega^4\eta^4}{4\rho c_\sigma \mu_2^{\,4}+8\rho c_\sigma \mu_2^{\,2}\omega^2\eta^2+4\rho c_\sigma \omega^4\eta^4} \\ -\dfrac{16\rho c_\sigma \mu_2^{\,5}\tau_2^{\,2}\omega^2\eta^2}{4\rho c_\sigma \mu_2^{\,4}+8\rho c_\sigma \mu_2^{\,2}\omega^2\eta^2+4\rho c_\sigma \omega^4\eta^4}+2\eta^3\tau_2^{\,2}\omega^4 t-\eta^3\tau_2^{\,2}\omega^3\sin(2\omega t) \\ -2\eta^2\tau_2^{\,2}\omega^2\mu_2\cos(2\omega t)+\eta\tau_2^{\,2}\omega\mu_2^{\,2}\sin(2\omega t) \\ +8\eta^2\omega^2\tau_2^{\,2}\mu_2\exp\left(-\dfrac{\mu_2}{\eta}t\right)-2\eta^2\omega^2\tau_2^{\,2}\mu_2\exp\left(-\dfrac{2\mu_2}{\eta}t\right)+2\eta\tau_2^{\,2}\omega^2\mu_2^{\,2}t\end{array}\right] \quad \text{(B.11)}$$

1.3 CONSTANT AXIAL STRESS RATE LOADING

For uni-axial loading, the governing equation for SLS model can be written as:

$$\frac{\partial\varepsilon_{11}(t)}{\partial t}+\frac{E_2}{\eta}\varepsilon_{11}(t)=\frac{1}{E_1}\frac{\partial\sigma_{11}(t)}{\partial t}+\frac{(E_1+E_2)}{\eta E_1}\sigma_{11}(t) \quad \text{(B.12)}$$

Let a constant stress rate of magnitude σ_0 is applied till time $t=t_1$.

$$\sigma_{11}(t)=\sigma_0 t \quad \text{(B.13)}$$

Substituting Eq. (B.13) into Eq. (B.12), taking Laplace transform and using initial condition $\varepsilon_{11}(0)=0$, we get

$$\bar{\varepsilon}_{11}(s)=\frac{\sigma_0(\eta s+E_1+E_2)}{E_1 s^2(\eta s+E_2)} \quad \text{(B.14)}$$

Taking inverse Laplace of Eq. (B.14), we get the expression for time-dependent strain as

$$\varepsilon_{11}(t)=\tau_0\left[\frac{t(E_1+E_2)}{E_1E_2}-\frac{\eta}{{E_2}^2}\left(1-\exp[-\frac{E_2}{\eta}t]\right)\right] \tag{B.15}$$

The energy equation, assuming an adiabatic process and no internal heating source, for an isotropic viscoelastic material can be expressed as:

$$\left(\rho c_\varepsilon+9KT_0\alpha^2\right)\dot{T}+\alpha T_0\dot{\sigma}_{11}=\dot{w}^t_{dis} \tag{B.16}$$

For SLS model the energy equation becomes

$$\left(\rho c_\varepsilon+9KT_0\alpha^2\right)\frac{\partial T(t)}{\partial t}+\alpha T_0\dot{\sigma}_{11}=\eta\left[\varepsilon_{11}(t)-\frac{1}{E_1}\frac{\partial\sigma_{11}(t)}{\partial t}\right]^2 \tag{B.17}$$

Substituting the expressions of $\varepsilon_{11}(t)$ and $\sigma_{11}(t)$ and solving the Eq. (B.17) using initial condition *T(0)=0*, we can obtained the expression for the evolution of temperature.

$$T(t)=\frac{\tau_0}{\left(\rho c_\varepsilon+9\alpha^2T_0K\right){E_2}^2}\left[\frac{2\tau_0\eta^2}{E_2}\exp[-\frac{2E_2}{\eta}t]-\frac{8\tau_0\eta^2}{E_2}\exp[-\frac{E_2}{\eta}t]+9\alpha T_0{E_2}^2t-4\tau_0\eta t\right]$$
$$-\frac{2{\tau_0}^2\eta^2}{3\left(\rho c_\varepsilon+9\alpha^2T_0K\right){E_2}^3}$$

2. INTEGRAL MODEL

2.1 SHEAR CREEP LOADING

For linear viscoelastic material, the shear strain can be expressed as

$$\varepsilon_{12}(t)=J_0{\sigma_{12}}^t+\int_0^t dJ\left(t-\tau\right)\frac{d{\sigma_{12}}^\tau}{d\tau}d\tau \tag{B.18}$$

Here J_0 and $dJ(t)$ are the shear instantaneous elastic and transient compliances. The shear transient creep compliance is expressed as:

$$dJ^t = \sum_{n=1}^{N} J_n \left(1 - \exp[-\lambda_n \left(t - \tau\right)]\right) \tag{B.19}$$

where J_n and λ_n are Prony coefficients and retardation times, respectively. Using the creep compliance data, the Prony series coefficients can be characterized. With one Prony coefficient, the integral model is equivalent to SLS model, the transient shear creep compliance become

$$dJ^t = J_1 \left(1 - \exp[-\lambda \left(t - \tau\right)]\right) \tag{B.20}$$

Apply a constant shear stress of magnitude τ_1 the strain can be obtained using Eq. (B.18) as

$$\varepsilon_{12}(t) = \left\{J_0 + J_1 \left(1 - \exp[-\lambda t]\right)\right\} \tau_1 H(t) \tag{B.21}$$

The energy equation (Schapery 1969, 1997), assuming an adiabatic process and no internal heating source, for an isotropic linear viscoelastic material can be expressed as:

$$\rho c_\sigma \dot{T} = \int_0^t \exp\left[-\lambda \left(t - \tau\right)\right] \frac{d\sigma_{12}^{\tau}}{d\tau} d\tau \left\{\frac{d}{dt} \int_0^t dD\left(t - \tau\right) \frac{d\sigma_{12}^{\tau}}{d\tau} d\tau\right\} \tag{B.22}$$

Substituting the expressions of $\varepsilon_{12}\left(t\right)$, $\sigma_{12}\left(t\right)$ and *dD(t)* and solving the Eq. (B.22) using initial condition *T(0)=0*, we can obtained the expression for the evolution of temperature.

$$T(t) = \frac{\tau_1^{\,2} J_1}{\rho c_\sigma} \left[-\frac{1}{2} H(t) \exp\left(-\lambda t\right)^2 + \frac{1}{2} H(t)\right] \tag{B.23}$$

2.2 CYCLIC STRESS LOADING

Under oscillating shear stress the expression for strain can be obtained using Eq. (B.18) as

$$\varepsilon_{12}(t) = J_0\tau_2 \sin(\omega t) + \frac{J_1\lambda\tau_2}{\lambda^2+\omega^2}\left[\omega\exp[-\lambda t] + \sin(\omega t)\lambda - \omega\cos(\omega t)\right] \tag{B.24}$$

Substituting the expressions of $\varepsilon_{12}(t)$, $\sigma_{12}(t)$ and *dD(t)* and solving the Eq. (B.24) using initial condition *T(0)=0*, we can obtained the expression for the evolution of temperature.

$$T(t) = \frac{1}{4\rho c_\sigma\lambda^4 + 8\rho c_\sigma\lambda^2\omega^2 + 4\rho c_\sigma\omega^4} \times \begin{bmatrix} -\dfrac{16\rho c_\sigma J_1\tau_2^2\omega^2\lambda^6}{4\rho c_\sigma\lambda^4 + 8\rho c_\sigma\lambda^2\omega^2 + 4\rho c_\sigma\omega^4} - \dfrac{32\rho c_\sigma J_1\lambda^4\tau_2^2\omega^4}{4\rho c_\sigma\lambda^4 + 8\rho c_\sigma\lambda^2\omega^2 + 4\rho c_\sigma\omega^4} \\ -\dfrac{16\rho c_\sigma J_1\tau_2^2\omega^6\lambda^2}{4\rho c_\sigma\lambda^4 + 8\rho c_\sigma\lambda^2\omega^2 + 4\rho c_\sigma\omega^4} + 2\lambda^3\tau_2^2\omega^2 J_1 t - \lambda^3\tau_2^2\omega J_1\sin(2\omega t) \\ -2\lambda^2\tau_2^2\omega^2 J_1\cos(2\omega t) - \lambda\tau_2^2\omega^3 J_1\sin(2\omega t) + 2\tau_2^2\omega^4\lambda J_1 t \\ +8\lambda^2\omega^2\tau_2^2 J_1\exp(-\lambda t)\cos(2\omega t) - 2\lambda^2\omega^2\tau_2^2 J_1\exp(-2\lambda t) \end{bmatrix} \tag{B.25}$$

2.3 CONSTANT AXIAL STRESS RATE LOADING

The uni-axial transient creep compliance *dD(t)* with one Prony coefficient can be expressed as:

$$dD^t = D_1\left(1 - \exp[-\lambda(t-\tau)]\right) \tag{B.26}$$

Under constant stress rate the expression for axial strain can be obtained using Eq. (B.18) as

$$\varepsilon_{11}(t) = D_0\sigma_0 t + \frac{D_1\sigma_0}{\lambda}\exp[-\lambda t]\left[\exp[\lambda t] - 1 - \lambda t\right] \tag{B.27}$$

where D_0 is an axial instantaneous elastic compliance. Assuming an adiabatic process and no internal heating source, for an isotropic thermo-viscoelastic material and assuming temperature independent material properties, the energy equation can be expressed as:

$$\left(\rho c_\varepsilon + 9KT_0\alpha^2\right)\frac{dT(t)}{dt} + \alpha T_0\dot{\sigma}_{11} = \int_0^t \exp\left[-\lambda(t-\tau)\right]\frac{d\sigma_{11}^\tau}{d\tau}d\tau\left\{\frac{d}{dt}\int_0^t dD(t-\tau)\frac{d\sigma_{11}^\tau}{d\tau}d\tau\right\} \tag{B.28}$$

Substituting the expressions of $\varepsilon_{11}(t)$, $\sigma_{11}(t)$ and *dD(t)* and solving the Eq. (B.28) using initial condition *T(0)=0*, we can obtained the expression for the evolution of temperature.

$$T(t) = \frac{\sigma_0}{\left(\rho c_\varepsilon + 9\alpha^2 T_0 K\right)\lambda}\left[\begin{array}{l} -\dfrac{D_1\sigma_0\left(-\dfrac{1}{2}\exp[-\lambda t]^2\lambda t - \dfrac{1}{4}\exp[-\lambda t]^2\right)}{\lambda} \\ +\dfrac{D_1\sigma_0\left(-\exp[-\lambda t]\lambda t - \exp[-\lambda t]\right)}{\lambda} \\ +\alpha T_0\exp[-\lambda t] + \dfrac{3D_1\sigma_0}{4\lambda} - \alpha T_0 \end{array}\right] \tag{B.29}$$

VITA

Name:	Kamran Ahmed Khan
Address:	Department of Mechanical Engineering, 3123 TAMU, College Station, TX 77843, USA
Email Address:	kamran026@yahoo.com
Education:	B.E., Mechanical Engineering, NED University of Engineering and Technology, Karachi, Pakistan, 2002
	M.S., Mechanical Engineering,, Texas A&M University, College Station, Texas, 2006
	Ph.D., Mechanical Engineering,, Texas A&M University, College Station, Texas, 2011